ISSN 1817-2954

HSIUPING UNIVERSITY OF SCIENCE AND TECHNOLOGY

修平學報

HSIUPING JOURNAL

第二十三期

修平科技大學編印
中華民國一〇〇年九月出版

修 平 學 報

第 二十三 期

修 平 科 技 大 學　　編印

中華民國一〇〇年九月出版

第二十三期學報中文目錄

Contents

修平學報 第二十三期 民國一〇〇年九月
HSIUPING JOURNAL VOL.23, pp.1-16 （September 2011） 1

Gait Analysis for Walking Paths Determination and Human Identification

Meng-Fen Ho , Chung-Lin Huang

Abstract

In this paper, we propose a gait analysis method to extract the dynamic and static information from the input video for walking path determination and human identification. Based on the periodicity of swing distances, we may estimate the gait period of each walking video sequence. For each gait cycle, we depict the dynamic information by analyzing the distribution of motion vectors, and then describe the static information by using Fourier descriptors. The extracted dynamic and static information is transformed into lower dimensional embedding space for human identity recognition. To solve the difference of walking velocity between the test and training human objects, a hybrid human ID recognition algorithm is developed to choose the effective feature. Given a test feature vector, the nearest neighbor classifier is applied for walking paths determination and human identification. The proposed algorithm is evaluated on the CASIA gait database, and the experimental results demonstrate a highly acceptable recognition rate, for example, 98% for normal walking dataset.

Keywords: Gait analysis, human identification.

Meng-Fen Ho, Associate Professor, Department of Electronic Engineering, HUST.
Chung-Lin Huang, Professor, Dept. of Electrical Engineering, National Tsing Hua University.
Received 16 December 2010; accepted 18 January 2011

步伐姿態分析運用於
人物步行路徑與身分識別

何孟芬、黃仲陵

摘　要

在這篇論文中，我們擷取動態與靜態資訊來進行人物步行路徑和身分的識別。首先利用步伐擺幅距離的週期特性,可以估測每段影像的步伐週期,針對每段步伐週期，分析其運動向量的分布，即可獲得所需的動態資訊，同時利用傅立葉描述取得靜態資訊，接著將這兩種資訊轉換至低維度空間以便進行人物識別。為了解決訓練影片與測試影片中，人物走路速度可能不同的問題，我們提出了一個混合人物識別演算法來選定最有效的特徵。每當測試特徵向量進來時，利用最鄰近分類法則進行路徑確認與人物識別。本系統利用 CASIA 步伐姿態資料庫進行評估，實驗結果證明的確獲得極高的辨識率，以正常走路的資料組而言，可達到約 98%。

關鍵詞：步伐姿態分析、人物辨識。

何孟芬：修平科技大學電子工程系副教授
黃仲陵：清華大學電機工程系教授
投稿日期：99 年 12 月 16 日　接受刊登日期：100 年 1 月 18 日

I. Introduction

Intelligent video surveillance system has been widely developed of which the human identification is one of the most important functionalities. Biometric features are regularly applied for human identification to express the unique property of human object. Common biometric features include iris, face, speech, fingerprints, hand geometry, voice, and gait. Here, we choose the gait posture as our main feature for human identification. Comparing with other biometrics, gait analysis has the advantage of non-contact and can generate the perceivable biometric feature for human identification at distance.

However, gait analysis also has some disadvantages [1]. In the internal factors, gait posture has a little change accompanying the mood or physical injury of the walking people. In the external factors, gait can be affected by clothing, shoes, walking surface, or other handbag-carrying conditions. Therefore, it will induce a large gait variation of the same person and reduce system discriminating ability. Excluding the internal factors, we attempt to construct a new system that can identify the human object based on the gait postures caused only by some external factors.

A. Related Works

Current approaches of gait analysis can be divided into two categories: appearance-based and model-based approaches [1-16]. The former deals directly with the image statistics, whereas the latter models the image data and then analyzes the variation of its parameters. The majority of current approaches are the appearance-based, because they are simple and fast.

Su et al. [2] propose a method which combines both the appearance-based approach and the model-based approach to analyze and extract human gait. The static features include body height, width, etc. Instead of modeling the human body, the limb angle information is extracted by analyzing the variation of silhouette width to represent the kinematic information of gait. Then the multi-class support vector machines are used to identify human object. In [3], a new feature extraction process is proposed for gait representation. Each gait sequence is described by using a low-dimensional feature vector consisting of selected Radon template coefficients. Identification is done by using linear discriminant analysis (LDA). A different approach called component-wise comparison is proposed by [4], which calculates the distances between silhouettes on a component by component basis, and then combines the component-wise distances into a common distance metric for the evaluation of similarity between two silhouettes.

Han et al. [5] propose a spatial-temporal gait representation, called Gait Energy Image (GEI), to characterize human walking posture. They combine Principal Component Analysis (PCA) and Multiple Discriminant Analysis (MDA) to transform datasets to a low-dimensional space and then separate the datasets to different classes. In [6], they improve temporal templates called Gait History Image (GHI). GEI only represents the static part and the dynamic part on moving subject, but GHI increases the temporal variation and provides the better performance. Equivalently, the other authors choose gait moment image (GMI) as features to emphasize the dynamic information of human gait in [7]. GMI is the gait probability image at each key moment in the gait period.

In [8], they propose an eigen-gait method to model human motion directly, and encode the dynamic feature of gait in pair-wise image similarities of gait images. Moreover, the authors employ PCA to reduce the self-similarity plot (SSP) and use K-nearest neighbor rule to recognize the human identification. Cheng et al. [9] propose a novel algorithm for both automatic viewpoint and person identification by using only the silhouette sequence of the gait. First, the gait silhouettes are nonlinearly transformed into low-dimensional embedding by Gaussian process latent variable model (GPLVM). Then the temporal dynamics of the gait sequences are modeled by hidden Markov models (HMMs). In [10], a gait is represented by a vector of affine invariant moments obtained from the binary silhouettes. With a combination of histograms of individual silhouette and contextual silhouette, a gait appearance model is represented by a shape descriptor and gait images plane [11]. The similarity of gait appearance models are measured by Jeffrey divergence and dynamic time warping.

B. System Overview

Generally speaking, the procedure of gait recognition includes human object segmentation, feature extraction, and classification. In this paper, we propose a method which is different from the previous works in using new gait characteristics for human identification without knowing the walking direction of the person. The novel system will identify the walking path of human object, and then recognize his/her identification. The overview of our proposed system is shown in Fig. 1.

This system is composed of four main stages: human silhouettes segmentation, static and dynamic feature extraction, dimension reduction of feature vectors, and the recognition of walking path and human identification. The first stage is developed to separate the human object from the background in binary image sequence, which includes foreground compensation, horizontal and vertical alignment, and size normalization. Then, gait period is estimated by utilizing the periodicity of swing distances, and then binary image sequence is divided into sub-cycles of silhouette.

The second stage is developed to extract the static and dynamic features in each sub-cycle of silhouette. The intersecting operation is applied to every silhouette in each sub-cycle to obtain the static region within each gait period. The contour of the static region is regarded as the static feature. Then, we analyze two continuous image frames in each sub-cycle to obtain the optical flow measurement as the motion vector field. By analyzing the statistics of the motion vector field, we generate the two-dimensional motion histogram of the magnitude and the direction of the motion vectors, which are regarded as the dynamic features.

In the third stage, we use PCA and MDA to transform the high-dimensional feature vectors to the low-dimensional subspace. In the fourth stage, the discriminant functions and the nearest neighbor classifier are applied to recognize the walking path and human identification respectively.

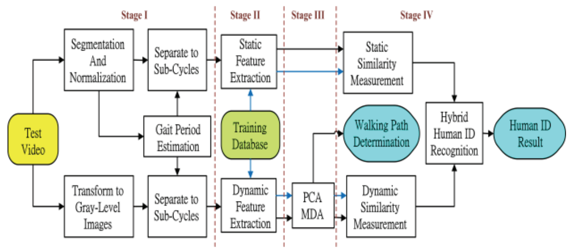

Fig. 1. System diagram of our main system.

II. Human Object Segmentation And Gait Period Estimation

A. Human Object Segmentation

In our system, we assume the camera is stationary and there is only one human object walking through the scene. We use the foreground video sequences from CASIA database. For each segmented human silhouette in each frame, we compute the centroid (xc, yc) of the human silhouette. Then, we compute the width W and the height H of the human silhouette. We use the centroid of the human silhouette to calibrate along the horizontal direction, and the vertical direction of the frames of size 320×240. Then we use the centroid to calibrate and then normalize the human silhouette within the bounding box of size 161x101 as shown in Fig. 2.

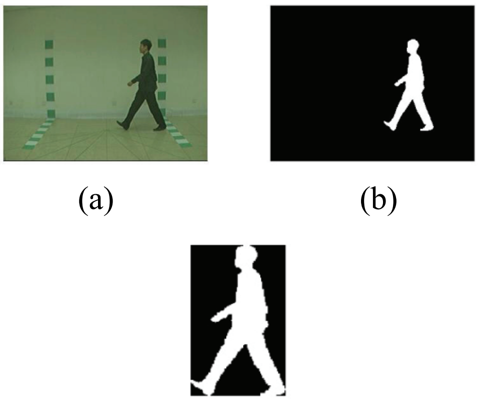

(a) (b) (c)

Fig. 2. Human segmentation results of the view angle 90 degree. (a) The original image. (b) The extracted silhouette. (c) The human silhouette after calibration and normalization.

B. Gait Period Estimation

The human walking is treated as a periodic activity which corresponds to the total average pixel width of the normalized foreground. For example, double-support stance corresponds to the local maximum average width and legs-together stance corresponds to the local minimum width. Therefore, swing distance [6] that computes the total average foreground pixels' distance from the normalized foreground center is applied to detect the started and end frames of the gait period. Swing distance is described as

$$sw = \sum_{y=y_b}^{y_t - \frac{(y_t - y_c)}{2}} \sum_{x=x_l}^{x_r} \left| (x - x_c) \times \frac{I(x, y)}{255} \right| , \quad (1)$$

where (xc, yc) is the centroid of the binary silhouette, xl and xr denote the horizontal positions of the left-most and the right-most boundary pixels of the silhouette respectively, yb and yt denote the vertical positions of the bottom-most and the top-most boundary pixels of the silhouette respectively, and I(x, y) represents the pixel intensity at (x, y).

The periodicity of gait is implied by the variation of swing distance. The gait period defined here starts from the legs-together stance and passes through two double-support stances and one legs-together stance and back to the same legs-together stance. Local minimum swing distance is detected and used to separate gait periods from the video since it is less affected by background noise than local maximum. The experimental results for measuring the periodicity of binary gate sequence are shown in Fig. 3. Finally, the binary gait sequence is separated to a number of sub-cycles.

III. Gait Feature Extraction

In order to get the higher recognition rate, we must find the discriminative characteristics for representing the walking style of each person. Using the motion vectors as the dynamic features is not effective when the walking velocities of the training video sequence and the test video sequence are different. It is necessary to utilize the static features which are independent of the walking velocity. Here, we use the Fourier descriptors to represent the contour of static region as the static features.

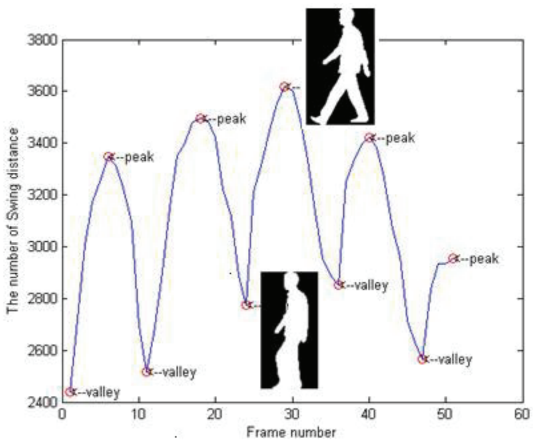

Fig. 3. The Swing distance corresponds to frame numbers. Local minimum of swing distance represents the legs-together stance, while, local maximum represents the double-support stance.

A. Dynamic Feature Extraction

After using the motion estimation to find the optical flow field of the video sequences, we evaluate the histogram distribution of the optical flow vector field, which are treated as the dynamic feature. From the experimental results, we find some useless motion vectors due to the variations of lighting condition, reflecting condition, shadow, and other reasons. By using the thresholding, we select only the meaningful and slightly larger motion vectors. We partition the magnitude and the direction of the motion vectors into 10 and 13 intervals respectively as shown in Table 1 and 2.

Table 1. Intervals of the magnitude of the optical flow vector, where mvm denotes the magnitude of every optical flow vector.

Level	**1**	**2**	**3**	**4**	**5**
MV_m	1~2	2~3	3~4	4~5	5~6
Level	**6**	**7**	**8**	**9**	**10**
MV_m	6~7	7~8	8~9	9~10	>10

Table 2. Intervals of the direction of the optical flow vector, where MVθ denotes the direction of every optical flow vector.

Interval	**1**	**2**	**3**	**4**	**5**
MV_θ	$\pi \pm \frac{\pi}{12}$	$\frac{5\pi}{6} \pm \frac{\pi}{12}$	$\frac{4\pi}{6} \pm \frac{\pi}{12}$	$\frac{3\pi}{6} \pm \frac{\pi}{12}$	$\frac{2\pi}{6} \pm \frac{\pi}{12}$
Interval	**6**	**7**	**8**	**9**	**10**
MV_θ	$\frac{\pi}{6} \pm \frac{\pi}{12}$	$0 \pm \frac{\pi}{12}$	$-\frac{\pi}{6} \pm \frac{\pi}{12}$	$-\frac{2\pi}{6} \pm \frac{\pi}{12}$	$-\frac{3\pi}{6} \pm \frac{\pi}{12}$
Interval	**11**	**12**	**13**		
MVθ	$-\frac{4\pi}{6} \pm \frac{\pi}{12}$	$-\frac{5\pi}{6} \pm \frac{\pi}{12}$	$-\pi \pm \frac{\pi}{12}$		

Then we combine the magnitude and

direction histograms to a 2-D histogram. Supposing there are N gait cycles in the sequence, after evaluating the overall N 2-D combinational histograms, we utilize the Bhattacharyya distance to measure the similarity between these 2-D combinational histograms. For two discrete probability distributions p(x) and q(x), over the same domain X, the Bhattacharyya distance dbhatt(p,q) is defined as

$$d_{bhatt}(p,q)=\sum_{x\in X}\sqrt{p(x)q(x)} \quad . \tag{2}$$

Let MVC(i) denote the 2-D combinational histogram belonging to the ith gait period interval. The 2-D combinational histograms, MVC(i), i=1,…,N whose dbhatt(p, q) is lower than the threshold are truncated as MVC(i), i= 1,…,Nt, where 1< Nt <N. Then, we take the average of the spare 2-D combinational histograms as

$$r=\sum_{i=1}^{N^t}\frac{MV_C(i)}{N^t} \quad . \tag{3}$$

Finally, we transform the average 2-D combinational histogram to a column vector of size 130×1. The column vector expresses the dynamic features in the video sequence. Figure 4(a) shows the silhouette sequence of one human object, and the corresponding average 2-D combinational histogram is demonstrated in Fig. 4(b).

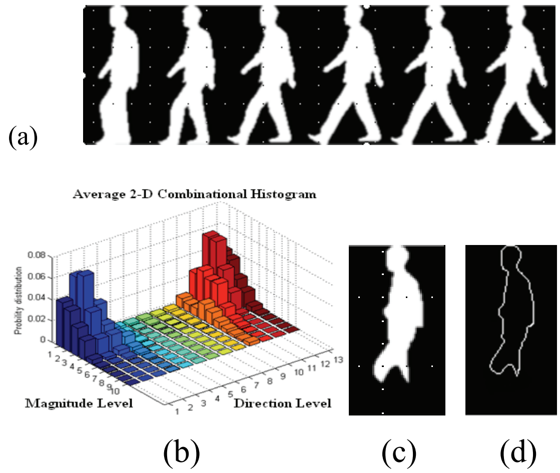

Fig. 4. (a) The silhouette sequence. (b) The average 2-D combinational histogram. (c) The static part of (a). (d) The extracted contour.

B. Static Feature Extraction

In this paper, we use Fourier descriptors (FDs) [17] to describe the contour of the static region within half cycle as the static feature. The static region of the human body represents the common region in each frame within one half cycle. Assuming S(x, y) represents the common region in each frame of one half cycle, where non-moving pixels are highlighted in binary image S, as shown in Fig. 4(c). For binary silhouette sequence BI, S can be obtained by utilizing the intersecting operation as

$$S(x,y)=\bigcap_{t=1}^{\tau}BI(x,y,t) \quad , \tag{4}$$

where BI(x,y,t) is the binary value of the pixel (x,y) in the tth frame, and τ is the time duration of the motion sequence.

FDs are invariant to translation, rotation and scaling of the object. Let the complex array p0, p1,…, pM-1 represent the boundary belonging to the region of static part, the kth Fourier transform coefficient can be calculated as

$$z_k = \sum_{n=0}^{M-1} p_n \, e^{-\frac{2\pi ikn}{M}} , \qquad (5)$$

zk describes the frequency contents of the shape. Lower frequency components depict the overall shape, whereas higher frequency components describe the details of the shape. The FDs are defined as

$$c_k = |z_{k+2}| / |z_1|, \; k = 0, \cdots, M-3 . \qquad (6)$$

Finally, we truncate the number of evaluated FDs to 30. Assuming N is the number of total gait cycles in the video sequence, the FDs of N static regions are combined as a matrix of size N×30 to represent the static features.

IV Human ID Recognition in Multiple Paths

Given the test video sequence, the purpose of the system is to recognize the human walking path and identify the human ID as well. In the learning procedure, we adopt the dimension reduction method to map the training feature vectors onto its embedding feature space. Then we continue the walking path classification and the human ID similarity measurement in the embedding feature space.

A. Learning Procedure by PCA and MDA

We combine PCA and MDA [5] to achieve the best trade-off between the data representation and the class separability. PCA is optimal in the sense that it minimizes the mean square error between the n d-dimensional dynamic features {x1, x2,…,xn} and their approximations {y1, y2,…, yn},

$$\mathbf{y}_k = [\mathbf{u}_1, \ldots, \mathbf{u}_{d'}]^T \mathbf{x}_k \;, k = 1, \ldots, n , \qquad (7)$$

where yk denotes the d′-dimensional feature vector, d′ << d, and u1, u2,…,ud′ represent the eigenvectors corresponding to the d′ largest eigenvalues.

Assuming that the principal component vectors {y1, y2,…, yn} belong to L classes (C1 to CL), MDA selects a transformation matrix W so that the ratio of the between-class scatter and the within-class scatter is maximized. Let the between-class scatter matrix be defined as

$$\mathbf{S}_b = \sum_{i=1}^{L} N_i(\overline{\mathbf{y}_{C_i}} - \overline{\mathbf{y}})(\overline{\mathbf{y}_{C_i}} - \overline{\mathbf{y}})^T \quad , \qquad (8)$$

and the within-class scatter matrix be defined as

$$\mathbf{S}_w = \sum_{i=1}^{L} \sum_{\mathbf{y}_{C_i}} (\mathbf{y}_{C_i} - \overline{\mathbf{y}_{C_i}})(\mathbf{y}_{C_i} - \overline{\mathbf{y}_{C_i}})^T \qquad (9)$$

where Ni is the number of feature vectors in class Ci, yCi and $\overline{\mathbf{y}_{C_i}}$ denote the feature vectors and the mean vector belonging to class Ci respectively, and $\overline{\mathbf{y}}$ is the mean for all feature vectors. The optimal projection Wopt is chosen as the matrix with the orthonormal columns which are the generalized eigenvectors corresponding to the m largest eigenvalues,

$$\mathbf{W}_{opt} = \arg\max_{\mathbf{W}} \frac{\left|\mathbf{W}^T \mathbf{S}_b \mathbf{W}\right|}{\left|\mathbf{W}^T \mathbf{S}_W \mathbf{W}\right|} = [\mathbf{w}_1, \mathbf{w}_2, \ldots, \mathbf{w}_{L-1}] \quad . (10)$$

There are at most L-1 nonzero eigenvalues and the corresponding eigenvectors. Finally, each training dynamic feature vector can be represented as

$$\begin{aligned}\mathbf{v}_k &= [\mathbf{w}_1, \ldots, \mathbf{w}_{L-1}]^T [\mathbf{u}_1, \ldots, \mathbf{u}_{d'}]^T \mathbf{x}_k \\ &= \mathbf{T}\mathbf{x}_k \ , k = 1, \ldots, n\end{aligned} \qquad (11)$$

In our experiments, the training dataset must be classified to three different groups according to three different walking paths of the video sequence. In testing procedure, given a testing dynamic feature vector, it can be projected into (L-1)-dimensional space.

B. Walking Path Determination

We apply Bayesian classifier to divide the feature space into three decision regions corresponding to three different walking paths. The feature vector v belonging to path i if

$$g_i(\mathbf{v}) > g_j(\mathbf{v}) \quad \textit{for all } j \neq i, \ \ i = 1,2,3 \quad , \qquad (12)$$

where gi(v) denotes a set of discriminant function. For multivariate normal densities $p(x|w_i) \sim N(\mu_i, \Sigma_i)$, the discriminant function can be evaluated and simplified as

$$\begin{aligned} g_i(\mathbf{v}) = &-\frac{1}{2}\mathbf{v}^t \Sigma_i^{-1}\mathbf{v} + (\Sigma_i^{-1}\mu_i)^t\,\mathbf{v} + \ln p(w_i) \\ &-\frac{1}{2}\ln\left|\Sigma_i\right| - \frac{1}{2}\mu_i^t \Sigma_i^{-1}\mu_i \ , \ \ i = 1,2,3. \end{aligned} \qquad (13)$$

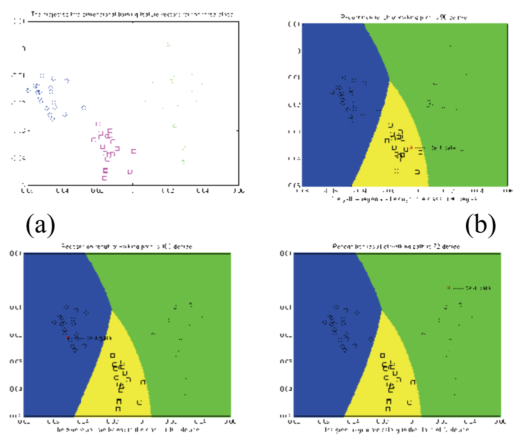

(a) (b) (c) (d)

Fig. 5. The classification results of test feature vectors. (a) The training feature vectors from three different classes are projected onto the two-dimensional feature space.

(circle: 108°, square: 90°, diamond: 72°) (b)-(d) The testing feature vector is correctly classified to its class.

Here, we suppose an equal prior probability for each class, i.e. p(w1) = p(w2)= p(w3)=1/3. Figure 5(a) shows the distribution for training data from three different walking paths.

Then using the following decision rule to divide the feature space into three decision regions, $\Re_1$, $\Re_2$, and $\Re_3$, which are referred as three different walking paths,

$$\mathbf{v} \in \Re_i,\ \ if\ g_i(\mathbf{v}) > g_j(\mathbf{v}) \quad for\ all\ j \neq i,\ \ i = 1,2,3 \ . \quad (14)$$

According to the decision rule, we can classify the feature vector v to the ith class. Figures 5(b) - 5(d) shows the classification results for the test data of three different walking paths.

C. Hybrid Human ID Recognition

Once the human walking path has been identified, the human identity can be recognized. Given a testing dynamic feature vector r, we transform it onto a low-dimensional feature space, i.e., $r' = Tr$. The similarity measurement for dynamic feature vectors is described as

$$D_i(\mathbf{r}', \mathbf{v}_i) = n(n-1)\|\mathbf{r}', \mathbf{v}_i\| \Big/ \sum_{i=1}^{n} \sum_{j=1, j\neq i}^{n} \|\mathbf{v}_i, \mathbf{v}_j\| \ , \quad (15)$$

where $\frac{1}{n(n-1)} \sum_{i=1}^{n} \sum_{j=1, j\neq i}^{n} \|\mathbf{v}_i, \mathbf{v}_j\|$ is the average distance between training feature vectors of every two classes, and n is the number of human objects in the database. Hence r' is classified to the kth-human object if and only if $D_k(\mathbf{r}', \mathbf{v}_k) = \min_i D_i(\mathbf{r}', \mathbf{v}_i),\ \ i = 1, \cdots, n$.

For the similarity measure of the static feature, assuming Ct =[c1t,…, cNtt]T is the testing static feature, and Ci =[c1i,…, cNii]T is the training static feature belonging to the ith-human object, where Nt denotes the number of gait cycles and ckt denotes the Fourier descriptors of the testing sequence. Ni represents the average gait cycles, and cki represents the evaluated Fourier descriptors for the ith-human object. Using Euclidean metric to measure the distance in the frequency domain as

$$D_i(C^t, C^i) = \left\|C^t - C^i\right\| = \frac{\sum_{k=1}^{\min(N_i, N_t)} \left\|c_k^t - c_k^i\right\|}{\min(N_i, N_t)} \ . \quad (16)$$

Finally, Ct is assigned to the kth-human object if and only if $D_k(C^t, C^k) = \min_i D_i(C^t, C^i),\ i = 1, \cdots, n$.

Here we propose a hybrid human ID recognition based on the walking velocity of human object. If the walking cycle period of the testing sequence is similar to the training sequence, the dynamic ranking is effective; otherwise, the static ranking is considered. The dynamic ranking identifies the human ID based on the similarity of the dynamic features, i.e., Eq. (15), whereas the static ranking recognizes the human ID based on the similarity of the static features, i.e., Eq. (16). The hybrid human identification process consists of the following steps: (1) The difference of gait period between the testing video sequence (Ptest) and the highest rank of human ID from the database ($\hat{P}_{train}$) is calculated. (2) If the difference is lower than threshold TP, we will recognize human ID by dynamic ranking. (3) If the difference of the periods is higher than threshold TP, we calculate the average similarity distance of static feature and compare with threshold TD to determine which ranking is better. (4) When the average similarity distance is lower than threshold TD, we will recognize the human ID by static ranking; otherwise, the dynamic ranking is chosen. The flowchart of the hybrid human ID recognition is described in Fig. 6.

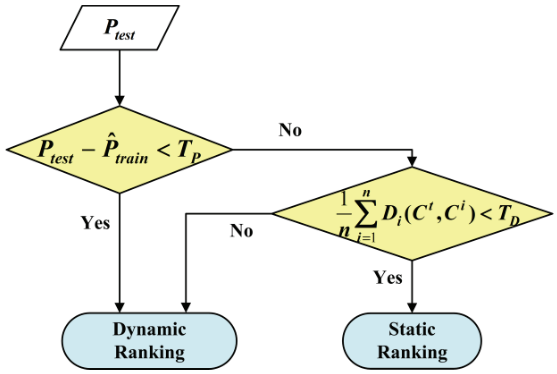

Fig. 6. The flowchart of the hybrid human ID recognition.

V. Experimental Results

The gait video sequences in CASIA database [18] are used to evaluate the effectiveness of our proposed system. The database consists of 124 subjects captured from 11 different views simultaneously, and has 10 walking sequences for each individual. There are six normal walking sequences (i.e., Set A), two carrying-bag sequences (i.e., Set B) and two wearing-coat sequences (i.e., Set C) as shown in Fig. 7. In our experiments, we collect the first four sequences of each individual in Set A as the training set (i.e., Set A1), and use the rest two sequences in Set A (i.e., Set A2), Set B and Set C as the test set. Here, we only select three walking paths, in 72° viewing direction (i.e., Path 1), in 90° viewing direction (i.e., Path 2), and in 108° viewing direction (i.e., Path 3), to test the performance of our proposed system. Figure 8 shows the images from three different walking paths in the perspective view.

(a) (b) (c)

Fig. 7. Three different sets from CASIA database. (a) Normal walking, (b) walking with wearing a coat, and (c) walking with carrying a bag.

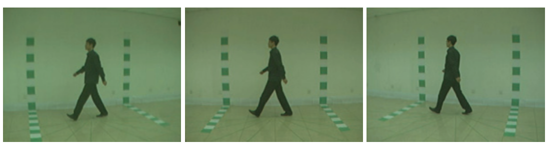

(a) (b) (c)

Fig. 8. Three different walking paths. (a) 72° (Path 1), (b) 90° (Path 2), and (c) 108° (Path 3)

A. Walking Path Recognition and Human ID Recognition

We select 124 human objects from Set A2, Set B, and Set C walking in three different paths. The accuracy of our system for identifying the correct walking path direction is shown in Table 3. Once the walking path is identified, we do the experiments of testing 124 human objects from Set A2, Set B, and Set C in the three different walking paths. The average human ID recognition rates are shown in Table 4. The results show that the recognition rates for the normal walking sequences (Set A2) are much higher than the other two sets. Besides, we can further increase the recognition rate by using the proposed hybrid features.

Table 3. The Walking Path Recognition Rate using CASIA Gait Database.

Correct Path Recognition Ratio				
Input	Path 1	Path 2	Path 3	Recognition Rate
Path 1	491	8	5	98.99%
Path 2	5	476	9	95.97%
Path 3	0	12	482	97.18%
Average success rate: 97.38%				

Table 4. The experimental results for average Human ID recognition in multiple paths.

	Human ID Recognition Rate			
	Dynamic Feature Only		Hybrid features	
Test Sequence	Rank1	Rank3	Rank1	Rank3
Set A2	97.45%	99.33%	97.98%	99.73%
Set B	86.02%	95.70%	86.02%	95.70%
Set C	83.06%	92.20%	85.22%	93.82%
Average Rate	90.99%	96.64%	91.80%	97.24%

B. Human ID Recognition Using Only Training Dataset from Path 2

In the 2nd experiment, we use only the video sequences in 90° viewing direction (i.e., Path 2) as our training sequence to recognize the walking people captured from three different viewing directions. This experiment aims to test the performance of different methods when the viewing direction of the test video sequence is different from the viewing direction of the training video sequence. Table 5 demonstrates the comparison of our system with other methods where "Sup" is the method of supervised feature selection [13], and "CAS" is the method of using direct GEI (Gait Energy Image) shape match [14]. The experimental results show that our proposed method is insensitive to different test paths by using only the training datasets of path 2. Compared with the supervised feature selection (Sup), which is computationally expensive, our method not only offers a similar performance for normal cases, but also performs better for the special cases of the input videos of people carrying a handbag.

Table 5. Comparison of recognition performance of our proposed method with others by using only the training dataset of path 2.

Comparison of the Recognition performance (%)									
	Set A			Set B			Set C		
Path	CAS	Sup	Ours	CAS	Sup	Ours	CAS	Sup	Ours
1	82.3	90.3	89.5	42.3	79.4	79.8	20.6	77.5	75.8
2	97.6	98.6	98.4	52	85.5	87.1	32.7	88.7	86.3
3	82.3	78.5	79.8	31.9	60.6	62.9	16.5	62.3	61.3

C. Comparison with Other Proposed Methods

We also do the experiments of using the input videos of 90° viewing direction for both the training and the testing datasets. Table 6 shows the comparison of the proposed method with four different existing methods. The results demonstrate that our method is efficient for human identification of different datasets under various clothing and handbag-carrying conditions.

Table 6. Comparison of recognition performance of our proposed method with other existing methods.

Comparison of the Recognition performance					
	CAS [14]	UCR [5]	Sup[13]	Un-Sup [13]	**Ours**
Set A2	97.6%	99.4%	98.6%	99.4%	98.39%
Set B	32.7%	60.2%	85.5%	79.9%	87.10%
Set C	52.0%	22.0%	88.8%	31.3%	86.29%

VI. Conclusion

In this paper, we propose a novel hybrid system using the dynamic feature extracted by optical flow estimation as well as the static feature to recognize the human walking path and human identification. The proposed method can be applied for different walking path and walking velocity of the gait video sequence. The experimental results show the effectiveness of our system and demonstrate its ability even for various clothing and carrying conditions.

Acknowledgment

This paper uses the CASIA Gait Database collected by Institute of Automation, Chinese Academy of Sciences.

References

[1] N.V. Boulgouris, D. Hatzinakos, and K.N. Plataniotis, "Gait Recognition: A Challenging Signal Processing Technology for Biometric Identification," IEEE Signal Processing Magazine, Vol. 22, No 6, pp.78 – 90, Nov. 2005.

[2] H. Su and F. G. Huang, "Human Gait Recognition Based on Motion Analysis," in Proceedings of the Fourth International Conference on Machine Learning and Cybernetics, Guangzhou, pp. 4464 – 4468, Aug. 2005.

[3] N. V. Boulgouris and Z. X. Chi, "Gait Recognition Using Random Transform and Linear Discriminant Analysis," IEEE Transactions on Image Processing, Vol. 16, No. 3, pp. 731 – 740, Mar. 2007.

[4] N. V. Boulgouris and Z. X. Chi, "Gait Recognition Based on Human Body Components," in ICIP 2007, pp. I–353–356.

[5] J. Han and B. Bhanu, "Individual Recognition using Gait Energy Image," IEEE Transactions on Pattern Analysis and Machine Intelligence, Vol. 28, No. 2, pp. 316 – 322, Feb. 2006.

[6] J. Liu and N. Zheng, "Gait History Image: A Novel Temporal for Gait Recognition," in ICME 2007, pp. 663 – 666.

[7] Q. Ma, S. Wang, D. Nie and J. Qiu, "Recognizing Humans Based on Gait Moment Image," in *Eighth ACIS International Conference on Software Engineering, Artificial Intelligence, Networking, and Parallel/Distributed Computing 2007 IEEE*, pp. 606 – 610.

[8] P. S. Huang, C. J. Harris, and M. S. Nixon, "Recognizing Humans by Gait via Parametric Canonical Space," *Artificial Intelligence in Eng.,* Vol. 13, pp. 359 – 366, 1999.

[9] M. H. Cheng, M. F. Ho and C. L. Huang, "Gait Analysis for Human Identification Through Manifold

Learning and HMM," *Pattern Recognition,* Vol. 41, No. 8, pp. 2541 – 2553, Aug. 2008.

[10] A. Bissacco, P. Saisan and S. Soatto, "Gait Recognition using Dynamic Affine Invariants," in *Proc. of the MTNS*, 2004.

[11] S. Chen and Y. Gao, " An Invariant Appearance Model for Gait Recognition," in *ICME* 2007, pp. 1375 – 1378.

[12] S. Sarkar, P. J. Phillips, Z. Liu, I. R. Vega, P. Grother, and K. W. Bowyer, "The HumanID Gait Challenge Problem: Data Sets, Performance, and Analysis," *IEEE Transactions on Pattern Analysis and Machine Intelli*gence, Vol. 27, No. 2, pp. 162 – 177, Feb. 2005.

[13] K. Bashir, T. Xiang, S. Gong and Q. Mary, "Feature Selection on Gait Energy Image for Human Identification," in *ICASSP* 2008, pp. 985 – 988 .

[14] S. Yu, D. Tan and T. Tan, "A Framework for Evaluating the Effect of View Angle, Clothing and Carrying Condition on Gait Recognition," in *ICPR* 2006, pp. 441 – 444.

[15] A. Kale, R. Chowdhury and R. Chellappa, "Towards a View Invariant Gait Recognition Algorithm," in *Proc. Of the IEEE Conf. on Advanced Video and Signal Based Surveillance*, 2003, pp. 143 – 150.

[16] X. Huang and N. Boulgouris, "Model-Based Human Gait Recognition Using Fusion of Features," in *ICASSP* 2009, pp. 1469 – 1472.

[17] R. C. Gonzales and R. E. Woods, *Digital Image Processing*, Prentice Hall.

[18] *CASIA Gait Database*, http://www.sinobiometrics.com, 2006.

The Verification Mode of Positioning Errors for Attacking Trajectory of The Aggressor

Shao-Chang Miao

Abstract

This paper probes into application and correction of the errors of the radars in the defensive system. The Utility Integration Algorithm (UIA) proposed in this paper can be used to create a correction database of the errors for the radar to correctly transmit the attacking trajectory of the aggressor. It also can simplify the calculation process and make the programmers to apply more efficiently, and these become its advantages. The RADAR/GNSS/RAIM integration systems (RGRIS) can offer the data of the target orientation to the interceptor then an optimal intercepting trajectory can be obtained. According to these, we can take necessary precautions, against attack and assignment of intercepted missions for destroyed the target and selecting the intercept points at an earlier time.

Keywords：Global Positioning System (GPS); Global Navigation Satellite System (GNSS); Inertial Navigation System (INS); Receiver Autonomous Integrity Monitoring (RAIM); RADAR/GNSS/RAIM Integration System (RGRIS)

Shao-Chang Miao, Office of Military Education, Hsiuping University of Science and Technology, Doctoral program student, Department of Statistics, TungHai University
Received 25 August 2010; accepted 20 January 2011

侵略者的攻擊彈道定位誤差之驗證法

繆紹昌

摘 要

本文是探討防禦系統中雷達的誤差之校正與運用，文中提出多用途整體演算法可用以建立誤差校正之資料庫，以利雷達能夠正確傳遞飛彈攻擊的軌跡，並且簡化演算過程使得程式設計者能有效的運用，此為本文之優點。RADAR/GNSS/ RAIM 整合系統可提供目標資料給飛彈攔截器而獲得一條攔截的最佳彈道，據此可啟動防禦系統之先期預警與進入備戰，並完成指派攔截之任務，故此目標資料有利於飛彈攔截器進行目標之標定與攔截點之選擇。

關鍵詞： 全球定位系統(GPS)、全球導航衛星系統(GNSS)、慣性導航系統(INS)、接收器自主性完整監測(RAIN)、RADAR/GNSS/RAIM 整合系統

繆紹昌：修平科技大學軍訓室軍訓教官、東海大學統計系博士生
投稿日期：99 年 8 月 25 日 接受刊登日期：100 年 1 月 20 日

1. Introduction

During the last decades, GPS (Global Positioning System) has replaced the conventional geodetic measurements and played the most important role in distortion monitoring [1][2]. The GPS provides aircraft's accurate position, velocity and time (PVT). GPS was officially launched in 1995. The United State launched many satellites and at least 24 of them are orbited six trajectories with an angle of 55 degrees around its continent. It provides an omnibus and an all-weather global positioning for users in navigation. However, the integrity and availability of the GPS are still imperfect. There are many methods of GPS modifications and integrations using statistics and mathematics to make up its disadvantages. For example, the Global Navigation Satellite System (GNSS) has been created to make up for the disadvantages of the GPS. Its receiver uses a direct signal line to provide stable and long-term positioning [3], so it can use continuous signal lines to provide the solutions of continual positioning. Despite this breakthrough, the GNSS is still impeded by obstacles that weaken and obstruct the signal [4]. Inertial Navigation System is another positioning system that has been widely used. It overcomes the GNSS disadvantage by using three orthogonal linear accelerators and their angles to calculate navigation information. The obstacle interference factor can be neglected for a high-flying aircraft.

Technological advances have rapidly decreased the errors of positioning for both the GPS and the GNSS. However, the International Civil Aviation Organization (ICAO) and Federal Aviation Administration (FAA) still plan to use the GPS to improve the efficiency of navigation and positioning. Thus, scholars have started to focus and research on the receiver's monitoring and measuring integrity [5,6] and navigation efficiencies [7,8]. Receiver Autonomous Integrity Monitoring (RAIM) uses the measurement values from satellites to detect errors and examine errors, namely, it can provide the integrity assistance for GNSS. RAIM uses the snapshot concept and takes a set of the GNSS measurement values to calculate the position of aircrafts by using the method of least square (MLS).

This paper has improved the disadvantage of the traditional MLS that only takes into consideration of the errors of measured variables. At the same time, the positioning error of the scaling factor matrix is considered to find out the aberration correction of radars in the defense system. This helps raising the interception rate of the guided missile. For example, the Patriot Advanced Capability-3 (PAC-3) needs the radar to correct its trajectory during flying. In relatively high-speed condition, inaccurate trajectory navigation causes PAC-3 incapable of accurate terminal interception in real time. Besides, it is hard to acquire, the system's accurate parameters of the weapons purchased from abroad, and the weapon systems are adopted into the defense system without correction. These can cause deviation for the weapon function. Now litter deviation can generate big mistake in future wars and make the weapon system inefficient. Hence, national weapon systems need to be established and applied carefully. The outline of the rest of this paper is below:

The second section introduces the Utility Integration Algorithms (UIA) of correction of the deviations in the positioning navigation system. The third section describes the architecture of implementation verification of the RADAR/GNSS /RAIM. The fourth section provides the analysis result of the calculations, and provides a compare and contrast with results of the common method. The last section provides a conclusion and future prospects.

2. The Utility Integration Algorithm (UIA)

The Utility Integration Algorithm used in this paper takes into consideration the error of the scaling factor matrix and measured variable. With GNSS/RAIM system and the single aircraft, the radars can be corrected through the positioning calculation of the total least-square method (TLSM) and obtain the corrections of parameters of the distance and the scaling factor matrix. Micro-Electro-Mechanical Systems (MEMS) technology, which is based on inertial systems, brings a new science for integrated GPS/RAIM system. The position, velocity and attitude (PVA) calculation is possible using MEMS principle (mechanization equations) from the inertial gyroscopes and accelerometers. The conceptual principle of the measurement simulator is shown in Fig. 2.1. However, use the Radar/GNSS/RAIM to improve the efficiency of navigation and positioning, which is still influenced by the factors of time and position. Therefore, the integrity and availability of the Radar/GNSS/RAIM are still imperfect. This paper develops the method of radar modifications and integrations using UIA to make up its disadvantages. This research gives a description of hypotheses and limitations:

All results of velocity, acceleration, angular velocity and each of their continued time should be expressed clearly in the same time.

It overcomes the GNSS disadvantage

by using three orthogonal linear accelerators and their angles to calculate navigation information.

The obstacle interference factor can be neglected for a high-flying aircraft.

Applying the mechanization equation (Yang et al., 2007) and considering an inverse process for the simulation, the inertial sensor outputs consist of two parts: error-free values and sensor errors. They are linearly combined. The error-free value is determined by the GNSS/RAIM system. In this simulation, the sensor model take into account the departure, scaling factor and the noise level (Bennour et al., 2005). From the following equation which is the same for both accelerometers and gyro-meters:

$$(\vec{S}^{n}_{i,M,t})^{T}\vec{M}_{i,M,t} = \left(\vec{S}^{T}_{i,M,t}, J\right)\left(\vec{M}^{T}_{0,M,t}, \vec{\sigma}_{i,\theta,\phi,d}, \vec{e}_{i,\theta,\phi,d}\right)^{T} \quad (1)$$

The notations are as following:

$\vec{M}_{i,M,t}$ = measurement variable of the Radar i for aircraft M at time t,

$\vec{M}_{0,M,t}$ = noise-free variable of the aircraft M at time t,

$\vec{S}_{i,M,t}$ = scaling factor matrix of noise-free variable of the Radar i measurement for aircraft M at time t,

$\vec{S}^{n}_{i,M,t}$ = scaling factor matrix of noise variable of the Radar i measurement for aircraft M at time t,

$\vec{e}_{i,\theta,\phi,d}$ = the measurement bias of the Radar i in a position (θ, ϕ, d),

$\vec{\sigma}_{i,\theta,\phi,d}$ = the scaling matrix errors of the Radar i in a position (θ, ϕ, d),

d = the distance from the origin to the aircraft M; we require $d \geq 0$,

θ = the polar angle (as in polar coordinates); we require $0 \leq \theta \leq 2\pi$,

ϕ = the angle measured down from the positive z-axis to the ray from the origin through M; we require $0 \leq \phi \leq \pi$,

J = having all elements unity.

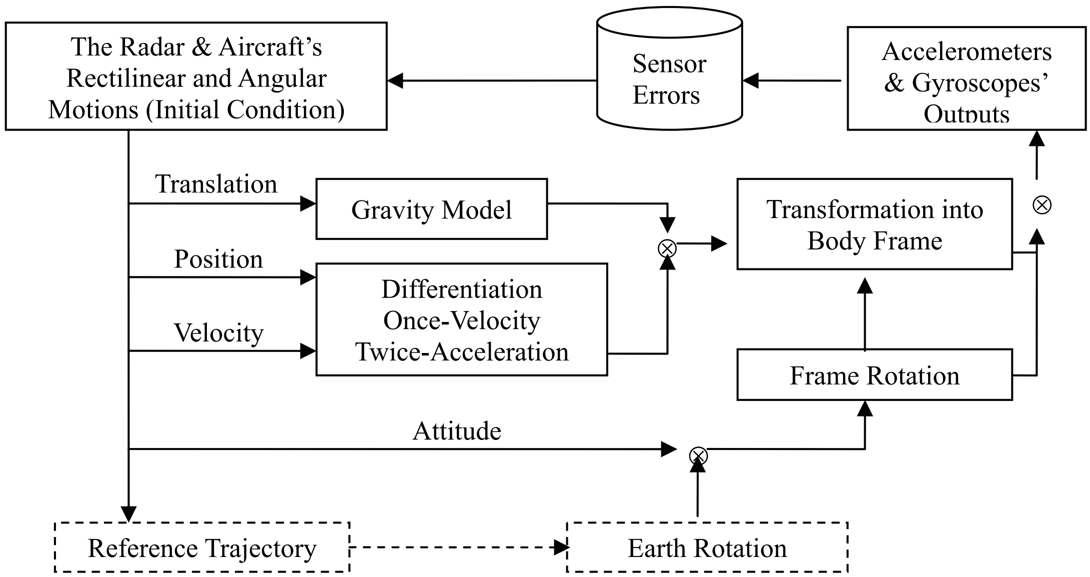

Figure 2.1 Principle of simulator (Modified to Yang et al., 2007)

Through the INS/GPS integration architecture concept, we have established the Radar/GNSS/RAIM integrated system (RGRIS). A GNSS simulator must be able to simulate the radar's distribution in the future as well as all error sources and aircraft dynamic trajectory. By inputting some elements, the simulator can calculate the trajectory and velocity of aircrafts. A widely used implementation is the error state space of a closed loop, such as the extended Kalman filter (EKF) implemented in coupled architecture as the core of the optimal estimation engine. The coupled RGRIS (or the closed loop) suggested in this paper is shown in Figure 2.2.

The coupled RGRIS performs all the GNSS calculations by itself. The virtual ranges, carrier phase and instantaneous Doppler measurements are processed by the RAIM instead of the position and velocity fixes.

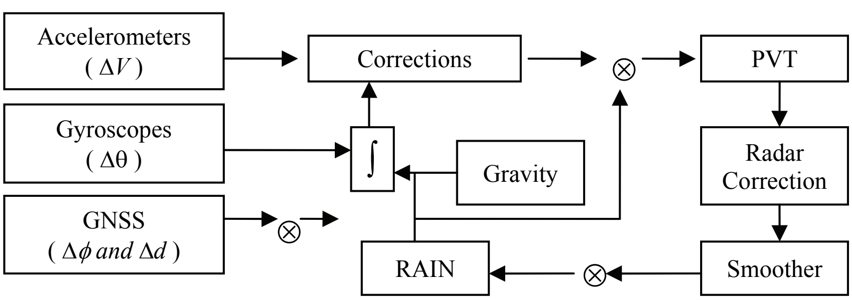

Figure 2.2: A coupled Radar/GNSS/RAIM integration

2.1 Principle of The Implementation Verification

We use Fig. 2.3 to describe the various courses and heights of flight within the radar's range. With the GNSS/RAIM tracking system, we can modify and correct the radar's flight trajectory. In order to set up the error correction under the various flight situations.

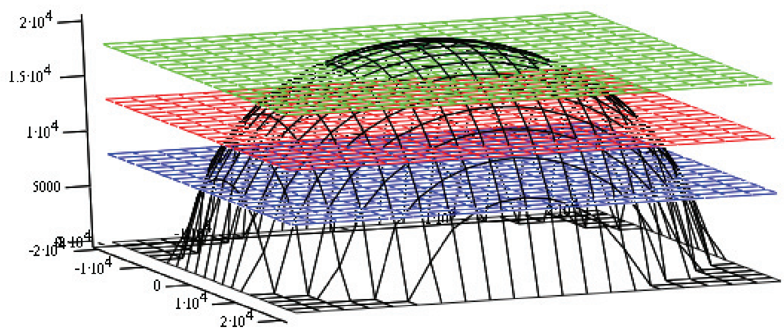

Figure 2.3 The contour surfaces of the radar cone in the navigating zones

R , z1 , z2 , z3

Firstly, we carefully observed the position of the aircraft in the cross-sectional zi-through the radar i, and from radar i we can detect the virtual distance $\vec{d}_{i,\mathrm{M},t}$ of the aircraft. The virtual distance is put into the RGRIS to calculate the distance error $\vec{\varepsilon}_{i,d}$ and bias $\vec{\rho}_{\mathrm{i},\theta,\phi,\mathrm{d}}$ on the scaling factors. The integration algorithms can be written as following:

$$\vec{\mathrm{S}}_{\mathrm{i,M,t}}\vec{\mathrm{M}}_{\mathrm{0,M,t}} - \vec{d}_{i,\mathrm{M},t} = \vec{\varepsilon}_{i,d}\,, \tag{2}$$

$$\vec{\mathrm{S}}^{\mathrm{n}}_{\mathrm{i,M,t}}\vec{\mathrm{M}}_{\mathrm{i,M,t}} = \vec{d}_{i,\mathrm{M},t}\,, \tag{3}$$

and

$$\vec{\mathrm{M}}_{\mathrm{i,M,t}} = \vec{\mathrm{X}}^{i}_{0} - \vec{\mathrm{X}}_{i,\mathrm{M},t}\,,$$

where $\vec{\mathrm{X}}_{\mathrm{0,M,t}}$ is the true coordinate of the testing missile (or flying device) in the GNSS/RAIM system at time t; $\vec{\mathrm{X}}_{\mathrm{i,M,t}}$ is the coordinate for the testing missile (or flying device) of the Radar system at time t. $\vec{\mathrm{S}}^{\mathrm{n}}_{\mathrm{i,M,t}}$ is the true scaling factor matrix of the testing missile (or flying device) of the GNSS/RAIM system. $\vec{\mathrm{S}}_{\mathrm{i,M,t}}$ is the scaling factor matrix of the testing missile (or flying device) of the Radar system. The difference between the two is the slight micro-noise matrix of the i-th Radar system. These differences have been modified into equations.

$$\left(\vec{\mathrm{M}}_{\mathrm{0,M,t}} - \vec{\mathrm{M}}_{\mathrm{i,M,t}}\right)/dt = \nabla\vec{\mathrm{X}}_{i,\mathrm{M},t}\,, \tag{4}$$

$$\vec{S}_{i,M,t} = \left(\vec{M}_{0,M,t} \big/ \left\|\vec{M}_{0,M,t}\right\|\right)^{T},$$

and $\vec{S}^{n}_{i,M,t} = \left(\vec{M}_{i,M,t} \big/ \left\|\vec{M}_{i,M,t}\right\|\right)^{T}$.

Through Eqs. (2) and (3) we can establish the error value $\vec{\varepsilon}_{i,d}$ when the i-th Radar is at a distance $\vec{d}_{i,M,t}$. The database of error values of various states of single aircrafts (such as fighter, transport, military aircraft and civil aircraft etc.) of various directions and altitudes can be found through using four different radars simultaneously to correct the bias. Nevertheless, we still need to figure out the bias $\vec{\rho}_{i,\theta,\phi,d}$ on the scaling factors of the i-th Radar in order to proceed with the calculation and solution of the Total least-square Method (TLSM). The method proposed by this paper is the backward algorithm. In other words, we can estimate the bias $\vec{\rho}_{i,\theta,\phi,d}$ of the rotation between coordinate frames through Eq. (4) and TLSM.

The rotation coordinate equation can be written as follow:

$$\vec{S}^{n}_{i,M,t} \nabla \vec{X}_{i,M,t} = \vec{\gamma}_{i,M,t}, \tag{5}$$

$$\operatorname{diag} \vec{\rho}_{i,\theta,\phi,d} \nabla \vec{X}_{i,M,t} = \vec{e}_{i,\theta,\phi,d}, \tag{6}$$

$$\left(\vec{S}^{n}_{i,M,t} - \operatorname{diag}\vec{\rho}_{i,\theta,\phi,d}\right) \cdot \nabla \vec{X}_{i,M,t} = \vec{\sigma}_{i,\theta,\phi,d}, \tag{7}$$

$$\vec{\rho}_{i,\theta,\phi,d} = \left(\vec{\gamma}_{i,M,t} - \vec{\varepsilon}_{i,d}\right)\left(\nabla \vec{X}_{i,M,t}\right)^{-1} \big/ N,$$

$$d_{i,M,t} = \sqrt{\vec{S}_{i,M,t}\vec{M}_{0,M,t}},$$

$$\phi = \cos^{-1}\left(z^{i}_{0} - z_{0,M,t} \big/ d_{i,M,t}\right),$$

$$\theta = \tan^{-1}\left(y^{i}_{0} - y_{0,M,t} \big/ x^{i}_{0} - x_{0,M,t}\right),$$

$$\vec{C}^{n}_{i,M,t} = \left(\left(\vec{S}^{n}_{i,M,t} - \operatorname{diag}\vec{\rho}_{i,\theta,\phi,d}\right)^{T}\left(\vec{S}^{n}_{i,M,t} - \operatorname{diag}\vec{\rho}_{i,\theta,\phi,d}\right)\right)^{-1} \times \left(\vec{S}^{n}_{i,M,t} - \operatorname{diag}\vec{\rho}_{i,\theta,\phi,d}\right)^{T} \cdot \vec{\sigma}_{i,\theta,\phi,d},$$

and $\vec{X}_{0,M,t} = \vec{X}_{i,M,t} + \vec{C}^{n}_{i,M,t}$ (8)

Through Eqs. (5)~(8) we can find out the amount of rotation coordinate.

On the other hand, the advantage of TLS algorithm is that while the traditional method of least squares (MLS) is able to filter out the noise in the measurement signal, the MTLS algorithm is capable of removing the implicit positioning errors in both the scaling factors and the measurement variables. Huffel and Vandewall (1991) proposed the both traditional methods of MLS (Eq. 9) and MTLS (Eq. 10), which are given below:

$$\vec{C}^{MLS}_{i,M,t} = \left(\left(\vec{S}^{n}_{i,M,t}\right)^{T}\vec{S}^{n}_{i,M,t}\right)^{-1} \times \left(\vec{S}^{n}_{i,M,t}\right)^{T} \cdot \left(\vec{\sigma}_{i,\theta,\phi,d} + \vec{e}_{i,\theta,\phi,d}\right), \tag{9}$$

and

$$\vec{C}^{MTLS}_{i,M,t} = \left(\left(\vec{S}^{n}_{i,M,t} - \sigma_{i+1} \cdot I\right)^{T}\vec{S}^{n}_{i,M,t}\right)^{-1} \times \left(\vec{S}^{n}_{i,M,t}\right)^{T} \cdot \left(\vec{\sigma}_{i,\theta,\phi,d} + \vec{e}_{i,\theta,\phi,d}\right). \tag{10}$$

The above MLS results given are inaccurate, and MLS singular value decomposition is difficult, because they are defined the non-negative definite (n.n.d.) matrices. Since the definition is in terms of quadratic forms, they are usually taken as being symmetric, and thus also have the following properties: (i) All eigenvalues are real. (ii) They are diagonable. (iii) Rank equals the number of nonzero eigenvalues.

3. RADAR/GNSS/RAIM Integration system

The RADAR/GNSS /RAIM integration system proposed in this paper uses the backward smoothing algorithm that is the fixed interval smoother. The Rauch-Tung-Striebel smoother (RTSS) was first presented in 1965 a few years after R. E. Kalman presented his filter in 1960 (Gelb, 1974). The Kalman filter (KF) is a recursive filter that optimally, by means of maximum-likelihood, estimates the state vector of a dynamic system on the condition that a linear (or linearized) system model, past and current noisy measurements are known. It is only applicable in post processing, but promises improved accuracy, especially during GNSS outages.

Figure 3.1 illustrates how the data is used. The upper part shows the forward run and the lower part the reverse run and the involved variables. Between two GNSS measurements, the KF predicts the system state $\vec{\varepsilon}_t$, by means of inertial navigation. When a new GNSS measurement becomes available, the KF calculates a new corrected prediction $\vec{\varepsilon}_t^-$, that is the smoother has the ability to level these discontinuities, by means of a new weighting of the previously calculated system states $\vec{\varepsilon}_t^-$, $\vec{\varepsilon}_{t+1}^-$ and $\vec{\varepsilon}_{t+1}^{sm}$.

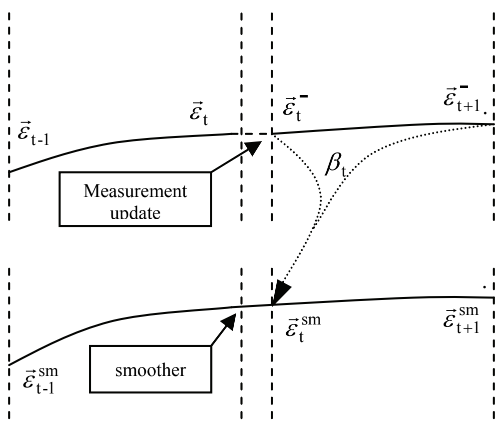

Figure 3.1: Forward and reverse run of the RTSS

The final trajectory therefore is smooth and contains no discontinuities. Where δ denotes the variance-covariance matrix (or dispersion matrix) of the random variables $\vec{\mathrm{M}}_{\mathrm{i,M,t}}$. The full smoother equations are given below:

$$\beta_{\mathrm{t}} = \delta_{\mathrm{t}} \cdot \nabla\vec{\mathrm{X}}_{\mathrm{i,M,t}}\left(\delta^{-}_{\mathrm{t+1}}\right)^{-1},$$

$$\vec{\varepsilon}^{\,sm}_{\mathrm{t}} = \vec{\varepsilon}^{\,-}_{\mathrm{t}} + \beta_{\mathrm{t}}\left(\vec{\varepsilon}^{\,sm}_{\mathrm{t+1}} - \vec{\varepsilon}^{\,-}_{\mathrm{t+1}}\right), \quad (11)$$

and

$$\delta_{\mathrm{t}} = \delta^{sm}_{\mathrm{t}} - \beta_{\mathrm{t}} \cdot \left(\delta^{sm}_{\mathrm{t+1}} - \delta^{-}_{\mathrm{t+1}}\right)\beta^{\mathrm{T}}_{\mathrm{t}}.$$

In this paper, the RGRIS has been very helpful for the choice of an intercepting point and the target orientation. Figure 3.2 illustrates the flow chart of the overall system. If it acts as KF, the logged measurement data can be processed forward or reverse in time, while resolved ambiguities are loaded from or saved to a file. All the state and covariance data of the permanent state variables is also written to a file for further use in smoother mode. Integrated Radar/GPS systems provide an enhanced navigation system that has superior performance in comparison with either stand-alone system as it can overcome their limitations. In this simulator, the corresponding GNSS signals (i.e. Position and Velocity information) are also simulated with a defined data format to offer an effective way for evaluating a specific integrated RAIM/GNSS loosely coupled and tightly coupled architectures under different operational environments. The proposed simulation platform is composed of three major components: (i) trajectory generator of Radar, (ii) measurement generators which include the measurements of Radar and GNSS, (iii) optimal estimation engine which integrates RAIM with GNSS with coupled architectures using KF and RTSS, respectively.

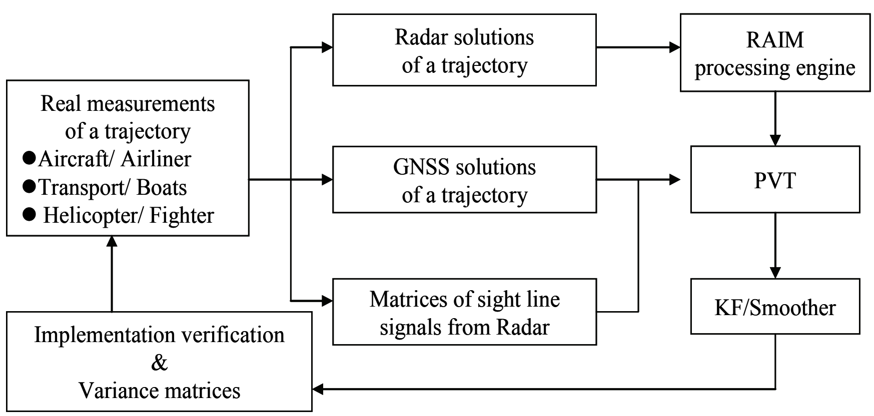

Figure 3.2: The flow chart of the Radar/GNSS/RAIM integration architecture

3.1 Estimations of The Aircraft's Trajectory

Through the TLSM proposed in this paper, we can establish the system of discrimination for the flight trajectory. This system model can derive the position of the next time point from existing position. We are unable to use all the data to estimate the future trajectory. The method described above is unnecessary to real application, and has increased the workload and error range. To illustrate our point, the following is a statement of the measured difference in scalar potential of a position through geometric condition in figure 3.3. Let C be a smooth curve, with positional equation R(t)={x(t), y(t), z(t)} for tk≤ t ≤ tk+1, that lies within the domain of a function G(t)=f (x(t), y(t), z(t)). We say that C is orient able if it is possible to describe direction along the curve for increasing t. Suppose F is a vector field that is continuous on C, and f is a scalar potential such that F=∇f, then

$$\int_C F\ dR = f(R(t_{k+1})) - f(R(t_k)) \quad (12)$$

where R(tk) and R(tk+1) are the endpoints of a piecewise smooth curve of C.

Proof

According to the chain rule

$$dG/dt = (\partial f/\partial x)(dx/dt) + (\partial f/\partial y)(dy/dt) + (\partial f/\partial z)(dz/dt)$$

and we have

$$\begin{aligned}\int_C F\ dR &= \int_C \nabla f\ dR \\ &= \int_{t_k}^{t_{k+1}} \left[(\partial f/\partial x)(dx/dt) + (\partial f/\partial y)(dy/dt) + (\partial f/\partial z)(dz/dt)\right]dt \\ &= \int_{t_k}^{t_{k+1}} \left[(dG/dt)\right]dt = G(t_{k+1}) - G(t_k) \\ &= f(R(t_{k+1})) - f(R(t_k))\end{aligned}$$

We outline the proof in the difference of scalar potential. Therefore a vector field F is said to be conservative in a region D if F = ∇f for some scalar function f in D. We know that F is a continuous vector field on the open connected set D. then the following three conditions are either all true or all false:

i. F is conservative on D; that is, F = ∇f for some scalar function f defined on D.
ii. $\oint_C F\ dR = 0$ for every piecewise smooth closed curve C in D.
iii. $\oint_C F\ dR$ is independent of path within D if for any two points tk and tk+1 in D the line integral along every piecewise smooth curve in D from tk to tk+1 has the same value.

For this (iii) implication, we obtain the equations as following:

$$f(R(t_{k+1})) - f(R(t_k)) = f(R(t_k)) - f(R(t_{k-1})) = f(R(t_{k-1})) - f(R(t_{k-2})), \quad (13)$$

$$R(t_{k+1}) = R(t_k) + 2f(R(t_{k-1})) - f(R(t_{k-2})). \quad (14)$$

It is a purely geometric relation to be

derived out above. Then, we consider predicting the subsequent position by three points already known as shown in Fig. 3.4.

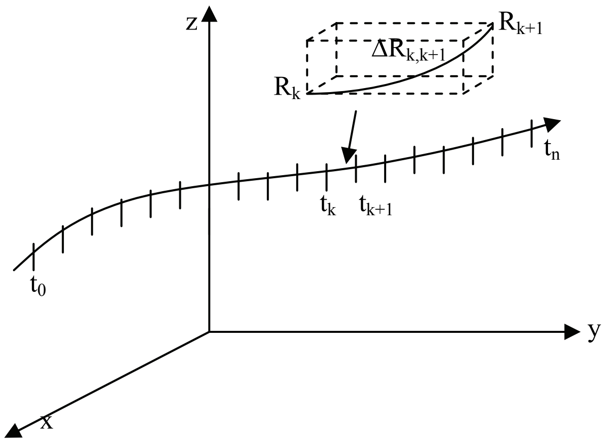

Figure 3.3: The curve C partitioned into subarcs

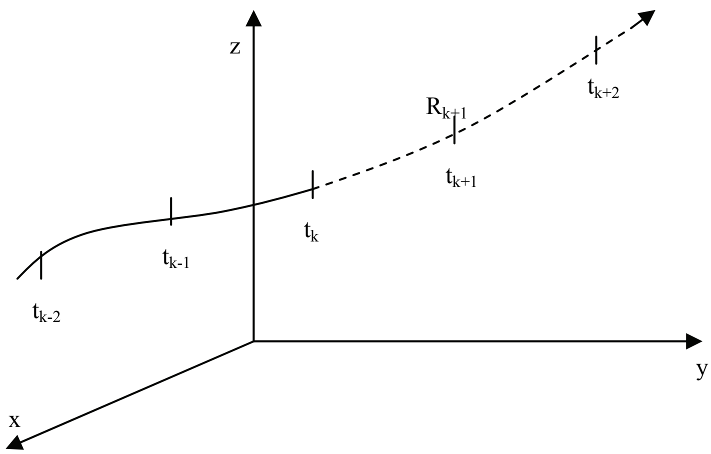

Figure 3.4: Estimations of the aircraft's trajectory

According to Eq. 14 can know that we unnecessary to know the position of two points outside of the flight trajectory, and only need to know its slope. Now, we suppose an extreme point Rt=(x, y, z), two adjacent points Rt-1 、Rt -2 , and two predictive points Rt+1 、Rt+2 on the trajectory. We can obtain Eq. 15 by the above-mentioned geometric meaning to be written as following:

$$R(t_{k+1}) = R(t_k) + 2\vec{m}_{k-1} - \vec{m}_{k-2}. \tag{15}$$

The coordinate vector function Rt of aircraft at time t, its derivative f(Rt) is a increasing tangent vector and f(Rt) ≠ 0 where is correspondent to the trajectory at time t, we call ΔRt that is unit tangent vector of Rt at time t to be written as following:

$$\Delta R_t = f(R_t) / \| f(R_t) \|,$$

and

$$\| f(R_t) \| = \sqrt{\left(\vec{M}_{0,M,t} - \vec{M}_{i,M,t}\right)^T \cdot \vec{C}^n_{i,M,t}}.$$

Through the TLSM proposed in this paper, when the system of discrimination for the flight trajectory was established, We need to build a known time sequence

ΔR =Δ(R1, R2,…, RT), T=2t-1.

We derive the n-th point of the flight trajectory by described above equations and the known k-th point as following:

$$\vec{X}_{i,M,N} = \vec{X}_{i,M,k} + \Delta R_{kN}, \quad (16)$$

$$\Delta R_{kN} = \Delta R_N \| f(R_N) \| - \Delta R_k \| f(R_k) \|,$$

$$\vec{m}_k = (\Delta R_{k,k+1} / \Delta t_k).$$

That is,

$$\Delta R_{kN} = \Sigma_{j=k}^{N} \begin{Bmatrix} (j-k) \cdot (2\vec{m}_{k-1} - \vec{m}_{k-2}) \\ - \varpi_k \cdot \vec{m}_{k-1} \end{Bmatrix}, \quad (17)$$

and $\varpi_k = \begin{cases} (j-k-1), & \text{if } (j-k-1) > 0, \\ 0, & \text{otherwise.} \end{cases}$

We change the time sequence into the Hessian matrix of the tangent vector, which is given below:

$$H_{t+1}(R) = \begin{bmatrix} \vec{m}_1 & \vec{m}_2 & \cdots & \vec{m}_{T-t} & \Delta R_{1(T-t+1)} \\ \vec{m}_2 & \vec{m}_3 & \cdots & \vec{m}_{T-t+1} & \Delta R_{2(T-t+2)} \\ \vdots & \vdots & \ddots & \vdots & \vdots \\ \vec{m}_{t+1} & \vec{m}_{t+2} & \cdots & \vec{m}_T & \Delta R_{(t+1)(T+1)} \end{bmatrix} \quad (18)$$

Through the coordinate vector function of three time points that have already known positions, we can establish the position at the new time point by successive approximation and compose a row of Hessian matrix. The new time point changes into the known time point at next time, thus we can establish the position again at the new time point by successive approximation and compose another row of Hessian matrix. We call the path search is iterative vector algorithm. The iterative vector algorithm is given below:

Ht+1(R) · [I3×(t×3), -I3×3]t=0,

$$\begin{bmatrix} M_{t+1} \\ \vdots \\ M_{T+1} \end{bmatrix} = \begin{bmatrix} M_1 \\ \vdots \\ M_{T-t+1} \end{bmatrix} + \begin{bmatrix} \Delta R_{1(t+1)} \\ \vdots \\ \Delta R_{(t+1)(T+1)} \end{bmatrix}. \quad (19)$$

The iterative vector algorithm proposed in this paper, which is a Hessian matrix composed of seven time points, that are t=3 and T=2t. The Hessian matrix can meet the needs of real environment which we can expand the Hessian matrix by k>3, that are ti=i×t and T=2× ti, where i is a row number.

3.2 Combat Management System (CMS)

According to the method that describes in the previous section, we can obtain the navigation trajectories of targets. For an interceptor of the missile that is dependent on radars, which offer the data of the target, we can succeed in getting the best trajectories under control. The above results given can achieve the second purpose of this article that is we can really carry out the command, control, fight, management and communication, in order to obtain better reliability and defensive capability in the simulating war or training bay. The section focuses on setting up the ability of the fight, management and communication. When the system obtains the best trajectories of intercepted targets, according to these, we can take necessary precautions, against attack and assignment of intercepting missions for destroyed the target and selecting the intercept points at an earlier time. At the same time, the radar offered the target's data to help the interceptor to implement the scaling variables. In other words, how to carry on the assignment of intercepting missions?

This paper suggests on a basis of intercepting range of the interceptor, when the best trajectory intercepted is through the intercepting range of the interceptor, whose volume is largest between minimum arc of the intercepting range and the best trajectory? The intercepting missions will be assigned to it that is a top priority. If there are other missiles attacked us, except that there is not the appropriate interceptor that can be appointed, otherwise the intercepting missions will be assigned to it that is a secondary priority. The rest may be inferred by analogy. We describe the model of the assignment of intercepting missions and iterated integration as following:

Definition 3.1 If f is defined on a closed, bounded region A in the level (x, y) of the radar cone, then the iterated integral of f over A is defined by

$$\iint_A f(\mathrm{x},\mathrm{y})dA = \lim_{\|\mathrm{a}\|\to 0} \Sigma_{\mathrm{i}=1}^{\mathrm{n}} f(\mathrm{x}_\mathrm{i},\mathrm{y}_\mathrm{i})\Delta A_\mathrm{i}$$

where A : a≤ x≤b, c≤ y≤d, therefore the iterated integral can be evaluated by

$$\iint_A f(\mathrm{x},\mathrm{y})dA = \int_c^d \int_a^b f(\mathrm{x},\mathrm{y})dxdy = V \quad .$$

By using a limit to add up the sum of volumes of all slabs on the region of integration D, so we obtain the volume, V, of the D. In essentially the same ways, a triple integral can be evaluated by the iterated integral.

In general, changing variables in an iterated integral is more complicated than in a single integral. In this section, we focus attention on using polar coordinates in an iterated integral, and we simplify the assigned model of intercepted missions from a more military standpoint.

Theorem 3.2 Let T be a subset of ℜn and f is continuous on the image g(T). If g: ℜn →ℜn is a linear coordinate transformation and T such that the Lebesgue integral ∫g(T)f(x) dx exists, then the Lebesgue integral ∫T f(g(x))·∣Jg(t)∣dt also exists, and the two are equal.

Proof Let $\tilde{f}(\mathrm{x}) = f(\mathrm{x})$ if x∈ g(T) , and let $\tilde{f}(\mathrm{x}) = 0$ otherwise. Then

$$\int_{g(T)} f(\mathrm{x})\, d\mathrm{x} = \int_{R^n} \tilde{f}(\mathrm{x})\, d\mathrm{x}$$

$$= \int_{R^n} \tilde{f}(\mathrm{g(T)})\, \mathrm{g}'(\mathrm{T})\, d\mathrm{t} = \int_T f(\mathrm{g(T)}) \cdot \left|J_{\mathrm{g}}(\mathrm{t})\right| d\mathrm{t}$$

Corollary 3.3 Let g: ℜn →ℜn be a linear coordinate transformation. If T be a subset of Rn with finite Lebesgue measure m(T), then g(T) also has finite Lebesgue measure and $m[\mathrm{g(T)}] = \left|\det \mathrm{g}\right| m(\mathrm{T})$.

Proof Write T=g-1(W), where W= g(T). Since g-1 is also a coordinate transformation, we find

$$m(\mathrm{T}) = \int_T d\mathrm{x} = \int_{g^{-1}(W)} d\mathrm{x} = \int_W \left|\det \mathrm{g}^{-1}\right| d\mathrm{t} = \left|\det \mathrm{g}^{-1}\right| \cdot m(\mathrm{W}).$$

This proves since
W=g(T) and det (g-1)=(det g)-1.

Now, let us extend its operations into spherical coordinates in ℜ3. We write t=(d,θ, ϕ) and we take

$$T = \{(d,\theta,\phi) : d > 0, 0 < \theta < 2\pi, 0 < \phi < \pi\}.$$

The coordinate transformation g maps each point (d,θ, ϕ) in T onto the point (x, y, z) in g(T) given by the equations

x =d cosθ sinϕ,
y = d sinθ sinϕ,
and z = d cosϕ.

If f is continuous on the bounded radar cone D, then the triple integral of f over D is given by

$$\iiint_D f(\mathrm{x,y,z}) = \iiint_T f(d\cos\theta\sin\phi, d\sin\theta\sin\phi, d\cos\phi)\cdot d^2 \cdot \sin\phi\, \mathrm{d}d\, \mathrm{d}\theta\, \mathrm{d}\phi \cdot$$

In geometry, it is shown that a sphere of radius r has volume V=4πd 3/3. The proof is left with readers. On the other hand, we simplify the assigned model of intercepted missions from a more military standpoint. When its volume is largest between minimum arc of the intercepting range and the best trajectory, that is, d is the biggest when they are all on the spherical coordinate system. Oppositely, We use (L-d/2) to replace d which intercepting best-trajectory has only a penetrating point (xm,0, ym,0, zm,0) and has not a breached point (xm,1, ym,1, zm,1), its (L- d/2) means too is minimum (L is the largest range). Therefore, this paper simplifies the triple integral described above into the following judgment equation:

$$m(D) = min\{ \mathrm{L}_{\mathrm{m}} - (d_{\mathrm{m}}/2) \}, d_{\mathrm{m}} = \sqrt{(\mathrm{x}_{\mathrm{m},1} - \mathrm{x}_{\mathrm{m},0})^2 + (\mathrm{y}_{\mathrm{m},1} - \mathrm{y}_{\mathrm{m},0})^2 + (\mathrm{z}_{\mathrm{m},1} - \mathrm{z}_{\mathrm{m},0})^2}, \quad (20)$$

where dm shows the navigation distance of the best trajectory intercepted in the range Lm of the interceptor m.

4. Analyzed The Various Tests for Both UIA and Flight Trajectories

In this section, we will utilize the methodology mentioned in the section 2 and 3. This paper builds the error correction under various states according to the result of the trajectories of GNSS/RAIM system, and traditional method to be compared with UIA suggested in this paper. Finally, this paper estimated the navigation trajectory of the back segment by the navigation trajectory of the aircraft.

4.1 Analysis and Building The Corrections of The Navigation Trajectories

The paper implements the estimation and intercepting of the trajectories with the following steps at first:

A. The paper adopts the military planes of some military airports, in order to observe various flight directions and heights by four radar stations. Intercepting 1000 data points from the navigation trajectory of the aircraft, the time interval of each point is the 10th part of a second. Thus far the navigation trajectory of the plane constructed in the coordinate system that is assumed, because the military confidentiality of both the radar station and the weapon. The orientation of the radar's coordinates in ℜ3 will be right-handed in the sense that if the aircraft flies to the west from the military airport (as at the origin) with its right wing along the positive X-axis (as the north) and its head along the positive Y-axis. The fly upwards will then point in the direction of the positive Z-axis (as the height).

B. To compare the trajectory of the GNSS/RAIM system with the observational trajectory of four radar stations, the paper can obtain distance corrections that be corrected. The paper derives the bias $\vec{\rho}_{i,\theta,\phi,d}$ on the scaling factors and the error vector $\vec{\sigma}_{i,\theta,\phi,d}$ of measured variable through Eqs. 5-8, hence we can set up the correction (ε, ρ, σ) of i-th radar in the (θ, ϕ, d).

C. We can finish the setting-up of the correction database through the steps described above, and link up it with the calculating parameters of the radar. To be embedded the corrections (ε, ρ, σ) of i-th radar in the (θ, ϕ, d) while observing the target, in order to obtain the correct coordinates, and estimated the navigation trajectory of the back segment by Eqs. 16-19.

This paper conducted a training event in which 1000 data points against each other in four radar stations. Multiple trials were held, and in each trial, the mission objectives were provided as verbal instructions to the radar teams. Pre-mission planning and post mission debriefing were performed in the commander. Observation of the target and comments from the intercepting tracks showed a rich set of interactions, a high level of interest, positive training potential for the scenario, and the ability to effectively reuse the same environment for various sets of intercepting targets. We can construct the components critical for teamwork training assessment, such as embedded tools for observation, in-maneuver-exercise performance of the aircraft's trajectory, and tools for supporting Radar.

This paper tries to intercept 300 data points from the first period of the navigation trajectory of the aircraft by the method of the step A., and simplifying the complexity of the figure. In order to obtain the navigation tracks of every observation unit, therefore use the interval of every 10 points of these data points to adopt the position of first points on this, we obtain the Fig. 4.1 as following:

(X, Y, Z): The black full line shows that GNSS/RAIM monitors the aggressor's trajectory,

(X1, Y1, Z1): The red full line shows that Radar 1 monitors the aggressor's trajectory,

(X2, Y2, Z2): The blue dotted line shows that Radar 2 monitors the aggressor's trajectory,

(X3, Y3, Z3): The black dotted line shows that Radar 3 monitors the aggressor's trajectory,

(X4, Y4, Z4): The purple dotted line shows that Radar 4 monitors the aggressor's trajectory.

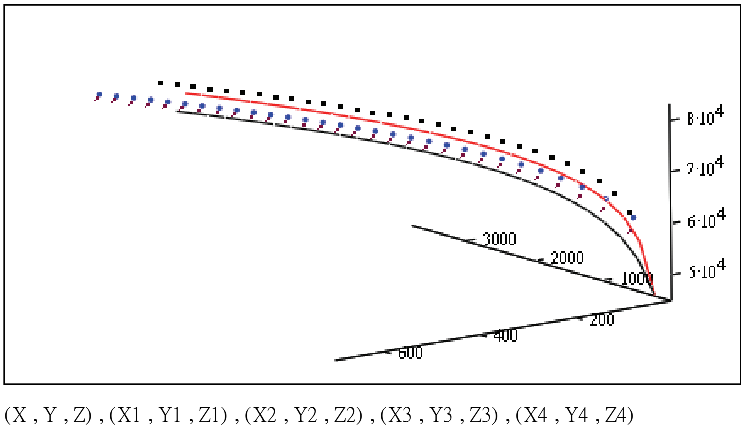

Fig. 4.1 The navigation trajectories of each observation

On the other hand, we can observe that radar-reality mismatch is sufficiently observable by Fig. 4.2~ Fig.4.4.

Now, the paper explains the UIA proposed in this paper by 20th data point in Fig. 4.1 that is an example for the reader. We have coordinates of the four radar stations that have already known:

R1(96,235,199), R2(125,295,239), R3(155,325,219) and R4(78,57,95).

We obtain both the matrix of scaling factors and distance errors for radars by $\vec{M}_{true,\ M,20}$ =(2000,400,76002) of the RGRIS:

$$\vec{S}^{n}_{i,M,20} = \begin{pmatrix} -0.029 & -1.361\cdot 10^{-3} & -1 \\ -0.032 & -2.103\cdot 10^{-3} & -0.999 \\ -0.032 & -1.919\cdot 10^{-4} & -1 \end{pmatrix},$$

d1,M=77230, ε1,d=1403,

d2,M=78420, ε2,d=2636,

d3,M=78600, ε3,d=2792,

d4,M=78300, ε4,d=2364.

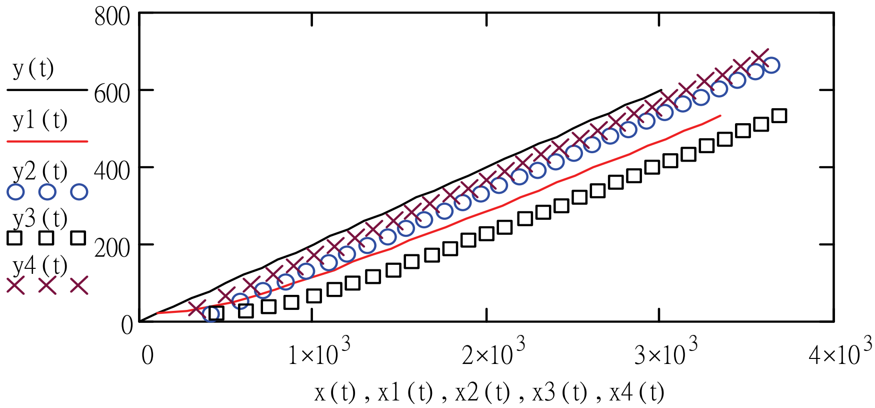

Fig. 4.2 Observation errors of the navigation trajectories of each observation

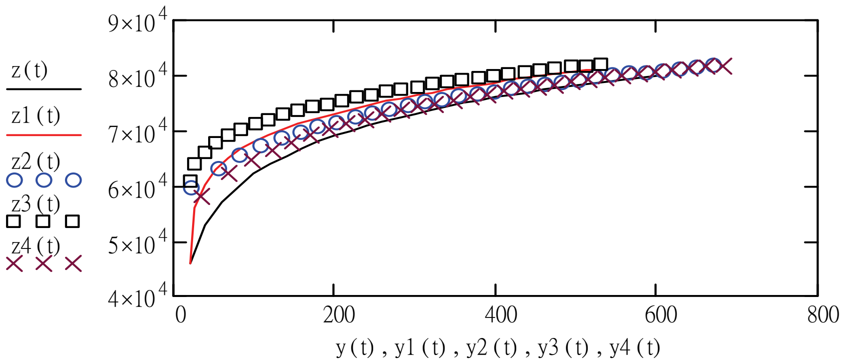

Fig. 4.3 Observation errors of the navigation trajectories of each observation unit in y-z axis

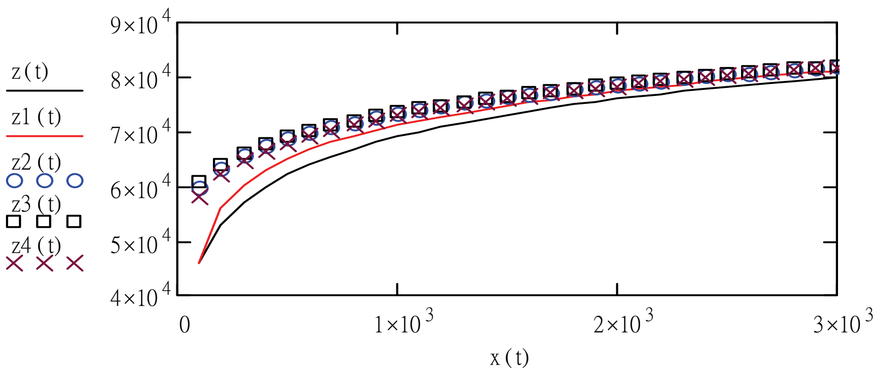

Fig. 4.4 Observation errors of the navigation trajectories of each observation unit in x-z axis

We calculate the solutions to the single radar by equations 5-8, which are given below:

$$\vec{S}_{1,M,20} = \begin{pmatrix} -0.0287 & 0 & 0 \\ 0 & -3.9268\cdot 10^{-3} & 0 \\ 0 & 0 & -0.996 \end{pmatrix},$$

$\mathrm{diag}\,\vec{\rho}_1$=(1.224·10-4,2.566·10-3, 3.493·10-6),

$$\vec{\sigma}_{1,\theta,\phi,d} = \begin{pmatrix} -8.58277 \\ 0.23528 \\ -1.39559\cdot 10^{3} \end{pmatrix},$$

$$\left[(\vec{S}_{1,M,20})^T \vec{S}_{1,M,20}\right]^{-1} (\vec{S}_{1,M,20})^T \vec{\sigma}_{1,\theta,\phi,d} = \vec{C}_{1,M,\theta,\phi,d} = \begin{pmatrix} 299.573 \\ -59.916 \\ 1.396\cdot 10^{3} \end{pmatrix},$$

θ1(M,20)=4.953 and ϕ1(M,20)=1.444. Consequently, the UIA suggested in this paper is compared with the traditional method, not only proves that is a feasible mode by the result of Fig. 4.5 but also reaches the paper's purpose that uses the statistical method to obtain the correction of biased test of the radar. To each radar be true to life, that is accurate and independent completion monitoring-control of the aggressor. An average of the errors ($\Delta x,\Delta y,\Delta z$) of the traditional method is compared with an average of the errors of UIA suggested in this paper as follows:

MLE= (34.456,112.31,99.847),

TLE= (6.873,2.847,19.969),

UIA= (0, 0.0013, 0.153).

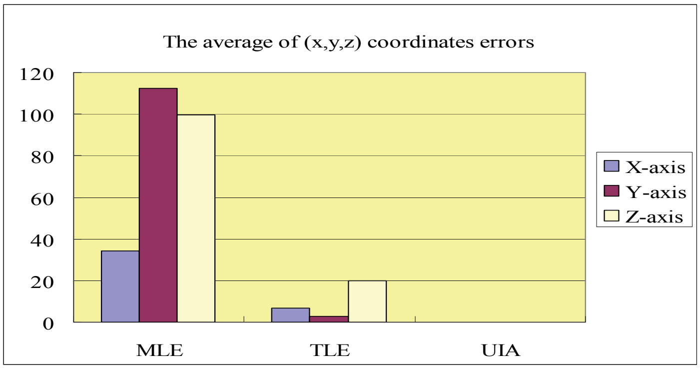

Figure 4.5: The average of (x,y,z) coordinates errors

4.2 Estimations of The Aircraft's Trajectory and Combat Management System (CMS)

To achieve the first purpose in this paper that can offer the data of the target orientation to the interceptor then an optimal intercepting trajectory can be obtained. We have already settled good foundation for this purpose in previous section, thus we can be used to create a correction database of the errors for the radar to correctly transmit the attacking trajectory of the aggressor. Now, we estimate the navigation trajectory of the back segment by Eqs. 20-23：

Ht+1(R)．[I3×(t×3), -I3×3]t=0，

$$\begin{bmatrix} \Delta R_{1(t+1)} \\ \vdots \\ \Delta R_{(t+1)(T+1)} \end{bmatrix}^T = \left[\begin{pmatrix} 300 \\ 60 \\ 1400 \end{pmatrix}^T, \begin{pmatrix} 300 \\ 60 \\ 1330 \end{pmatrix}^T, \begin{pmatrix} 300 \\ 60 \\ 1280 \end{pmatrix}^T, \begin{pmatrix} 300 \\ 60 \\ 1220 \end{pmatrix}^T \right],$$

$$H_{t+1}(R)=\begin{bmatrix} \begin{pmatrix}100\\20\\487.781\end{pmatrix}=a & \begin{pmatrix}100\\20\\465.083\end{pmatrix}=b & 2b-a & \Delta R_{1(T-t+1)} \\ b & \begin{pmatrix}100\\20\\444.404\end{pmatrix}=c & 2c-b & \Delta R_{2(T-t+2)} \\ c & \begin{pmatrix}100\\20\\425.486\end{pmatrix}=d & 2d-c & \Delta R_{3(T-t+3)} \\ d & \begin{pmatrix}100 & 20 & 408.113\end{pmatrix}^T=e & 2e-d & \Delta R_{(3+1)(T+1)} \end{bmatrix}^T,$$

$$\begin{bmatrix}M_4\\ \vdots \\ M_7\end{bmatrix}=\begin{bmatrix}M_1\\ \vdots \\ M_4\end{bmatrix}+\begin{bmatrix}\Delta R_{1(t+1)}\\ \vdots \\ \Delta R_{(t+1)(T+1)}\end{bmatrix}, \quad M_1=\vec{M}_{true,M,20}=\begin{bmatrix}2000\\400\\76000\end{bmatrix}$$

$$\begin{bmatrix}M_4\\ \vdots \\ M_7\end{bmatrix}=\begin{bmatrix}\begin{pmatrix}2300\\460\\77400\end{pmatrix}^T, \begin{pmatrix}2400\\480\\77820\end{pmatrix}^T, \begin{pmatrix}2500\\500\\78230\end{pmatrix}^T, \begin{pmatrix}2600\\520\\78620\end{pmatrix}^T\end{bmatrix}^T,$$

the paper describes the result in Fig. 4.6.

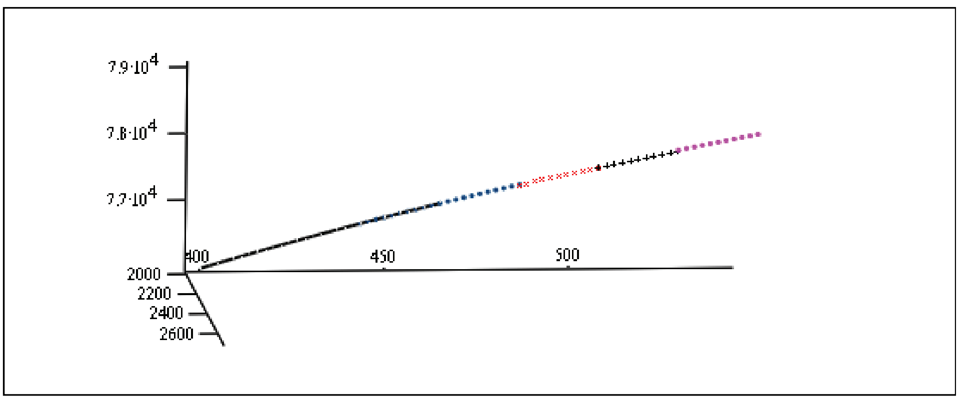

(X20 , Y20 , Z20) , (X21 , Y21 , Z21) , (X22 , Y22 , Z22) , (X23 , Y23 , Z23) , (X24 , Y24 , Z24)

Fig. 4.6 An estimate of the navigation trajectory of the target

The Hessian matrix can be also expand by t>3 to conform to the need of the real environment, that are t=6, ti=i×t and T=2×ti, i is a row number. We describe the result in Fig. 4.7.

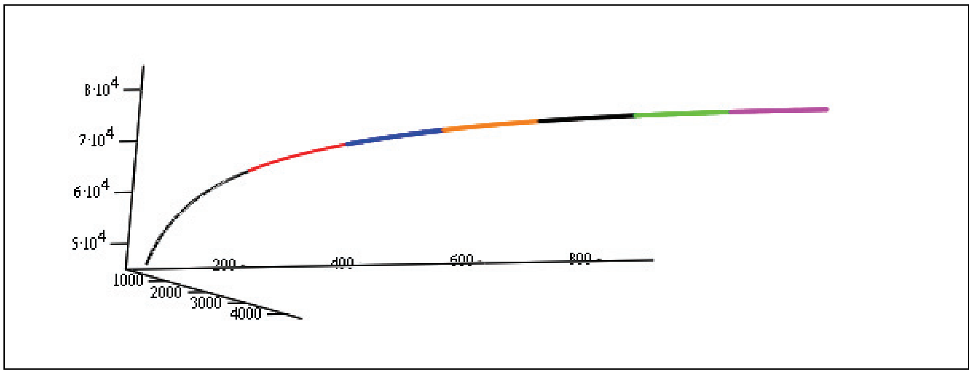

(x1 , y1 , z1) , (x7 , y7 , z7) , (x13 , y13 , z13) , (x19 , y19 , z19) , (x25 , y25 , z25) , (x31 , y31 , z31) , (x37 , y37 , z37)

Fig. 4.7 An expansive estimate of the navigation trajectory of the target

From what has been said above, the radar offered the target's data to help the interceptor to implement the scaling variables at the same time. In addition to obtain the best trajectories of intercepted targets, the CMS can take necessary precautions, against attack and assignment of intercepted missions for destroyed the target and selecting the intercept points at an earlier time. The system constructs three interceptors with different coordinates but their range is the same (Rm=18 kilometers)：

m1=(44394, 153763, 100),
m2=(40468, 154320, 1000),
m3=(41910, 154381, 1000).

The paper can estimate the entry Ri0 and the exit Ri1 of the defending range of the interceptor each by the navigation trajectory of the target:

R10 = (46300, 9260, 107400)T,
R11 = (58000, 11600, 109700) T;
R20 = (45300, 9060, 107200) T,
R21 = (48000, 9600, 107800) T;
R30 = (47000, 9400, 107600) T,
R31 = (51000, 10200, 108400) T.

Then we calculate the solutions dm to each the radar by Eqs. 16-19, which are given below:

d1=12140 > d3=4160 > d2=2814.

Therefore, the optimal policy of the assignment of intercepted missions is obtained and dm*= d1.

5. Conclusion and future research

The research works concerning RADAR/ GNSS/ RAIM integration algorithms is the core to improve the quality of the interceptor. This paper probes into application and correction of the errors of the radars in the defensive system. The Utility Integration Algorithm (UIA) proposed in this paper can be used to create a correction database of the errors for the radar to correctly transmit the attacking trajectory of the aggressor. It also can simplify the calculation process and make the programmers to apply more efficiently, and these become its advantages. The other advantages are using simple matrix calculation and modeling process. We combine GNSS with RAIM system to form the implementation architecture of the verification mode of the positioning errors for the radar. The RGRIS can offer the data of the target orientation to the interceptor then an optimal intercepting trajectory can be obtained. According to these, we can take necessary precautions, against attack and assignment of intercepted missions for destroyed the target and selecting the intercept points at an earlier time. At the same time, the radar offered the target's data to help the interceptor to implement the scaling variables.

However, the required accuracy of the involved estimation process is not easily achieved in practice, which may result in low tolerance to localization and association errors. Additionally, the military is interested in supporting effective, large-scale, distributed, simulation-based training that will enhance and expedite instruction of interceptor. The "weakly-scripted" approach of the weapon purchased proved to be effective for eliciting military teamwork with high error overhead. Analyzed the various tests demonstrated that teamwork does occur during RGRIS maneuver-exercise, in the form of coordination, leadership, monitoring, radar orientation, back-up, adaptability, RGRIS pushing and pulling, and closed-loop RGRIS. The RGRIS environment, therefore, is sufficient to produce instances of military teamwork, and may provide an appropriate medium for instruction of military teamwork skills.

However, a number of capabilities gaps exist in the large-scale maneuver-exercise, the distributed teamwork, and the simulation-based training. If these capabilities gaps are met successfully, then existing technology tracked and corrected will provide a powerful tool for the development of effective, large scale, military training environments. In other words, while Ministry of National Defense carried on the large amount of the dearly purchased weapons at the same time, we should think about the performance of the best weapons to establish a link between build up the army and fight against the enemy, so the variance factor existed still on this. Through the models of the RGRIS, TLSM and CMS proposed in this paper have been very helpful for the improvement of the weapon performance. If the construction unit of the weapon only knows to buy the weapon to use, and wonder whether the performance to the existing weapon is deeply analyzed and accurately corrected. This present situation causes millions kinds weapon to be collected in a place, but it is difficult to be the essential function of frightened and hindered the enemy in the war. The paper considers both the guidance law and the dynamic characteristic of the three-dimensional relative motion of the missile in future research direction.

Acknowledgments

The author would like to thank the Editor-in-Chief and Referees for their comments and suggestions that are the mother of innovation.

Reference

[1] Zou, X., Deng, Z., Ge, M., Dick, G., Jiang, W., Liu, J. (2010) "GPS data processing of networks with mixed single- and dual-frequency receivers for deformation monitoring," Advances in Space Research, 46, 130–135.

[2] Jin, S.G., Park, P.H., Zhu, W. (2007) "Micro-plate tectonics and kinematics in Northeast Asia inferred from a dense set of GPS observations," Earth Planet, Sci. Lett. 257, 486–496.

[3] El-Sheimy, N. (2004) Inertial Techniques and INS/DGPS Integration, ENGO 623 lecture notes, Department of Geometrics Engineering, The University of Calgary.

[4] Chiang, K.W. (2004) INS / GPS Integration Using Neural Networks for land Vehicular Navigation Applications, Department of Geometrics Engineering, The University of Calgary, Canada, UCGE Report 20209,.

[5] Washington Y. Ochieng, Knut Sauer, David Walsh, Gary Brodin, Steve Griffon, Mark Denney (2003) "GPS Integrity and Potential Impact on Aviation safety," The Royal Institute of Navigation, 56, 51-65.

[6] Šegvić, S., Remazeilles A., Diosi, A., Chaumette, F. (2009) "A mapping and localization framework for scalable appearance- based navigation," Computer Vision and Image Understanding, 113, 172–187.

[7] Kelly, R. J., Davis J.M. (1994) "Required Navigation Performance (RNP) for Precision Approach and Landing GNSS Application," Journal of The Institute of Navigation, Spring 41 (1), 94-108.

[8] Per Enge, Todd Walter, Sam Pullen, Changdon Kee, Yi-Chung Chao, and Yeou-Jyh Tsai (1997) "Wide Area Augmentation of the Global Positioning System," U.S. Patent, April 15 (5), 621-646.

[9] Yang, Y., El-sheimy, N., Goodall, C. and Niu, X. (2007) IMU Signal software Simulator, ION NTM 2007, San Diego, CA.

[10] Bennour, Z., Landy, R. Jr., Giroux, R., Constantinescu, A., and Gavidia, G. (2005) Web-based MEMS Inertial Navigation Simulator, ION 61st Annual Meeting 2005, Cambridge, MA.

[11] Huffel, S. V. and Vandewall, J. (1991) The Total Least Squares Problem: Computational Aspect and Analysis. Philadelphia: Society for Industrial and Applied Mathematics.

Practical Algorithms for The Optimal Operation Management of Distributed Supply Chain System with Multi–Lot-Size of Deteriorating Items

Shao-Chang Miao

Abstract

This paper uses the Optimal Operation Management (OOM) to deal with the replenishment strategies in the Distributed Supply Chain (DSC) system and simplifies the Markov Decision Process for the managers to apply efficiently. Its advantages are using simple modeling processes and the manager only needs to enter the inventory amount to obtain the demand quantity, the stationary distribution, the reorder point, the order quantity and the expected cost of the DSC system. In the numerical examples of this paper, the wrong replenishment strategies have risen 47.23 %~110.02 % of the expected cost on the civil gas station. In addition, we also analyzed how to distribute the stock under the condition of insufficient supply from the supplier in a non-cooperative behavior distributed supply chain system while minimizing the total cost.

Keywords： Optimal Operation Management (OOM); Markov Decision Process (MDP); Deteriorating item; Distributed supply chain (DSC); Practical Algorithm (PA).

Shao-Chang Miao, Office of Military Education, Hsiuping University of Science and Technology, Doctoral program student, Department of Statistics, TungHai University.
Received 1 December 2010; accepted 9 March 2011

具退化性商品多批量配送供應鏈系統之最佳作業管理的實用演算法

繆紹昌

摘　要

本文採用最佳化作業管理以獲得在 DSC 系統的補充的策略，並且簡化馬可夫決策過程使得經營者能夠有效地應用。　它的優點是使用簡單的建模過程和經營者只需要輸入觀察點的存貨數量便可獲得 DSC 系統的需求量、穩定的分配、再訂購點、訂購的數量和期望成本。在本文的數例中 民營加油站錯誤的補充策略已經使期望成本上升 47.23 %~110.02 %。此外，我們也分析了非合作行為的 DSC 系統的供應商在供應不足的條件下如何分配可使得系統總成本最小化。

關鍵詞：最佳化作業管理、馬可夫決策過程、退化性商品、配送供應鏈、實用演算法。

繆紹昌：修平科技大學軍訓室軍訓教官、東海大學統計系博士生
投稿日期：99 年 12 月 1 日　接受刊登日期：100 年 3 月 9 日

1. Introduction

In this paper, we study the replenishment strategies of a deteriorating item in a Distributed Supply Chain (DSC) system for a producer that consists of a distribution center, a supplier and multiple retailers. In a traditional distribution system, each retailer holds a certain amount of inventory to keep adequate service. The right amount of inventory can avoid the loss of customers and the damage of good will. It can minimize the total cost and serves as the buffer of another replenishment time. However, if inventory levels are not evaluated by cost analysis, the above-mentioned objectives are hard to accomplish. Therefore, the replenishment strategies are worthy not only discussing but also needing more attention. The supplier can be a distribution center or upstream supplier who purchases items in batches and sells or distributes these items to the downstream retailers. In this system, the supplier and retailers are independent and face the stochastic demand. Their behavior influences the whole supply chain system. The inventory model of these stochastic demands is based on the (s, S) inventory policy. The inventory level is reviewed periodically. As the inventory level decreases under the reorder level s, an order is given to increase the level up to the replenishment level S. In this study, we use the Markov Decision Process (MDP) and the Practical Algorithm (PA) to deal with the Optimal Operation Management (OOM) in the DSC system. The optimal strategy is derived efficiently to determine the reorder points and the replenishment amount, to minimize the total cost, and to decide which retailers' demands to be satisfied first and which retailers' demands to be backlogged.

OOM can be treated with MDP and PA, but many experts don't see the need. They suggest having a regular delivering schedule. As simple as this may seem, it is not at all uncommon for an organization to expend considerable time, money, and effort to generate customer demand and then fail to have product available to meet customer requirements. The traditional practice in many organizations is to stock inventory in anticipation of customer orders. Typically an inventory stocking plan is based on forecasted demand for products and may include differential stocking policies for specific items as a result of sales popularity, profitability, and importance of an item to the overall product line and the value of the merchandise.

The remainder of this paper is organized as following: Section 2 reviews relevant literatures. Section 3 describes both the problem and the assumptions about our research. Sections 4 and 5 introduce the

OOM, Markov Decision Process and the Practical Algorithm and develop a distributed supply chain inventory model to decide when to order and how much to order. Section 6 constructs a case study about inventory management of the oil Distributed Supply Chain (DSC) system; numerical examples and a sensitivity analysis are illustrated. Section 7 presents a discussion about the results and the final section presents the conclusions and a brief planning on the future research and extensions.

2. Literature review

2.1 The deterioration inventory

The classical economic order quantity (EOQ) model was developed in 1915 with the theory of unlimited stock in general inventory models. However, it lacked statement of the deterioration phenomenon of the items in stock. In the practical situation, the deterioration phenomenon of goods is common. Goods may not function properly because of decay, corruption, volatilization, degradation or expiration within the holding period. These goods include food items, photographic films, pharmaceuticals, chemicals, electronic components, volatile commodities and radioactive substances. These kinds of items are usually known as deterioration inventory.

Ghare and Schrader [7] were the two earliest researchers to develop an EOQ model with an exponential decay and a deterministic demand. They categorized the deterioration phenomena into three types: direct spoilage, physical depletion and deterioration. Since then, a lot of work has been done on deterioration inventory systems. Papachristos and Skouri [18] established a partially backlogged inventory model with deterministic varying demand and constant deterioration rate, in which the backlogging rate decreases exponentially as the waiting time increases. Goyal and Giri [9] investigated a similar production-inventory situation in which the demand, production and deterioration rates of a product were assumed to vary with time. However, pricing was not under consideration and the backlogging rate was assumed to be a constant fraction.

Some scholars consider product life to be a random variable that follows Weibull distribution, which is constantly applied to describe the failure and the life expectancy of items. Covert and Philip [5] obtained an inventory model for items with a variable rate of deterioration. They assumed that the time of deterioration of an item obeys the two-parameter Weibull distribution. Chang and Dye [2] considered a temporary sale price inventory model for a varying rate of deterioration which is assumed to obey a two-parameter Weibull distribution. Wu [21] proposed an inventory model of deteriorating items with Weibull distribution. The model allows the item shortage and a demand of time variance.

Gradually, many managers and researchers accepted the concept of deterioration in the inventory system because they realized that the effect of deterioration of products could not be ignored in many inventory systems. Therefore, the deterioration inventory models have been paid much attention and studied widely in past years by fellow researchers Gupta and Vrat [11]; Aggarwal and Bahari-Kashani [1]; Goswami and Chaudhuri [8]; Howard [13].

2.2 The multiple-echelon deterioration inventory in the DSC system

The multiple-echelon inventory is the most complex and changeable inventory system in the DSC system. It is different from the single-echelon inventory system in which each member of the DSC system has to satisfy its own external demand and choose its own inventory policy to chase the minimum cost or the maximum profit. Therefore, the members' behavior will influence the whole supply chain and makes it more complicated. Among the models of the DSC system, Graves [10] studied the situation between one-supplier (or one-warehouse) and multi-retailer with independent demands across retailers and this model is under a periodic review policy. Cheng and Sethi [4] studied the optimal promotion decision and order quantity for a retailer. They applied a Markov decision model to obtain the minimum total cost. Smith and Agrawal [20] and Howard [13] studied the situation of jointly deciding the stocking levels and the assortment under probabilistic substitution. Iyer and Ye [15] used a newsboy-type inventory model that included customer heterogeneity and promotion information to examine the expectant profit for the retailer and the manufacturer.

In recent years, other researchers (Netessine et al. [17]; Sarmah et al., 2006; Zhang et al. [22]) tried to resolve the problems of coordination between different business entities and determine the optimal investment and replenishment decisions in competitive environments. In addition, some researches have studied two or multiple echelon inventory model with deteriorating items in the DSC system. Huang and Yao [14] studied a deteriorating item in a DSC system with a single vendor and multiple buyers and proposed a search algorithm to minimize the average total costs. Lin et al. [16] considered a cooperative inventory with deteriorating items. It allowed complete back-order without the equal replenishment periods and presented a procedure to find the optimal solution for the replenishment strategy. Feng et al. [6] researched for a deterioration inventory model for a single product under a two-echelon DSC system with a manufacturer and a retailer. An algorithm for a retailer to minimize the average total cost and for a manufacturer to optimize production time was derived.

3. Problem description

Sections 3 and 4 introduce the Markov chain and its analysis. We will also discuss a discrete-time Markov chain, e.g. it is observed at the end of each day. This paper focuses on how to design the operation of a discrete-time Markov chain to optimize its performance in the DSC system. Chazan and Gal [3] treated the inventory control as selecting a policy at each possible state of the Markov chain. Therefore, for each possible state of the Markov chain, we make a decision on which one of the several alternative actions should be taken. The decision affects the transition probabilities and system costs in the distributed supply chain. We want to choose the optimal decisions for the respective states when considering the long-run expected cost (LEC) during the observed period time in the DSC system. The decision process for doing this is referred to as a Markov decision process.

The main purpose of this paper is to investigate the inventory models for the deteriorating/distributing items in the DSC system (shown in Figure 1) to develop the optimal inventory and replenishment strategies by applying MDP. According to the retailers' order demand, which was reacted to their supplier, the MDP and PA were used to model the supply chain, and the optimal inventory policy was given to the supplier and retailers.

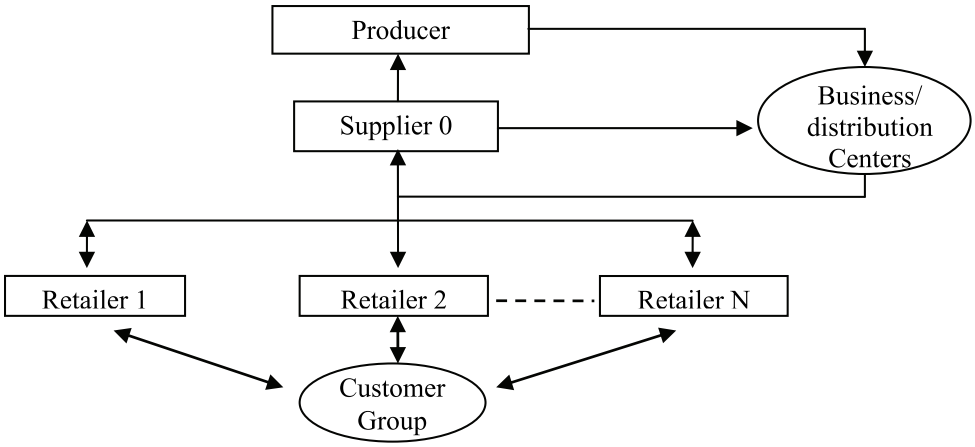

Figure 1 Conceptual Model for Distributed Supply Chain

Therefore, depending on the operational mission of a particular performance cycle in a supply chain structure, the associated work may be under the complete control of a single enterprise or may involve multiple firms. For example, manufacturing support cycles are often under the operational control of a single enterprise. In contrast, performance cycles related to customer accommodation and procurement typically involve multiple firms. The goal of performance cycle synchronization is to achieve the planned time performance. Delayed performance at any point along the supply chain results in potential disruption of operations. Such delays require that safety stocks be established to cover variances. When performance occurs faster than expected, unplanned work will be required to handle and store inventory that arrives early. Given the inconvenience and expense of either early or late delivery, it is no wonder that logistics managers place a premium on operational consistency.

Blood or Oil is a deteriorating item, and a highly volatile liquid, which undergoes physical depletion over time through the process of evaporation. Consequently, for the deteriorating items it is necessary to consider potential loss due to deterioration while determining the optimal inventory strategies. To describe the model, we summarized the descriptions as following:

- The inventory is monitored only at the beginning of each period, and orders are placed only at these times.
- The stochastic demand and a fixed delivery lead-time are considered in this model.
- Backlog is allowed for the retailers but not for the customers.

- There is no rebalancing allocation among retailers.
- The model's basic concepts stem from (*s*, *S*)-type polices.

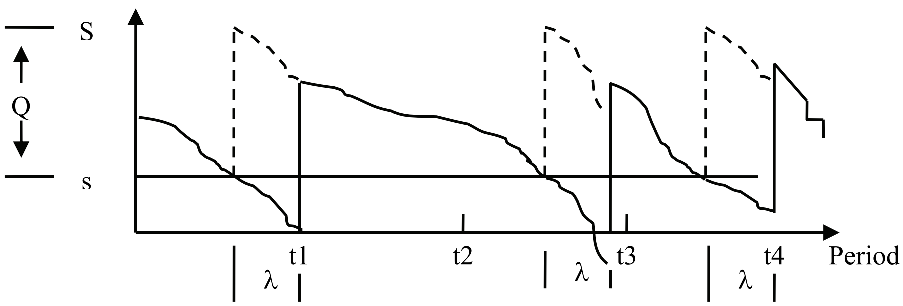

Figure 2 Diagram of the inventory level (the solid curve) and the inventory position (the dashed curve) as a lot-size reorder-point for multi-period

Fig. 2 can be viewed as a series of fixed cycles with the order points where sometimes the demand during period λ is so large that the inventory level becomes negative. The inventory strategies are used to determine the inventory level S. When it reaches order point s, an order of size Q is placed.

Remark 3.1 A delivery lead-time λ is so small that it has never been more than a single order, and reorder point s is always nonnegative.

The above descriptions guarantee that the inventory on hand always falls above the reorder point s when an order is received. Otherwise, more than one order would be outstanding. We were able to determine the optimal reorder points and replenishment policy that resulted in minimizing the expected cost (EC). The cost depends upon the probability of Q, which can be found by actual statistic observation of the order lot-size. It is difficult to solve the model analytically. Therefore, a discrete-time MDP is employed to formulate the structure of the supply chain in this paper to derive an optimal policy by PA.

The primary value of OOM is to accommodate customer requirements in a cost effective manner. Although most senior managers agree that customer service is important, they sometimes find it extremely difficult to explain what it is and what it does. While common expressions of customer service include "easy to do business with" and "responsive to customers" to develop a full understanding of customer service, a more thorough cost framework is required.

4. Model development

The paper has what developed some important foundations of the logistical discipline and how it creates value in a supply chain context. These insights regarding the nature of OOM, the importance of achieving internal operational integration through managing inventory and information flow, viewing the performance cycle structure as the basic unit of analysis, and the management of operational uncertainty combine to form a logically consistent set of concepts essential to supporting supply chain management. Logistics and supply chain are not the common and the same concepts. Supply chain is a strategy that integrates all aspects of satisfying customer requirements. Logistics is the process of positioning and managing inventory throughout the supply chain. To understand basic principles, it is useful to understand inventory relationships under conditions of certainty. Formulation of inventory policy must consider uncertainty. Two types of uncertainty directly influence inventory policy. Demand uncertainty is rate of sale during inventory replenishment. Performance cycle uncertainty involves inventory replenishment-time variation.

Sales forecasting estimates unit demand during the inventory replenishment cycle. Even with good forecasting, demand during replenishment cycle typically exceeds or falls short of what is planned. To protect against a stock-out when demand exceeds forecast, safety stock is added to base inventory. Under conditions of demand uncertainty, average inventory represents one-half order quantity plus safety stock. Figure 2 illustrates the inventory performance cycle under conditions of demand uncertainty. The solid line represents the forecast. The line illustrates inventory on hand across multiple performance cycles. The task of planning safety stock requires three steps. First, the likelihood of stock-out must be gauged. Second, demand during a stock-out period must be estimated. Finally, a policy decision is required concerning the desired level of stock-out protection.

The lot size refers to the number of units to be purchased in each transaction. When customers are required to purchase in large quantities, they must incur costs of product storage and maintenance. When the supply chain allows them to purchase in small lot sizes, they can more easily match their consumption requirements with their purchasing. In developed economies, alternative supply chains frequently offer customers a choice of the level of lot-size service output. Of course, the supply chain that allows customers to purchase in small quantities normally experiences higher cost and therefore demands higher unit prices from customers.

In this section, we will introduce MDP and PA to develop our inventory model for the DSC system with deteriorating items.

4.1 The Markov Decision Process (MDP) model

In this study, we explore a two-echelon inventory system in the DSC system, which includes a single distribution center and a single supplier, multiple-retailers and various products, shown in Fig. 1. The deteriorating items storage cannot be monitored continuously and the customer demand timing is only related with the current state, which is irrelevant with the pass event. Hence, the stochastic process {S(n)} holds the Markov property (see Hillier & Lieberman [12]), when S(n)=j , it represents the storage amount in state j after exactly n-step. The observation frequency is limited if we observe weekly or daily. A deteriorating/ distributing item in the industry is stable and because there are regular distribution activities, so it exists with a stationary transition probability. We can gain the initial probability or the probability of state i through long periods of observation and data-collection. The purposes of this research adopt the optimal policy in the limited decision point n, which keeps the EC minimum. The process conforms to MDP. It is interpreted below.

Definition 4.1.1 A stochastic process { S(n), n = 0, 1,⋯} is a Markov chain with n-step if it has the Markovian property.

A Markov chain { S(n)(j), n = 0, 1,⋯} of the inventory level S in state j after n-step is completely defined by its (n-step) transition probability matrix and its initial distribution as Eq. (1).

$$P\left(S^{(n)}(j)\right)=\sum_{i=0}^{\infty} P\left(S^{(0)}(i)\right) p_{i,j}^{(n)} \geq 0, \ \forall \ j, \quad S^{(n)}(i)+Q^{(n)}-\varepsilon_{\lambda}=S^{(n)}(j), \quad D_{d,e}^{(n)}=\left|S^{(n)}(j)-S^{(n)}(i)\right|, \ \forall n, \quad \sum_{j=0}^{\infty} P\left(S^{(n)}(j)\right)=1. \tag{1}$$

We drop the superscript n when n =1. Moreover we can calculate all the transition probabilities by specifying the transition probability matrix P=[pi,j] and the initial distribution S=[S(1)(j), j = 0, 1,⋯]. This paper considers only Markov chains with the following properties: (1) A finite number of states, (2) Stationary transition probabilities.

4.2 The steps of Markov Decision Process

In this section, an MDP approach is used to model the supply chain. The steps are shown below:

- After each transition, observe the Markov chain state i ($i = 0, 1, \cdots\cdots, S$).
- After each observation, select a policy Q from (S-i) policy set，S-i = 0 represents no decision.
- If select policy Q at state i, an expected cost $C(i, Q)$ can be obtained.
- If select policy Q at state i, the system moves to state j at next observed time period, with the transition probability $P_{ij}(Q)$, for $j = 0, 1, \cdots, S$.
- The policy set ($Q^{(0)}, Q^{(1)}, \cdots, Q^{(n)}$) is the policy of MDP at time n.
- The goal to find the optimal policy according to each cost function is decided by the minimum expected cost.

4.3 *The notations of the inventory model*

This paper kicked the DSC system model off with the notations that are defined below:

d	Members of the supplier chain, for d =0, 1, 2…, N, when d =0 it stands for the supplier; when d =1, 2…, N it stands for the retailer.
ε_λ	The demand during delivery lead-time λ.
$D_{d,e}$	Demand state of item e for member d, for 0, 1, 2⋯, $M_{d,e}$.
$M_{d,e}$	Maximum storage amount of item e for member d .
$S_{d,e}$	Inventory level of item e for member d , $S_{d,e} \le M_{d,e}$.
$Q_{d,e}$	Policy (replenishment amount) of item e for member d .
$C_{d,e}$	Purchase cost of item e for member d.
$h_{d,e}$	Holding cost of item e for member d.
$R_{d,e}$	Set up cost of item e for member d.
$b_{d,e}$	Shortage cost of item e for member d.
$L_{d,e}$	Deterioration cost of item e for member d.
$\theta_{d,e}$	Deterioration rate of item e for member d.
$P_{i,j}(Q_{d,e})$	Conditional probability for selected policy $Q_{d,e}$ from state i transferred to state j.
$C_{i,j}(Q_{d,e})$	The cost for selected policy $Q_{d,e}$ from state i transferred to state j.
$EC(i, Q_{d,e})$	The expected cost for selected policy $Q_{d,e}$ from state i transferred to state j.
$g^{(n)}(Q_{d,e})$	The long-run expected cost (LEC) during the observed period time n when using policy $Q_{d,e}$.

4.4 The Model development

Pi,j(Q) is transferred to a conditional probability Pi,Qd,e by the relative function (j - i = Qd,e). Thus Pi,Qd,e =P{policy Qd,e|state i} of stochastic policy Qd,e will derive a probability matrix at state i.

$$P_{i,Q_{d,e}} = \begin{cases} P(D_{d,e} > i + Q_{d,e}) \ \ if\ j = 0, 0 \le i \le M_{d,e} - Q_{d,e} \\ P(D_{d,e} > i + Q_{d,e} - j) \ if\ 0 < j < i + Q_{d,e}, \\ \qquad\qquad 0 \le i \le M_{d,e} - Q_{d,e} \\ 0 \qquad ,\quad otherwise \end{cases}$$

$$\sum_{Q_{d,e}=0}^{M_{d,e}} P_{i,Q_{d,e}} = 1,\ P_{i,Q_{d,e}} \ge 0,\ \forall \quad i \qquad (2)$$

Lemma 4.4.1 The Chapman-Kolmogorov equation calculates the (n+m)-step transition probability Pn+m by summing over all the intermediate states of k at time n and moving to state j from state k at the remaining time m.

Pn+m=pij[Q(n+m) /(i, Q(0))]=
pij[Q(n+m) /(i,Q(0)),
(k,Q(n))]·pik[Q(n) /(i,Q(0))]=
Σk p(n)ik·p(m)kj=Pn Pm.

Since arguments of the proof of *Lemma 4.4.1* can be found in many textbooks [12][13], therefore, the proof of *Lemma 4.4.1* is omitted in this paper.

Remark 4.4.1 Let Wi=p(0)iQ, W= [W0, W1, …] and ∑Wi=1. Then W is said to be a stationary distribution for the Markov chain if W·P=W. Clearly, if W is a stationary distribution, then ∀ n ≥1, W·Pn =…=W P= W.

Nevertheless, Eq. (2) is a constraint condition and a one-step transition-probability matrix. We drop the subscripts d and e from Qd,e in order to simplify the equations and to make reader understand. Recall that P(n)i,Q is just the conditional probability of being in state Q after n steps, starting in state i. In this paper, P(n)i,Q can identify an irreducible finite-state Markov chain by the property (2). In other words, the distribution of Q is independent of n. The conditional probability Pi,Q of DSC system will be transferred to state Q after a large number of transitions

$$\lim_{n\to\infty} P_{i,Q}^{(n)} = P_Q > 0,\ \forall \quad i \quad ,$$

where the PQ , uniquely satisfies the following stationary equations

$$P_Q = \sum_{i=0}^{M_{d,e}} P_i \cdot P_{i,Q}^{(n)},\quad \forall \quad Q \text{ and } n \ ,$$

$$\sum_{Q=0}^{M_{d,e}} P_Q = 1 \qquad (3)$$

The PQ is called the stationary probability matrix of the Markov chain. According to stationary probability matrix of Eq. (1) ~ (3), we can find the shortage amount Ad,e and expected storage amount Bd,e :

$$A_{d,e}(i) = \begin{cases} \sum_{D=i+1}^{M_{d,e}} [P_D(D-i) + \\ \sum_{k=Q+1}^{M_{d,e}-Q} P_k(k-Q)]\ ,\quad j=0 \\ 0\ ,\ otherwise\ , \end{cases}$$

$$B_{d,e}(i)=\begin{cases}\sum_{D=0}^{i}P_D[(i-D)+\\ \sum_{j=1}^{M_{d,e}}\sum_{k=0}^{i+Q-j-D}(Q+i-D-k)]+\\ \sum_{D=i+1}^{M_{d,e}}\sum_{j=1}^{M_{d,e}}\sum_{k=0}^{i+Q-j-D}P_k\cdot(Q+M_{d,e}-D-k),\\ \qquad 0<j<i+Q, 0\le i\le M_{d,e}-Q,\\ P_{i+Q}(i+Q)\ ,\ otherwise\ .\end{cases} \quad (4)$$

From the above statement of Eq. (4), we can derive a policy Q at state i, and obtain an expected cost function EC(i,Q), presented as Eq. (5)

$$EC(i,Q)=\sum_{j=0}^{M_{d,e}}[C_{i,j}(Q)\cdot P_{i,Q}]=$$

$$C_{d,e}\times Q+b_{d,e}\times A_{d,e}(i)+B_{d,e}(i)\times (h_{d,e}+\theta_{d,e}\times L_{d,e})+R_{d,e} \quad (5)$$

4.5 *Practical Algorithm (PA)*

By PA, let A(i) denote the space of all possible states. We assume A(i) to be countable. If at time n the system is observed in state i∈S, S ={0, 1, 2,…,M} then an action Q(n) must be chosen from a given set A(i). We assume that for each Q∈ A(i) the set of actions Q is countable. If the system is in state i at time n and action Q is chosen, then, regardless of the history of the system, two things occur: (1) We incur a known cost Ci,j(Q). (2) At time n+1 the system will be in state j with probability Pi,Q. An optimal stationary deterministic policy exists and such a policy can be determined by Howard [13].

4.5.1 *Preliminary relationships*

We drop all the subscripts d and e in order to simplify the equations. We will obtain an expected cost function EC(i,Q) when the decision-maker selects policy Q at state i. If the cost is affected by inventory level j =Q+i (i.e., next state j), then it can be denoted as Eq. (5). Denoted by Vi (n) the total expected cost of a system starting in state i and policy Q and evolving for n time periods. Then Vi(n) has a total expected cost $\sum_{j=0}^{M}P_j\cdot V_j^{(n-1)}$ of a system evolving over the remaining n-1 time periods and policy Q, where Vi(1) = EC(i,Q) for all i, $\sum_{j=0}^{M}P_j=1$. It will be useful to explore the history of Vin as n grows large. g(n)(Q) denotes the long-run expected cost (LEC) during the observed period time n when using policy Q. By Markov Decision Process, we can obtain $g(Q)=\sum_{i=0}^{M}P_i\cdot EC(i,Q)\ ,\ \forall Q\in A(i),\ A(i)=\{0,1,2,\cdots,M\}$.

Sufficient conditions for the existence of an optimal stationary deterministic policy are stated in the following theorem.

Theorem 4.5.1 Suppose there exists a set of finite numbers {g(Q) , Vi, i∈S} such that $g(Q)=\{EC(i,Q)+\sum_{j=0}^{M}P_{i,j}\cdot V_j\}-V_i$,

(6) we can find that, for any given policy Q , there exist values g(Q) and Vi, i∈S that satisfy Eq. (6).

We now shall use a heuristic justification of these relationships for these values. Referring to the description for Markov decision processes given at the beginning of this section, that gives the recursive equation

$$V_i^{(n)} = EC(i,Q) + \Sigma_{j=0}^{M} P_{i,j} \cdot V_j^{(n-1)} . \qquad (7)$$

It will be useful to explore the behavior of Vi(n) as n grows large. By Markov Decision Process, we can obtain $g(Q) = \Sigma_{i=0}^{M} P_i \cdot EC(i,Q)$, which is independent of the starting state i. Hence, Vi(n) behaves approximately as ng(Q) for large n, then we obtain the equation

$$V_i^{(n)} = ng(Q) + V_i(Q) \ ,$$

where Vi(Q) can be interpreted as the effect on the total expected cost due to starting in state i. Similarly, this gives $V_j^{(n-1)} = (n-1)g(Q) + V_j(Q)$ in state j. We now can substitute Vi(n) and Vj(n-1) into the Eq. (7). This leads to the Eq. (6) given in the Theorem 4.5.1. We obtain the desired results as given in Hillier & Lieberman [12].

Practical Algorithm Originated in Revised Policy Improvement Algorithm

The statements in equations (6) and (7) should be understood to hold with any stationary deterministic policy *Q** which, when in the i, prescribes an action which minimizes the right-hand side of Eq. (6) is optimal, that is

$$g(Q^*) = \min_{Q \in A(i)} \left\{ EC(i,Q) + \Sigma_{j=0}^{M} P_{i,j} \cdot V_j \right\} - V_i \ ,$$

and for policy *Q** the limit inferior in g(Q) can be written as follows

$$g^{(n)}(Q) = EC(i,Q) + \Sigma_{j=0}^{M} P_j \cdot V_j^{n-1}(Q) - V_i(Q) \geq \min_{Q \in A(i)} \left\{ EC(i,Q) + \Sigma_{j=0}^{M} P_{i,j} \cdot V_j^{n-1}(Q) - V_i(Q) \right\}$$

$$= G_n(i^*, Q^*) \Leftrightarrow g^{(n)}(Q) \geq G_n(i^*, Q^*) \ ,$$

where $G_n(i^*, Q^*) = \min_{Q \in A(i)} \left\{ g^{(n)}(Q) \right\}$.

Since *Q** is defined to take a minimizing action. Hence,

$$g^{(n)}(Q^*) = G_n(i^*, Q^*) \ ,$$

with equality for *Q* = *Q**. Letting n →∞, we obtain the desired results as given in Ross [19].

Remark 4.5.2 Note that recursive equation of Eq. (6) has M+1 equations with M+2 unknown, so that one of these variables may be chosen arbitrarily. But after each observation in the real world, we must select a policy $Q \subseteq$ policy set *(S-i)*，if S-i = 0, it represents no decision. In this paper, we use Gn*(i*,Q*)* to substitute LEC g*(Q*)* to obtain the optimal reorder point and order quantity. Gn*(i*,Q*)* denotes the obtained optimal solution of the pair-wise policy (i,Q) during period time n. In other words, Gn(i,Q) is the LEC matrix during the observed period time n for all applied pair-wise policies *(i,Q)*. Conventionally, VMn is chosen equal to zero, therefore, by solving the system of linear equations, we can obtain Vin and Gn*(i,Q)*. By recursive equation, we can gain the expected cost matrix of improvement policy shown as Eq. (8):

$$G_n(i,Q) = EC(i,Q) + [\sum_{k=i+Q+1}^{M} P_{i,k} \cdot V_0^{(n)} + \sum_{k=0}^{i+Q} P_{i,i+Q-k} \cdot V_{k+1}^{(n)}] - V_i^{(n)} . \quad (8)$$

In this paper, computational results pointed out the *Gn(i*, Q*) ≤ g(n)(Q)*, for all n. We obtained the results that might decide on the maximum inventory level (MIL) and reorder state (RS) such that they improved benefit realization in the DSC system, and therefore denoted by Gn*(i*, Q*)* the punitive profit of the system starting in state i and policy *Q* and evolving for n time periods. The results of the above described process can make the manager obtain the optimal pair-wise policy *(i,Q)*, which is an innovation of this paper. To perfect the PA′s calculation process, its properties are revised as following:

This algorithm has two key properties:

- $g^{(n+1)}(Q) \le g^{(n)}(Q)$ and $G_n(i^*, Q^*) \le g^{(n)}(Q)$, for n =1,2,⋯.
- After limited iterations, we can find the optimal policy S_n at reorder point i and stop. Therefore, the algorithm terminates with an optimal solution in a finite number of iterations in the DSC system.

According to the first key property of Practical Algorithm, $g^{(n+1)}(Q) \le g^{(n)}(Q)$ and $G_n(i^*, Q^*) \le g^{(n)}(Q)$ at n period, we get an optimal policy $S^{(n)}=i^* +Q^*$ into the Practical Algorithm in next iteration step n +1 as Eq. (8).

This method decreases the problems of scales/complexities, and the solution method is easy when the transformed matrix is large. Furthermore, there is a jumping solution that is produced in the next iteration stage where we can judge by $S^{(n+1)} \le S^{(n)} \le S^{(n-1)}$ (or $S^{(n-1)} \le S^{(n)} \le S^{(n+1)}$) and get a small $G_{n+1}(i^*, Q^*)$ into Eq. (8) and perform the following iteration steps of PA. Therefore, PA is a more efficient algorithm than Linear Programming [12]. We will explain the steps for this algorithm below:

4.5.2 Steps of Practical Algorithm

Set n=1, select the initial policy (0, M), and then proceed to policy improvement steps.

Step 1 Long-run expected value determination

At policy $Q^{(n)}$, applying P_{i,Q_n}, $V_M^{(n)}=0$ and $EC(0,Q^{(1)}) = EC(0,M)$ to solve Eq. (6), there will be M+1 equations and M+1 unknown values of $g^{(n)}(Q)$, $V_0(Q^{(n)})$, $V_1(Q^{(n)}),\cdots, V_{M-1}(Q^{(n)})$ will be obtained.

Step 2 Policy improvement

Get substituting solution of step 1 or 3 for Eq. (8) and calculate the minimized value of $G_n(i, Q)$ at state i of $Q^{(n)}$. The optimal solution $d_i(S^{(n)})= Q^{(n)}$ will be found and $(i, Q^{(n)})$ is the new policy and get into the next iteration step.

Step 3 Optimality judgment condition

When the current policy (i^*, Q^*) is the optimal solution for determining the reorder points $i^* + \lambda \cdot E(S)$ and $S^{(n)} = i^* + Q^*$, minimizes the expected average cost, but if this policy is identical to policy $(i^*, Q^{(n-1)*})$ or $G_n(i^*, Q^*) = g^{(n)}(Q)$, stop calculation. Otherwise get (i^*, Q^*) into Eq. (8), then reset $n= n+1$ and proceed policy improvement from 2^{nd} step to 3^{rd} step. The mean of the demand during period λ is given by $E(S)$.

$E(S) = \sum_{i=0}^{S} P_i \cdot \bar{S}_i \cdot \lambda / t_i$ ($\bar{S}_i$: the lower bounds of storage level in state i).

5. Linear programming for distribution center with deteriorating items

In this section, we point out how to make the adjustments required for other legitimate forms of the LP model.

5.1 Problem description

The problem is to determine which plan for assigning these demands $Q_{d,e}$ to the various supplier-retailer combinations would minimize the total distribution cost Z_e. The problem is actually a linear programming problem of the distribution problem type that called distributed programming problem.

For the distribution center's viewpoint, each node of retailers through MDP can gain the upper bound S_d of optimal policy. After deciding the storage upper bound $S_{d,e}$ of each retailer for item e, how to allot the item to the retailers for satisfying their demand should be considered. In this section we utilize the concept of network theory and linear programming method to resolve the problem. The constraint conditions are shown below:

- Balancing the available quantity in the distribution center;
- Balancing the demand quantity for each retailer;
- The available quantity of the supplier should not exceed the current storage amount;
- Replenishment amount + current storage amount ≤ the maximum

capability.

5.2 Model development

This problem can be circumvented in the following way. Construct an artificial problem that has same optimal solution as the real problem. Assign an overwhelming penalty to having ($Q_{d,e}$ - $X_{d,e}$) ≥0 by changing the objective function. The distribution problem is concerned with distributing any degenerate commodity from a supply center to any group of retailers in such a way as to minimize the total distribution cost. Therefore, it is not the general transportation problem. For many applications, the supply and demand quantities in the model (the $Q_{d,e}$ and $T_{d,e}$) have integer values, and implementation will require that the distribution quantities $X_{d,e}$ also have integer values.

Using this distributed programming we can find the upper bound of the supplier, and combine it with retailers' response demand to gain the optimal distribution amount of deteriorating items that distribution center allots to each retailer. The notations and model construction are showed below:

k Number of types of deteriorating items;

e Types of deteriorating items, for e=1,2,⋯,k (such as: 1 gasoline, 2 diesel, 3 kerosene, 4 special engine oil, 5 general engine oil, 6 ethane, …);

$X_{d,e}$ Distribution amount of item e for member d;

COT The capacity of a delivery tanker;

$T_{d,e}$ Current amount of item e for member d;

$W_{d,e}$ Impact degree of shortage of item e for member d, $W_{d,e}$ represents as money, we assumed M stands for a very large impact, where $W_{d,e}$ >>1;

$a_{d,e}$ Shortage frequency of item e for member d, it is a positive integer.

Objective function

$$Min \quad Z_e = \sum_{d=1}^{N} \begin{bmatrix} R_{d,e} + (a_{d,e}+1)\cdot \\ W_{d,e}\cdot b_{d,e}(Q_{d,e} - \mathrm{COT}\cdot X_{d,e}) + \\ (h_{d,e} + L_{d,e}\cdot\theta_{d,e} + C_{d,e})\cdot \mathrm{COT}\cdot X_{d,e} \end{bmatrix}$$

$$s.t \;\; 0 \le S_{d,e} - T_{d,e} = Q_{d,e},$$

$$0 \le \sum_{d=1}^{N} X_{d,e} \le T_{o,e}, \quad 0 \le X_{d,e} + T_{d,e} \le S_{d,e},$$

$$X_{d,e} \ge 0, \quad d = 1,2,\cdots,N, \quad e = 1,2,\cdots,k \qquad (9)$$

5.3 The procedure for preemptive distribution programming

The procedure finds an optimal solution for a preemptive distributed programming problem by solving just one linear programming model. Thus, the procedure is able to duplicate the work of the sequential procedure with just one run of the simplex method. To find optimal solutions is based on first-priority goals and breaks binds among these solutions are by considering lower-priority goals. The concept comes from the Big M method that we retain the symbolic quantity M in the sequence of simplex method.

The distributed programming formulation for the procedure with two priority levels would include all the goals in the usual model, but with basic penalty weights of $W_{d,e}$ and 1 assigned to deviations from first-priority and lower-priority goals, respectively. If different penalty weights are desired within the same priority level, these penalty weights then are multiplied by the individual penalty weights assigned within the level. There are more than two priority levels shown as

$$W^{1}{}_{d,e} \geq W^{2}{}_{d,e} \geq \ldots \geq W^{N-1}{}_{d,e} \geq 1.$$

Each coefficient in the objective function of each simplex tableau is now a linear function of all these quantities, where the multiplicative factor of $W^{1}{}_{d,e}$=*maximize* $\{(a_{d,e}+1)\cdot W_{d,e}$ of the item e for all $d\}$ is used to make the first priority decision. Accordingly that of $W^{k}{}_{d,e}$ is used to make the m th priority decision, m =1, 2,…,N-1. Then additive term is dealt with last. Mathematical-programming computer packages retain the exceptional computational efficiency to handle very large problem. The optimal distribution policy is solved by LINGO as shown in subsection 6.1. The preemptive distribution programming and its solution procedures provide an effective way dealing with the problems. The key of the procedure is introducing auxiliary variables that enable one to convert the problem to a linear programming format.

6. Case study

This research took an interest in the Taiwanese civil gas stations and its demand system, which contains three sections: Randomly generated test cases, empirical results observed under different items and computational experiments are demonstrated below:

6.1 Randomly generated test cases

In this research there is an oil DSC system which includes a single distribution center and a single supplier, two retailers and a single product. Four thousand randomly generated demand numbers with a mix of normal distribution and uniform distribution are used to illustrate that our proposed model is feasible and efficient. The unit cost is shown in Table 1, and state probability and the capacity of an oil tanker (*COT*) are shown in Table 2 ~4.

Table 1 Related unit cost for supplier and retailers.

Cost	Retailer 1	Retailer 2	Supplier 0
C	20	21	18
h	0.15	0.16	0.1
B	25	26	20
θ	0.04	0.05	0.02
L	10	10	10
R	1000	1000	10000
λ	0.5	1	0.5
t	1.5	3	3

Table 2 State probability of retailer 1

State	Storage	Number	Probability
0	0-10	0	0
1	11-1000	175	0.15
2	1001-2000	183	0.15
3	2001-3000	362	0.3
4	3001-4000	302	0.25
5	4001-5000	178	0.15

COT=10

Table 3 State probability of retailer 2.

State	Storage	Number	Probability
0	0-10	0	0
1	11-1000	123	0.1
2	1001-2000	237	0.2
3	2001-3000	302	0.25
4	3001-4000	295	0.25
5	4001-5000	178	0.15
6	5001-6000	65	0.05

COT=1000

Table 4 Joint probability of supplier

State	Storage	Number	Probability
0	0-10	0	0
1	11-2000	157	0.1
2	2001-4000	323	0.2
3	4001-6000	399	0.25
4	6001-8000	397	0.25
5	8001-10000	238	0.15
6	10001-12000	86	0.05

COT=2000

Stage 1

Substituting the values in Table 1 and 2 for Eq. (5), then a cost matrix $EC(i, Q)$ is obtained. Let $Q_{d,e}^{(n)}= Q^{(n)}$ and get cost matrix into Practical Algorithm step n=1, substitute initial value $(i, Q^{(n)})$ =(0,5000) for Eq. (8), then $EC(i,Q)$ =

$$\begin{bmatrix} 263500 & 211000 & 177332 & 159407 & 165633 & 187630 \\ 198500 & 153582 & 127745 & 121895 & 139743 & M \\ 107415 & 82828 & 81565 & 97338 & M & M \\ 34242 & 40480 & 59590 & M & M & M \\ 10810 & 29920 & M & M & M & M \\ 6638 & M & M & M & M & M \end{bmatrix}$$

$$g(Q^{(n)}) = 119527, V_0(Q^{(n)}) = 180993,$$
$$V_1(Q^{(n)}) = 146574, V_2(Q^{(n)}) = 106244,$$
$$V_3(Q^{(n)}) = 79333,\ V_4(Q^{(n)}) = 35489.$$

By substituting above values for Eq. (8) to solve $Q^{(n)}$, the cost matrix $G_n(i, Q)$ is obtained, $G_n(i^*, Q^*)$=105353 ≤ $g^{(n)}(Q)$= 119527. We can know $(i,Q^{(n)})$= (3,1000)≠ (0,5000), so reset $n = n +1$ and perform another iteration, substitute $(i,Q^{(n)})$= (3,1000) for Eq. (8), then $G_n(i,Q)$ =

$$\begin{bmatrix} 263500 & 211000 & 172169 & 143032 & 128845 & 300519 \\ 232919 & 182838 & 145789 & 119527 & 252631 & M \\ 177001 & 141202 & 119527 & 210226 & M & M \\ 119527 & 105353 & 172479 & M & M & M \\ 119527 & 156953 & M & M & M & M \\ 119526 & M & M & M & M & M \end{bmatrix}$$

$$g(Q^{(n)}) = 97016, V_0(Q^{(n)}) = 117292,$$
$$V_1(Q^{(n)}) = 133834, V_2(Q^{(n)}) = 93504,$$
$$V_3(Q^{(n)}) = 52419, \quad V_4(Q^{(n)}) = 22749.$$

By substituting above values for Eq. (8) to solve $Q^{(n)}$, the cost matrix $G_n(i,Q)$ is obtained.

$$\begin{bmatrix} 263500 & 211000 & 179813 & 158320 & 157296 & 278009 \\ 181958 & 139521 & 110116 & 97016 & 230121 & M \\ 133684 & 105529 & 97016 & 187716 & M & M \\ 98028 & 97016 & 149969 & M & M & M \\ 97016 & 120299 & M & M & M & M \\ 97016 & M & M & M & M & M \end{bmatrix}$$

We can know $(i,Q^{(n)})$= (3,1000)=$(i,Q^{(n-1)})$, and then stop the *PA*. Therefore, the optimal policy of retailer 1 is obtained and $E(S)$=701. The reorder state is $T_{1,e} \leq 3701$，optimal storage amount is $S_{1,e}$= 4000, and the *LEC* is $g^{(n)}(Q)$ =97016.

Therefore, by substituting the values in Table 1 and 3 for Eq. (5), the optimal policy $(i,Q^{(n)})$=(3,2000)=$(i,Q^{(n-1)})$ of retailer 2 is obtained and $E(S)$=767. The reorder state is $T_{2,e} \leq 3767$, optimal storage amount is $S_{2,e}$= 5000 and the *LEC* is $g^{(n)}(Q)$ = 106453.

$$g(Q^{(n)}) = 106453 \ , V_0(Q^{(n)}) = 114414 \ ,$$
$$V_1(Q^{(n)}) = 164598 \ , V_2(Q^{(n)}) = 121280 \ ,$$
$$V_3(Q^{(n)}) = 81882 \ , V_4(Q^{(n)}) = 48254 \ ,$$
$$V_5(Q^{(n)}) = 19973,$$

$$\begin{bmatrix} 357200 & 282000 & 227484 & 200381 & 195595 & 204799 & 329143 \\ 248516 & 182300 & 135301 & 111127 & 106453 & 275213 & M \\ 199484 & 149885 & 117515 & 106453 & 227117 & M & M \\ 135981 & 115311 & 106453 & 186531 & M & M & M \\ 107511 & 106453 & 153798 & M & M & M & M \\ 106453 & 128126 & M & M & M & M & M \\ 106453 & M & M & M & M & M & M \end{bmatrix}$$

Stage 2

Based on the replenishment amount for retailers' response to the supplier and the replenishment frequency gained, as shown in Table 4, we can solve the optimal policy for the supplier. Substituting the values in Table 1 and Table 4 for Eq. (5), then a cost matrix $EC(i, Q)$ is obtained. Get $EC(i, Q)$ into the Practical Algorithm step n=1, substitute initial value $(i,Q^{(n)})$=(0,12000) for Eq. (8), then $EC(i,Q)$ =

$$\begin{bmatrix} 558000 & 446000 & 358060 & 310780 & 305390 & 333600 & 379361 \\ 468000 & 362060 & 284420 & 249950 & 258180 & 297060 & M \\ 318120 & 236480 & 189650 & 188800 & 221700 & M & M \\ 150660 & 121830 & 124620 & 156440 & M & M & M \\ 54160 & 68950 & 102410 & M & M & M & M \\ 21430 & 58890 & M & M & M & M & M \\ 21460 & M & M & M & M & M & M \end{bmatrix}$$

$$g(Q^{(n)}) = 228357 \ , V_0(Q^{(n)}) = 357901 \ ,$$
$$V_1(Q^{(n)}) = 330441 \ , V_2(Q^{(n)}) = 224750 \ ,$$
$$V_3(Q^{(n)}) = 202321 \ , V_4(Q^{(n)}) = 134651 \ ,$$
$$V_5(Q^{(n)}) = 57380.$$

By substituting the above values for Eq. (8) to solve Q_n, a cost matrix $G_n(i,Q)$ is obtained, $G_n(i^*,Q^*)$=186606 ≤

$g^{(n)}(Q)$= 228357. We can know $(i,Q^{(n)})$= (3,4000)≠(0,12000), so reset $n = n + 1$ and perform another iteration, substitute $(i,Q^{(n)})$=(3,4000) for Eq. (8),

then $G_n(i,Q)$ =

$$\begin{bmatrix} 558000 & 446000 & 355314 & 291973 & 256337 & 240006 & 586258 \\ 495460 & 386774 & 293073 & 228357 & 192046 & 503957 & M \\ 448525 & 350824 & 273748 & 228357 & 428597 & M & M \\ 287433 & 228357 & 186606 & 363337 & M & M & M \\ 228357 & 198606 & 309307 & M & M & M & M \\ 228357 & 265787 & M & M & M & M & M \\ 228357 & M & M & M & M & M & M \end{bmatrix}$$

$g(Q^{(n)}) = 180885$, $V_0(Q^{(n)}) = 203686$, $V_1(Q^{(n)}) = 275260$, $V_2(Q^{(n)}) = 205880$, $V_3(Q^{(n)}) = 141700$, $V_4(Q^{(n)}) = 86030$, $V_5(Q^{(n)}) = 38510$.

By substituting above values for Eq. (8) to solve $Q^{(n)}$, then a cost matrix $G_n(i,Q)$ is obtained.

$$\begin{bmatrix} 558000 & 446000 & 365217 & 325314 & 317524 & 327879 & 538786 \\ 396426 & 297643 & 227380 & 190510 & 180885 & 456485 & M \\ 323083 & 248820 & 199590 & 180885 & 379345 & M & M \\ 227180 & 195950 & 180885 & 315865 & M & M & M \\ 183950 & 180885 & 261835 & M & M & M & M \\ 180885 & 218315 & M & M & M & M & M \\ 180885 & M & M & M & M & M & M \end{bmatrix}$$

We can know $(i,Q^{(n)})$= (3,4000)=(i,Q_{n-1}), and stop *PA*. Therefore, we derive the optimal policy of supplier and $E(Q)$ =767. The reorder state is $T_{0,e} \leq 6767$，optimal storage amount is $S_{0,e}$=10000 and the expected cost is $g^{(n)}(Q)$=180885.

Table 5 Oil current storage and demand amount.

Members	0	1	2
State	4	1	1
Storage	7500	500	500
Order amount	0	3500	4500
Backlog	0	0	2
Impact degree	M	1	2

Table 6 The optimal replenishment amount.

Members	Retailer 1	Retailer 2
Replenishment	3000	4500

Members	Supplier 0	Total cost
Replenishment	10000	458050

Stage 3

From stage 1 to stage 2, the optimal policies for the supplier and retailers are obtained. According to the current storage and demand amount at that time, we substitute the replenishment situation for the linear programming of Eq. (9) to gain the solution shown as Table 5. By substituting the values in Table 1 and 5 for Eq. (9), then the optimal replenishment policy is solved by LINGO as shown in Table 6. In this circumstance, retailer 1 and retailer 2 apply for 3500 liters and 4500 liters respectively, but the supplier only has 7500 liters can be distributed. After computing with our proposed Linear Programming process model, retailer 2 should be satisfied first, and retailer 1 will have 500 liters backlog replenishment.

6.2 Empirical results observed under different oils at civil gas station

Table 7 summarizes the descriptive statistics that collected oil data for 90 days from a civil gas station in Taiwan in 2009. The parameters of unit costs for the civil gas station are in Table 1, and the recorded position data of the oil meter serves as statistics for oil demands. The introduction of oil variety and computational experiments are shown in Table 8.

Table 7 State probability of the unleaded gasoline 95 & 98.

State	Storage 95	Number	Probability
0	0-10	0	0
1	11-1000	17	.19
2	1001-2000	41	.46
3	2001-3000	21	.23
4	3001-4000	11	.12
5	4001-5000	0	0

State	Storage 98	Number	Probability
0	0-10	0	0
1	11-1000	2	.02
2	1001-2000	21	.23
3	2001-3000	19	.21
4	3001-4000	40	.44
5	4001-5000	9	.1

Substituting the values in Table 1 and 7 for Eq. (5), then a cost matrix $C(i, Q)$ is obtained. Insert the cost matrix into Practical Algorithm step n=2, then the optimal policy of the civil gas station is obtained and $E(S_{95})$=428 and $E(S_{98})$=368. The reorder states are $T_{95} \leq 1428$ and $T_{98} \leq 3368$，optimal storage amounts are $S_{95} = 4000$ and $S_{98} = 4000$, and the expected costs are $g(Q_{95}) = 64425$ and $g(Q_{98}) = 116978$.

$$\begin{bmatrix} 249500 & 176500 & 136860 & 150611 & 158762 & 227492 \\ 149473 & 90833 & 69562 & 64425 & 177762 & M \\ 116605 & 87084 & 64425 & 135306 & M & M \\ 85084 & 64425 & 106391 & M & M & M \\ 64425 & 83875 & M & M & M & M \\ 64425 & M & M & M & M & M \end{bmatrix}$$

$$g(Q_{95}) = 64425, V_0(Q^{(n)}) = 58173,$$
$$V_1(Q^{(n)}) = 108200, V_2(Q^{(n)}) = 70288,$$
$$V_3(Q^{(n)}) = 47639,\ V_4(Q^{(n)}) = 18373.$$

$$\begin{bmatrix} 281500 & 235750 & 192581 & 172358 & 157726 & 303137 \\ 217994 & 175325 & 140296 & 116978 & 256129 & M \\ 144380 & 129851 & 116978 & 210898 & M & M \\ 120351 & 116978 & 172230 & M & M & M \\ 116978 & 138983 & M & M & M & M \\ 116978 & M & M & M & M & M \end{bmatrix}$$

$$g(Q_{98}) = 116978, V_0(Q^{(n)}) = 1424393,$$
$$V_1(Q^{(n)}) = 145945, V_2(Q^{(n)}) = 95651,$$
$$V_3(Q^{(n)}) = 57539,\ V_4(Q^{(n)}) = 19041.$$

6.3 Computational experiments demonstration

The computational experiments demonstrate the correctness of our theory in this section. According to section 5.1 and 5.2, we divide the administrators into two kinds: C1 is an optimistic manager, who wants to increase order amount or reorder point in order to improve inventory level; C2 is a pessimistic manager who has reduced order amount or postponed replenishment and caused the inventory level to drop. We compared the respective results in Table 8. At present, the civil gas stations adopt the proportion rule to control the inventory position by 60%. In other words, the manager issued an order of full-inventory at once when the inventory level has decreased by 40%.

Table 8 Comparison of the respective results of part A, B, and C.

	Part A retailer & C						Part B civil gasoline & C			
Strategies	Optimal-1	Optimal-2	C1-1	C1-2	C2-1	C2-2	Optimal 98	Optimal 95	60% rule 98	60% rule 95
i	3701	3767	3701 ≤	3767 ≤	3701>	3676>	3368	1428	3000<	3000<
S	4000	5000	4000<	5000<	4000>	5000>	4000	4000	5000	5000
PRT	1	2	1 ≤	1 ≤	1 ≤	1 ≤	1	2	1 ≤	1 ≤
LEC	97016 = g*	106453 (g*)	120299~ 278009	153798~ 392143	105529~ 211000	115311~ 357200	116978 (g*)	64425 (g*)	172230~ 210898	106391~ 135306
€C	LEC - g* =0	0	23283~ 180993	47345~ 285690	8513~ 113984	8858~ 250747	0	0	55252~ 93920	41966~ 70881
€C/g^*	0	0	24%~ 186.56%	44.48~ 268.37%	8.78%~ 117.49%	8.32%~ 135.54%	0	0	47.23%~ 80.29%	65.14%~ 110.02%

According to Table 8, we were able to know that the control of the inventory level is extremely important. The wrong strategies of inventory have already caused the *EC* to rise 47.23%~110.02% in the civil gas station. Furthermore, according to both inventory strategies of C1 and C2, they have risen 24%~268.37% and 8.32%~ 135.54% respectively, in their weighty *EC*. When the periodic review time (*PRT*= *j*-*i*) and maximum inventory level (*MIL*) *S* are increased, it brings with it a massive drop in competitiveness.

6.4 Sensitivity analysis

In this section, the sensitivity of parameters involved in the model will be analyzed. To do so, we change the value of one parameter and keep the other parameters at their base values. They are shown in Tables 9 and10. The qualitative effect of changing each parameter on the *EC*, reorder state (*RS*) *i*, *PRT* and maximum inventory level (*MIL*) $S_{d,e}$ are summarized in Tables 11-13.

Table 9 Value of state probability $P(S_i)$ where they are changed in the DSC

Members	Retailer 1		Retailer 2		Supplier 0	
State	Low	High	Low	High	Low	High
0	0.45	0	0.5	0	0	0
1	0.3	0	0.2	0	0.5	0
2	0.2	0	0.2	0	0.18	0
3	0.05	0	0.1	0	0.14	0.1
4	0	0.4	0	0	0.1	0.2
5	0	0.6	0	0.3	0.08	0.3
6	0	0	0	0.7	0	0.4

Table 10 Value of cost and COT parameters where they are changed in the DSC

Members	Retailer 1		Retailer 2		Supplier 0	
Parameter	Increase	Decrease	Increase	Decrease	Increase	Decrease
C	64	0.2	65	0.21	72	0.18
h	15	0	16	0	10	0.01
L	500	0	600	6.8	1500	0
θ	0.8	0.0004	0.7	0.025	0.9	0.0002
b	75	10	78	13	80	6
COT	1500	500	1500	500	3000	1000

Table 11 Sensitivity analyses of the change of state probability P(S)

Members	Retailer 1		Retailer 2		Supplier 0	
Results	Low	High	Low	High	Low	High
RS	1(↓)	5(↑)	1(↓)	6(↑)	1(↓)	6(↑)
MSL	3000(↓)	5000(↑)	3000(↓)	6000(↑)	5(–)	12000(↑)
PRT	2(↑)	0(↓)	2(–)	0(↓)	4(↑)	0(↓)
EC	50187(↓)	189173(↑)	82631(↓)	241920(↑)	104053(↓)	307091(↑)

(↑):Shows increase; (–):Shows no change; (↓):Shows decrease

Table 12 Sensitivity analyses of the change of cost parameters

Members		Retailer 1		Retailer 2		Supplier 0	
Parameter	Results	Increase	Decrease	Increase	Decrease	Increase	Decrease
C	RS	1(↓)	5(↑)	1(↓)	6(↑)	1(↓)	6(↑)
	MSL	1000(↓)	5000(↑)	3000(↓)	6000(↑)	2000(↓)	12000(↑)
	PRT	0(↓)	0(↓)	2(–)	0(↓)	0(↓)	0(↓)
	EC	184219 (↑)	42576(↓)	209017(↑)	48141 (↓)	307982(↑)	69642(↓)
h	RS	0(↓)	5(↑)	1(↓)	6(↑)	1(↓)	6(↑)
	MSL	3000(↓)	5000(↑)	4000(↓)	6000(↑)	4000(↓)	12000(↑)
	PRT	3(↑)	0(↓)	3(↑)	0(↓)	2(–)	0(↓)
	EC	164666(↑)	96253(↓)	197453(↑)	101383(↓)	316307(↑)	176700(↓)
L	RS	1(↓)	5(↑)	0(↓)	6(↑)	0(↓)	6(↑)
	MSL	3000(↓)	5000(↑)	3000(↓)	6000(↑)	4000(↓)	12000(↑)
	PRT	2(↑)	0(↓)	3(↑)	0(↓)	2(–)	0(↓)
	EC	173005(↑)	86752(↓)	215651(↑)	101383(↓)	358760(↑)	169683(↓)
θ	RS	0(↓)	5(↑)	1(↓)	6(↑)	1(↓)	6(↑)
	MSL	4000(–)	5000(↑)	4000(↓)	6000(↑)	8000(↓)	12000(↑)

	PRT	4(↑)	0(↓)	3(↑)	0(↓)	3(↓)	0(↓)
	EC	158701 (↑)	86769(↓)	177389(↑)	100588(↓)	308116(↑)	174779(↓)
b	RS	5(↑)	1(↓)	6(↑)	1(↓)	6(↑)	1(↓)
	MSL	5000(↑)	3000(↓)	6000(↑)	3000(↓)	12000(↑)	4000(↓)
	PRT	0(↓)	2(↑)	0(↓)	2(–)	0(↓)	1(↓)
	EC	174660(↑)	67561 (↓)	186623(↑)	75331(↓)	363956(↑)	103527(↓)

(↑):Shows increase; (–):Shows no change; (↓):Shows decrease

Table 13 Sensitivity analyses of the change of the COT parameters

Members		Retailer 1		Retailer 2		Supplier 0	
Parameter	Results	Increase	Decrease	Increase	Decrease	Increase	Decrease
COT	RS	3000(–)	2500(↓)	1500(↓)	500(↓)	6000(–)	4000(↓)
	MSL	4500(↑)	4000(–)	4500(↓)	6000(↑)	9000(↓)	9000(↓)
	PRT	1500(↑)	1500(↑)	3000(–)	3500(↑)	3000(↓)	5000(↑)
	EC	117147 (↑)	79535(↓)	122171(↑)	99280 (↓)	205498(↑)	179425(↓)

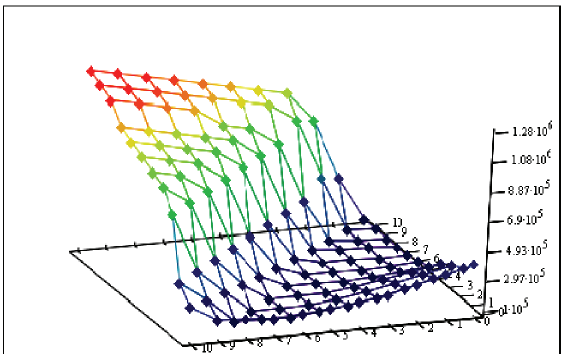

Figure 3 Diagram of the EAC of the unleaded gasoline 98 at the civil gas station.

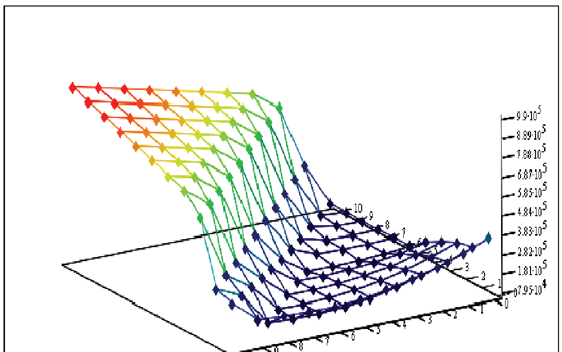
Figure 4 Diagram of the expected average cost matrix of retailer 1 in the DSC

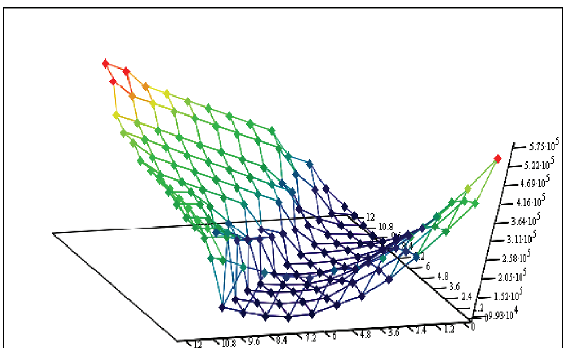
Figure 5 Diagram of the expected average cost matrix of retailer 2 in the DSC

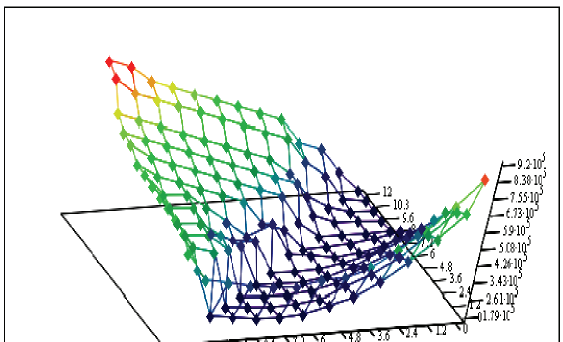
Figure 6 The expected average cost of distribution center 0 in the DSC

Finally, descriptions of the above results in Table 11~13 and Figure 3~6 imply that the constant change toward replenishment strategies is to the advantage of the DSC competition to reduce costs (such as the *EC*, the purchase cost, the holding cost, the deteriorating cost and shortage cost). The manager can reduce RS and cause EC to drop when the capacity of oil tanker (*COT*) drops and vice versa. As the manager is expecting a drop in the market price, one thing leads to another and he reduces the RS and the MSL. We provided plenty of information from sensitivity analyses to managerial changes of the replenishment strategies, and they occur without difficulty in real-time. For example, a producer can be suitably modified by 3000-liters and 2000-liters of oil tankers in real-time to satisfy the supplier under high frequency (i.e. low-COT) demand, as shown in Table 13. In addition, Figure 4~6 show EC evaluation results under various states that are used to illustrate that our proposed model is feasible and efficient.

7. Discussion

We summarize the descriptive statistics as follows:

—When *MSL* doesn't change, the change of *RS* and *PRT* are inversely proportional to each other.

—If *MSL* changes, the change of *RS* and *PRT* will be directly proportional to each other.

—When *PRT* is affected by the changes of *RS* and *MSL*, and if the change of *RS* is greater than *MSL*, then the change of *RS* and *PRT* can be inversely proportional to each other, directly proportional, or have no change.

—According to recursive equations, we discovered that with the rapid decrease of V_i^n, the *EC* alternation works better than *EC* in increasing calculation speed.

In this study, the proposed inventory model considered a single supplier, multiple retailers and various products with deteriorating item in a distributed supply chain. We utilized discrete-time *MDP* and *PA* to develop an efficient algorithm for finding the optimal reorder states and replenishment quantity to minimize the *EC*. Therefore, the control of inventory level is extremely important. The wrong strategies of inventory have risen 47.23%~110.02% *EC* on the civil gas station. Furthermore, the optimistic manager and the pessimistic manager also have risen 24%~268.37% and

8.32%~135.54% of their weighty *EC* in this paper. Efficient is the key advantage of *PA*, because it usually reaches an optimal policy in a relatively small number of iterations. By this inventory replenishment method, the members of the supply chain can improve distribution efficiency and reduce logistic cost with little calculation tasks. Each member of the supply chain can also decide its own optimal reorder states and replenishment quantity individually for minimizing total operating costs. From Figure 3~6 *EC* evaluation results under various states are used to illustrate that our proposed model is feasible and efficient.

8. Conclusion and future extensions

The objective of this paper is to solve the problem of merchandise management in DSC system by applying MDP, and to simplify MDP for the manager to use efficiently. Its key factors are state partition and demand probability obtaining. They have been proved and skills are offered in section 6 case study. Its advantages are using simple matrix calculation and modeling process. Through the linked information technology with this paper's viewpoints and models, we find that to obtain customer demand, stationary distribution, reorder point, order quantity and expected cost, the manager only needs to enter the inventory level when parameter dates are not changed. This paper's viewpoints and models also suit for DSC system using other random demand items. They can also be extended to management system using multi-echelon and multi-merchandise.

In addition, we also analyzed how to distribute under the condition of insufficient supply from the supplier in a non-cooperative behavior distributed supply chain system. Finally, we contribute another possible main benefit for the supplier and the producer. If the supplier can control its supply quantity and reduce its backlogs, then the lead-time variability can be mastered.

For a multiple inventory manager, the ultimate goal is to obtain a system that can offer decision support in the process of replenishment and control. This is because not only there is a complexity of the problem domain, but also there is difficulty in obtaining help from the information ability. This is the reason why we want to develop a methodology which incorporates decision support systems to simulate the inventory operation process in the decision making process of replenishment and control. All of these could be directions of future research.

Acknowledgments

The author would like to thank the Editor-in-Chief and Referees for their comments and suggestions that are the mother of innovation.

References

[1] Aggarwal V, Bahari-Kashani H., 1991. Synchonized production policies for deteriorating items in a declining market. IIE Trnsc. 23 (2), 185-197.

[2] Chang HJ, Dye CY., 2000. An EOQ model with deteriorating items in response to a temporary sale price. Production Planning & Control 11 (5), 464-473.

[3] Chazan D, Gal S., 1977. A Markovian Model for A Perishable Product Inventory. Management Science 23 (5), 512-521.

[4] Cheng F, Sethi SP., 1999. A periodic review inventory model with demand influenced by promotion decisions. Management Science 45 (11), 1510–1523.

[5] Covert RP, Philip GC., 1973. An EOQ model for items with Weibull distribution deterioration. AIIE Transactions 5 (4), 323-326.

[6] Feng Y, Cai XQ, Tu FS., 2008. Deteriorating inventory model under two-echelon integrated supply chain environment. Computer Integrated Manufacturing 14 (2), 300-305.

[7] Ghare PM, Schrader GF., 1963. A model for exponentially decaying inventory. Journal of Industrial Engineering 14 (5), 238-243.

[8] Goswami A, Chaudhuri KS., 1992. Variations of order-level inventory models for deteriorating items. International Journal of Production Economics 27 (2), 111-117.

[9] Goyal SK, Giri BC., 2003. The production-inventory problem of a product with time varying demand, production and deterioration rates. European Journal of Operational Research 147 (3), 549–557.

[10] Graves S., 1996. A multi-echelon inventory model with fixed replenishment intervals. Management Sciences 42 (1), 1–18.

[11] Gupta R, and Vrat P., 1986. Inventory models with multi-items under constraint systems for stock dependent consumption rate. Operations Research 24, 41-42.

[12] Hillier FS, Lieberman G J., 1997.

Introduction to Operations Research", 6th ed., Singapore: MCGRW-HiLL.

[13] Howard, R., 1960. Dynamic Programming and Markov Process. Cambridge, Mass.

[14] Huang JY, Yao MJ., 2005. On optimally coordinating inventory for a deteriorating item in a supply chain system with a single vendor and multiple buyers. Journal of the Chinese Institute of Industrial Engineers 22 (6), 473-484.

[15] Iyer AV, Ye J., 2000. Assessing the value of information sharing in a promotional retail environment. Manufacturing & Service Operations Management 2 (2), 128–143.

[16] Lin C, Lin Y., 2007. A cooperative inventory policy with deteriorating items for a two-echelon model. European Journal of Operational Research 178 (1), 92-111.

[17] Netessine S, Rudi N, Wang Y., 2006. Inventory competition and incentives to back-order. IIE Transactions 38 (11), 883–902.

[18] Papachristos S, Skouri K., 2000. An optimal replenishment policy for deteriorating items with time-varying demand and partial—exponential type—backlogging. Operations Research Letters 27 (4), 175–184.

[19] Ross, S. M., 1968. Arbitrary start Markovian decision processes, Ann. Math. Statistic 39, 2118-2122.

[20] Smith SA, Agrawal N., 2000. Management of multi-item retail inventory systems with demand substitution. Operations Research 48 (1), 50–64.

[21] Wu KS., 2002. EOQ inventory model for items with Weibull distribution deterioration, time-varying demand and partial backlogging. International Journal of Systems Science 33 (5), 323-329.

[22] Zhang T, Lianga L, Yua YG, Yua Y., 2007. An integrated vendor-managed inventory model for a two-echelon system with order cost reduction. International Journal of Production Economics 109 (1-2), 241–253.

工業常用吸附劑之熱分析研究

蔣忠誠、陳耀漢、吳勝宏、徐啟銘

摘 要

近十幾年來多孔洞性材料因具有極高的表面積，被廣泛應用為吸附劑 (adsorbent) 、觸媒 (catalyst) 及離子交換劑 (ion exchange) 等技術層面上以去除空氣或水中污染物質。針對工業界常用的吸附劑包含沸石 (zeolite) 、活性碳 (activated carbon) 、矽膠 (silica gel) 以及活性氧化鋁 (activated alumina) ，可依不同性質使用於水或空氣中吸附有機污染物、重金屬污染物等，如：揮發性有機物 (volatile organic compounds, VOCs) 、二氧化碳 (carbon dioxide, CO2) 、水中之餘氯等。

目前許多專家學者研究均針對於吸附劑之吸附效率、脫附效率與標的污染物，但卻僅有少數研究針吸附劑本質安全性及再生性加以評估。本研究將針對工業界常用四種吸附劑運用熱分析技術加以分析其材料本身熱穩定性及安定性。

本研究使用微差掃描熱卡計 (differential scanning calorimetry, DSC) 以及熱重分析儀 (thermogravimetric analyzer, TGA) 針對沸石、活性碳、矽膠以及活氧化鋁進行材料本質安全及再生性脫附處理時材料本身之安全條件分析與測試，以提供相關研究與應用之參考並適當選擇吸附劑使用。

本研究中得知，活性碳具有高的放熱能量並不適合做為高溫吸脫附之材質儘可能成為前處理或後處理的吸附材料。活性氧化鋁與矽膠之吸附操作溫度範圍為 30－150^{o}C 與 30－150^{o}C，而沸石則為 30－150^{o}C。活性碳則於 500°C 後會產生熱危害 (thermal hazard)。活性氧化鋁、沸石、矽膠本身皆不具有放熱效應 (exothermic effect)，可安心使用於相關工業吸脫附製程，但使用這些材料吸附相關汙染物時仍需注意汙染物之燃燒性 (flammable) 與反應性 (reactivity)。

關鍵詞：吸附劑、多孔性沸石、活性碳、微差掃描熱卡計、熱重分析儀。

蔣忠誠：修平科技大學電機工程系助理教授
陳耀漢：吳鳳科技大學消防學系助理教授
吳勝宏：國立雲林科技大學通識中心講師
徐啟銘：國立雲林科技大學環境與安全衛生工程系教授
投稿日期：99 年 8 月 31 日　接受刊登日期：100 年 3 月 14 日

Thermal analyses and safety evaluation of Industrial adsorbents in industry

Chung-Cheng Chiang, Yao-Han Chen, Sheng-Hung Wu, Chi-Min Shu

Abstract

Industrial material including zeolite, activated carbon, activated alumina, silica gel, etc are widely used as adsorbents for volatile organic compounds (VOCs), carbon dioxide (CO2) or residual chlorine in air or water adsorption, catalyst and ion exchange because of its high surface area. Differential scanning calorimetry (DSC) and thermogravimetric analyzer (TGA) were applied to determine and analyze thermal hazard and safety of four adsorbents for control their regenerative process and provide a reference for relevant research and application.

The best operating temperature range of zeolite, activated alumina and silica gel were discovered to be 30－150oC in this study. According to the experimental results, zeolite is an adsorbent with low cost, good structural stability and better adsorption efficiency in industries. Thermal hazard of activated carbon was investigated occurring after 500°C of process temperature.

Keywords：adsorbent, zeolite, activated carbon, differential scanning calorimetry (DSC), thermogravimetric analyzer (TGA)

Chung-Cheng Chiang, Assistant Professor, Department of Electrical Engineering, Hsiuping University of Science and Technology (HUST).
Yao-Han Chen, Assistant Professor, Department of Fire Science, WuFeng University.
Sheng-Hung Wu, Lecturer, General Educational Center, National Yunlin University of Science & Technology (NYUST)
Chi-Min Shu, Professor, Institute of Safety, Health, and Environmental Engineering, National Yunlin University of Science & Technology (NYUST).
Received 31 August 2010; accepted 14 March 2011

一、前言

近數十幾年來台灣地區工商業發達，無論於空氣或水質污染皆大幅上昇，在許多污染的處理技術上，吸附劑皆佔有很重要的地位。

1970年代，各國開始採用活性碳 (activated carbon, AC)、沸石 (zeolite)、活性氧化鋁 (activated alumina)、矽膠 (silica gel) 以及氧化鎂 (MgO) 等乾濕吸附方法處理硫烟氣，甚至運用於處理揮發性有機物 (volatile organic compounds, VOCs)，如甲苯 (benzene)、丙酮 (acetone) 等 [1]。

目前許多專家學者研究均針對於吸附劑之吸附效率、脫附效率與標的污染物，但卻僅有少數研究針對吸附劑本質安全性及脫附再生性安全評估與預防。

沸石轉輪製程中置入大量沸石並將轉輪分成幾個區塊，其中包含汙染物吸附區、汙染物脫附區 (再生性脫附區域)。當轉輪走到吸附區時，工業氣體汙染物則會穿過沸石進行吸附行為，並經過一段時間後，轉輪轉至另一吸附區繼續進行吸附行為，但剛吸飽汙染物之沸石區塊則轉至脫附再生區以高溫進行脫附且進入濃縮汙染物階段。一般性吸附時並需考量吸附材質本身與汙染物、氧氣、溫度是否有其危險性或不相容性，而再生性脫附時則考量氧氣濃度是否達到燃燒界限 (flammable limit) 內、再生性溫度、吸附材料水氣問題所引發之燃燒、火災，甚至爆炸事故 [2]。

本研究的主要目的在於應用四大工業界常用吸附劑以熱卡計加以評估其材料本身吸放熱行為，提供給工業界較好的吸附劑材料選擇並防止材料本身所引起之熱危害或反應。沸石屬於多孔性物質，因具有極高的表面積，而被廣泛的應用作為吸附劑、觸媒及觸媒載體並且對不同有機物質之吸附行為與物種之極性、分子量，有著絕對之關係，沸石之矽鋁比與孔洞大小亦有相對的影響 [3–5]。活性碳為多孔性碳體之集合名稱，主要是由木頭、木屑、水果殼或煤炭等物質經高溫 (600–800°C) 乾餾，將含碳物質碳化 (carbonization) 後，使其分解形成低分子性的碳氫化合物和多孔性的碳殘留物，再通以熱空氣或水蒸氣加以活性化。活性碳的吸附容量可以有效的從廢水中去除 COD、色度、酚類、氯酚類及臭味物質等，活性碳因具有特殊的表面物化性質，於焚化系統空氣污染防治中，多應用於有機物的去除，活性碳具有大的比表面積、多孔性的結構，與表面含有多種的官能基位等性質，對於活性碳的吸附特性，影響甚大 [6–10]。

活性氧化鋁 (activated alumina) 具有特殊的多孔性結構，吸濕能力強，可承

受急遽的溫度變化 [11],結構安定性佳，即使浸泡於水中也不會收縮、膨脹、軟化或分解,最常應用於乾燥機內的吸附床，可乾燥各式各樣的氣體及液體,如：乙炔 (acetylene)、甲烷 (methane)、苯 (benzene) 等,並可有效去除某些有害的酸性物質，藉以保護昂貴設備。

氧化矽即矽膠 (silica gel),此為一種非晶型固體 (amorphous form),的 $SiO_2 \cdot xH_2O$ 乃是矽酸 (silicic acid) 經縮合作用形成 Si-O-Si (siloxane) 之半聚合體，之後再形成水凝膠 (hydrogel),而生成之凝膠。在適當之控制條件下可具有高度多孔性結構且表面積極高。矽膠吸濕力強，吸濕容量大,吸濕後不膨脹,仍然保持乾燥狀態，無毒、無腐蝕性，為國家標準 (Chinese National Standards, CNS) 唯一具有標準規範之乾燥劑。一般而言,加熱到 390 度時只有物理吸附之水份被趕出，超過此溫度則造成表面之矽羥基脫水。

二、研究方法與設備

1. 樣本

沸石為自製材料，運用二氧化矽 (SiO_2) 混合矽鋁酸鈉 (sodium silicoaluminate) (Si/Al 比為 30) 並於混合時加入氫氧化鈉水溶液 (NaOH) 加以成型後，置入烘箱中以 100°C 烘乾八小時後即為工業用沸石,其吸附表面積大約為 400 m^2 g^{-1} [2]。活性碳 (activated carbon)、矽膠 (silica gel) 以及活性氧化鋁 (activated alumina) 直接向元虹儀器有限公司購買標準品。

2. 儀器設備

(1) 微差掃描熱卡計

微差掃描熱卡計 (differential scanning calorimetry, DSC) 為瑞士商梅特勒托利多股份有限公司所出產儀器,用以測量物質精細的熱量變化與溫度之間的關係。目前普遍使用的微差掃描熱卡計以熱流式 (heat-flux) 為主。其原理乃是將參考體與樣品放置於加熱爐中,加熱爐四周佈有一組加熱器用以控制加熱爐溫度。在參考體與樣品下方有一熱流感溫體 (thermal resistance material),熱流感溫體上有一對熱電偶 (thermocouple) 可以偵測出參考體與樣品間的溫度差。當樣品昇溫到轉移點如晶態轉變、熔點、沸點或者產生熱分解反應,此時加熱器所供應之能量 (mW) 為樣品所吸收（吸熱反應），或樣品釋放能量（放熱反應）均能使樣品與參考體間的溫度不再維持平衡,而有熱流的產生。此種差異對溫度的關係圖,即該樣品的熱譜圖 (thermoanalytical curves)。本研究溫度範圍以 30 至 600°C 為主，其掃描速率為每分鐘 4°C [2]。

(2) 熱重分析儀

熱重分析儀 (thermogravimetric analyzer, TGA) 出產於 TA 儀器公司，其熱重量測定是加熱時反應導致樣品質量的變化而加以連續測定之方法。換言之，熱重量測定即是以程式控制調節物質之溫度，使其連續變化再將其物質重量以溫度函數加以測定之方法，其結果之紀錄即為熱重量曲線。

大部份重量測定法之高溫爐其溫度範圍是從室溫到 1,500°C。通常高溫爐之加熱及冷卻速率可自行選擇。隨溫度昇高，高溫爐外部需絕緣及冷卻，以避免將熱傳導至天秤。通常使用氮氣或氬氣淨化高溫爐，以防止樣品氧化。

本研究之 TGA 使用白金秤盤量秤樣品之重量，以得知實驗過程中重量損失百分比。TGA 內之懸吊臂乃由耐高溫之石英製成，此精密懸吊臂懸掛在天秤與加熱爐之間，其末端連接著白金秤盤，加熱爐之昇溫速率可從 0.1–200°C min–1，而加熱爐之昇溫範圍可從 25–1,000°C。本研究溫度範圍以 30 至 600°C 為主，其掃描速率為每分鐘 4°C。

三、結果與討論

1. TGA 試驗之結果

四種吸附劑於氮氣 (無氧下) 中之熱重損失比較如圖 1 所示，因四種熱重損失率分別為 95 (沸石)、92 (矽膠)、86 (活性氧化鋁) 以及 85% (活性碳)，可由圖譜瞭解於 100°C 時四種吸附劑皆有熱重損失情形，表示本身於空氣中皆有吸水氣效應。但超過 500°C 後僅有沸石未有第二階段熱重損失，第二階段熱重損失則代表可能結構性有所破壞導致有物質釋出。可得知沸石於熱環境吸脫附時有較佳的行為。由圖 2 顯示可得知，四種吸附劑於空氣中燃燒之情況，其中顯示活性碳於空氣中燃燒情形較為嚴重，活性碳超過 500°C 則產生燃燒現象，快速燃燒下可透過 TGA 圖譜瞭解熱重損失非常明顯，最後僅剩下一些碳黑。沸石、矽膠、活性氧化鋁於空氣載體下並未發生燃燒現象，可運用於工業高溫吸脫附製程。

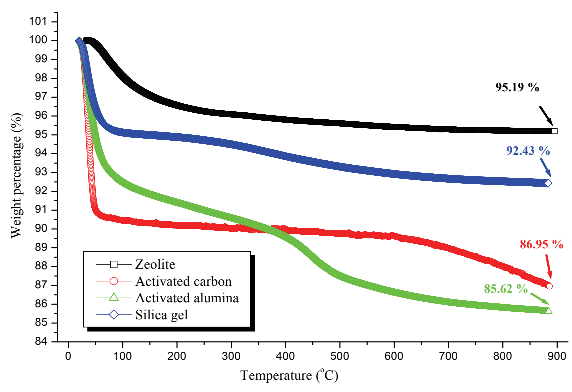

圖 1 運用 TGA 測得四種吸附劑於氮氣中之熱重分析圖

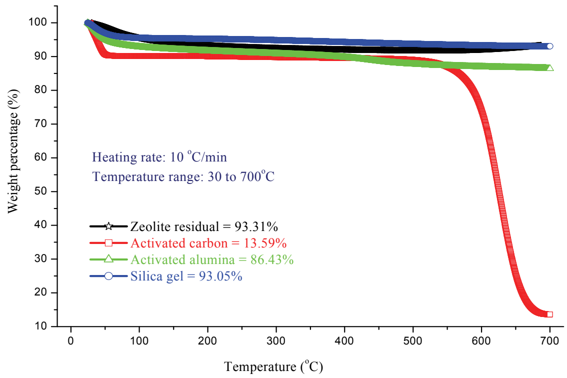

圖 2 運用 TGA 測得四種吸附劑於空氣中之熱重分析圖

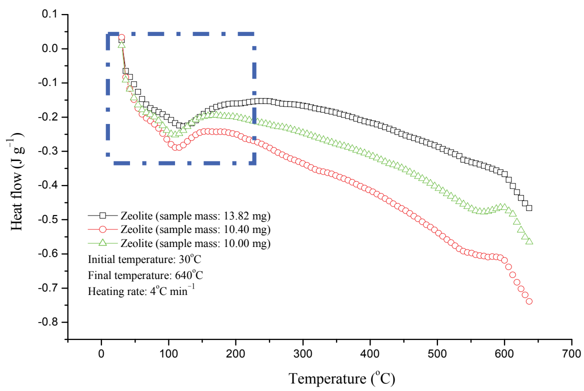

圖 3 沸石之重複性實驗

2. DSC 昇溫掃描熱分析結果

(1).沸石

本研究首先採用微差掃描熱卡計 (DSC) 進行吸附材料之基礎熱測試，以瞭解沸石等吸附劑之基礎熱特性。首先將自製之沸石進行熱重複性測試，以檢視實驗之可信度。

由圖 3 可得知，運用 DSC 以 4°C min–1 掃描速率下分別呈現相同熱分解狀況，可知沸石結構於 30–150°C 間有一只吸熱波峯 (endothermic reaction)。由此圖可知沸石為一穩定性極高之吸附劑。

(2) 活性碳

於先前已分別做過活性碳於各種不同溫度之恆溫烘箱試驗，以及運用 TGA 測得活性碳於不同氣體中之結構穩定性，並且可知活性碳於烘箱測試中，一旦高於 400°C會有燃燒之現象，因此接著，再使用微差掃描熱卡計測其是否有吸熱或放熱行為。由 DSC 測得如圖 4、5 所示。

於各種不同的昇溫速率下，顯示出活性碳於 30–100°C 有一只吸熱波峯，與 TGA 測得相符，而於 4, 6 及 10°C 昇溫時，因昇溫速率大而產生熱延遲現象，因此僅觀察出圖譜於 400°C 後，其熱流有上昇之現象，而使用 1°C 昇溫時，即能觀察出活性碳整體放熱行為，其於 300°C 開始即有放熱之現象。

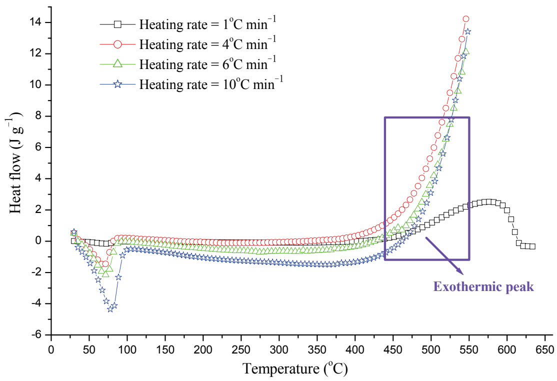

圖 4 以 DSC 進行不同昇溫速率活性碳之熱分析

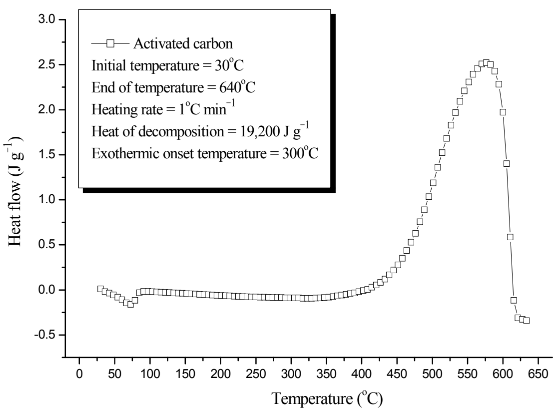

圖 5 運用 DSC 測得活性碳之熱譜圖(昇溫速率=1°C min－1)

(3) 活性氧化鋁

由圖 6 所示，於不同昇溫速率下，由 DSC 測得活性氧化鋁有兩只吸熱波峯，分別於 30–150°C 及 350–500°C 之間，而因其昇溫速率大小，可觀察到其波峯於昇溫速率較大時，有熱延遲之現象，此外並無其他放熱波峯。

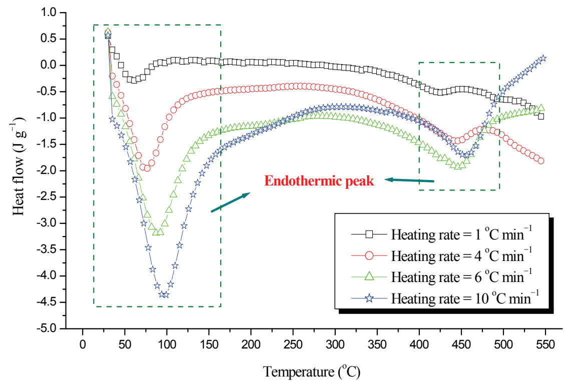

圖 6 運用 DSC 於不同昇溫速率下測得活性氧化鋁之熱譜圖

(4) 矽膠

由圖 7 將四種吸附劑之 DSC 圖譜做比較可知，僅有活性碳於 400°C 有放熱的現象，其他三種吸附劑安全性質良好，僅有於 100°C 時有吸附現象。

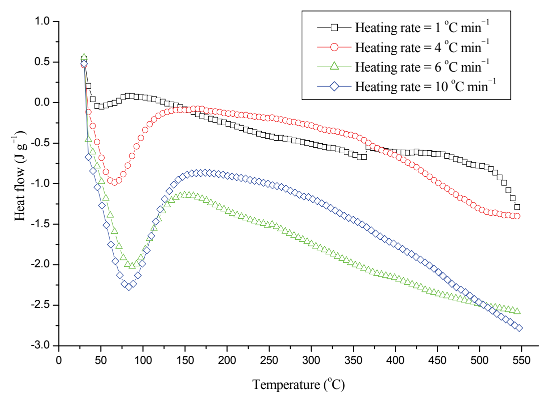

圖 7 運用 DSC 於不同昇溫速率下測得矽膠之熱譜圖

五、結論

沸石材料穩定度極佳，但於 100°C 左右有一只吸熱波峯，其原因為沸石可於室溫下吸附空氣中水分或雜質，結果發現沸石有一只波峯，顯示極易吸附與反應。因此於操作吸附污染物時，須先進行超過 100°C 以上之加熱脫附為必要之流程，以提昇其吸附效率。由 TGA 以及 DSC 之測試活性氧化鋁，可知其吸熱波峯與裂解皆分為兩階段，其結構穩定性相當良好，亦不會產生任何熱危害，也因其兩段之吸熱波峯，30–150°C 及 350–500°C，對於吸附材料之吸附操作溫度範圍為 30–150°C 時效率較高，脫附溫度範圍則為 150–350°C 之間效率較好。矽膠亦為一穩定且無危害之吸附劑，其適當之吸附操作溫度約 30–150°C，脫附溫度範圍為 150–280°C。相較於四種吸附劑之熱穩定性而言，活性碳則於 500°C 後會產生熱危害 (thermal hazard)。

六、參考文獻

[1] 翁瑞 (2001)，環境材料學。新竹：清華大學。

[2] Su, C. H., Wu, S. H., Shen, S. J., Shiue, G. Y., Wang, Y. W. & Shu, C. M. (2009). "Thermal characteristics and regeneration analyses of adsorbents by differential scanning calorimetry and scanning electron microscope", Journal of Thermal Analysis and Calorimetry, 96, 765–769.

[3] Baerheim, S. A. and Verpoorte, R. (1983). "Chromatography of alkaloids: Thin-layer chromatography", *Journal of Chromatography Library*, 23, 35.

[4] Mansoor, M. A. and Beverly, J. S. (2003). Applied Physical Pharmacy. New York: McGraw-Hill.

[5] Yuranov, I., Renken, A. and Kiwi, M. L. (2005). "Zeolite/sintered metal fibers composites as effective structured catalysts", Applied Catalysis A: General, 281, 55–60.

[6] 吳萬全 (2001)，活性碳。台灣鑛業，53 (3)，37–51。

[7] Boehm, H. P. (1994). "Some aspects of the surface chemistry of carbon blacks and other carbons", Carbon, 32, 759–769.

[8] Corapcioglu, M. O. & Huang, C. P. (1987). "The surface acidity and characterization of some commercial activated carbon", Carbon, 25, 569.

[9] 謝建德 (1998)，活性碳孔隙結構與製備條件對液相吸附的影響。中原大學化學工程學系研究所碩士

論文。全國博碩士論文資訊網，086CYC0063001。

[10] 周佳慧 (2001)，活性碳孔洞結構對不同氣體有機物吸附之影響。國立成功大學化學工程學系碩士論文。全國博碩士論文資訊網，089NCKU0063078。

[11] Ankur, S. and Vimal, C. S. (2009). “Adsorptive desulfurization by activated alumina”, Journal of Hazardous Materials, 170, 1133–1140.

A Nonlinear programming method for time-optimal control of an omni-directional mobile robot

Shi-Min Wang, Chia-Ju Wu, Jia-Yan Wei

Abstract

The time-optimal control problem of a three-wheeled omni-directional mobile robot is addressed in this paper. Different from usual cases, in which the Pontryagin’s Minimum Principle (PMP) is used, an iterative procedure is proposed to transform the time-optimal problem into a nonlinear programming (NLP) one. In the NLP problem, the count of control steps is fixed initially and the sampling period is treated as a variable in the optimization process. The optimization object is to minimize the sampling period such that it is below a specific minimum value, which is set in advance considering the accuracy of discretization. To generate initial feasible solutions of the formulated NLP problem, genetic algorithms (GAs) are adopted. Since different initial feasible solutions can be generated, the optimization process can be started from different points to find the optimal solution. In this manner, one can find a time-optimal movement of the omni-directional mobile robot between two configurations. To show the feasibility of the proposed method, simulation results are included for illustration.

Keywords: Time-optimal control, nonlinear programming, omni-directional robots.

Shi-Min Wang, Lecturer, Department of Electrical Engineering, Hsiuping University of Science and Technology.
Chia-Ju Wu,Professor, Department of Electrical Engineering,
National Yunlin University of Science and Technology.
Jia-Yan Wei, Lecturer, Department of Electrical Engineering, Hsiuping University of Science and Technology.
Received 12 January 2011; accepted 28 March 2011

可全方位運動機器人之非線性規劃最佳時間控制法

王世民、吳佳儒、魏嘉延

摘　要

本論文為探討一部三輪可全方位運動機器人的時間最佳化控制問題，這裏所提出的方法為 Pontryagin 的最小原則（PMP）。所使用的迭代法為非線性規劃（NLP）方法的時間最佳化題型，NLP 問題的初始值在控制過程中為常數，而取樣週期在做最佳化過程中為變數，最佳化的目的是希望取樣週期要比設定的最小值更低，如此一來才可確保它的準確度。本論文所制定的 NLP 問題初始可行解可由遺傳演算法(GAs)來求得，因為初始可行解可求得，所以時間最佳化問題便可進行計算而得到最佳解。在這種模式下，可全方位運動機器人在空間移動時就可以找到最佳的時間運動方式。本論文所提出的方法可經由模擬結果來作說明得到驗證。

關鍵詞：時間最佳化控制，非線性規劃，全方位機器人

王世民：修平科技大學電機系講師
吳佳儒：國立雲林科技大學電機工程系教授
魏嘉延：修平科技大學電機系講師
投稿日期：2011 年 1 月 12 日　接受刊登日期：2011 年 3 月 28 日

1. Introduction

In recent years, mobile robots have been used widely in many occasions [1]. Among several kinds of mobile robot, the omni-directional ones have attracted much attention since they have the ability to move simultaneously and independently in translation and rotation [2]. A typical application of omni-directional mobile robots is the annual international Robocup competition [3], in which omni-directional mobile robots are used to play soccer-like games.

Many researchers have studied omni-directional mobile robots and most research has been focused on the mechanical design and dynamic analysis. Pin and Killough [2] presented the concepts for a family of holonomic wheeled platforms that feature full omni-directionality with simultaneous and independent controlled rotational and translational capabilities. Jung *et al*. [4] developed an omni-directional mobile robot, derived its kinematic and dynamic models, and used a fuzzy logic controller for the shooting action control. Kalmar-Nagy *et al.* [5] proposed an innovative method to generate near-optimal trajectories for an omni-directional robot. This method provided an efficient method for path planning and allowed a large number of possible scenarios to be explored in real time. William II *et al*. [6] presented a dynamic model for omni-directional wheeled mobile robots, considering the occurrence of slip between the wheels and motion surface. Chen *et al*. [7] presented an off-road omni-directional robot, which can run on an uneven road and obstacles. They also designed a position and velocity control system for the robot such that the robot can be automatically controlled to run in an optional direction and to track an orbit. With the same kind of omni-directional robot in [7], Chen *et al*. [8] developed an intelligent genetic programming method to search for an optimum route leading the robot to given destination and avoiding obstacles. Liu *et al*. [9] designed a nonlinear controller for an omni-directional mobile robot utilizing the so-called linearization control method such that robust stability and performance can be provided. In [10,11], the dynamic model of an omni-directional mobile robot is developed, and several control strategies are discussed based on linear control methods while the robot dynamics is nonlinear. A resolved-acceleration control with PI and PD feedback is developed in [10] and PID control, self-tuning PID control, and fuzzy control of the omni-directional mobile robot are introduced in [11].

From the robot testing and the competition experience of Robocup games, it is realized that a time-optimal control method for the mobile robots between configurations can improve their performance significantly. In the past few years, the time-optimal problem of mobile robots has attracted the attention of several researchers [12-14]. However, to the best knowledge of the authors, previous researchers have not addressed the time-optimal control problem of an omni-directional mobile robot yet. This motivates the research in this paper and a NLP method will be proposed to carry out the motion maneuver of an omni-directional mobile robot between two configurations in minimum-time.

The time-optimal motion-planning (TOMP) problem for an omni-directional mobile robot is to find the time-optimal motion in a smooth flat surface between two configurations, where the initial and final velocities are zero. Usually, this TOMP problem leads to the utilization of the PMP [15], in which one needs to solve a set of differential equations. Since these equations are usually nonlinear and highly coupled, one will have two-point boundary value problems, which are intractable in numerical computation.

Recently, a NLP method that does not utilize the PMP was developed by one of the authors of this paper to solve the time-optimal control problem of linear systems [16]. The basic idea of this method is that instead of considering a fixed sampling period, the count of control steps is fixed initially and the sampling period is treated as a variable in the optimization process. The optimization object is to minimize the sampling period such that it is below a specific minimum value, which is set in advance considering the accuracy of discretization. With this approach, the optimization procedure requires only two iterations in most linear cases, thereby reducing the computation time dramatically.

Extending the concept in [16] to nonlinear systems, this paper shows the generation of time-optimal motion between two configurations for an omni-directional mobile robot with three independently driven individual wheels. In the beginning, dynamical equations of the omni-directional mobile robot are introduced and an iterative procedure will be proposed to transform the time-optimal problem into a NLP one. However, since the dynamics of the omni-directional robot is highly nonlinear, it is a difficult task to find a feasible solution for the formulated NLP problem. Therefore, a GA-based approach is proposed to generate feasible solutions for the formulated NLP problem. In this manner, since feasible solutions can be obtained easily, the optimization process can be started from many different starting points to find the optimal solution. Simulation examples are given to verify the feasibility of the proposed method.

The rest of this paper is as follows. In Section 2, dynamical equations of the omni-directional mobile robot are derived. Then the TOMP problem between two configurations of the omni-directional mobile robot is formulated as a NLP one by an iterative procedure in Section 3. In Section 4, GAs are used to generate initial feasible solutions of the NLP problem. Problem solution and simulation results are shown in Sections 5 and 6, respectively. Finally, conclusions and discussion are given in Section 7.

2. Dynamic Equations of the Omni-directional Robot

In this section, it is assumed that the omni-directional robot consists of the orthogonal-wheel assembly mechanism proposed in [2] and a schematic diagram to illustrate the motion of the omni-directional robot is given as shown in Figure 1. In the working space of the robot, a world-frame $[x_w, y_w]^T$ and a moving-frame $[x_m, y_m]^T$ are defined as shown in Figure 2. The world-frame denotes a frame that everything discussed can be referenced and the moving-frame is a frame attached to the center of the gravity of the robot. The transformation between these two frames is described by

$$\begin{bmatrix} \dot{x}_w \\ \dot{y}_w \end{bmatrix} = \begin{bmatrix} \cos\phi & -\sin\phi \\ \sin\phi & \cos\phi \end{bmatrix} \begin{bmatrix} \dot{x}_m \\ \dot{y}_m \end{bmatrix} \tag{1}$$

where ϕ is the angle between these two frames.

With the transformation in (1) and according to the Newton's Second Law of Motion, one can obtain

$$M(\ddot{x}_m - \dot{y}_m\dot{\phi}) = -\frac{1}{2}D_1 - \frac{1}{2}D_2 + D_3 \tag{2}$$

$$M(\ddot{y}_m + \dot{x}_m\dot{\phi}) = \frac{\sqrt{3}}{2}D_1 - \frac{\sqrt{3}}{2}D_2 \tag{3}$$

$$I_v\ddot{\phi} = (D_1 + D_2 + D_3)L \tag{4}$$

where M is the mass of the robot, I_v is the moment of inertia of the robot, L is the distance between any wheel and the center of gravity of the robot, and D_i $i = 1,2,3,$ are the driving forces of the wheels.

In addition, the driving system property for each wheel is assumed to be given by [17]

$$I_w\ddot{\theta}_i + c\dot{\theta}_i = ku_i - RD_i, \; i = 1,2,3 \tag{5}$$

where c is the viscous friction factor of the wheel, R is the radius of the wheel,

I_ω is the moment of inertia of the wheel around the driving shaft, k is the driving gain factor, and u_i is the driving input torque.

From (1) through (5), and the geometrical relationships among variables $\dot{\phi}, \dot{x}_m, \dot{y}_m$, and $\dot{\theta}_i$, it is found that

$$\ddot{x}_m = a_1\dot{x}_m + a_2\dot{y}_m\dot{\phi} - b_1(u_1 + u_2 - 2u_3), \quad (6)$$

$$\ddot{y}_m = a_1\dot{y}_m - a_2\dot{x}_m\dot{\phi} + \sqrt{3}b_1(u_1 - u_2), \quad (7)$$

$$\ddot{\phi} = a_3\dot{\phi} + b_2(u_1 + u_2 + u_3), \quad (8)$$

where

$$a_1 = -3c/(3I_\omega + 2MR^2) \quad (9)$$

$$a_2 = 2MR^2/(3I_\omega + 2MR^2) \quad (10)$$

$$a_3 = -3cL^2/(3I_\omega L^2 + I_v R^2) \quad (11)$$

$$b_1 = kR/(3I_\omega + 2MR^2) \quad (12)$$

$$b_2 = kRL/(3I_\omega L^2 + I_v R^2) \quad (13)$$

From (6) through (13), and the transformation between the world-frame and the moving-frame, the dynamical equations of the omni-directional robot are given as

$$\frac{d}{dt}\begin{bmatrix}\dot{x}_w\\ \dot{y}_w\\ \dot{\phi}\end{bmatrix} = \begin{bmatrix}a_1 & -a_4\dot{\phi} & 0\\ a_4\dot{\phi} & a_1 & 0\\ 0 & 0 & a_3\end{bmatrix}\begin{bmatrix}\dot{x}_w\\ \dot{y}_w\\ \dot{\phi}\end{bmatrix} + \begin{bmatrix}b_1\beta_1 & b_1\beta_2 & 2b_1\cos\phi\\ b_1\beta_3 & b_1\beta_4 & 2b_1\cos\phi\\ b_2 & b_2 & b_2\end{bmatrix}\begin{bmatrix}u_1\\ u_2\\ u_3\end{bmatrix} \quad (14)$$

where

$$a_4 = 3I_\omega/(3I_\omega + 2MR^2) \quad (15)$$

$$\beta_1 = -\sqrt{3}\sin\phi - \cos\phi \quad (16)$$

$$\beta_2 = \sqrt{3}\sin\phi - \cos\phi \quad (17)$$

$$\beta_3 = \sqrt{3}\cos\phi - \sin\phi \quad (18)$$

$$\beta_4 = -\sqrt{3}\cos\phi - \sin\phi \quad (19)$$

3. TOMP between Two Configurations

3.1 Problem Formulation

The TOMP problem of the omni-directional mobile robot between two configurations is to find the control inputs that will move the system from an initial configuration to a desired final configuration while minimizing the traveling time. With the dynamics in (14) through (19), the TOMP problem can be formulated as follows:

PROBLEM 1: For the omni-directional mobile robot described in (14) through (19), assuming that the initial configuration is given as

$$(x_w(0), y_w(0), \phi(0)) = (x_0, y_0, \phi_0) \quad (20)$$

$$(\dot{x}_w(0), \dot{y}_w(0), \dot{\phi}(0)) = (0, 0, 0) \quad (21)$$

determine the control inputs $u_1(t)$, $u_2(t)$, and $u_3(t)$ for $t \in [0, t_f]$ to minimize

$$J = t_f \tag{22}$$

subject to

$$(x_w(t_f), y_w(t_f), \phi(t_f)) = (x_f, y_f, \phi_f) \tag{23}$$

$$(\dot{x}_w(t_f), \dot{y}_w(t_f), \dot{\phi}(t_f)) = (0, 0, 0) \tag{24}$$

and

$$u_{i,\min} \le u_i(t) \le u_{i,\max} \quad \text{for}$$

$$t \in [0, t_f];\ i = 1, 2, 3 \tag{25}$$

where (x_f, y_f, ϕ_f) is the desired final configuration.

It is obvious that Problem 1 is a very difficult problem due to the nature of the nonlinear and coupled relation of the omni-directional mobile robot. To cope with the difficulty, Problem 1 will be formulated and solved in the discrete-time domain by numerical methods. By extending the concept in [16], it will be shown how to determine the time-optimal movement of an omni-directional mobile robot between configurations. The first step is to divide the interval $[0, t_f]$ into N equal time intervals, where N is the number of control steps [16]. That is

$$t_i - t_{i-1} = \Delta t = t_f / N \qquad \text{for } i = 1, 2, \cdots, N \tag{26}$$

If the acceleration is assumed to be constant for each sub-interval, then one obtains

$$\begin{bmatrix} \dot{x}_w(i) \\ \dot{y}_w(i) \\ \dot{\phi}(i) \end{bmatrix} = \begin{bmatrix} \dot{x}_w(i-1) + \ddot{x}_w(i-1)\cdot\Delta t \\ \dot{y}_w(i-1) + \ddot{y}_w(i-1)\cdot\Delta t \\ \dot{\phi}_w(i-1) + \ddot{\phi}_w(i-1)\cdot\Delta t \end{bmatrix} = \begin{bmatrix} \dot{x}_w(0) + \sum_{k=0}^{i-1} \ddot{x}_w(k)\cdot\Delta t \\ \dot{y}_w(0) + \sum_{k=0}^{i-1} \ddot{y}_w(k)\cdot\Delta t \\ \dot{\phi}(0) + \sum_{k=0}^{i-1} \ddot{\phi}(k)\cdot\Delta t \end{bmatrix} \tag{27}$$

$for \quad i = 1, 2, \cdots, N$

$$\begin{bmatrix} x_w(i) \\ y_w(i) \\ \phi(i) \end{bmatrix} = \begin{bmatrix} x_w(i-1) + 0.5\times(\dot{x}_w(i) + \dot{x}_w(i-1))\cdot\Delta t \\ y_w(i-1) + 0.5\times(\dot{y}_w(i) + \dot{y}_w(i-1))\cdot\Delta t \\ \phi(i-1) + 0.5\times(\dot{\phi}(i) + \dot{\phi}(i-1))\cdot\Delta t \end{bmatrix} \tag{28}$$

$$= \begin{bmatrix} x_w(0) + 0.5\times\sum_{k=1}^{i}(\dot{x}_w(k) + \dot{x}_w(k-1))\cdot\Delta t \\ y_w(0) + 0.5\times\sum_{k=0}^{i-1}(\dot{y}_w(k) + \dot{y}_w(k-1))\cdot\Delta t \\ \phi(0) + 0.5\times\sum_{k=0}^{i-1}(\dot{\phi}(k) + \dot{\phi}(k-1))\cdot\Delta t \end{bmatrix}$$

$for \quad i = 1, 2, \cdots, N$

where $(x_w(i), y_w(i), \phi(i))$ and $(\dot{x}_w(i), \dot{y}_w(i), \dot{\phi}(i))$ are used to denote $(x_w(i\cdot\Delta t), y_w(i\cdot\Delta t), \phi(i\cdot\Delta t))$ and $(\dot{x}_w(i\cdot\Delta t), \dot{y}_w(i\cdot\Delta t), \dot{\phi}(i\cdot\Delta t))$, respectively, for notational simplicity.

If $(u_1(0), u_2(0), u_3(0))$ are substituted into (14), with the given $(x_w(0), y_w(0), \phi(0))$ and $(\dot{x}_w(0), \dot{y}_w(0), \dot{\phi}(0))$, then the values of $(x_w(1), y_w(1), \phi(1))$ and $(\dot{x}_w(1), \dot{y}_w(1), \dot{\phi}(1))$ can be obtained from (27) and (28). Applying input torques to (14) sequentially and repeatedly using (27) and (28), the final configuration of the robot can be expressed as functions of $(x_w(0), y_w(0), \phi(0))$, $(\dot{x}_w(0), \dot{y}_w(0), \dot{\phi}(0))$, the input variables $(u_1(0), u_2(0), u_3(0)), \cdots, (u_1(N-1), u_2(N-1), u_3(N-1))$, and the sampling period Δt. This means that

$$x_w(N) = f_1(x_w(0), y_w(0), \phi(0), \dot{x}_w(0), \dot{y}_w(0), \dot{\phi}(0), u_1, u_2, u_3, \Delta t) \quad (29)$$

$$y_w(N) = f_2(x_w(0), y_w(0), \phi(0), \dot{x}_w(0), \dot{y}_w(0), \dot{\phi}(0), u_1, u_2, u_3, \Delta t) \quad (30)$$

$$\phi(N) = f_3(x_w(0), y_w(0), \phi(0), \dot{x}_w(0), \dot{y}_w(0), \dot{\phi}(0), u_1, u_2, u_3, \Delta t) \quad (31)$$

$$\dot{x}_w(N) = f_4(x_w(0), y_w(0), \phi(0), \dot{x}_w(0), \dot{y}_w(0), \dot{\phi}(0), u_1, u_2, u_3, \Delta t) \quad (32)$$

$$\dot{y}_w(N) = f_5(x_w(0), y_w(0), \phi(0), \dot{x}_w(0), \dot{y}_w(0), \dot{\phi}(0), u_1, u_2, u_3, \Delta t) \quad (33)$$

$$\dot{\phi}(N) = f_6(x_w(0), y_w(0), \phi(0), \dot{x}_w(0), \dot{y}_w(0), \dot{\phi}(0), u_1, u_2, u_3, \Delta t) \quad (34)$$

where $\mathbf{u_1} = (u_1(0), u_1(1), \cdots, (u_1(N-1))$, $\mathbf{u_2} = (u_2(0), u_2(1), \cdots, (u_2(N-1))$, and $\mathbf{u_3} = (u_3(0), u_3(1), \cdots, (u_3(N-1))$. A flowchart to illustrate the derivation of (29) through (34) is shown in Figure 3. With (29) through (34), Problem 1 is now turned into a standard constrained NLP problem as follows:

PROBLEM 2: Given the initial configuration in (20) and (21), determine the values of $u_1(0), u_1(1), \cdots, u_1(N-1)$, $u_2(0), u_2(1), \cdots, u_2(N-1)$, $u_3(0), u_3(1), \cdots, u_3(N-1)$, and Δt to minimize

$J = N \cdot \Delta t$ (35)

subject to

$\Delta t > 0$ (36)

$(x_w(N), y_w(N), \phi(N)) = (x_f, y_f, \phi_f)$ (37)

$(\dot{x}_w(N), \dot{y}_w(N), \dot{\phi}(N)) = (0, 0, 0)$ (38)

$u_{i,\min} \le u_i(j) \le u_{i,\max}$ for $i = 1, 2, 3;\ j = 0, 1, \cdots, N-1$ (39)

where $(x(N), y(N), \phi(N))$ and

$(\dot{x}(N), \dot{y}(N), \dot{\phi}(N))$ are defined in (29) through (34).

3.2 Choice of Control Steps and Sampling Period

Although the TOMP problem of an omni-directional mobile robot can be formulated as shown in Problem 2, there still exist several difficulties to be solved. One difficulty is the choice of the value of control steps N. It is obvious that a larger value of N gives more freedom for the input variables. However, this also means more computation burden for Problem 2. For linear system without constraints on the input variables, it has been shown that the initial choice of N must be greater than the dimension of state variables [16]. Though no similar rules can be followed for nonlinear systems, an integer that is large than the dimension of state variables will be chosen as an initial value of N in this paper.

Another difficulty is the choice of the sampling period. From the viewpoint of discretization accuracy, it is obvious that smaller sampling period value will result in a more accurate model. Therefore, a limitation of the sampling period, say Δt_{limit}, should be chosen. If the value of Δt obtained in Problem 2 is greater than Δt_{limit}, then a new value of control steps will be chosen according to

$$N_{\text{new}} > \frac{N \cdot \Delta t}{\Delta t_{\text{limit}}} \tag{40}$$

4. Initial Feasible Solutions

Most NLP algorithms usually need an initial feasible solution to start the optimization process. In Problem 2, an initial feasible solution means a set of $u_1(0), u_1(1), \cdots, u_1(N-1)$, $u_2(0), u_2(1), \cdots, u_2(N-1)$, $u_3(0), u_3(1), \cdots, u_3(N-1)$, and Δt satisfying the constraints in (36) through (39). It is obvious that these solutions are not easy to be found since the constraints are highly nonlinear and coupled. Therefore, an approach based on GAs is developed to generate initial feasible solutions.

The theoretical basis of GAs is that chromosomes (solutions) better suited to the environment (evaluation) will have greater chance of survival and better chance of producing offspring. The evolutionary process is based primary on the mutation and crossover operators. The crossover operator combines the features of two parents to form two offspring. The mutation operator arbitrarily alters one or more genes of a selected chromosome, which increases the variability of the population. These two operators can further be divided into static and dynamic, where static ones do not change over the life of the population while dynamic ones are functions of time.

In the evolutionary process to generate initial feasible solutions of Problem 2, genetic operators such as real number encoding, arithmetical crossover and non-uniform mutation will be implemented. Moreover, dynamic mutation and crossover, enlarged sampling space and ranking mechanism will also be used to expedite the convergence of the evolutionary process.

4.1 Chromosome Representations

How to encode a solution of the problem into a chromosome is a key issue for GAs. In this paper, since the parameters to be determined are all real, real number encoding technique will be used. Once the real-code chromosomes are used, the next step is to determine the number of genes in a chromosome. If the number of control steps is *N*, then the chromosomes will contains (3*N*+1) genes, which denote $u_1(0), u_1(1), \cdots, u_1(N-1)$, $u_2(0), u_2(1), \cdots, u_2(N-1)$, $u_3(0), u_3(1), \cdots, u_3(N-1)$, and Δt, respectively. For a chromosome $\mathbf{x} = [x_1, x_2, x_{3N+1}]$, one can find that the first 3*N* genes are within the ranges $[u_{i,\min}, u_{i,\max}]$ for $i = 1, 2, 3$, and the lower bound of the last gene is greater than zero.

4.2 Crossover and Mutation Operations [18]

Arithmetical crossover and non-uniform mutation will be introduced in this section. For two real-coded chromosomes $\mathbf{x}_1$ and $\mathbf{x}_2$, the operation of arithmetical crossover is defined as follows:

$$\mathbf{x}_1' = \lambda \mathbf{x}_1 + (1-\lambda)\mathbf{x}_2 \tag{41}$$

$$\mathbf{x}_2' = \lambda \mathbf{x}_2 + (1-\lambda)\mathbf{x}_1 \tag{42}$$

where $\lambda \in (0,1)$.

For a given parent $\mathbf{x}$, if a gene x_k of it is selected for mutation, then the resulting offspring will be randomly selected from one of the following two choices.

$$x_k' = x_k + (x_k^U - x_k) \cdot r \cdot \left(1 - \frac{gen}{G}\right)^b \tag{43}$$

$$x_k' = x_k - (x_k - x_k^L) \cdot r \cdot \left(1 - \frac{gen}{G}\right)^b \tag{44}$$

where x_k^U and x_k^L are the upper and lower bounds of x_k; r is a random number from $[0,1]$; gen is the generation number; G is the maximal generation number, and b is a parameter determining the degree of non-uniformity.

In addition to arithmetical crossover and non-uniform mutation, dynamic crossover and mutation probability rates will also be used for fast convergence. The crossover and mutation rates are defined as follows:

$$\text{crossover rate} = \exp\left(-\frac{gen}{G}\right) \tag{45}$$

$$\text{mutation rate} = \exp\left(-\frac{gen}{4G}\right) - 1 \tag{46}$$

4.3 Enlarge Sampling Space

To generate good offspring, a method for selection of parents will be necessary. For selection methods that are developed based on regular sampling space, parents are replaced by their offspring soon after they give birth. In this manner, some fitter chromosomes will be worse than their parents. To cope with this problem, the selection method in this paper will be performed in enlarged sampling space, in which both parents and offspring have the same chance of competition for survival. Moreover, since more random perturbation is allowed in enlarged sampling space, high crossover and mutation will be allowed in the evolutionary process.

4.4 Ranking Mechanism

In proportional selection procedure, the selection probability of a chromosome is proportional to its fitness. This scheme exhibits some undesirable properties such as a few super chromosomes will dominate the process of selection in early generations. Moreover, competition among chromosomes will be less strong and a random search behavior will emerge in later generations. Therefore, the ranking mechanism is used in this paper to mitigate these problems, in which the chromosomes are selected proportionally to their ranks rather than actual evaluation values. This means that the fitness will be an integer number from 1 to P, where P is the population size. The best chromosomes will have a fitness value equal to P and the worst one will have a fitness value equal to 1.

5. Problem Solution

The details of the proposed method can be summarized as follows:

Algorithm A : (Generating an initial feasible solution)

Step 1: Define the fitness function.

Step 2: Determine the population size, the crossover rate according to (45), and the mutation rate according (46).

Step 3: Produce an initial generation in a random way.

Step 4: Evaluate the fitness for each member of generation.

Step 5: With the crossover rate in Step 2, generate offspring according to (41) and (42), in which the ranking mechanism is used for selection of chromosomes.

Step 6: With mutation rate in Step 2, generate offspring according to (43) and (44).

Step 7: Select the members of the new generation from the parents in the old generation and the offspring in Step 5 and Step 6 according to their fitness values.

Step 8: Repeat the procedure in Step 5 through Step 7 until the number of generations reaches a prescribed value.

Algorithm B：(Solution of Problem 2)

Step 1: Choose a value of Δt_{limit} and an integer N.

Step 2: Formulate the TOMP problem as a NLP problem as shown in Problem 2 with the chosen value N.

Step 3: Use Algorithm A to find an initial feasible solution of Problem 2.

Step 4: Use any NLP algorithm to determine the minimum value of Δt in Problem 2 based on the initial feasible solution obtained in Step 3.

Step 5: If $\Delta t > \Delta t_{\text{limit}}$, then choose a new value of N according to (40) and go to Step 2. Otherwise, continue.

Step 6: $N \cdot \Delta t$ is the minimal traveling time.

6. Simulation Results

In this simulation example, the omni-directional mobile robot is to be moved from the initial configuration

$$(x_w(0), y_w(0), \phi(0)) = (0\text{ m}, 0\text{ m}, 0^\circ) \quad (47)$$

$$(\dot{x}(0), \dot{y}(0), \dot{\phi}(0)) = (0\text{ m}, 0\text{ m}, 0^\circ) \quad (48)$$

to the desired final configuration

$$(x_w(N), y_w(N), \phi(N)) = (1\text{ m}, 0\text{ m}, 180^\circ) \quad (49)$$

$$(\dot{x}(N), \dot{y}(N), \dot{\phi}(N)) = (0\text{ m}, 0\text{ m}, 0^\circ) \quad (50)$$

in a time-optimal manner.

For convenience, the dynamical equations used in this example are the same as those in [10,11]. This means that the parameters of the mobile robot are chosen as $M = 9.4$ kg, $L = 0.178$ m, $I_v = 11.25\ \text{kg}\cdot\text{m}^2$, $I_\omega = 0.02108\ \text{kg}\cdot\text{m}^2$, $c = 5.983\times10^{-6}\ \text{kg}\cdot\text{m}^2/\text{s}$, $R = 0.0245$ m, and $k = 1$, respectively. Meanwhile, the constraints on the input torques are assumed to be

$$-10\text{Nm} \le u_1 \le 10\text{Nm} \quad (51)$$

$$-10\text{Nm} \le u_2 \le 10\text{Nm} \quad (52)$$

$$-10\text{Nm} \le u_3 \le 10\text{Nm} \quad (53)$$

In applying Algorithm A to generate an initial feasible solution, the fitness function is defined as

$$fitness = \frac{1}{1+e^2+\dot{e}^2} \quad (54)$$

where

$$e^2 = (x_f - x_w(N))^2 + (y_f - y_w(N))^2 + (\phi_f - \phi(N))^2 \quad (55)$$

and

$$\dot{e}^2 = (\dot{x}_w(N))^2 + (\dot{y}_w(N))^2 + (\dot{\theta}(N))^2 \quad (56)$$

In applying GAs, the population size and the maximal generation number are chosen to be 50 and 100, respectively. During the simulation, the MATLAB Optimization Toolbox will be used, and the value of Δt_{limit} and the initial value of N are chosen to be 0.05 (sec.) and 11, respectively.

Applying Algorithm B with N=11, the values of Δt and $N \cdot \Delta t$ are found to be 0.0985 (sec.) and 1.0835 (sec.), respectively. Since $\Delta t > \Delta t_{\text{limit}}$, the value of N will be updated according to (40), and the new value of N is chosen to be 22. Applying Algorithm B with N=22, the values of Δt and $N \cdot \Delta t$ are found to be 0.0475 (sec.) and 1.0461 (sec.), respectively, and the simulation results are shown in Figure 4.

7. Conclusions and Discussion

This paper presented a novel method to solve the TOMP problem of a three-wheeled omni-directional mobile robot. The first step is to transform the problem into a NLP problem by an iterative procedure. Then a GA-based method is proposed for generation of initial feasible solutions since an initial feasible solution is usually needed in solving a NLP problem. Different from the methods that utilizing the PMP, the major advantage of the proposed method is that one does not need to solve a set of highly nonlinear differential equations.

In the proposed method, one may ask why the optimal solution cannot be obtained by applying the GAs directly. From theoretical point of view, this task is possible to be done. However, in practice, the major difficulty is that the feasibility of the solution is very easy to be violated during the evolutionary process. This explains why the time-optimal solution cannot be obtained by applying the GAs directly.

It can be proved that the solution obtained satisfying the Kuhn-Tucker condition [19], which is a criterion used to check a local minimum. In addition, from the simulation results in Figure 4, one also can find that at least one of the four control inputs saturated at any time instant. This means that the solution is in the form of bang-bang control [20]. If a solution does not satisfy the Kuhn-Tucker condition or not in the form of bang-bang control, then one can conclude that the solution is not a global minimum. However, since the solution obtained meets both criterions simultaneously, it will be hard to determine whether the solution is globally optimal or not. More effort will be needed if one is interested in this issue.

References

[1] R. D. Schraft & G. Schmierer, *Service Robots* (A K Peters, Ltd., 2000).

[2] F. G. Pin & S. M. Killough, "A new family of omnidirectional and holonomic wheeled platforms for mobile robots," *IEEE Trans. on Robotics and Automation*, *10*, 1994, 480-489

[3] http://www.robocup.org/

[4] M. J. Jung, H. S. Shim, H. S. Kim, & J. H. Kim, "Omni-directional mobile base OK-II," *Proc. of the IEEE International Conference on Robotics and Automation*, 2000, 3449-3454.

[5] T. Kalmar-Nagy, P. Ganguly, & R. D'Andrea, "Real-time trajectory generation for omnidirectional vehicles," *Proc. of the American Control Conference,* 2002, 286-291.

[6] R. L. Williams, II, B. E. Carer, P. Gallina, & G. Rosati, "Dynamic Model with slip for wheeled omnidirectional robots," *IEEE Trans. on Robotics and Automation*, *18*, 2002, 285-293.

[7] P. Chen, S. Mitsutake, T. Isoda, & T. Shi, "Omni-directional robot and adaptive control metod for off-road running," *IEEE Trans. on Robotics and Automation*, *18*, 2002, 251-256.

[8] P. Chen, S. Koyama, S. Mitsutake, & T. Isoda, "Automatic running planning for omni-directional robot using genetic programming," *Proc. of the IEEE International Symposium on Intelligent Control*, 2002, 485-489.

[9] Y. Liu, X. Wu, J. J. Zhu, & J. Lew, "Omni-directional mobile robot controller design by trajectory linearization," *Proc. of the American Control Conference*, 2003, 3423-3428.

[10] K. Watanabe, "Control of an omnidirectional mobile robot," *Proc. of the Second International Conference on Knowledge-Based Intelligent Electronic Systems,* 1998, 51-60.

[11] K. Watanabe, Y. Shiraishi, & S. G.

Tzaffestas, "Feedback control of an omnidirectional autonomous platform for mobile serve robots," *Journal of Intelligent and Robotic Systems, 20*, 1998, 315-330.

[12] P. Soueres & J. P. Laumond, "Shortest paths synthesis for a car-like robot," *IEEE Trans. on Automatic Control, 41*, 1996, 672-688.

[13] W. Wu, H. Chen, & P. Y. Woo, "Optimal motion planning for a wheeled mobile robot," *Proc. of the IEEE International Conference on Robotics and Automation*, 1999, 41-46.

[14] Y. Zheng & P. Moore, "The design of time-optimal control for two-wheel driven carts tracking a moving target," *Proc. of the IEEE International Conference on Decision and Control*, 1995, 3831–3836.

[15] L. S. Pontryagin, V. G. Boltyanskii, R. V. Gamkrelidze, & E. F. Mishchenko, *The Mathematical Theory of Optimal Processes* (New York: Gordon and Beach, 1986).

[16] T. S. Chung & C. J. Wu, "A computationally efficient numerical algorithm for the minimum-time control problem of continuous systems," *Automatica*, *28*, 1992, 841–847.

[17] M. Saito & T. Tsumura, "Collision avoidance among multiple mobile robots – A local approach based on nonlinear programming, *Trans. of the Institute of Systems, Control, and Information Engineers*, *3*, 1990, 252-260.

[18] M. Gen & R. Cheng, *Genetic Algorithm and Engineering Design* (New York: Wiley, 1997).

[19] D. G. Luenberger, *Linear and Nonlinear Programming* (Addison-Wesley, 1973).

F. L. Lewis, *Optimal Control* (New York: Wiley, 1986).

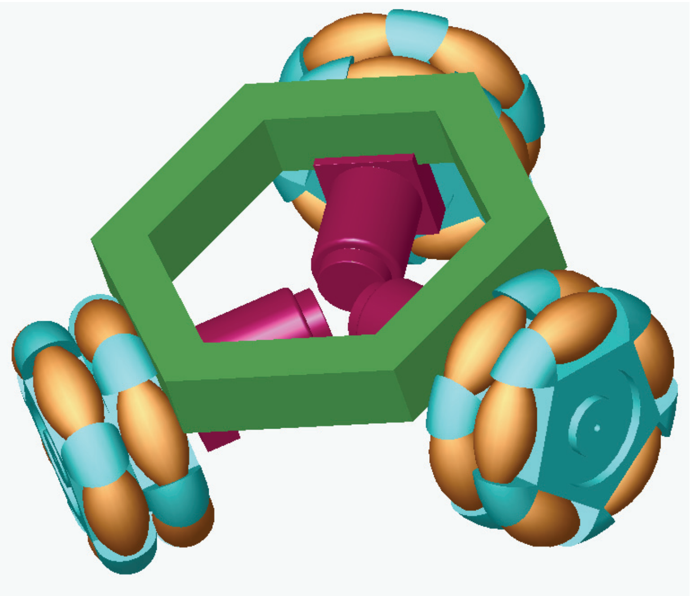

Figure 1. A schematic diagram of the omni-directional robot.

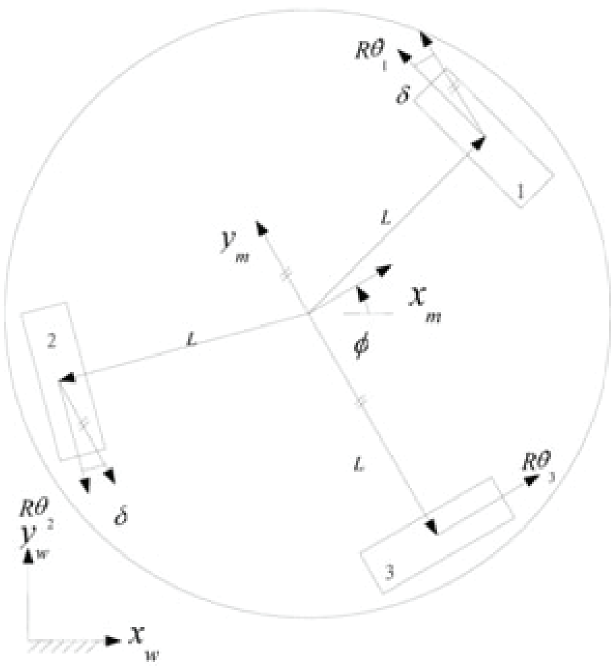

Figure 2. Definitions of the word-frame $[x_w, y_w]^T$ and the moving-frame $[x_m, y_m]^T$.

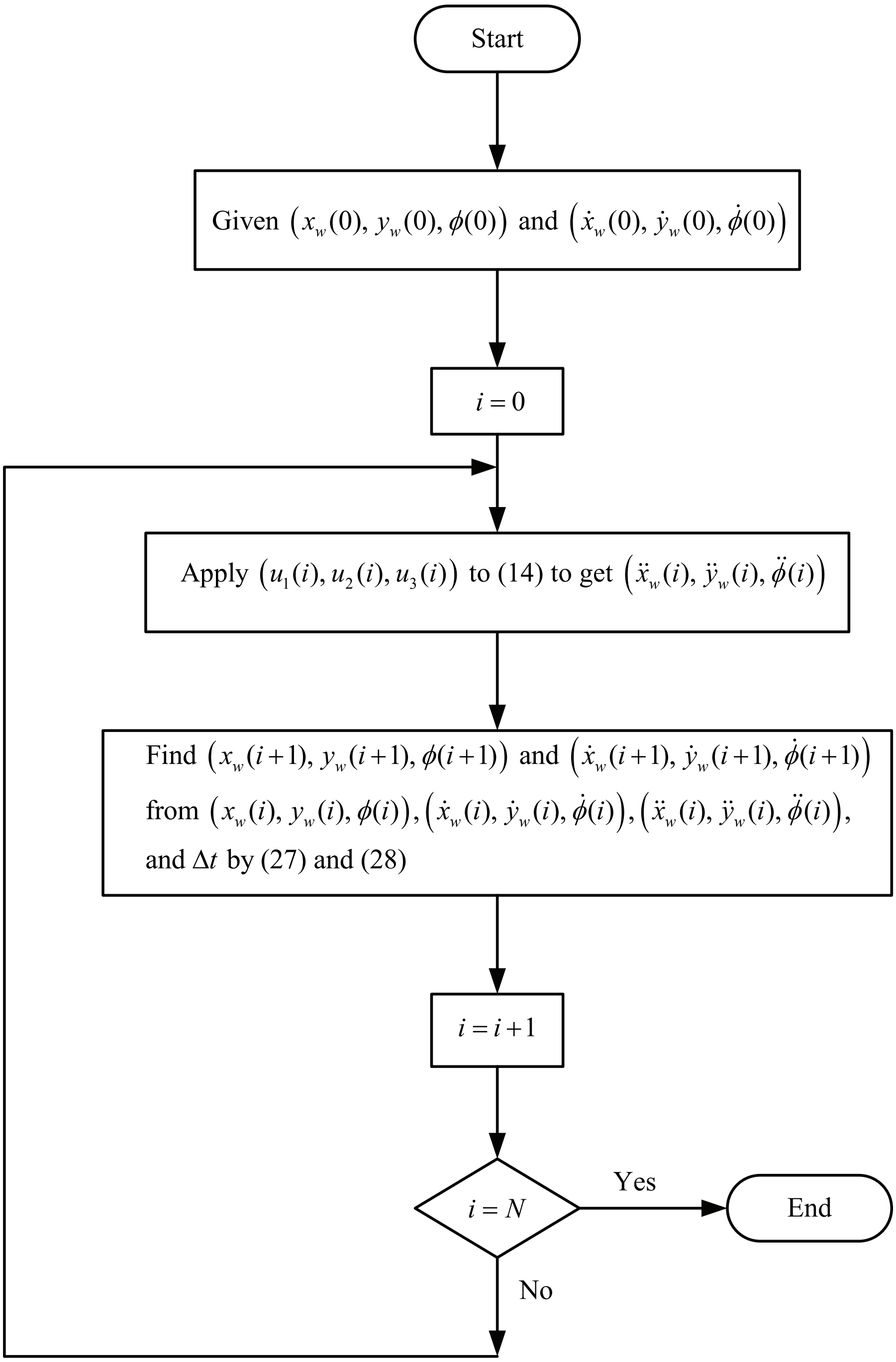

Figure 3. A flowchart to illustrate the derivation of equations (29) through (34).

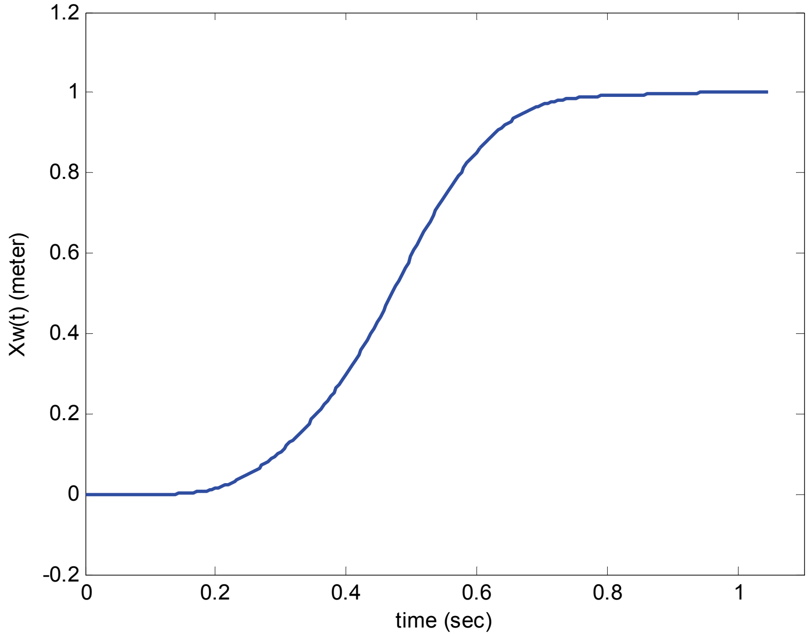

Figure 4(a). Plot of $x_w(t)$ for $N = 22$.

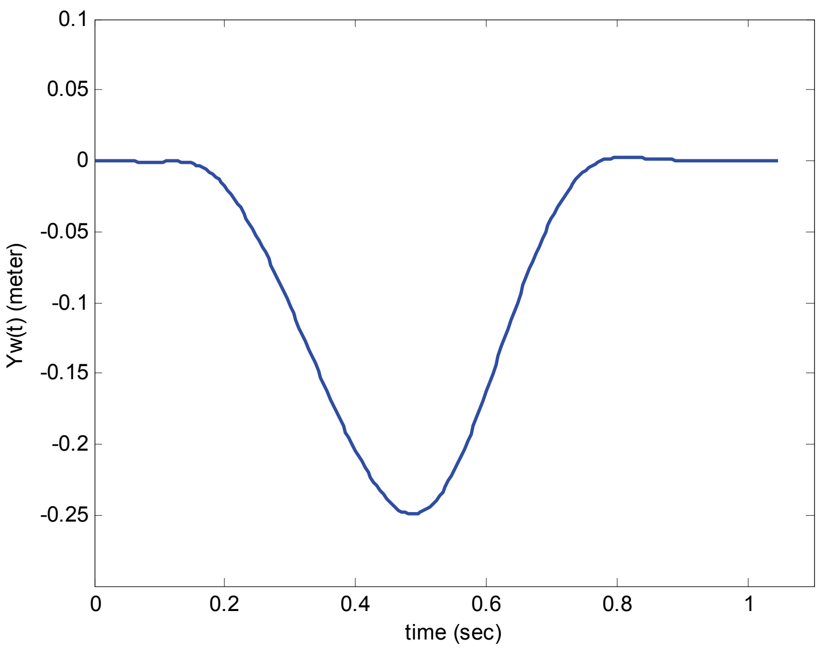

Figure 4(b). Plot of $y_w(t)$ for $N = 22$.

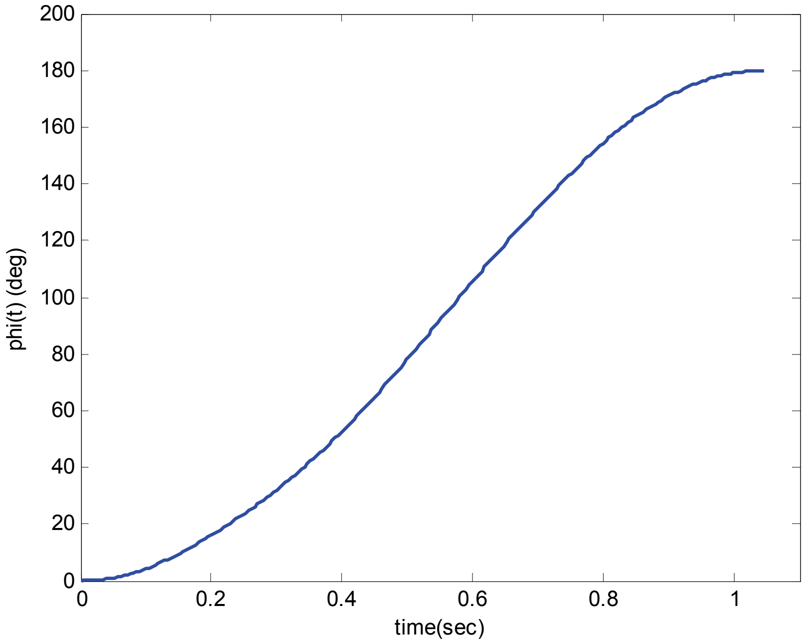

Figure 4(c). Plot of $\phi(t)$ for $N = 22$.

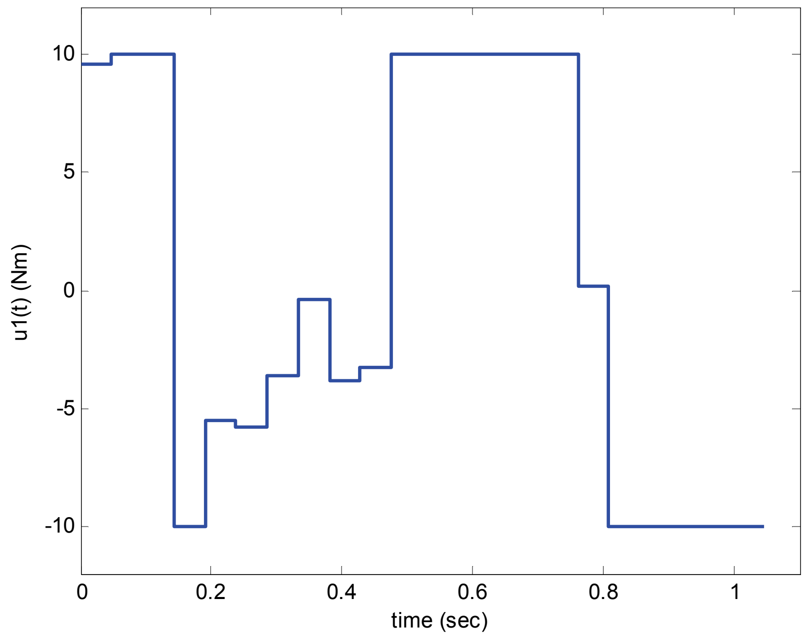

Figure 4(d). Plot of $u_1(t)$ for $N = 22$.

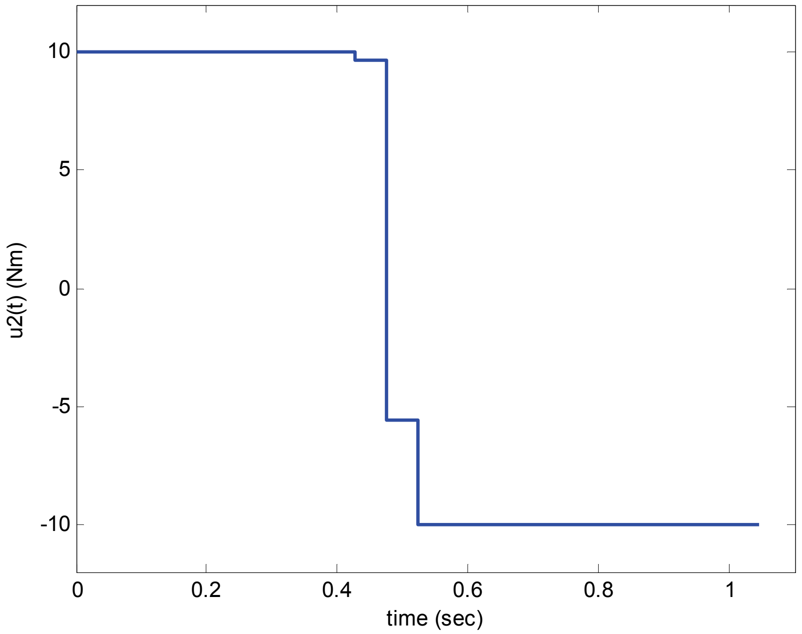

Figure 4(e). Plot of $u_2(t)$ for $N = 22$.

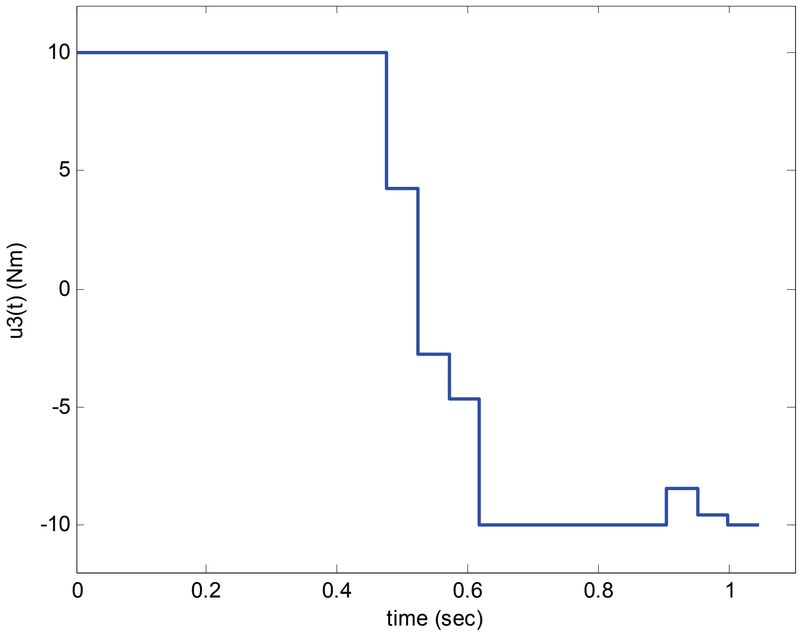

Figure 4(f). Plot of $u_3(t)$ for $N = 22$.

以 Kano 二維模型探討醫療服務品質與住院病患滿意度之研究：以中部某區域型醫院爲例

林芷薐、程建銘、馬志豪

摘 要

本研究以中部某區域型教學醫院為研究範圍，針對住院病患及醫院員工為對象，並利用 Kano 二維品質特性分類方法進行問卷設計，以探討住院病患及醫院員工對醫療機構服務品質之分類及關鍵因素之確認與住院病患滿意度分析。問卷資料之分析以 SPSS 統計套裝軟體進行敍述統計分析、信度分析、t 檢定、單因子變異數及 LSD 事後檢定等分析。本文依 Kano 二維分類方法設計調查問卷，研究結果發現住院病患與醫院員工對醫療服務品質上之看法有所差異，住院病患以一元品質居多，其次為無差異品質及當然品質，而醫院員工則以當然品質居多，其次為無差異品質及一元品質，顯示一般病患與醫院員工對品質要項的重視程度不同。另外，本研究探討住院病患對醫院服務品質之滿意度，並且依據「顧客滿意係數」以確認針對某品質要素進行改善時，其可能增加顧客滿意度與減少顧客不滿意度各為多少，以得出優先改善之順序，進而提供管理當局提昇服務品質、病患滿意度與競爭優勢之參考。

關鍵詞：病患滿意度、醫療服務品質、Kano 二維模型。

林芷薐：通訊作者；中臺科技大學國企系助理教授
程建銘：行政院衛生署豐原醫院心臟內科醫師
馬志豪：行政院衛生署豐原醫院小兒科醫師
投稿日期：100年1月20日 接受刊登日期：100年4月13日

A Study of Medical Service Quality and In-Patients' Satisfaction by Using Kano's Model－An Example of Certain District Hospital in Taichung

Chih-Ling Lin, Chien-Ming Cheng, Chin-Hao Ma

Abstract

This study explores the classification of service quality attributes and identification of critical improvement service quality attributes for patients and employees based on the certain hospital by applying Kano’ s model. The study also discusses the important degree and consciousness satisfactory of service quality for patients and employee of hospital. The SPSS statistical software was used for statistical analysis including t-Test, reliability analysis, ANOVA and LSD post hoc comparison. The questionnaire was designed on Kano’ s two-dimension model to evaluate the quality of hospital service. The results show that there is a statistically significant difference between the in-patients and employees in most items assessing quality elements. This study also implements the patient’ s satisfaction of perspective of healthcare service analysis. In addition, we use “Customer Satisfaction index matrix” to access critical service quality dimensions. These research results can be used by the document hospital management to improve service quality satisfaction to create competitive advantage.

Keywords：Patient satisfaction, Healthcare service quality, Kano’ s model.

Chih-Ling Lin*, Assistant Professor, Department of International Business, CTUST.
Chien-Ming Cheng, Doctor, Cardiology, FYH.
Chin-Hao Ma, Doctor, Pediatrics, FYH.
Received 20 January 2011; accepted 13 April 2011

壹、前言

醫療產業面臨政府推行全民健康保險的政策以來，即感受到競爭時代的來臨，而其政策的目的乃期望將有限的資源做最有效的運用，以提升人民福址，然而於資源運用移轉之間與組織權力的調整，使得醫師診療行為、醫院經營模式、管理模式及財務結構面臨空前的考驗[4,5]，而台灣的醫療產業的變革，除了來自政府推行全民健康保險的政策影響之外，再加上目前全球化與高科技化的衝擊之下，更使得醫療院所的競爭進入了白熱化的時代[6]。對於醫療產業而言，除了低廉的價格及先進的醫療設備外，最重要的是「以客為尊」的服務精神，所有服務的提供皆以顧客的角度來思考，讓病患或病患家屬都能感受到醫院的用心和專業[19]。為了提昇競爭優勢，近年來，台灣許多醫療院所亦積極推行品質管理活動，如：全面品質管理(Total Quality Management)、品管圈、流程再造、5S運動、六個標準差等[2,11]。醫院既屬於服務業的一環，所提供服務的對象為顧客，更應重視服務品質的提升，以滿足國人就醫服務的品質需求，而增進病患的滿意度更是廣為各大醫療院所及一般社會大眾所關注，也是各大醫療院所努力追求並致力達成的目標。

醫療服務品質定位於顧客的主觀感受程度而給與評定的。同時病患的服務品質需求會隨著環境而產生轉變，因此服務的「品質」也應該持續的不斷改善。提升服務品質是經營成功的重要因素，而好的醫療服務品質就是如何讓病人感受到滿意，病人感受到不滿意就是品質不好。Bolton & Drew [13]與Boulding, Kalra, Staelin & Zeithaml [14]指出服務品質與顧客滿意度二項指標，是加強顧客忠誠度的主要因素，即愈高的服務品質與顧客滿意度，愈能獲得顧客忠誠度及提高向他人推薦的意願，可見欲追求永續經營，對於服務品質之提升刻不容緩。

提升品質改善的成效，醫療部門及管理者必須著手改善服務品質並找出病人的需要[39]；過去相關研究文獻對於服務品質要素的認知往往以單一維度的思考方式來進行，亦即當某一品質要素具備則促使顧客滿意，反之不具備時顧客就感到不滿意，此種服務品質的衡量乃透過一維模型來區分出滿意與不滿意[15,23,32]。但實際上，服務品質反應的是消費者的主觀認定，是一種抽象的模糊概念，因而對於服務品質的衡量方式，較難單純應用一般二分法的方式來認定，根據Carson, Carson & Roe [17]的研究，病患的期望分為三層的需求，包括第一層的絕對的需求(implicit need)列為基本需求，如缺乏時就會造成不滿意，第二層為明顯的需求(explicit need)，缺乏時並不會使病人不滿

意，但若滿足時則可使病人感到滿意，第三層的需求是病患未期望的部份，缺乏時並不會影響服務的滿意度，但如具備時則會使顧感到愉快，其研究說明了衡量病患滿意度，二分法的方式認定較不適當。

本研究的範圍主要針對中部某區域醫院之醫院員工及住院病患為主，希望藉由Kano二維模型設計之問卷，來了解醫院員工與住院病患是否具有二維之品質特性，並探討不同族群對於品質看法的差異，同時利用「顧客滿意係數」分析找出關鍵服務品質特性。本研究之目的如下：

一、透過二維品質模型分析住院病患與醫院員工對服務品質要素之屬性分類。

二、探討住院病患與醫院員工所重視的服務品質要素是否有所不同。

三、由服務品質要素歸類與滿意度分析之結果，提出改善服務品質之建議。

貳、文獻探討

一、醫療服務品質

對於醫療服務業而言，其所提供的服務不同於一般企業機構，醫療服務提供的商品相當多包括專業、技術、知識、空間及時間等。韓揆[12]指出醫療服務品質即醫院臨床品質加服務品質。臨床品質指以醫師為主的醫事人員對臨床作業規範及行為規範的奉行狀況，服務品質指臨床周邊設施與工作，其中包括硬體環境、規章制度、行政手續、醫療費用及服務態度等之品質，並以病人滿意度為依歸，符合顧客需求，學者Plymire [37]亦指出適當並重視顧客抱怨或建議，對企業的營運具有正面的幫助。

而有關醫療服務品質的衡量，在過去之研究文獻大部份引用自服務業之Parasuraman, Zeithaml & Berry (以下稱PZB)的SERVQUAL模式測量服務品質[34,35,36]，PZB模式乃界定品質乃是顧客期望與實際評做績效間之差異，並以此概念發展SERVQUAL模式衡量服務品質，其構面分別為有形性、可靠性、反應性、確實性與關懷性。而Cronin & Taylor [20,21]認為品質是不包括消費者期望的部份，僅是消費者評估產品或服務績效，因此PZB模式運用只衡量績效部份構面，不採納期望部份構面；在醫療服務品質衡量方面，Robert & Kathleen[38]認為衡量醫療服務品質時需依照醫療行業特性來設計衡量模式，應包括醫療結構、醫療過程與結果三者。Bowers, Swan & Koehler [15]則認為使用SERVQUAL模式調查醫院服務品質，需要增加看護（Nursing）與醫療結果（Medical Outcome）二個構面，較能符合醫療服務品質的衡量。Georgette, Zifko-Baliga, & Krampt [23]也提出應採用學者Donabedian [22]的三構

面：結構、過程、結果來探討醫療服務品質。

其他國內外學者有關醫療服務品質構面與特性之研究，例如：Carey & Seibert [16]衡量住院病患對於服務品質認知的問卷，其衡量指標包括八個構面：醫師照護、護理照護、醫療結果、禮儀、飲食服務、舒適與清潔、入院/費用與宗教關懷，目前廣泛應用於醫療服務品質之研究。Coddington, Fischer & Moore [18]認為21世紀醫療服務的轉變包括市場與環境的變遷，其所帶來的轉變除了成本面的影響外，最重要的是以顧客為中心的概念，好的醫療服務品質衡量需具備的特性包括友善的員工、能快速預約醫生看診、簡單易於了解的付款程序、清潔且簡要的服務流程聲明、醫師與病患能充分溝通、醫師問診時間充足、具備良好的醫療記錄保存系統、定期的進行檢核確認單等。國內學者湯玲郎與鄭博仁[7]則採用學者Donabedian[22]年所提出的結構、過程、結果三個服務品質構面，結構包括軟、硬體環境，而過程則取自PZB模式問項。

而根據過去之研究文獻指出醫療服務品質與病患滿意度兩者之間相關性甚高，病患滿意度是衡量服務品質的重要指標之一[20,33,41]。而影響醫療服務業之病患滿意度的原因，根據郭德賓[3]的研究可歸納為醫院形象、醫療設備、醫護人員、便利性與醫療費用等五大構面，其中以醫護人員為最高，其次為醫院形象。其他有關住院病患服務品質及滿意度問卷設計的相關研究有Gonzalez, Quintana, Bilbao, Escobar, Aizpuru, Thompson, Esteban, Sebastian & Sierra [24]以西班牙境內的醫院之住院病患為研究對象設計出一套服務品質問卷，並利用因素分析結果，歸納出六個構面：訊息與醫療照護、護理照護、舒適、探訪、隱私與清潔，其團隊之研究發現病患對於舒適構面的滿意度最低，而個人隱私的滿意度最高。Lee, Chang & Chao[29]則採用Carey[16]的服務品質構面設計來研究醫療服務品質與顧客滿意度之關連性。

二、Kano 二維模型

狩野紀昭(Noriaki Kano)、瀨樂信彥、高橋文夫與迂新一[1]引申心理學家赫茲柏格(Frederick Herzberg)於1959年所提出的二因子理論(two-factor theory of jog attitude)，赫茲柏格(Herzberg)所提出的二因子理論(two-factor theory)，又稱激勵－保健理論(motivation-hygiene theory)，主要探討員工的工作滿意度，其將工作滿意度區分為二種因子：激勵因子(motivators)與保健因子(hygiene factors)，並且打破傳統的觀點，認為滿足的反面為“非滿足”，不滿足的反面為“非不滿足”，換言之，當激勵因素具備時會增加滿意程度，但是缺

乏時不會不滿意；當具備保健因子時，不會提高滿程度，但缺乏時則會造成不滿足。赫茲柏格(Herzberg)的二因子理論雖然開創了二元品質的概念，但後來也遭受批評，部分學者認為二因子理論忽略工作滿足與生產力之間的關係，產生滿意未必可以提高生產力，又評估者對於調查結果的解釋容易因人而異，而產生信度的偏差等缺點。但二因子這個概念發展出品質要素的二維度模式，認為品質要素充足時不一定會獲得滿足，有時可能會造成不滿意或沒有感覺。

二因子理論後來經由高橋文夫、狩野紀昭引用定名為“品質的M-H性”，後來更名為魅力品質(Attractive quality)及當然品質(Must-be quality)的名稱。由狩野紀昭(Noriaki Kano)、瀨樂信彥、高橋文夫與迂新一[1]的研究乃將二維概念運用於製造業的品質實證研究，定名為”Kano二維品質模型”並將品質要素區分成二維模型：魅力品質(Attractive quality)與當然品質(Must-be quality)。這套方法被後來的學者運用於製造業與服務業[8,9,27,31,40,42,43]的產品創新與開發。而於醫療業運用則在服務品質的重視下相關研究有逐漸增加的趨勢[7,26,28,29]。

狩野紀昭等人的二維品質模型把品質要素分成下列五大屬性[10]，詳述如下：

魅力品質要素(Attractive Quality Element, A)：當此要素充足時即感到滿足，不充足時顧客也會接受但不會感到不滿意。

一元化品質要素(One-dimensional Quality Element, O)：又稱為線性品質要素，當此品質要素充足時，顧客會感到滿意，但不充足時，會讓顧客感到不滿意。

當然品質要素(Must-be Quality Element, M)：當此品質要素充足時，會讓顧客認為理所當然，因此不會因為具備此項品質要素而讓滿意度上升，但缺乏時，則會使顧客不滿意。

無差異品質要素(Indifferent Quality Element, I)：不論此項品質要素充足與否，都不會引起顧客的滿意或不滿意。

反轉品質要素(Reverse Quality Element, R)此項品質要素充足時，會讓顧客感到不滿意，如果不充足時，反而會讓顧客感到滿意。

二維品質和一維品質的最大差別在於思考邏輯不同，二維品質突破一般線性思考的空間，可以有效洞悉顧客的想法，將品質要素區分成不同屬性與品質，其所代表的意義也都不同，故若將二維品質模型妥善的運用在服務品質上，將有助於明瞭不同服務品質在品質要素分類上的差異，以便能針對其差異之特質提出適當之

改善策略。為了能更進一步找出關鍵品質要素，Matzler & Hinterhuber [30]提出了「顧客滿意係數」的衡量方式，定義出改善品質之指標，其以「魅力品質(A)」加上「一元品質(O)」做為提高滿意之指標，而「一元品質(O)」加上「當然品質(M)」做為改善不滿意之指標，此「顧客滿意係數」主要用以確認針對某品質要素進行改善時，其可能增加顧客滿意度與減少顧客不滿意度各為多少，以得出優先改善之順序。本文亦採用此改善品質指標係數，做為改善服務品質之參考，其公式如下：

式一：增加顧客滿意指標

＝(A+O)／(A+O+M+I)

式二：減少顧客不滿意指標

＝(O+M)／(A+O+M+I)

將Kano二維模型應用於醫療服務品質之相關研究，例如：湯玲郎與鄭博仁[7]以Kano二維模型評估醫療機構服務品質及改善，其研究對象包括六家醫院（成大醫院、亞東醫院、豐原醫院、楊敏盛醫院、桃新醫院及華濟醫院）的醫生、護士及桃園與台北地區的民眾三個族群，結果發現醫療服務品質以一元品質項目居多，再來才是當然品質與魅力品質，且民眾與醫護人員所重視之醫療服務品質要項亦有所不同。Lee, Chang & Chao[29]運用Kano二維模型來進行品質要素之分類，研究醫療服務品質與顧客滿意度之關連性，研究對象為來自二家醫院（一家公立醫學中心與一家私立區域醫院）之病患與員工，病患樣本取自二家醫院，員工樣本則取自私立區域醫院，其研究發現病患最重視的是醫師照護，而最不重視醫院成本。

學者Hu, Cheng, Chiu, & Hong [26]結合二維模型的概念及顧客滿意度指標模型來研究醫療服務品質滿意度與忠誠度之關係，發現一元品質素及魅力品質要素品質對於顧客滿意度有較佳的提升效果。

本研究於醫療服務品質與住院病患滿意度之衡量，依據二維品質模型與顧客滿意度係數，來確認個案醫院之服務品質特性及關鍵服務品質。

參、研究方法

一、研究假設

研究假設如下（以虛無假說之方式表示）：

H1: 不同族群對醫療服務品質特性之認知為一維品質。

H2: 不同族群(醫院員工及住院病患)在品質要素充足及不充足時看法相同。

H3: 不同人口統計變項的住院病患對醫院各項服務品質構面滿意度無顯著差異。

二、問卷設計與研究對象

本研究以調查研究方法為主,依研究目的本問卷的設計分為二方面來調查,一為Kano二維品質特性模型問卷調查及服務品質滿意度之問卷調查,研究對象為個案醫院之醫院員工及住院病患,以確認研究對象對於醫療服務品質之二維品質特性分類及關鍵服務品質特性,同時瞭解醫院員工及住院病患對於醫院服務品質之滿意度程度。服務品質要項的問卷設計參考前述學者之相關研究構面[22,7,16]所提出之適合醫院服務品質的構面,共八個構面包括軟、硬體環境、專業性及可靠性、溝通能力與反應性、保證性、友善及關懷性、國際化及就醫結果。並親自參訪醫院及聽取院方人士簡介並依其作業特性,得出本研究之初步50項服務品質特性要項後,再經前測修正後為縮減為39問項。問卷的問題設計方式分為二大部份,第一部份為醫院員工及住院病患對Kano二維模型之「正向」及「反向」服務品質特性之認知調查與滿意度調查,第二部份則為個人基本資料,包括個人身份、性別、年齡、婚姻、教育程度、居住的區域、住院科別等。第一部份之Kano二維模型,其服務品質特性設計為正向(品質要素充足時)與反向(品質要素不充足時)的39個成對問題,問卷問題答案分為五個衡量選項,分別為滿意、理所當然、沒感覺、能忍受及不滿意,而服務品質特性問卷之問題答案則採李克特(Likert)五點量尺,受訪人員依一分到五分選擇填答,一分為極不滿意,二分為不滿意,三分表普通,四分表滿意,五分為非常滿意。

本研究主要以中部某個案醫院的醫院員工及住院病患為對象,調查日期乃自民國96年10月中旬到11月中旬,本問卷調查方式採用簡單隨機抽樣,並排除死亡、待轉院、加護病房、精神科、隔離病房及安寧病房之住院病患,由護理站提供住院病患名單並以符合調查對象為樣本。由調查人員於各病房對住院病患進行現場問卷調查,調查之抽樣樣本包括醫院員工及住院病患,問卷實施期間為民國96年10月中旬到11月31日止,調查的時段平均分散於平日及假日的時段,以提高樣本之代表性,問卷共發放350份,回收350份(其中醫院員工之問卷150份,住院病患問卷200份),扣除無效問卷61份(員工50份及住院病患11份),共得有效樣本289份(員工100份及住院病患189份),有效回收率達82.57%。

肆、資料分析

本研究藉由SPSS for Window 12.0版統計套裝軟體進行問卷資料處理,此部份之分析包括:敍述統計分析、信度分析、t檢定、單因子變異數分析與LSD事後檢

定等。

一、基本資料分析

有效問卷受測者(醫院員工與住院病患)之基本資料整理(如表1)，分別說明如下。醫院員工部份的基本資料結構中男性佔16%，女性佔84%；年齡層則多為21-30歲居多，其次為31-40歲；婚姻方面，未婚或單身佔54%，已婚但未有子女佔4%，已婚但已有子女佔42%；教育程度則以專科及大學最多，佔全體員工之93%；身份則以聘僱居多佔50%，公務人員則佔39%；服務年資則多數為5年以上；專業方面則以醫師佔16%、護士佔50%、一般行政人員佔19%、醫檢人員佔11%、藥劑人員及營養人員分佔2%及1%；

住院病患部份中，於性別方面，以女性居多(66.1%)，男性則為(33.9%);年齡層以21-30歲之年輕群居多(23.3%)，以31~40歲者最少(19%)；婚姻方面大部份受測病患為已婚且已有子女居多(58.2%)，其次為未婚且單身(37.6%)；教育程度國中以下佔32.8%，高中職族群為27.5%，專科大學以上為39.1%；職業則以學生居多(18.5%)；居住地區則以豐原市為主(39.2%)；住院科別以內科為多數(29.1%)，其次為外科(23.8%)；病房單位則大多為16病房之住院病患(38.1%)，其餘則均勻分配；主要照顧者方面以家屬居多佔86.8%，完成問卷者則以家屬居多佔60.3%，由於某些病患不方便填寫問卷，在訪問人員之陪同下，由家屬代為詢問並填寫，但仍以病患之意見為主。

表 1　醫院員工與住院病患基本資料結構

醫院員工				住院病患			
基本資料	項目	人數	百分比(%)	基本資料	項目	人數	百分比(%)
性別	男	16	16%	性別	男	64	33.9%
	女	84	84%		女	125	66.1%
年齡	20 歲以下	1	1%	年齡	20 歲以下	31	16.4%
	21-30 歲	49	49%		21-30 歲	44	23.3%
	31-40 歲	32	32%		31-40 歲	21	11.1%
	41-50 歲	12	12%		41-50 歲	36	19.0%
	51-60 歲	3	3%		51-60 歲	33	17.5%
婚姻	未婚或單身	54	54%		61 歲以上	24	12.7%
	已婚但未有子女	4	4%	婚姻	未婚或單身	71	37.6%
	已婚但已有子女	42	42%		已婚但未有子女	8	4.2%

	國中	1	1%		已婚但已有子女	110	58.2%
教育程度	高中職	3	3%	教育程度	小學以下	33	17.5%
	專科	44	44%		國中	29	15.3%
	大學	49	49%		高中職	52	27.5%
	研究所以上	3	3%		專科	25	13.2%
身份	公務人員	39	39%		大學	46	24.3%
	聘僱	50	50%		研究所以上	3	1.6%
	臨時約僱	6	6%		未填	1	0.5%
	其他	5	5%	職業	無	29	15.3%
服務年資	1 年以下(含1 年)	21	21%		軍公教人員	5	2.6%
	1-3 年	19	19%		農	7	3.7%
	3-5 年	14	14%		工	30	15.9%
	5-10 年	20	20%		商	20	10.6%
	10 年以上	24	24%		學生	35	18.5%
	未填	2	2%		自由業	21	11.1%
專業	住院醫師	12	12%		服務業	26	13.8%
	主治醫師	3	3%		其他	16	8.5%
	主任或主任級醫師	1	1%	居住地區	豐原	74	39.2%
	護理人員	49	49%		潭子	38	20.1%
	專科護理師	1	1%		后里	11	5.8%
	醫檢人員	11	11%		神岡	12	6.3%
	藥劑人員	2	2%		大雅	5	2.6%
	營養人員	1	1%		其他	49	25.4%
	一般行政人員	19	19%	住院科別	內科	55	29.1%
	其他	1	1%		外科	45	23.8%
					婦產科	31	16.4%
					牙科	1	0.5%
					兒科	6	3.2%
					復健科	3	1.6%
					耳鼻喉科	3	1.6%
					骨科	39	20.6%
					其他	6	3.2%
				病房單位	13 病房	29	15.3%
					15 病房	13	6.9%
					16 病房	72	38.1%

					17 病房	10	5.3%
					18 病房	27	14.3%
					22 病房	15	7.9%
					23 病房	3	1.6%
					其他	20	10.6%
				主要照顧者	家屬	164	86.8%
					看護	12	6.3%
					朋友	8	4.2%
					無人照顧	5	2.6%
				完成此問卷者	病患本人	50	26.5%
					家屬	114	60.3%
					看護	12	6.3%
					朋友	13	6.9%

二、信度分析

本研究以Cronbach’s α分析內部一致性，檢定Kano二維設計之問卷量表及住院病患滿意度之信度，Cronbac’s α值如表2所示。Guilfold[25]指出Cronbach α係數大於0.7則具有高信度值，如低於0.35則為低信度值，應予以拒絕。本研究之分析結果問卷整體信度皆大於0.7以上，顯示問卷資料屬於高信度值。

表 2　問卷之 Cronbach’s α 係數表

構面	信度 Cronbach α 值				
	Kano 二維模型				滿意度
	正面問項		反面問項		
	員工	病患	員工	病患	病患
硬體環境	0.897	0.783	0.880	0.937	0.898
軟體環境	0.826	0.781	0.881	0.845	0.786
專業性等	0.838	0.826	0.898	0.896	0.896
溝通力等	0.814	0.749	0.866	0.879	0.879
保證性	0.803	0.735	0.887	0.862	0.862

關懷性等	0.907	0.857	0.948	0.857	0.914
國際化	0.772	0.701	0.724	0.771	0.757
醫療結果	0.821	0.781	0.896	0.781	0.877
整體信度	0.964	0.951	0.977	0.978	0.957

三、Kano 二維品質分析

住院病患與醫院員工之Kano二維品質特性分類之結果分別列示於表3及表4，而不同身份群之服務品質特性分類結果比較列示於表5；其構面分類品質特性歸類，係根據Kano文獻之分類步驟，將構面中之各問項所歸類出的不同之品質特性頻次進行加總，找出相對最高頻次來決定其分類。

首先，表3針對住院病患之39個問項之二維品質分類，有30個問項被歸類為一元品質(O)，當然品質(M)有2個問項，而無差異品質(I)則有7項；而醫院員工的Kano二維品質特性歸類如表4，其中以當然品質(M)居多佔22個問項，一元品質(O)則為1個問項，無差異品質(I)則有16個問項。以構面來看，在住院病患方面，除了國際化與醫療結果二個構面為無差異品質(I)外，其餘皆為一元品質(O)；在醫院員工方面，硬體環境、軟體環境、專業性及可靠性、醫療結果等四個構面為當然品質(M)，溝通能力與反應性、保證性、友善及關懷性、國際化為無差異品質(I)。因此不論以問項來看或是以構面來看，整體而言，個案醫院之服務品質特性具有二維品質特性。就住院病患與醫院員工而言，其Kano二維品質特性分類之看法之異同茲詳述如下：

(一) 住院病患與醫院員工意見一致的品質要素為：

1. 「醫院的環境及衛生狀況良好」之品質要素而言，醫院員工與住院病患均認為是當然品質，因此醫院在環境整體規劃與清潔方面，兩者均認為是理所當然，如果未能充足時，則會引起不滿，因此醫院在環境及清潔方面應保持一定的水準，才能符合大眾的需求與期望。
2. 於「醫院有良好的伙食時」、「醫師時常發表研究計劃時」、「醫護人員保持對病患的禮貌態度時」、「醫護人員及員工具備基礎的英語能力」、「醫院提供國際語言（英語）的咨詢服務」等之品質要素方面，不論是醫院員工或住院病患皆認為是無差異品質，因此兩者均認為這些品質要項充足與否，都不會引起不滿。

(二) 住院病患與醫院員工意見不一致的品質要素為：

1. 「醫院交通便利」住院病患認為是當然品質，而醫院員工認為是無差異品質，此項品質就住院病患而言，到達醫院的交通工具或交通方便性是理所當然，如果不充足則會引起不滿意。顯見醫院員工則與住院病患存在認知上的差異，住院病患比醫院員工更重視醫院交通便利性。
2. 「完善先進的醫療設備」、「無障礙設施環境」、「各科別標示很清楚」、「現代化與電腦化的服務」、「完善的醫療保險服務」、「容易找到所需的醫護人員」、「能按時執行對病患的承諾」、「能迅速處理抱怨」、「醫師與護理人員良好的專業訓練與技術」、「醫師有良好的診斷能力」、「回答諮詢」、「收費合理」、「醫師能詳細診察並詳細說明病情」、「醫師能詳細說明病人的治療方式」、「護理人員能給予適切的護理指導」、「醫護人員能詳細說明藥劑服用的方式」、「就醫後，病情能有很好的改善」等品質要素，住院病患認為是一元品質，而醫院員工認為是當然品質。可見醫院員工對醫院服務品質的要求，比住院病患更高，可能是因為住院病患已習慣一般醫院的服務品質，因此，如具備時則會感到滿意，不具備會引起不滿，然而醫院員工則可能因為目前醫療市場的競爭所致，體認到目前以顧客為導向的市場，對於醫療服務品質的重視更甚於住院病患。
3. 「醫院能設置兒童遊戲室並有專人看顧」、「醫院有各項簡介或衛教資料」、「醫院聲譽良好時」、「掛號（候診、檢驗、領藥、批藥、注射）時，等待時間比較短」、「快速辦妥住院手續並住入病房」、「對訪客人數與探訪時間進行管理，維持病房安寧」、「醫院和社區關係良好，經常舉辦義診、健康檢查及疾病防治等活動」、「醫師能耐心傾聽病人之病情時」、「醫師能詳細說明處方時」、「醫護人員能傾聽病患之需求時」等品質要素，住院病患認為是一元品質，而醫院員工認為是無差異品質。由此結果知，醫院員工對於這些醫療服務品質的重視與住院病患有認知上的差異，可能原因是醫護人員，普遍認為專業技術品質比週邊服務更重要，然而病患所重視的除了專業技術外，尚期望醫院能提供更多的友善與關懷，畢竟住院病患是在生理上承受病痛之苦，故會更希望能在心理上獲得友善與關懷的對待，因此醫院應特別重視這個層面的服務。

住院病患對問題的反應，大部份都歸類在一元品質，因此這部份可用傳統的滿

意度調查來衡量其滿意程度大小。另外，大部份都歸類在一元品質可能原因，可能問卷設計的問項內容為一般公認的服務品質項目，所以提愈完善則滿意度愈高，亦有可能問卷大多由家屬代為填答，因此回答問題的角度與認知有別於病患本身的看法，再加上問卷的問項較多，受測者在填答時，較無法耐心並仔細的審視問題，回答較無法深入。

4. 「醫護人員的工作時數正常」、「醫院能在病人出院後，定期追踪病人的癒後狀態」、「醫院能在病人出院前，做詳細的衛教」等之品質要素，住院病患認為是無差異品質，而醫院員工認為是當然品質。住院病患對於醫護人員的工時正常與否，並沒有特別的感受，而醫院員工則因切身問題而較重視，另外，在病人癒後狀態追踪與衛教方面，病患與醫院員工認知不同，對於住院病患而言需求不高。

茲就上述結果，可知本文所提之H1假設是被拒絕的，即住院病患與醫院員工對醫療服務品質特性之問卷調查結果可歸類出一維品質以外之品質特性，顯示存在二維品質特性。另外，整體而言，39個品質要素中，醫院員工與住院病患看法一致的只有7項品質要素，其餘皆有不同看法，此結果拒絕H2假設。

表 3　住院病患之 Kano 二維品質屬性分類

構面	品質要素	魅力品質 (A)	一元品質 (O)	當然品質 (M)	無差異品質 (I)	品質歸類
硬體環境	1.醫院交通方便	30	55	59	38	M
		15.87%	29.10%	31.22%	20.11%	
	2.醫院有完善先進的醫療設備	27	64	53	39	O
		14.29%	33.86%	28.04%	20.63%	
	3.醫院能提供無障礙設施環境	25	62	41	55	O
		13.23%	32.80%	21.69%	29.10%	
	4.醫院能設置兒童遊戲室並有專人看顧	40	53	41	48	O
		21.16%	28.04%	21.69%	25.40%	
	5.醫院各科別上標示很清楚	28	58	55	39	O
		14.81%	30.69%	29.10%	20.63%	
	6.醫院的環境及衛生狀況良好	25	53	56	43	M
		13.23%	28.04%	29.63%	22.75%	
	7.醫院有良好的伙食時	27	47	44	61	I
		14.29%	24.87%	23.28%	32.28%	
	8.醫院有各項簡介或衛教資料	36	56	35	53	O
		19.05%	29.63%	18.52%	28.04%	
構面服務品質屬性		125.93%	237.03%	203.17%	198.94%	O

軟體環境	9.醫院有現代化與電腦化的服務	31	60	48	41	O
		16.40%	31.75%	25.40%	21.69%	
	10.醫院提供完善的醫療保險	20	73	38	46	O
		10.58%	38.62%	20.11%	24.34%	
	11.醫院聲譽良好時	39	55	36	53	O
		20.63%	29.10%	19.05%	28.04%	
構面服務品質屬性		47.61%	99.47%	64.56%	74.07%	O
專業性及可靠性	13.住院病患有需要可以立刻找到所需的醫護人員	22	69	46	42	O
		11.64%	36.51%	24.34%	22.22%	
	14.對病患的承諾，醫護人員都能按時執行	20	70	50	38	O
		10.58%	37.04%	26.46%	20.11%	
	15.病人抱怨時，醫護人員能迅速處理時	22	71	43	44	O
		11.64%	37.57%	22.75%	23.28%	
	22.醫師與護理人員有良好的專業訓練與技術	17	78	52	31	O
		8.99%	41.27%	27.51%	16.40%	
	23.醫師有良好的診斷能力	16	80	54	33	O
		8.47%	42.33%	28.57%	17.46%	
	33.醫護人員的工作時數正常	29	53	44	57	I
		15.34%	28.04%	23.28%	30.16%	
構面服務品質屬性		44.44%	149.21%	102.11%	87.30%	O
溝通與反應性	16.不論是向醫護人員或服務人員諮詢時，都能快速得到回答時	25	64	41	51	O
		13.23%	33.86%	21.69%	26.98%	
	17.掛號(候診、檢驗、領藥、批藥、注射)時，等待時間比較短	28	57	51	44	O
		14.81%	30.16%	26.98%	23.28%	
	18.住院病患能快速辦妥住院手續並住入病房(手續簡便)	32	71	38	37	O
		16.93%	37.57%	20.11%	19.58%	
構面服務品質屬性		44.97%	101.59%	68.78%	69.84%	O
保證性	19.在醫院中進行治療感到十分安全(診療隱密性)時	29	64	41	45	O
		15.34%	33.86%	21.69%	23.81%	
	20.訪客人數與探訪時間進行管理，維持病房安寧	35	55	45	48	O
		18.52%	29.10%	23.81%	25.40%	
	21.醫院各項收費合理時(掛號、診療，收費明細完整)	26	63	50	43	O
		13.76%	33.33%	26.46%	22.75%	
	24.醫師能詳細診察並詳細說明病情	25	74	45	36	O
		13.23%	39.15%	23.81%	19.05%	

	25.醫師能詳細說明病人的治療方式	18	75	49	39	O
		9.52%	39.68%	25.93%	20.63%	
	32.醫師時常發表研究計劃時	25	46	31	81	I
		13.23%	24.34%	16.40%	42.86%	
構面服務品質屬性		83.60%	199.46%	138.10%	154.50%	O
友善及關懷性	12.醫院和社區關係良好，經常舉辦義診、健康檢查及疾病防治等活動	32	59	37	52	O
		16.93%	31.22%	19.58%	27.51%	
	26.醫師能耐心傾聽病人之病情時	23	72	43	44	O
		12.17%	38.10%	22.75%	23.28%	
	27.醫師能詳細說明處方時	24	66	46	44	O
		12.70%	34.92%	24.34%	23.28%	
	28.醫師能每日探視住院病患	30	70	39	43	O
		15.87%	37.04%	20.63%	22.75%	
	29.護理人員能給予病人適切的護理指導	25	73	40	42	O
		13.23%	38.62%	21.16%	22.22%	
	30.醫護人員能傾聽病患之需求時	22	71	47	41	O
		11.64%	37.57%	24.87%	21.69%	
	31.醫護人員保持對病患的禮貌態度時	29	59	34	60	I
		15.34%	31.22%	17.99%	31.75%	
	34.醫護人員能向病患詳細說明藥劑服用的方式	26	58	40	54	O
		13.76%	30.69%	21.16%	28.57%	
構面服務品質屬性		111.64%	279.38%	172.48%	201.05%	O
國際化	38.醫護人員及員工具備基礎的英語能力	34	34	27	85	I
		17.99%	17.99%	14.29%	44.97%	
	39.醫院提供國際語言(英語)的咨詢服務	16	18	17	80	I
		8.47%	9.52%	8.99%	42.33%	
構面服務品質屬性		26.46%	27.51%	23.28%	87.30%	I
醫療結果	35.您在就醫後，病情能有很好的改善	24	64	43	53	O
		12.70%	33.86%	22.75%	28.04%	
	36.醫院能在病人出院後，定期追踪病人的癒後狀態	30	54	35	62	I
		15.87%	28.57%	18.52%	32.80%	
	37.醫院能在病人出院前，做詳細的衛教	20	57	27	75	I
		10.58%	30.16%	14.29%	39.68%	
構面服務品質屬性		39.15%	92.59%	55.56%	100.52%	I

表 4　醫院員工之 Kano 二維品質屬性分類

構面	問項	魅力品質 (A)	一元品質 (O)	當然品質 (M)	無差異品質 (I)	品質歸類
硬體環境	1.醫院交通方便	17	12	27	40	I
		17%	12%	27%	40%	
	2.醫院有完善先進的醫療設備	4	18	49	25	M
		4%	18%	49%	25%	
	3.醫院能提供無障礙設施環境	14	16	36	30	M
		14%	16%	36%	30%	
	4.醫院能設置兒童遊戲室並有專人看顧	13	7	31	43	I
		13%	7%	31%	43%	
	5.醫院各科別上標示很清楚	8	12	43	32	M
		8%	12%	43%	32%	
	6.醫院的環境及衛生狀況良好	5	16	46	28	M
		5%	16%	46%	28%	
	7.醫院有良好的伙食時	10	6	31	45	I
		10%	6%	31%	45%	
	8.醫院有各項簡介或衛教資料	10	12	33	44	I
		10%	12%	33%	44%	
構面服務品質屬性		81%	99%	296%	287%	M
軟體環境	9.醫院有現代化與電腦化的服務	16	6	41	36	M
		16%	6%	41%	36%	
	10.醫院提供完善的醫療保險	10	13	45	31	M
		10%	13%	45%	31%	
	11.醫院聲譽良好時	16	8	34	39	I
		16%	8%	34%	39%	
構面服務品質屬性		42%	27%	120%	106%	M
專業性及可靠性	13.住院病患有需要可以立刻找到所需的醫護人員	9	10	38	40	M
		9%	10%	38%	40%	
	14.對病患的承諾，醫護人員都能按時執行	12	5	46	35	M
		12%	5%	46%	35%	
	15.病人抱怨時，醫護人員能迅速處理時	13	6	47	32	M
		13%	6%	47%	32%	
	22.醫師與護理人員有良好的專業訓練與技術	4	17	51	26	M
		4%	17%	51%	26%	
	23.醫師有良好的診斷能力	5	11	42	41	M
		5%	11%	42%	41%	
	33.醫護人員的工作時數正常	2	16	38	29	M
		2%	16%	38%	29%	
構面服務品質屬性		45%	65%	262%	203%	M

溝通與反應性	16.不論是向醫護人員或服務人員諮詢時，都能快速得到回答時	11	8	44	35	M
		11%	8%	44%	35%	
	17.掛號(候診、檢驗、領藥、批藥、注射)時，等待時間比較短	8	9	33	46	I
		8%	9%	33%	46%	
	18.住院病患能快速辦妥住院手續並住入病房(手續簡便)	16	5	24	53	I
		16%	5%	24%	53%	
構面服務品質屬性		35%	22%	101%	134%	I
保證性	19.在醫院中進行治療感到十分安全(診療隱密性)時	13	10	43	33	M
		13%	10%	43%	33%	
	20.訪客人數與探訪時間進行管理，維持病房安寧	12	9	33	40	I
		12%	9%	33%	40%	
	21.醫院各項收費合理時(掛號、診療，收費明細完整)	13	14	37	34	M
		13%	14%	37%	34%	
	24.醫師能詳細診察並詳細說明病情	5	13	44	37	M
		5%	13%	44%	37%	
	25.醫師能詳細說明病人的治療方式	4	12	53	29	M
		4%	12%	53%	29%	
	32.醫師時常發表研究計劃時	13	3	22	61	I
		13%	3%	22%	61%	
構面服務品質屬性		60%	61%	232%	234%	I
友善及關懷性	12.醫院和社區關係良好，經常舉辦義診、健康檢查及疾病防治等活動	25	9	28	34	I
		25%	9%	28%	34%	
	26.醫師能耐心傾聽病人之病情時	4	12	40	42	I
		4%	12%	40%	42%	
	27.醫師能詳細說明處方時	8	7	33	50	I
		8%	7%	33%	50%	
	28.醫師能每日探視住院病患	6	9	41	43	O
		6%	9%	41%	43%	
	29.護理人員能給予病人適切的護理指導	11	10	43	36	M
		11%	10%	43%	36%	
	30.醫護人員能傾聽病患之需求時	12	10	38	40	I
		12%	10%	38%	40%	
	31.醫護人員保持對病患的禮貌態度時	13	11	35	41	I
		13%	11%	35%	41%	
	34.醫護人員能向病患詳細說明藥劑服用的方式	9	14	49	26	M
		9%	14%	49%	26%	
構面服務品質屬性		88%	82%	307%	312%	I

國際化	38.醫護人員及員工具備基礎的英語能力	6	6	26	57	I
		6%	6%	26%	57%	
	39.醫院提供國際語言(英語)的咨詢服務	6	6	21	61	I
		6%	6%	21%	61%	
構面服務品質屬性		12%	12%	47%	118%	I
醫療結果	35.您在就醫後，病情能有很好的改善	11	9	56	23	M
		11%	9%	56%	23%	
	36.醫院能在病人出院後，定期追踪病人的癒後狀態	14	7	40	39	M
		14%	7%	40%	39%	
	37.醫院能在病人出院前，做詳細的衛教	12	7	45	36	M
		12%	7%	45%	36%	
構面服務品質屬性		37%	23%	141%	98%	M

表 5 不同身份群對於服務品質特性之歸類比較

構面	品質要素	品質特性歸類	
		醫院員工	住院病患
硬體環境	1.醫院交通方便	I	M
	2.有完善先進的醫療設備	M	O
	3.提供無障礙設施環境（如:愛心鈴、斜坡道等）	M	O
	4.設置兒童遊戲室並有專人看顧，以方便問診	I	O
	5.各科別上標示很清楚	M	O
	6.環境及衛生狀況良好	M	M
	7.有良好的伙食時	I	I
	8.有各項簡介或衛教資料	I	O
	構面品質特性歸類	M	O
軟體環境	9.有現代化與電腦化的服務	M	O
	10.提供完善的醫療保險服務（如：健保）時	M	O
	11.聲譽良好時	I	O
	構面品質特性歸類	M	O
專業性及可靠性	13.住院病患有需要能立刻找到所需的醫護人員	M	O
	14.對病患的承諾，醫護人員都能按時執行	M	O
	15.病人抱怨時，醫護人員能迅速處理時	M	O
	22.醫師與護理人員有良好的專業訓練與技術	M	O
	23.醫師有良好的診斷能力	M	O

構　　面	品　質　要　素	品質特性歸類 醫院員工	 住院病患
	33.醫護人員的工作時數正常	M	I
	構面品質特性歸類	M	O
溝通能力與反應性	16.病患諮詢能快速得到回答時	M	O
	17.掛號時，等待時間比較短	I	O
	18.住院病患能快速辦妥住院手續並住入病房	I	O
	構面品質特性歸類	I	O
保證性	19.在醫院中進行治療感到十分安全	M	O
	20.醫院能對訪客人數與探訪時間進行管理	I	O
	21.醫院各項收費合理時	M	O
	24.醫師能詳細診察並詳細說明病情	M	O
	25.醫師能詳細說明病人的治療方式	M	O
	32.醫師時常發表研究計劃時	I	I
	構面品質特性歸類	I	O
友善及關懷性	12.醫院和社區關係良好	I	O
	26.醫師能耐心傾聽病人之病情時	I	O
	27.醫師能詳細說明處方時	I	O
	28.醫師能每日探視住院病患	O	O
	29.護理人員能給予病人適切的護理指導	M	O
	30.醫護人員能傾聽病患之需求時	I	O
	31.醫護人員保持對病患的禮貌態度時	I	I
	34.醫護人員能向病患詳細說明藥劑服用的方式	M	O
	構面品質特性歸類	I	O
國際化	38.醫護人員及員工具備基礎的英語能力	I	I
	39.醫院提供國際語言（英語）的咨詢服務	I	I
	構面品質特性歸類	I	I
醫療結果	35.您在就醫後，病情能有很好的改善	M	O
	36.醫院能在病人出院後，定期追踪病人的癒後狀態	M	I
	37.醫院能在病人出院前，做詳細的衛教	M	I
	構面品質特性歸類	M	I

註：A:魅力品質， I:無差異品質， O:一元化品質， M:當然品質

四、醫療服務品質改善指標

為有效的提升滿意度，並了解哪些執行改善作業能對住院病產生最大效益，本研究利用「顧客滿意係數」之計算，此法可找出優先改善之參考順序服務品質問項，以確認針對某品質要素進行改善時，能找出優先改善之參考順序。其分析方式，首先根據前述之公式計算出醫院員工與住院病患各問項之顧客滿意係數值，其次計算二族群之增加滿意度係數總平均值與減少不滿意度係數之總平均值，找出高於平均係數值之服務品質問項，最後落於高度增加住院病患滿意度與高度減少住院患滿意度之品質要素，便是個案醫院的關鍵服務品質特性及應優先改善之項目。

而有關不同族群對於服務品質改善指標，根據總平均值來看，不論問項或構面來看，有些項目可同時提高全體人員之滿意度，但大部份以住院病患的期望最高，所以在提升滿意度上應優先以住院病患的意見為考量。茲就表6之統計結果敘述如下：

(一) 同時為高度增加滿意度與高度減少不滿意度之服務品質問項

1. 住院病患部份：落於高度增加滿意度與高度減少不滿意度之關鍵服務品質問項共有17項，包括Q2「醫院有完善先進的醫療設備」、Q9「醫院有現代化與電腦化的服務」及Q10「醫院提供完善的醫療保險服務（如：健保）時」；專業性及可靠性有2項：Q13「住院病患有需要可以立刻找到所需的醫護人員」、Q 14「對病患的承諾，醫護人員都能按時執行」、Q 15「病人抱怨時，醫護人員能迅速處理時」、Q 16「不論是向醫護人員或服務人員諮詢時，都能快速得到回答時」、Q 18「住院病患能快速辦妥住院手續並住入病房」、Q 19「在醫院中進行治療感到十分安全」、Q 21「醫院各項收費合理時」、Q 22「醫師與護理人員有良好的專業訓練與技術」、Q 23「醫師有良好的診斷能力」、Q 24「醫師能詳細診察並詳細說明病情」、Q 26「醫師能耐心傾聽病人之病情時」、Q 27「醫師能詳細說明處方時」、Q 29「護理人員能給予病人適切的護理指導」、Q30「醫護人員能傾聽病患之需求時」所有的關鍵服務品質要素皆為一元品質，因此若能加強相關服務與設施，則能增加的滿意度與減少的不滿意均較高。

2. 醫院員工部份：落於高度增加滿意度與高度減少不滿意度之關鍵服務品質問項共有11項，包括Q2「有完善

先進的醫療設備」、Q3「醫院能提供無障礙設施環境(如:愛心鈴、斜坡道等)」、Q 4「醫院能設置兒童遊戲室並有專人看顧，以方便問診」、Q 6「醫院的環境及衛生狀況良好」、Q 10「醫院提供完善的醫療保險服務(如：健保)時」、Q 22「醫師與護理人員有良好的專業訓練與技術」、Q 33「醫護人員的工作時數正常」、Q 19「在醫院中進行治療感到十分安全」、Q 21「醫院各項收費合理時」、Q 29「護理人員能給予病人適切的護理指導」、Q 34「醫護人員能向病患詳細說明藥劑服用的方式」。

綜合上述之結果，其中於有6項Q2、Q10、Q22、Q19、Q21、Q29可同時提升醫院員工與住院病患之滿意度。

(二) 同時為高度增加滿意度與高度減少不滿意度之服務品質構面

就構面而言,醫院管理當局應優先改善「硬體環境」、「軟體環境」、「專業性及可靠性」、「溝通能力與反應性」、「保證性」、「友善及關懷性」等方面以提升較多的住院病患滿意度(滿意指標較高)。綜合上述「顧客滿意係數」之分析，可提供醫院管理當局做為改善服務品質之參考指標，以提升其服務品質之滿意度。

表 6 醫院員工與住院病患之「顧客滿意係數」分析表

構面	問項	依問項分析				依構面分析			
		醫院員工		住院病患		醫院員工		住院病患	
		增加滿意	減少不滿意	增加滿意	減少不滿意	增加滿意	減少不滿意	增加滿意	減少不滿意
	1	**0.30**	0.41	0.47	**0.63**				
	2	**0.23**	**0.70**	**0.50**	**0.64**				
	3	**0.31**	**0.54**	0.48	0.56				
硬體環境	4	**0.21**	0.40	**0.51**	0.52	**0.24**	**0.52**	**0.47**	**0.58**
	5	**0.21**	**0.58**	0.48	**0.63**				
	6	**0.22**	**0.65**	0.44	**0.62**				
	7	0.17	0.40	0.41	0.51				
	8	**0.22**	0.45	**0.51**	0.51				
	9	**0.22**	0.47	**0.51**	**0.60**				
軟體環境	10	**0.23**	**0.59**	**0.53**	**0.63**	**0.23**	**0.50**	**0.51**	**0.57**
	11	**0.25**	0.43	**0.51**	0.50				
	13	0.20	0.49	**0.51**	**0.64**				
專業性等	14	0.17	**0.52**	**0.51**	**0.67**	0.19	**0.57**	**0.51**	**0.66**
	15	0.19	**0.54**	**0.52**	**0.63**				
	22	**0.21**	**0.69**	**0.53**	**0.73**				

構面	問項	依問項分析				依構面分析			
		醫院員工		住院病患		醫院員工		住院病患	
		增加滿意	減少不滿意	增加滿意	減少不滿意	增加滿意	減少不滿意	增加滿意	減少不滿意
	23	0.16	**0.54**	**0.52**	**0.73**				
	33	**0.21**	**0.64**	0.45	0.53				
溝通能力	16	0.19	**0.53**	**0.49**	**0.58**				
	17	0.18	0.44	0.47	**0.60**	0.20	0.42	**0.51**	**0.60**
	18	**0.21**	0.30	**0.58**	**0.61**				
保證性	19	**0.23**	**0.54**	**0.52**	**0.59**				
	20	**0.22**	0.45	**0.49**	0.55				
	21	**0.28**	**0.52**	**0.49**	**0.62**	0.21	**0.50**	**0.49**	**0.59**
	24	0.18	**0.58**	**0.55**	**0.66**				
	25	0.16	**0.66**	**0.51**	**0.69**				
	32	0.16	0.25	0.39	0.42				
關懷性	12	**0.35**	0.39	**0.51**	0.53				
	26	0.16	**0.53**	**0.52**	**0.63**				
	27	0.15	0.41	**0.50**	**0.62**				
	28	0.15	**0.51**	**0.55**	**0.60**	0.22	**0.49**	**0.51**	**0.59**
	29	**0.21**	**0.53**	**0.54**	**0.63**				
	30	**0.22**	0.48	**0.51**	**0.65**				
	31	**0.24**	0.46	0.48	0.51				
	34	**0.23**	**0.64**	0.47	0.55				
國際化	38	0.13	0.34	0.38	0.34	0.13	0.31	0.33	0.31
	39	0.13	0.29	0.26	0.27				
醫療結果	35	0.20	**0.66**	0.48	**0.58**				
	36	**0.21**	0.47	0.46	0.49	0.20	**0.55**	0.46	0.51
	37	0.19	**0.52**	0.43	0.47				
總平均		0.21	0.50	0.49	0.57	0.22	0.47	0.47	0.55

註：
1. 「增加滿意」表示增加滿意係數，其計算公式為（A+O）/（A+O+M+I）；
2. 「減少不滿意」表示減少不滿意係數，其計算公式為（O+M）/（A+O+M+I）
3. 黑色粗體表示高於增加滿意度係總平均值與減少不滿意度係數之總平均值之「顧客滿意度係數值」
4. 陰影表示落於高度增加顧客滿意與高度減少顧不滿意之服務品質特性

五、不同人口統計變項之住院病患對服務品質滿意度與差異性分析

(一) 住院病患滿意度分析

根據統計分析結果，住院病患之滿意度平均值及標準差分析結果得知整體的滿意度平均值為3.65，標準差為0.61，可

知住院病患對於個案醫院之整體滿意度是介於普通到滿意之間。以構面來看，「友善與關懷性」為病患評價最高之構面，其次為「專業及可靠性」。

以39項醫院服務品質要素來看，住院病患認為最佳的項目依序為：醫護人員能傾聽病患之需求時(3.82)、醫院有完善先進的醫療設備(3.81)、護理人員能給予病人適切的護理指導(3.81)、醫護人員能向病患詳細說明藥劑服用的方式(3.78)、在醫院中進行治療感到十分安全(診療隱密性)(3.77)、醫師能每日探視住院病患(3.77)，而住院病患認為相對較不滿意的項目依序為:醫院提供國際語言(英語)的咨詢服務(3.52)、掛號(候診、檢驗、領藥、批藥、注射)時(3.52)、醫院能設置兒童遊戲室並有專人看顧，以方便您問診(3.57)、醫院有良好的伙食時(3.58)、醫院聲譽良好時(3.58)。

(二)差異分析

為了解不同的人口統計變數對醫院服務品質之滿意程度是否有差異，茲分別就住院病患之性別、年齡、婚姻、教育程度、職業、居住地區、住院科別、病房單位等方面，進行醫院服務品質構面差異性分析。不同性別間，由於探討男女兩群體，故採用t分配檢定，其餘人口統計變項之群體則大於2群，採單因子變異數之F檢定。由表7之分析結果敘述如下：

1. 不同年齡之住院病患，對醫院服務品質滿意度的「專業性及可靠性」、「溝通能力與反應性」、「保證性」、「友善及關懷性」等四個構面，具有顯著差異。
2. 不同婚姻狀況之住院病患在「專業性及可靠性」、「溝通能力與反應性」、「保證性」、「友善及關懷性」、及「醫療結果」等五個構面，具有顯著差異。
3. 其餘之人口統計變項之住院病患，對醫院服務品質之構面無顯著差異。

綜合上述，虛無假設H3在年齡與婚姻狀況二項人口統計變數上，結論為不成立，其餘人口統計變數之檢定結果無法拒絕虛無假設，結論成立。又在不同年齡與不同婚姻狀況下其ANOVA檢定之F值達顯著水準，表示群族之間具有顯著差異，因此進行LSD事後檢定（見表8）。依住院病患人口統計變數與醫院服務品質之事後檢定，結果顯示，以年齡來看「41-50歲」與「61歲以上」之族群有較高之滿意度，在婚姻狀況來看，已婚且已有子女者對醫院服務品質滿意度較高，因此醫院在提升服務品質時，應留意不同年齡層與單身或已婚人士等族群之服務品質需求來改善。

表 7 不同人口統計變數之住院病患對服務品質之整體滿意度之差異性分析表

構面＼屬性	性別		年齡		婚姻狀況		教育程度		職業		居住地區		住院科別		住院單位	
	T 值	P 值	F 值	P 值	F 值	P 值	F 值	P 值	F 值	P 值	F 值	P 值	F 值	P 值	F 值	P 值
硬體環境	0.83	0.41	1.47	0.20	1.50	0.23	0.73	0.63	1.88	0.07	0.49	0.82	0.58	0.79	1.07	0.39
軟體環境	0.67	0.49	0.94	0.46	1.17	0.31	1.25	0.28	1.71	0.10	0.53	0.78	0.46	0.88	0.62	0.74
專業性等	1.01	0.31	2.65	**0.02***	4.55	**0.01****	1.27	0.27	1.33	0.23	0.54	0.77	1.42	0.19	0.81	0.58
溝通力等	0.36	0.72	2.46	**0.04***	4.25	**0.02***	1.26	0.28	0.90	0.52	0.53	0.79	0.87	0.55	0.60	0.76
保證性	1.59	0.11	2.48	**0.03***	5.35	**0.01****	1.02	0.41	1.85	0.07	0.79	0.58	1.25	0.27	0.73	0.65
關懷性	1.39	0.17	2.33	**0.04***	8.23	**0.00****	1.10	0.36	1.79	0.08	1.01	0.42	1.07	0.38	1.48	0.18
國際化	.230	0.82	0.94	0.46	0.99	0.38	1.32	0.25	0.38	0.93	1.26	0.28	0.88	0.53	1.02	0.42
醫療結果	0.88	0.38	2.21	0.06	4.42	**0.01****	0.62	0.72	0.93	0.49	0.50	0.81	1.74	0.09	0.65	0.72
整體滿意度	1.14	0.25	2.46	**0.04***	4.43	**0.01****	1.16	0.33	1.36	0.22	0.47	0.83	1.02	0.42	0.90	0.50

註：1.*表 p 值< 0.05; ** p 值< 0.01

2.粗體表示具有顯著差異

表 8 住院病患在年齡與婚姻狀況的人口統計變數對服務品質之整體滿意度事後檢定表

變項＼平均數＼構面		專業性等	溝通力等	保證性	關懷性	醫療結果
年齡	a. 20 歲以下	3.59	3.51	3.51	3.58	3.52
	b. 21-30 歲	3.47	3.37	3.50	3.51	3.37
	c. 31-40 歲	3.83	3.73	3.71	3.80	3.63
	d. 41-50 歲	3.91	3.86	3.88	3.91	3.90
	e. 51-60 歲	3.64	3.59	3.68	3.75	3.77
	f. 61 歲以上	3.96	3.91	3.89	3.95	3.74
	LSD 事後檢定	d > b f > b	d >b f > b ; f > a	d > a ; d > b f > b ; f > a	d > a ; d > b f > b ; f > a	
婚姻	g. 未婚或單身	3.56	3.52	3.49	3.53	3.47
	h. 已緍未有子女	3.31	3.04	3.65	3.31	3.25
	i. 已婚已有子女	3.83	3.75	3.81	3.89	3.78
	LSD 事後檢定	i > g	i > h	i > g	i > g	i > g

伍、結論與建議

經由研究之資料分析結果與討論後，本研究的結論與建議如下：

(一) 結論

1. 依Kano二維模型進行服務品質之分析，發現某些服務品質項目確實具有二維品質特性，以住院病患而言，被歸類為一元品質的有30個服務品質要素，而當然品質有2個問項，無差異品質則有8項；在醫院員工方面，以當然品質居多佔22項，一元品質則有一項，無差異品質則有17個問項。
2. 住院病患與醫院員工在Kano二維品質特性之看法上有所不同，以構面來看，住院病患方面，除了「醫療結果」為無差異品質外，其餘皆為一元品質；在醫院員工方面，「硬體環境」、「軟體環境」、「專業性及可靠性」、「醫療結果」為當然品質，而「溝通能力與反應性」、「保證性」、「友善及關懷性」為無差異品質。此結果與過去文獻之研究結論一致，同時藉由此二維品質分類，可提供個案醫院參考，以了解醫院員工與住院病患對服務品質特性為何種二維特性，以進行服務品質之改進及行銷策略之研擬。
3. 為有效改善服務品質及增加病患的就醫意願，本研究利用「顧客滿意度係數」找出之關鍵服務品質要素皆為一元品質，而根據Kano二維品質分類中因素中，一元品質項目為僅次於當然品質為重要之優先改善項目，當服務品質要素不充足時會引起不滿意，充足時則可增進滿意度。由前述結果知，當醫院管理當提供相關服務與設施或改進策略時，應以住院病患的感受為第一優先，其所能增加的滿意度與減少的不滿意會較高，有助於改善服務品質及增加住院病患的就醫意願。其中最具關鍵性及有效的構面為「硬體環境」、「軟體環境」、「專業性及可靠性」、「溝通能力與反應性」、「保證性」、「友善及關懷性」等方面。
4. 住院病患之服務品質滿意度之分析結果顯示，住院病患整體的滿意度是介於普通到滿意之間，以構面來看，「友善與關懷性」為病患評價最高之構面，其次為「專業及可靠性。國際語言咨詢服務是病患較不滿意的項目，因此醫院如欲發展國際醫療，對於一般服務人員之基礎外語能力提升有改善空間；其他在掛號、候診、檢驗、領藥、批藥、注射的等待時間上，對病患而言需要等待時間較久而致不滿意，因此醫院可進行各項作業之流程與管控上的評估及改善；在硬

體設備上有二個項目，病患的滿意偏低，分別為兒童遊戲室與伙食方面，兒童遊戲室來說，針對已婚且已有子女之病患來說，年幼的孩童抵抗力弱，不宜病房中或診間久待，因此對兒童遊戲室的需求較高，然而，這項設施與醫院之空間及成本相關，因此，當局可進一步審評估，再進行改善，而伙食方面，病患對醫院的伙食的滿意度偏低，故對於醫院伙食供應有進行深入了解病患需求與改善的必要；最後，對於醫院聲譽方面，病患的滿意度亦偏低，在聲譽方面，病患大多以醫療人員名氣、技術及設備面來評估，可能因為醫院的型態為區域型的醫院，因此病患對此滿意度較低，因此為提升聲譽，醫院可以透過醫療人員及醫療技術的品質的加強來進行改善。最後依據住院病患認為應具備之服務品質項目，於滿意度分析中呈現不滿意的項目為兒童遊戲室的設置，因此院方可以針對此項進行評估改進。依住院病患人口統計變數與醫院服務品質之差異分析，結果顯示年齡與婚姻狀況是具有顯著差異，因此醫院在提升服務品質時，應留意不同年齡層與單身或已婚人士等族群之服務品質需求來改善。

(二) 研究限制與未來研究建議：

本研究由於為醫院之委託計畫且因時間之限制，而未能對更多醫院的病患進行醫院服務品質之調查工作，同時本研究對象只針對住院病患來分析，缺乏大量之門診病患部份，建議後續研究者可針對這些部份加以改善，以增進文章學術價值及更客觀之結論。

陸、誌謝

本研究承蒙行政院衛生署豐原醫院補助研究經費，計劃編號CTU95-產-52，謹此誌謝。

參考文獻

[1] 狩野紀昭、瀨樂信彥、高橋文夫、迂新一著，(l984)，有魅力的品質與應該有的品質」(Attractive Quality and Must-be Quality)，*品質管制月刊*，21(5)，33-41，譯自日本 “品質”雜誌，4(2)，pp.147。

[2] 馬震中，(1994)，如何在醫院推展整體的品質管理，*醫院雜誌*，27(6)，pp.19-20。

[3] 郭德賓，(2000)，醫療服務業顧客滿意與競爭策略之研究，*產業管理學報*，1(2)，pp231~256。

[4] 孫智麗，(2007)，台灣醫療產業發展關鍵因素與趨勢分析，*台灣經濟研究*

月刊，30(5)，pp.1-11。

[5] 陳惠芳、謝明娟、陳俞成，(2006)，全民健保實施前後醫院財務面經營績效之研究，*嘉南學報*，32，pp.303-316。

[6] 黃雅琳、孫智麗，(2005)，台灣醫療產業結構與發展趨勢，*台灣經濟研究月刊*，28(2)，pp.1-10。

[7] 湯玲郎、鄭博仁，(2001)，以KANO的二維品質模型，探討醫療服務品質特性，*工業工程學刊*，18(2)，pp.71-80。

[8] 湯玲郎、莊泰旭，(2004)，Kano二維模式在開發汽車配備品質功能之研究，*管理學報*，21(3)，pp.311-330。

[9] 鄧維兆、李友錚，(2006)，臺北市立美術館關鍵觀眾服務品質屬性之確認：Kano模式之應用，*博物館學季刊*，20(4)，pp.27-47。

[10] 楊錦洲，(2004)，服務業品質管理，*中華民國品質管制學會出版*，台北：三民。

[11] 蔡嘉韡、王佳惠、郭乃文，(2006)，臺灣醫院品質管理活動數量與績效關係之縱貫性研究，*北市醫學雜誌*，3(5)，pp.61-70。

[12] 韓揆，(1994)，醫療品質管理及門診服務品質定性指標，*公共衛生雜誌*，13(1)，pp.35-53。

[13] Bolton, R. N., & Drew, J.H.(1991), A multistage model of customers' assessments of service quality and value, *Journal of Consumer Research*, 17(4), pp.375-383.

[14] Boulding, W. K., Kalra, A., Staelin, R., & Zeithaml, V. A.(1993), A dynamic process model of service quality: from expectations to intentions, *Journal of Marketing Research*, 30, pp.7-27.

[15] Bowers, M.R., Swan, J.E., & Koehler, W.F.(1994).,What attributes determine quality and satisfaction with health care delivery, *Health Care Manage Review*, 19(4), pp.49-55.

[16] Carey, R.G., & Seibert, J.H.(1993), A patient survey system to measure quality improvement questionnaire reliability and validity, *Medical Care*, 31(9), pp.834-845.

[17] Carson, P.P.,Carson, K.D.,& Roe, C.W. (1998), Toward understanding the patient's perception of quality, *The Health Care Supervison*,16, pp.36-42.

[18] Coddington, D. C., Fischer, E. A., & Moore, K. D. (2001), Strategies for the new health care marketplace: Managing the Convergence of Consumerism and Technology, *San Francisco Jossey Bass*.

[19] Cheng, S. H., Yang, M. C., & Chiang, T. L. (2003), Patient satisfaction with and recommendation of a hospital:

Effects of interpersonal and technical aspects of hospital care, *International Journal for Quality in Health Care,* 15(4), pp.345-355.

[20] Cronin, J.J., & Taylor, S. A. (1992), Measuring service quality: a reexamination and extension, *Journal of Marketing*, 56, pp.55-68.

[21] Cronin,J.J.,&Taylor S.A.(1994), SERVPERF vs SERVQUAL ： Reconciling performance based-perception-minus-expectations measurement of service quality, *Journal of Marketing*, 58(1), pp.125-131.

[22] Donabedian, A..(1988), The quality of care, how can it be assessed?, *JAMA*, 260(12), pp.1743-1748.

[23] Georgette, M., Zifko-Baliga, & Krampt, R. F.(1997), Managing perceptions of hospital quality, *Marketing Health Service,* 17(2), pp.28-35.

[24] Gonzalez, N., Quintana, J.M., Bilbao, A., Escobar, A., Aizpuru, F., Thompson, A., Esteban, C., Sebastian, J.S., & Sierra E.L.(2005), Development and validation of an in-patient satisfaction questionnaire, *International Journal for Quality in Health Care*, 17(6), pp.465-472.

[25] Guilfold, J. P. (1965), Fundamental statistics in psychology and education (4ed), New York: *McGraw-Hill*.

[26] Hu, H.Y., Cheng, C.C., Chiu, S.I., &Hong, F.Y.(2011), A study of customer satisfaction, customer loyalty and quality attributes in Taiwan's medical service industry, *African Journal of Business Management* 5(1), pp.187-195.

[27] Kuo, Y.F. (2004), Integrating Kano's model into web-community service quality, *Total Quality Manag.*, 15(7), pp.925-939.

[28] Lee, Y.C., Hu, H.Y., Yen, T.M. & Tsai, C.H. (2009), An Integration of Kano's Model and Exit-Voice Theory: A Case Study, Asian Journal on Quality, 10(2), pp.109 -126.

[29] Lee, W.I., Chang, T.H., & Chao, P.J. (2007), The relationship between quality of healthcare service and customer satisfaction-an example of hospital in taiwan, *Journal of the Chinese Institute of Industrial Engineer*, 24(1), pp.81-95.

[30] Matzlar, K., & Hinterhuber, H.H.(1998), How to make Product Development Projects More Successful by Integrating Kano Model of Customer Satisfaction into Quality Function Deployment?, *Technovation*, 18(1), pp.25-38.

[31] Matzler K., Bailom F., Hinterhuber, H.H., Renzl B., & Pichler J. (2004),

The asymmetric relationship between attribute-level performance and overall customer satisfaction: a reconsideration of the importance performance analysis, *Ind. Mark. Manag*., 33(4), pp.271-277.

[32] Minjoon J,Robin T.P., & George A .Z.(1998), The identification and Measurement of quality dimensions in health care：Focus Group interview results, *Health Care Management Review*, 23, pp.81-94.

[33] O'Connor, G. G,. (1988), Case management: System and practice, *Social casework*, 69(2), pp.97-106.

[34] Parasuraman, A., Zeithaml, V.A., & Berry, L. L. (1985), A conceptual model of service quality and its implications for future research, *Journal of Marketing*, 49, pp.41-50.

[35] Parasuraman, A., Zeithaml, V.A., & Berry, L. L. (1988), SERVQUAL: a multiple-item scale for measuring consumer perceptions of service quality, *Journal of Retailing*, 64(1), pp.12-40.

[36] Parasuraman, A., Berry, L. L., & Zeithaml, V.A.(1991), Refinement and reassessment of SERVQUAL scale, *Journal of Retailing*, 67, pp.420-450.

[37] Plymire, J. (1991), Complaints as opportunities, *Journal of Consumer Marketing*, 8, pp.39-43.

[38] Robert, H. B., & Kathleen, N. L.(1987)., Monitoring quality of care in medicare program, *Journal of American Association,* 258(21), pp.3138-3141.

[39] Sage.G.C.(1991), Customers and the NHS, *International Journal of Health Care Quality Assurance*, 4, pp11-14.

[40] Schvaneveldt, S. J., Enkawa, T., & Miyakawa, M. (1991), Consumer Evaluation Perspectives of Service Quality: Evaluation Factors and Two-Way Model of Quality, *Total Quality Management*, 2, pp.149-161.

[41] Woodside, A., Frey, L., & Daly, R. (1989), Linking service quality, customer satisfaction and behavioral intention, *Journal of Health Care Marketing*, 9, pp.5-17.

[42] Yu, C.M.J, Wu L.Y, Chiao, Y.C., &Tai H.S. (2005), Perceived Quality, CustomerSatisfaction, and Customer Loyalty: the Case of Lexus in Taiwan, *Total Qual. Manage. Bus. Excel*, 16(6), pp.707-719.

[43] Zhang, P & Von Dran, G.M. (2002), User expectations and rankings of quality factors in different Web site domains, *Int. J. Elect.Com*, 6(2), pp.9-33.

大學生參與偏鄉地區縮短數位落差的自我成長之初探：以修平技術學院爲例

張夏青、姜文忠、林素穗

摘 要

本研究者著力於服務偏鄉地區的數位落差能力之縮短，已有多年時間，除了長期參與教育部學產基金縮短城鄉數位落差計畫外，也參與教育部 97-98 年度偏鄉地區中小學網路課業輔導服務計畫，落實縮短城鄉數位落差之服務。其間帶領二、三十位大學生共同從事貢獻服務，深感大學生因為參與此類活動後轉變，由生澀到自信，由衝動到內斂、體諒等，皆值得探討。所以，本研究的目的為探討大學生參與服務偏鄉地區縮短數位落差所產生的自我成長。

本研究發現以大學生自我特質而言(耐心、自信心、成就感、同理心)，受訪者認為參與城鄉數位落差計畫的執行，可以增加本身的耐心、自信心、成就感與同理心；至於人際溝通方面，發現受訪者在參與課輔活動後，懂得如何找出方法與學童溝通，並在無形中改變了自我的溝通模式，也多了觀察的能力，同時由經驗中找出溝通有效的方法；最後，探討人文素養培養，受訪者積極參與原住民文化認識課程以及體驗當地生活的活動，同時學習態度良好，由此可發現社會人文的關懷情操及服務學習的精神已逐漸深耕於受訪者身上。

關鍵詞：數位落差、遠距教學、自我成長。

張夏青：修平科技大學資訊管理系講師
姜文忠：修平科技大學資訊網路技術系助理教授
林素穗：修平科技大學資訊管理系助理教授
投稿日期：100 年 3 月 10 日　接受刊登日期：100 年 4 月 27 日

A Study on Self-growth Assessment of the College Students for Reducing Digital Divide in Rural Areas: with College Students of Hsiuping Institute of Technology as a Case Study

Hsia-Ching Chang, Wen-Chung Chiang, Su-Sui Lin

Abstract

Our efforts in reducing digital divide in rural areas has been undergoing for many years. The purpose of this plan is to increase the learning ability of school students from minor groups via e-learning. The previous study is to continue the above mentioned purpose, putting forth efforts on reducing digital divide in rural areas. The result of the previous study based on the reducing digital divide in rural area was not satisfied. Therefore, this study is changed to self-growth assessment of the college students who are involved in reducing the digital divide in the rural areas.

This study is to compile the self-assessment surveys from those who have involved in distance education project. From the conclusion of this study will find out which areas of the self-growth they have made and make the participation more meaningful.

Keywords: Digital divide, e-learning, Self-Growth.

Hsia-Ching Chang, Lecturer, Department of Information Management, HUST.
Wen-Chung Chiang, Assistant Professor, Department of Information Networking Technology, HUST.Su-Sui Lin, Assistant Professor, Department of Information Management, HUST.
Received 10 March 2011; accepted 27 April 2011

一、動機與目的

教育部學產基金縮短城鄉數位落差計畫以及教育部偏遠地區網路課輔計畫等，皆都落實於提升偏鄉地區學童的數位能力以及學習績效，期許能為弱勢的偏鄉學童增長競爭力，讓偏鄉學童也具有較豐富的學習資源。

本研究者著力於服務偏鄉地區的數位落差能力之縮短。在長期參與教育部縮短數位落差相關計畫並帶領二、三十位大學生共同從事貢獻服務，深感大學生因為參與此類活動後的轉變，由生澀到自信，由衝動到內斂、體諒等，皆值得加以探討大學生參與服務偏鄉地區縮短數位落差所產生的自我成長之改變為何。

本研究的目的希望藉由本研究的結論，可以回饋給擔任課輔老師的大學生，使他們可以了解參與計劃對自我的影響，同時，也嘗試了解此活動是否可以提升本校學生的自我氣質及能力，增強多元能力。再者則是希望能延續改善城鄉數位落差之實務工作，繼續為更多的偏遠地區學童帶來學習數位資訊的機會，畢竟，數位落差需要多年的耕耘才可能見其效果，所以要有成效，就必須長期執行。

二、文獻探討

Banduray 在 1986 年提出社會認知理論(Social Cognitive Theory, SCT)，社會認知理論認為個人的行為是由環境因素(environment factor)、個人因素(personal factor)及其行為(behavior)等三個構面，持續不斷地交互作用而形成的，而自我效能則為理論中之概念，指的是「個人判斷其執行某特定行為時之自信程度」，因此，自我效能越高也就越能完成所設之目標[5]。

費茲(Fitts，1965)認為自我概念可分為外在架構與內在架構。外在架構分為(1)生理自我，是指對自己身體、外貌、技能等之看法；(2)道德倫理自我，其為對於自己的道德、舉止、和意志之看法；(3)心理自我，則是對自己的評價、情緒與人格之看法；(4)家庭自我，作為家庭中一份子的價值感及勝任感；(5)社會自我為與他人交往中的價值感及勝任感。

而內在架構則有(1)自我認同也就是所認識的自己之現況；(2)自我滿意或接納則是對自己現況的滿意或接納的程度；(3)至於自我行動是指實際所採取之應對行動。

另外，成長是指個人的眼界在內在深度或是外在廣度上的擴展，也是邁向更寬廣的歷程[3]，而自我成長的首先步驟應是培養自我覺察的能力，進而學習接納自我[1]，另一方面，自我成長除了包含具體技能的獲得外、更應該涵蓋提升自我價值感以及增進人際關係技巧[2]。

1970 年 Maslow 解釋其需求層次論(need-hierarchy theory)，包含七個層次，由低至高分別為(1)維持生命必須的生理需求；(2)免於遭受威脅或希望被保護的安全需求；(2)被人接納、關心愛護與鼓勵等隸屬與愛的需求；(4)被人認可與讚許等自尊需求；(5)希望理解自己不懂之事物的知的需求；(6)對美好事物欣賞的美的需求；(7)理想全部實現的自我實現需求,而這七個層次就是自我成長的發展歷程。

而過去研究發現,自我成長也應是志願服務的主要動機來源，高以緯(2003)的研究中指出,影響高中生參與志願服務的動機最主要的因素是實現自我成長,而且所抱持的參與動機越高,則會產生越高的滿足感覺。在相關課後照顧的研究中，也發現志工是會獲得成長、自我肯定等結論的[2]。

若考量同理心，1984 年 Hoffman 提出了同理心理論,認為同理心包含三種認知、情感與動機。同理心的認知有四個階段，包含減少自我的觀點、個體的持久性、觀點的取替與個體的認同。新生兒的反射性哭泣、制約反應、直接聯想、模仿、象徵的聯想與角色取替六種能力可以用來說明同理心的情感。至於動機部分，Hoffman 認為個人必須滿足(1)他人的不幸事件，而非自己發生不幸事件；(2)行為的目的在於幫助別人，而非自己；(3)行為是為了減低別人的痛苦此三種條件，才能同理他人的感受。

在人際關係方面，Newcomb 在 1958 年提出人際關係之平衡論(Balance Theory)，其認為人際關係為自己、他人與事件或第三者的交互作用,當自己和他人對某件事或某個人態度不同時,就出現人際關係不平衡,這時自己為了人際關係平衡會與他人溝通協調。

三、研究對象與實驗平台

本研究的研究對象為修平技術學院參與教育部 97-98 年度偏遠地區網路課輔計畫的部分課輔老師，共計有 21 位大學生。每個人負責一位南投縣信義鄉地利國小的學童的課輔,每周一次時間為兩小時，科目則有數學或國語。

課輔老師中男生有 9 位，女生有 12 位。其中四年級生有 8 位，三年級生有 11 位，二年級有 2 位。受訪者中擔任課輔的經驗超過 6 個月的有 17 位，未超過的有 4 位，課輔老師的基本資料如表 1 所示。

表 1　課輔老師基本資料

編號	性別	科系	年級	課輔經驗
id1	男	資管系	4	1 年
id2	男	資管系	4	1 年

id3	女	資管系	4	1 年
id4	男	資管系	4	9 月
id5	女	資管系	4	1 年
id6	男	資管系	4	7 月
id7	女	資管系	3	7 月
id8	女	資管系	3	7 月
id9	女	資管系	3	7 月
id10	男	資管系	3	7 月
id11	男	資管系	3	7 月
id12	男	資管系	3	7 月
id13	女	資管系	3	7 月
id14	女	資管系	3	7 月
id15	女	資管系	3	7 月
id16	女	資管系	3	7 月
id17	女	資管系	3	7 月
id18	男	人資系	2	5 月
id19	男	人資系	2	4 月
id20	女	應日系	4	5 月
id21	女	應日系	4	5 月

該計畫利用視訊會議 JoinNet 平台以及輔仁大學開發的課輔日誌平台，利用網路同步教學進行每周兩次的課業輔導，而執行成效受到國小端的師長的認同，輔導團隊也對參加的課輔老師進行教育訓練，包含教學方法與技巧、兒童情緒的了解以及原住民文化認識的課程，期許課輔老師能順利的執行計畫。

偏鄉地區網路課業輔導服務計畫的執行過程就是自我成長的最佳學習機會，從準備教學內容到執行課輔時間的行動付出，以及對學童的觀察、了解，省思課輔過程中的優缺處及找出解決方法等，都足以培養自我成長的能力，另外對於社會人文的關懷情操及服務學習的精神，也都內化於課輔老師心中。因此，參與此計畫的課輔老師成為本研究之研究對象，目的在於探討大學生參與課輔計畫對自己自我成長的改變。

四、資料收集

本研究者藉由執行教育部網路課業輔導計畫的機會，從旁參與協助課輔計畫的執行，並彙整追蹤參與計畫的課輔老師整個教學歷程對自己所產生的自我成長，以便發掘參與偏鄉遠距教學活動對大學生的影響。

本研究採用質性研究的行動研究法(action research)，藉由教學觀察法及開放式問卷訪談彙集資料，再由研究者進一步將資料分類與分析，最後，獲得結果。

首先，本研究將所收集到的受訪者之逐字稿加以編列行號，檔名以受訪者編號命名。在資料分析時，若用到受訪者的逐字稿，則在受訪者的談話內容後加上受訪者編號加上行號作為佐證。

參與課輔的課輔老師皆是本校的同學們，本校學生對自己的能力信心，表現

出較為不足的現象，加上幾乎都無家教的經驗，因此對參與教學計劃的自我信心顯示出較為低落，但是秉持愛心的熱忱以及該計畫的教育訓練課程，才讓本校學生提高參與課輔計畫的意願，而隨著計畫的進行，多次的教學經驗，逐漸的讓課輔老師表現出較高的自信，從他們的言談中就可明顯感受到。

另外，選課時間的不同或個人因素等，都有可能是課輔老師異動的原因，所以大學生的參與熱誠以及持續性略顯不足。長期參與課輔的老師才能感受到自我成長的不同，若是異動頻繁將會影響本研究資料的蒐集。所以在研究過程中，必須主動了解關懷課輔老師的狀態，隨時記錄從旁協助所遇到的困難，協助維持擔任課輔老師的熱誠。

本研究將以大學生自我特質部分(耐心、自信心、成就感、同理心)來進行探討大學生參與網路課業輔導服務計畫後，所產生的自我成長變化，但不受限於此範圍內。研究者在協助課輔計畫一段時日後，設計訪問問卷，且逐一進行個人訪談，訪談後並擅打為個人訪談之逐字稿，最後，將資料分類彙整，得到結論。

五、研究結果

本研究將以大學生自我特質部分(耐心、自信心、成就感、同理心)、人際溝通以及人文素養等三方面進行探討大學生參與網路課業輔導服務計畫後，所產生的自我成長變化。而以下則分類詳述本研究發現：

1. 自我特質的部分

(1)耐心

關於耐心，大部分的大學生皆認同參與計畫確實對自己的耐心有所增加，且耐心的自我成長效果是最為明顯的。其中部分的大學生提到：

”我覺得自己變的有耐心了一些了，因為小朋友是需要耐心和關懷。有時候你要觀察他今天的心情怎麼樣之類的，所以會學習到一些如何觀察和帶小朋友的小技巧。” (id6-line22~23)

“小文讓我多了份耐性，因為她本身是屬於看心情上課的，心情好就好上課；反之，心情如果不好的話，就會變的比較皮，不好教，就要多了點耐性、慢慢教導。”(id5-line25~26)

“我覺得最大的改變是自己對小朋友的耐心，以前我對小孩的耐心真的是不足的，每次他們頂嘴或者是愛鬧的時候，就會受不了也會變得不喜歡小孩子，可是參加課輔計畫之後，會覺得自己對小孩的耐性變大了，會想要很努力的跟他們溝通，讓他們知道我想要表達的是什麼，他們必須做到的是什麼。”(id9-line30~33)

“信心與耐心上，增加了許多，對小

孩子的學習上，變的比較有耐心的教導。相對的，也學會了適時的給予鼓勵，對小朋友的影響是很大的。"(id13-line24~25)

"多訓練了點耐心，可是被小朋友拒絕潑冷水還是會很灰心吧，多了很多想法，知道自己要多點耐心，打進小朋友的心中，是件難事，但也很有挑戰性，我想需要長時間的互動吧，也許要很多吸引小朋友的樂趣與幽默(就像 X 傑會打籃球)"(id17-line19~21)

"變的更有耐心，懂得如何吸引她的注意力，增加自己與小朋友溝通上的信心與技巧，學會如何用更清楚、適合她的方法，教導她讀書。"(id16-line24~25)

"我覺得最大的改變是，如何跟小朋友玩在一起，如何帶動他們。還有就是學會忍受和耐性。"(id10-line23)

綜合以上的引證，以及本研究者經過一年的從旁觀察，亦可以發現同學在教學時對學童的等待耐性以及學童情緒問題上，都比剛開始教導上課時較有耐性輔導，的確證明大部分擔任課輔老師的大學生，在教導學童的過程中，逐漸增加對學童的耐心。

(2)自信心

部分課輔老師則認為參與計畫對自己的自信心有增加，大部分的大學生原本都不認為自己能夠擔任家教的工作，但是參與課輔計畫後，發現原來自己也是可以勝任的，相對的也對自己產生自信心。

對於自信心，大學生提到：

"自信心，耐性，以及表達能力都有很大的轉變，也學會怎麼樣去了解一個人的個性、想法...等等，並且學會面對問題，想盡辦法解決、處理。"(id15-line23~24)

"會對自已的教學情況變的有比較信心，跟其他人的相處也會比較熱絡，也會想要再幫助更多像這樣偏遠地區的計劃。"(id14-line23~24)

由訪談的資料可以看出經由教學經驗的處理，擔任課輔老師的大學生可以建構出自我的自信心，此外，經由與國立大學的大學生一同參與跨校的教育訓練，發覺本校學生發覺自己可以跟自己認為優秀的學生一同從事相同的工作，也連帶的增加了自己的信心。

(3)成就感

若考量擔任課輔老師的大學生之成就感，可以由訪談紀錄中發現大學生在課輔的過程中成就感的獲得是有所增加的。

對於成就感，大學生提到：

"....*就在某些稍微困難的題型，能把她點通的瞬間，大家笑了一下，就這幾秒鐘得成就感就出現了，也讓他多學了些知識。" (id19-line26~28)*

"……，因為許多邏輯沒有融會貫通，怎麼解釋，別人都聽不懂，不過這次發現，

原來...”我行” (id19-line12~13)

”從遠距課輔過程中，學習如何用簡單易懂的方式教導小朋友，並且從中得到了成就感。” (id15-line29~30)

”最大的感受是成就感,當我聽到偉祥的數學考到 92 分時,我真的很高興,很滿足.證明了我這學期來的努力沒有白費.希望下學期回更好.我會加油,努力的.“(id12-line29~30)

部分課輔老師有增加自信心以及成就感等自我評價，以費茲所提及的心理自我解釋，部分課輔老師在課輔過程中增加自信心、成就感、愛心、勇氣等，也就是擔任課輔老師的大學生們對自己的價值評價、情緒與人格的看法因為參與此活動而有不同的領悟。

至於擔任課輔老師的大學生在和小學生的互動中也增加自己的價值感，同時，小學生對課輔老師的依賴以及信任也會讓擔任課輔老師的大學生更肯定自我價值，大多數的課輔老師也自認可以勝任這份工作，進而從中獲得成就感，此一發現可以呼應費茲所提之社會自我，即個人與他人交往過程中，獲得價值感及勝任感。

此外，由參與課輔活動中課輔老師所獲得之自信心與成就感則符合 Maslow 需求層次論中的被人接納、關心愛護與鼓勵等隸屬與愛的需求與被人認可與讚許等自尊需求。

(4)同理心

同理心是建立人際關係中很重要的因素，根據 1996 年 William 對於同理心的分類，包含仁慈、寬容與尊重、服務他人三項而言，大學生對於仁慈提到:

“...，讓我從中了解如何看小朋友的心情和如何去解決。像是如果小朋友心情不好，就要先讓他講出來，從中了解後讓他知道什麼是對的是錯。”(id7-line11~13)

“...，還有就是如何去觀察小朋友，我覺得上完這個課後，我更容易與他們互動，而且透過觀察更了解他了.”(id11-line12~13)

至於寬容與尊重，大學生們說到:

“體會到老師真的很辛苦，以前的不懂事真是造成老師太多麻煩啦!! 限在才可以站在老師的立場想...”(id20-line21~22)

“以前從沒想過當一個老師教人上課,參加這個計畫後,體會到原來當一個老師不是只要把課文上的東西教會小朋友，還要教他如何面對事情解決事情，而且還要影響他們正確的道德觀念.”(id11~line23~24)

“體會到當老師不是那麼容易的，得花好多心思與耐心去教導學生，我們還只是一對一教學，只需要顧到一個而已，老師幾乎都是一對多... 覺得老師真的很辛苦。”(id8-line31~32)

“讓我體會到當一個老師的辛苦,以前老師上課時我都不聽,當我叫她們上課時他們不聽課時得那種感受...我體會到了...”(id11-line29~30)

“最大的感受就是覺得老師實在是太偉大了!! 一日為師，終身為父→是沒那麼誇張啦!!但~就是學生做的一切都跟老師很有關係，是相輔相成的!!” (id20-line26~27)

“真正自己去體會那種當教師的心情，當老師真的不是那麼容易的。” (id3-line24)

而服務他人，大學生描述:

“這次執行課輔，讓我覺得我可以再盡自已的一份力幫助更多人。相處之中很愉快，也很謝謝可以給我這次服務的機會。”(id14-line29~30)

“跟其他人的相處也會比較熱絡，也會想要再幫助更多像這樣偏遠地區的計劃。” (id14-line23~24)

本研究發現課輔老師在陪伴學童的過程中，讓大學生增加了同理心，也藉由孩童本身問題發覺擔任課輔老師大學生自身問題的答案，進而更加珍惜自身所擁有的與更加體諒感恩老師或是身旁的人。此研究發現符合 Hoffman 提出同理心理論之同理心認知階段中之減少自我的觀點，亦能夠站在他人的立場來瞭解他人的想法或情緒，並感受到他人的感受，進而理解與表達。

2. 人際溝通

指的是發覺需要溝通的問題，並能尋找出方法來達成溝通，另一方面增強溝通技能，以改善自我的人際關係。在訪談結果中可以發掘大學生經由與孩童的溝通或是處理孩童問題中，在溝通技巧上有所增長。

關於溝通能力部分，大學生提到：

”懂得如何吸引她的注意力，增加自己與小朋友溝通上的信心與技巧，學會如何用更清楚、適合她的方法，教導她讀書。” (id16 -line24~26)

”學會怎麼樣去了解一個人的個性、想法...等等，並且學會面對問題，想盡辦法解決處理。” (id15 -line23 ~ 24)

”有時候你要觀察他今天的心情怎麼樣之類的，所以會學習到一些如何觀察和帶小朋友的小技巧。”(id6-line22~23)

”參加課輔計畫之後，會覺得自己對小孩的耐性變大了，會想要很努力的跟他們溝通，讓他們知道我想要表達的是什麼，他們必須做到的是什麼。”(id9-line31~33)

綜合以上的引證可以發掘大學生在參與課輔活動後，懂得如何找出方法與學童溝通，並在無形中改變了自我的溝通模式，也多了觀察的能力，並由經驗中找出溝通有效的方法，此部分亦能增加自我的成就感。而此研究結果也印證 Newcomb

提出人際關係之平衡論，當大學生在參與課輔活動時，發現學童無法吸收所教授的內容時，為了人際關係平衡大學生們會選擇了解學童並與學童溝通協調。

3. 人文素養

在計劃執行過程中，亦設計認識布農族文化的活動來增加大學生社會人文素養的養成，並且利用多次的討論方式來引導課輔老師自我省思歸納，逐步讓課輔老師自我蛻變。以下是針對參與活動的訪談結果之部分節錄。

”應該是去山上的相見歡吧，可能是因為我們大部分的人都一直生長在平地的關係，所以有些地方都沒有實際去看一看或者是了解原住民的一些生活跟習俗，不過這次上山讓我真的學到了很多有關於原住民他們在當地的習俗跟族群裡的劃分。” (id4-line11~13)

”最大感受就是那次相見歡到地利國小吧! 以前對原住民的認識僅限於課本上，從沒想過自己會到地方去深入的了解原住民文化、環境方面與我們平地上的不同。” (id8-line11~12)

”之前到地利國小的兩天一夜，讓我印象特別深刻。因為從來沒有這麼深入的去了解原住民文化、生活特色，還有那些孩子們的學習環境，原住民的小孩確實跟一般都市的孩子不太一樣，不管是行為、語言上，都有些許的不同，例如他們很喜歡討論男女感情的問題，或者是喜歡你就黏著你不放，很真也很直接，另外讓我很深刻的是，我到輔導的學生家參觀，家長都很熱情的歡迎，學生也會紛紛拿出自己的法寶，一一介紹，他們總是很大方的，不過有些小地方也是會害羞，所以我覺得在他們身上我也學習到很多。” (id9-line11~16)

“山地小朋友和平地小朋友有很明顯的不同，她們很率直也很活潑，因為資訊上的不足，導致很多方面她們是不懂如何處裡和學習的，但是她們給我的體會很真實一點也不會掩蓋自己的一面。訓練課程，給我們增加許多互動學習的能力，以及培養我們的耐心與信心。”(id13-line11~13)

”這兩個學期下來，有辦了許多活動，特別讓有我有心得的是我們上山的相見歡，以及去暨南大學參觀，讓我對於地利村的文化和山上小孩們有不同的認識，跟我之前的印象有大不相同。” (id14-line11~12)

因為參與輔導計畫，引發出對人文關懷的情懷及服務精神，都是最佳的自我成長機會，而藉由原住民文化認識課程以及體驗當地生活的活動，本研究發現課輔老師的積極參與與學習態度良好，可以看出社會人文的關懷情操及服務學習的精神已逐漸深耕於參與的同學身上。

除了預訂的研究範圍之外，另外本研

究也發現不少的大學生提到，參與課輔活動有助於大學生自我生命價值的探索，以及體會到學校沒有教過的事情以及想法。以下是訪談的結果：

“這次執行課輔，讓我覺得我可以再盡自已的一份力幫助更多人。相處之中很愉快，也很謝謝可以給我這次服務的機會。”(id14-line29~30)

”我覺得參加這次的課輔計畫後，讓我感覺又更長大了一點，也對山上小孩子有所了解，以前我都覺得做這種事情，真的很無聊!不過後來聽了一些師長的話，之後讓我覺得非常有意義。”(id4-line25~26)

”更體會到了，小朋友的天真活潑，山地小孩的那份熱情，因為這計畫，讓我更了解了原住民，使我對課本上的認知改變成了實際上得認識。”(id18-line27~28)

”我參加課輔後,覺得自己的想法改變了.會用另一個方向來想.要用怎樣的方法教,學生才會明白.有自己的想法,就會有很多的感想.“(id12 –line 23~24)

”在執行課輔這項計劃裡，我認識率直的涵涵，他帶給我很大的成就和快樂，雖然他的中性化，但是在學習這條路上，我體會到很多，我們仍需要再學習的東西。例如：相處模式以及如何掌控自己的小朋友，上課的狀況等。”(id13-line30~32)

”再一個大家都一起在學習的空間裡，他們不斷的學習，當然，我們也是，在每個人每個不同的角度中，他們學到了好多課本沒有教的方式，而我們，則是學到許多課堂沒有教的知識。”(id19-line32~33)

“感受就是自己可以，親自帶下小朋友，明白要帶領別人的辛苦，並不是想像中的那麼簡單。一定是要親自下來感受、接觸才會真正的明白。這一些心得，只有自己的心中才會明白。”(id6-line28~30)

“從來都沒有想過自己會有這種機會去教原住民的小朋友，可是當真正去執行了之後才覺得，這不只是我在對他們上課，也是在為自己上另外一堂課。跟小朋友之間的交談不太能用一般自己跟同學間的詞語，他們雖然有些時候想法比較另類，但基本上他們還都是單純的孩子，一舉一動他們都會觀察的很詳細，也會很貼心。還有他們的真，生氣的時候就生氣，開心的時後就大笑，把情緒都很真實的表現出來，這我覺得他們很可愛，因為他們不太懂得去掩飾，這也是他們跟現在一般孩子比較不同的地方，所以現在我越來越喜歡他們，也希望能藉由他們讓我學到更多不一樣的事物。” (id9-line38~44)

“不斷學習與進步，剛開始有很多抱負，但是會隨著學童的反應有所改變，總之，能有這方面的體驗感覺真是挺不賴。” (id3-line19~20)

經由以上的訪談結果中，可以發現大學

生在參與縮短數位落差的計畫中，獲得很多的心得以及成長，其中包含有對不同文化的衝擊、自我溝通技能的提升以及服務學習的最佳體驗等，相對的，也較其他未參與課輔活動的大學生提早對自己的未來有生涯規劃，從助人助己中得到滿足感以及信心。

六、研究建議

本研究希望藉由探討大學生參與縮短數位落差計畫對自我效能的改變，來吸引更多的大學生投入意願，因為縮短數位落差是需要經過多年的耕耘後才可能見其效果的，所以要有一定的成效，就必須長期的執行，而大學生就是耕耘的主力，本研究認為越多的大學生參與將會提升縮短數位落差計畫的成效。

若能理解參與計畫可以增強自我的效能，應可提升大學生參與改善城鄉數位落差之實務工作的意願，如此也可為更多的偏遠地區學童帶來學習數位資訊的機會，本研究建議在研究計畫推廣時，可以引述研究結果並呈現給大學生，讓大學生理解參與計畫時所能獲得的自我成長，即能提升大學生參與的意願，而未來在推廣上相信也能更佳的順利，引入更多大學生的加入，為國家未來增加資訊素養的競爭力，這也是本研究希望對縮短數位落差的具體貢獻。

七、結論

本研究希望藉由研究回饋擔任課輔的大學生了解自己在參與計劃中對自我的影響，以及提升自我能力，結果發現網路線上課業輔導活動確實可以讓參加的大學生增加耐性、信心、同理心等自我概念。也對大學生個人的人際溝通能力亦有相對的增加，此外對大學生的生涯探索也有不少的獲得。

網路教學突破了距離的限制，讓遠距離的人可以有互動的機會，而參與網路課業輔導計畫讓偏鄉地區的學童增加學習的機會，更可以讓從事課輔的大學生們有自我成長的機會，共同提升國家未來的競爭力。

八、參考文獻

1. 朱湘吉。2000。自我成長--理論與實踐。空大社會科學學報，頁 133-164。
2. 何亭嫻。2008。小手牽大手-大學生擔任弱勢家庭課輔志工之實踐與成長。國立花蓮教育大學多元文化教育研究所碩士論文，花蓮，未出版。
3. 高以緯。2004。台北縣市高中生參與志願服務動機與滿足感相關之研究。中國文化大學青少年兒童福利研究所碩士論文。台北，未出版。
4. Bandura, A. (1986). Social foundations of thought and action: A social

cognitive theory. Englewood Cliffs, NJ: Prentice- Hall, Inc.

5. Bandura, A. (1997). Self-efficacy: The exercise of control. New York: Freeman.
6. Fitts, W.H.(1965).Tennessee Self-Concept Scale: Manual. Los Angeles : Western Psychological Services.
7. Hoffman, M. L. (1984). Interaction of affect and cognition in empathy. In C. E. Izard, J.Kagan & R. B. Zajonc (Eds.), Emotion, cognition, and behavior (pp. 103-131). Cambridge, England: Cambridge University Press.
8. Maslow, A.H.(1970).Motivation and personality, New York: Harper & Row.
9. Newcomb, T.M.(1985).The Cognition of Persons as Cognizers, In R. Tagiuri & Petrullo(eds.)Person, Perception and Interpersonal Behavior. California Stanford university press.

修平學報 第二十三期 民國一〇〇年九月
HSIUPING JOURNAL VOL.23, pp.147-156 （September 2011） 147

視窗化電梯控制系統之設計與應用

劉國華

摘　要

在資訊科技時代進步裡，工作繁忙及時間緊迫，平均每個人每天都會搭乘電梯，所以「 搭電梯」已經成為日常生活的一部份，從走出家門、進入辦公場所、外出洽公、甚至停車場內，無一處不使用電梯。本文主旨即在利用可程式控制器(PLC，Programmable Logic Controller)做為電梯控制系統的主體架構設計；視窗化部分則透過圖控方式規劃製作。視窗化電梯控制系統採用 Delta 圖控軟體在電腦上直接對電梯做監控導引，再經由電腦與可程式控制器的通訊連線實現完成之，並且利用模糊理論(Fuzzy Logic)之邏輯推理控制方法應用於電梯運行情況規則，通過進一步處理所選模糊控制法則，最終確定電梯運行程序，提供搭乘者更短的搭乘時間及樓層距離定位更精準。最後將有模糊邏輯控制及無應用此模糊邏輯推理控制方法作一比較，經由實驗數據結果，得知前者展現了較佳的效能。

關鍵詞：可程式控制器、模糊理論、圖控軟體、電梯。

劉國華：修平科技大學電機工程系專任講師
投稿日期：100 年 4 月 7 日　接受刊登日期：100 年 5 月 12 日

Design and application of an elevator control system based on window

Kuo-Hua Liu

Abstract

In the era of information technology, due to busy work and tight schedule, almost everyone takes elevator daily. Taking elevator has become a part of our daily life, as elevators are used at home, in office building, and even in parking lots. This study applied PLC (Programmable Logic Controller) in an architectural design for the elevator control system and used the graphic control planning to produce the window display. The windowing elevator control system adopts Delta graphic control software to directly monitor and direct the elevator, and establish the communication between the computer and PLC. In addition, the fuzzy logic control method is applied in the design of elevator operating rules. The final elevator operating procedure is determined by further processing of the selected fuzzy control rules to provide elevator riders with shorter riding time and more accurate positioning of floor distances. Finally, comparison of the fuzzy logic inference control methods with those without fuzzy logic control found that the former has a better performance.

Keywords：programmable logic controller, fuzzy logic control method, graphic control software, elevator .

Kuo-Hua Liu, Instructor, Department of Electrical Engineering, HUST.
Received 7 April 2011; accepted 12 May 2011

壹、研究動機與目的

由於科技的高度發展和國內經濟的起飛及人口向都會區集中，因而使都會區的建築物普遍朝高樓大廈發展，電梯即是在這種情況下的時代產物，因為可以提供人們上下高樓的便利性。

電梯的控制方式普遍採用下列三種控制方式：(1)、繼電器控制方式。(2)、可程式控制器(PLC)控制方式。(3)、微處理機之單晶片控制方式，上述之三種控制方式其繼電器控制系統較可能發生故障率高、可靠性差、接線複雜、通用性差等缺點。1983 年微處理晶片數位式邏輯系統控制器導入電梯使用，此後正式成為電梯控制之主要發展方向，致使電梯的電氣控制方式進入了一個新的發展時期。可程式控制器控制系統及微處理機之單晶片控制系統具有控制系統體積減小、節能、可靠性提高，尤其是對群控、通訊等複雜電梯控制功能更具優越性，因此，可程式控制器(PLC)之程式編輯採用易學易懂的梯形圖語言，且具有控制靈活方便、可重複使用、程式記憶體與外部輸出容量可彈性擴充、抗干擾能力強、運行穩定可靠、能與電腦連線操作等特點[1-2]。

由於電梯不再只是輸送的工具而已，都希望加強運輸調整功能，提供順暢便捷的運作服務，因而發展不僅僅快而且又要舒適的電梯成為生產電梯業界的主要課題。然而每天出入大樓的經常人來人往，致使電梯的使用頻率也因乘用時段而有所不同，控制器之管理系統能隨時配合乘客的流量變動[3]。

電梯控制系統是大部分都是藉由微電腦的軟硬體結構，並搭配週邊的各式各樣的感應器及預先所規劃之複雜的各式操作程式，結合成所謂之人工智慧，精準的監控及導引各部電梯的動作，是以下列方法為基礎：

(一)、模糊邏輯(Fuzzy Logic)：

模糊理論是根據不明確的訊號，透過近似推理的過程，且經過運算而得到明確的結論，類似人頭腦中「過程模糊，結果明確」之思維特徵相類似。使用模糊邏輯數學分析統計法，能快速的找出任何時刻最適合的運行模式[4]。

本文主要以小型電梯控制系統，結合 PLC 控制技術的特點，提出了一套結合模糊邏輯理論，將推理、判斷、決策、控制等之知識思考行為，轉化成為知識庫及規則庫儲存於電腦中，再經由模糊理論法(fuzzy theory)以數值計算方法完成推論，實現於此電梯控制系統的視窗化之設計與應用。 本文主要是針對電梯等待時間及搭乘時間做一完整分析，並利用可程式控制器(PLC)為控制核心，視窗化圖控採用 Delta 圖控軟體 Delta Screen Editor，在

電腦上直接對電梯做監控導引，再經由電腦與可程式控制器的通訊連線實現完成之。本系統是一種機電整合之教材，是電機、電腦與控制工程的融合，所得成果可作為機電整合或科學教育之教學教材。

貳、模糊理論介紹說明

模糊理論從最早十年間的理論發展到後來各式各樣的應用，其理論講究的是近似推理(Approximation reasoning)，不以精確計算為手段，只要差不多就好，如今差不多精神卻成為了模糊理論解決問題的利器，但這個差不多指的是根據不清晰的資訊，透過差不多的推論過程而得到精確的結果。

模糊控制主要是在直覺和人工經驗的基礎上，建立所需的知識庫，並可看成一組決策法則，根據輸入值滿足系統條件(歸屬函數)的程度，給予一個特定值，稱作 grade(歸屬度)其範圍為 0 ～ 1。若完全屬於系統條件時，其值為 1；完全不屬於系統條件時，其值為 0，則是傳統的集合；其他屬於系統條件中間的，依其所屬程度給予 0 和 1 之間的任意值，則是屬於模糊集合。模糊邏輯(fuzzy logic)設計方法主要可以分為四個部份：即模糊化介面(Fuzzification Interface)、知識庫(Knowledge)、模糊推論機構(Fuzzy Inference)與解模糊化介面(Defuzzification Interface)，如圖一所示，其中知識庫又可分為資料庫(Data Base)及規則庫(Rule Base)[5-8]。

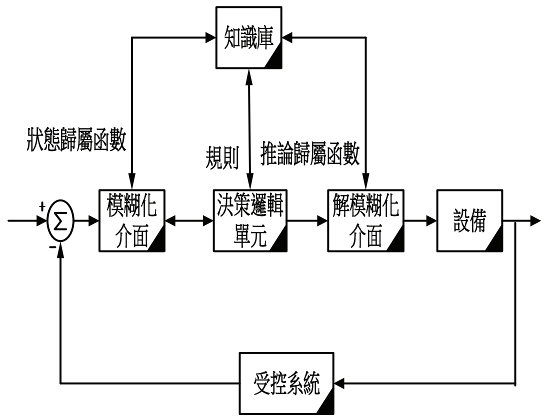

圖一：模糊控制器系統架構圖

模糊控制是以語言化控制規則為主體，為了將輸入的明確值與語言化的控制規則結合，必須將輸入值做模糊化處理以便對映到資料庫裡語言變數的論域中，再配合規則庫及推論機構推導出結果。因結果仍然是模糊值，所以必須再做解模糊化工作，其輸出才是明確值。本文中藉由每個樓層之感測器做為取樣輸入，再透過步進馬達之驅動模組做為輸出控制。本電梯控制系統之每個模糊集合皆有語性值代表其模糊涵意，如表一所示。系統所建立之模糊控制規則表，如表二所示，根據此法則利用編輯軟體 Delta WPLSot 程式化於可程式控制器系統之內部，以達成系統之閉迴路控制。

表一：語言變數

語言變數名稱	代表語意	
NB	Negative big	負大
NM	Negative Medium	負中
NS	Negative Small	負小
ZO	Zero	零
PS	Positive Small	正小
PM	Positive Medium	正中
PB	Positive Big	正大

表二：模糊控制法則

E(error) / ΔE (error dot)	NB	NM	NS	ZO	PS	PM	PB
NB	NB	NB	NB	NM	NS	NS	PS
NM	NB	NB	NM	NS	NS	PS	PS
NS	NB	NM	NS	NS	PS	PS	PM
ZO	NM	NM	NS	ZO	PS	PM	PM
PS	NM	NS	NS	PS	PS	PM	PB
PM	NS	NS	PS	PS	PM	PB	PB
PB	NS	PS	PS	PM	PB	PB	PB

叁、系統架構

本研究的硬體架構係由可程式控制器、步進馬達及驅動器、感測器等所組成，其整體系統架構如圖二所示。本系統完成實現表二之內容於可程式控制器內部時，可先定義誤差量(E)與誤差偏差量(ΔE)兩軸，誤差量是由軟體設定之參考距離與回授距離之差值。誤差偏差量之計算是目前誤差 En 減去前一次的誤差量 En-1，當程式連續執行下，循環一次的時間步距 Δt 很短時，可視為一個誤差偏差量 ΔE 或稱之為誤差微分量 ΔE / Δt。

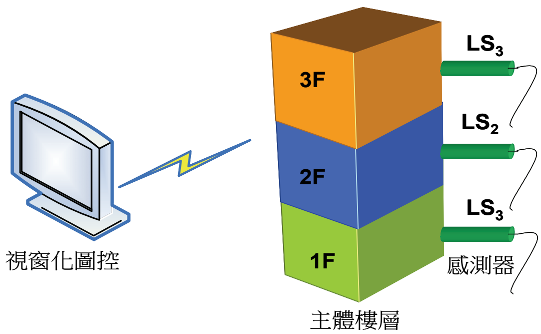

圖二：本研究系統架構圖

一、可程式控制器

本文所使用的控制器是利用台達公司之產品，其硬體結構如圖三所示。此系列 PLC 在電腦通訊的模式中，其交信資料的型式如圖四及圖五所示，分別為讀取 PLC 元件及交信資料的交信型式和寫入 PLC 元件及交信資料的交信型式[9-10]。

圖 三: 可程式控制器實體圖

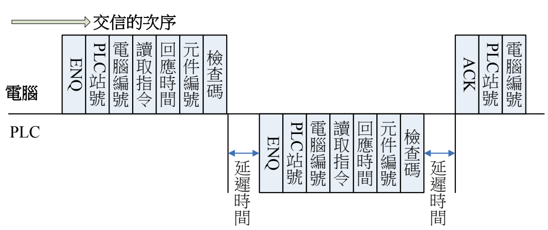

圖四：讀取 PLC 元件及交信資料的交信型式

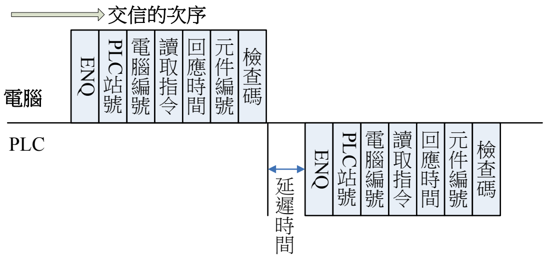

圖五：寫入 PLC 元件及交信資料的交信型式

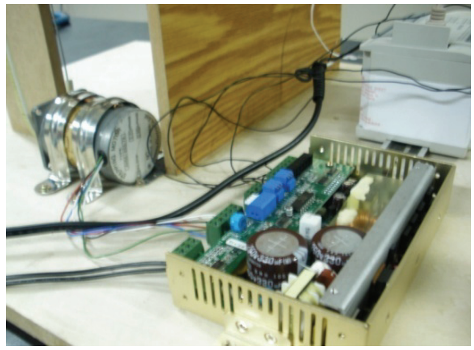

圖六：步進馬達及驅動器硬體架構

二、步進馬達及驅動器

本文所使用的步進馬達及驅動器，其硬體結構如圖六所示，完成實現輸出距離，提供搭乘者更短的搭乘時間及更精準之樓層距離定位。步進馬達的結構不論是 PM 式、VR 式或複合式步進馬達，其定子均設計為齒輪狀，這是因為步進馬達是以脈波訊號依照順序使定子激磁，以數位電壓輸入來控制其轉速及轉動方向[9-10]。圖七為步進馬達驅動原理，將其脈波激磁訊號依序傳送至 A 相、A+相、B 相、B+相則轉子向右移動(正轉)，相反的若將順序顛倒則轉子向左移動(反轉)。圖八為 PLC 與步進馬達之控制驅動器之正轉／反轉脈波信號交信原理。圖九-十為當設定為 2pulse 輸入方式時及 1 pulse 輸入方式時之運轉脈波信號波形。

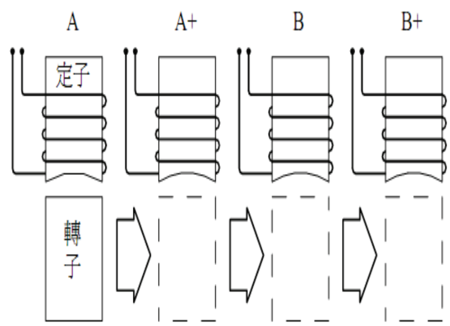

圖七：步進馬達驅動原理圖

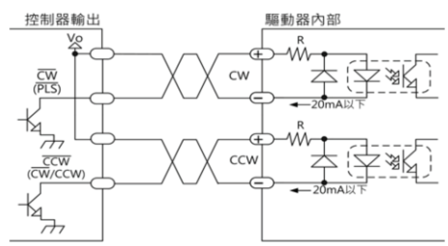

圖八：正轉／反轉脈波信號交信原理圖

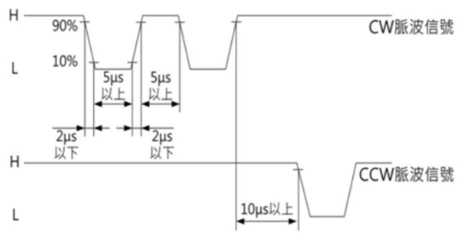

圖九：脈波波形為 2pulse

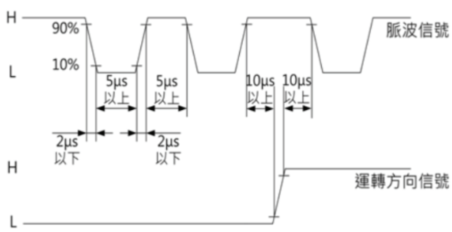

圖十：脈波波形為 1pulse

三、感測器

本文所使用的感測器，其硬體結構如圖十一所示，完成實現取樣輸入信號，提供給可程式控制器之輸入端，進入控制器內部做運算處理。

圖十一：感測器硬體架構圖

肆、研究結果

本研究實體為一部三樓層電梯如圖十二所示[4]，本系統結構可將應用技術進行下列各項教學之規劃：(1)步進馬達控制；(2)驅動器應用；(3)可程式應用；(4)圖控軟體設計。本研究之經驗可作為技專院校「機電整合」課程之教學應用，以協助學生結合相關領域之知識理論與實務結合之教學目標。

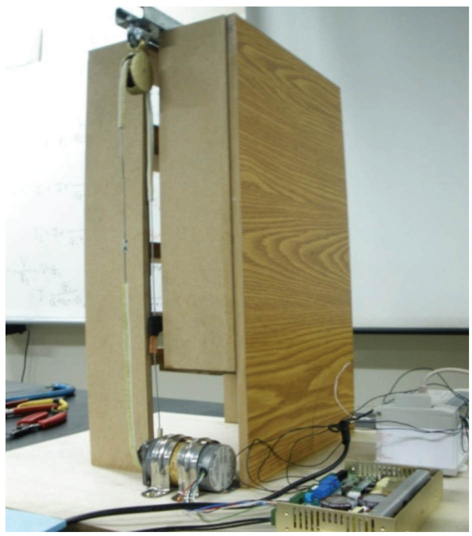

圖十二：本研究系統實體架構圖

表三所列為各個實際樓層相互距離各為 14.4cm，加入 Fuzzy 控制時，可測得之距離分別為 14.3 cm、14.2 cm、14.3 cm，未加入 Fuzzy 控制時，可測得之距離分別為 13.8 cm、14.0 cm、13.9cm，可知經由模糊理論控制可實現精準之樓層距離定位，。表四所列為樓層搭乘時間，

加入 Fuzzy 控制時，可測得之搭乘時間分別為 18.6 sec、18.7 sec、18.6 sec，未加入 Fuzzy 控制時，可測得之搭乘時間分別為 19.1 sec、19.2 sec、19.1 sec，可知經由模糊理論控制可實現縮短的搭乘時間。操作者透過 Delta 圖控軟體進行視窗化控制，如圖十三所示[11-16]。

表 三: 樓層距離定位

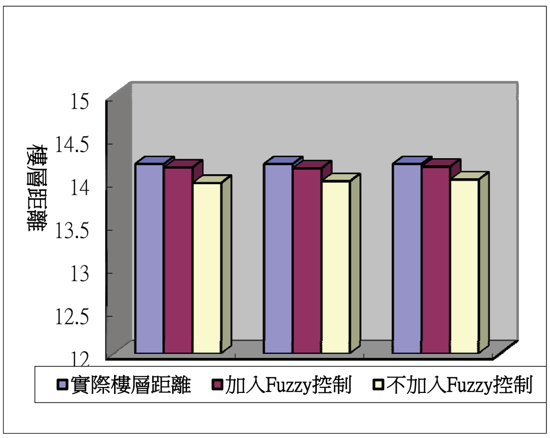

表 四: 搭乘時間

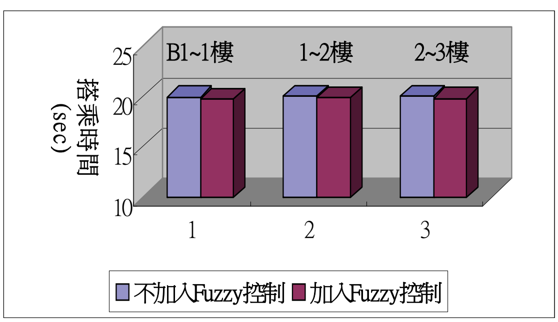

圖十三：電梯控制系統之控制視窗圖

視窗中之按鍵，可對電梯控制系統進行模糊邏輯控制設定、樓層控制、樓層距離顯示、搭乘時間顯示等進行自動化設計。

伍、結論

本文利用可程式控制器完成實現模糊理論(Fuzzy Logic)，提供搭乘者更短的搭乘時間及樓層距離定位更精準。本系統在硬體部分，自行設計及組裝一小型電梯之實驗模型進行實驗，軟體部分則透過圖控方式製作人機界面應用程式建構出視窗化電梯控制系統，最後由實驗結果驗證所發展之軟硬體之可行性。

並且比較了有模糊理論及無模糊理論之應用，經由實驗數據結果，得知前者展現了較佳的效能。所研製之經驗可作為機電整合的教學教材，達成理論與實務結合的教學目標。

參考文獻

[1] 陳盟吉（2010），以可程式控制器為核心之伺服馬達定位控制方法，崑山科技大學電機工程研究所碩士論文。

[2] 劉國華、魏嘉延、江奕旋、鄭喬臨、柳志維（2011），模糊控制的電梯控制系統之研製，第九屆現代通訊科技應用學術研討會，第 108-112 頁。

[3] 游逸峰（2000），電梯控制系統之研究與設計，中央大學機械工程研究所碩士論文。

[4] 汪惠健（2006），模糊理論與應用，高立圖書公司。

[5] 馮國臣、趙忠賢、張宏志、溫坤禮（2007），模糊理論基礎與應用，新文京開發出版有限公司。

[6] 王進德（2007），類神經網路與模糊控制理論入門與應用，全華圖書公司。

[7] G.J. Klir and B.Yuan, , Fuzzy sets and fuzzy logic: theory and applications, Prentice-Hall Inter., Inc., Upper Saddle River, NJ, USA, 1995.

[8] Yung-Hsin Wang, Kuang-Hsuan Hsia, and Yo-Ping Huang, “Elevator Group Control with Fuzzy Logic and Genetic Algorithms”, Journal of Chinese Fuzzy Systems Association, Vol.5, No.2, 1999.

[9] 許溢适、陳坤正（2005），步進馬達使用法，全華圖書公司。

[10] 許允傑（1994），馬達控制，全華圖書公司。

[11] DVP-PLC 應用技術手冊【程式篇】，台達電子工業股份有限公司。

[12] DVP 系列 PLC 使用手冊【目錄】，台達電子工業股份有限公司。

[13] DVP-PLC 應用技術手冊【101 例】，台達電子工業股份有限公司。

[14] DVP 系列人機介面使用手冊，台達電子工業股份有限公司。

[15] 王進德（2003），機電整合－圖形監控應用實務，全華圖書公司。

[16] 宓哲民、顏見明、劉春山（2009），人機介面圖形監控，全華圖書公司。

隨機外彈道六自由度模型與蒙地卡羅法

王旭萍、楊伯華、洪浚瑋

摘 要

傳統六自由度理論計算彈體飛行軌跡，輸入起始條件後，解算六自由度微分方程組，計算在相同起始條件下之彈體飛行軌跡，其軌跡為唯一解，亦即其每一發彈的飛行軌跡與彈著點都是相同的。但在實際射擊上，在相同的射擊起始條件下，彈體在射擊過程中會受到砲口的初速變化、砲口跳躍、砲口的噴流及空氣動力改變等隨機因素影響，造成在相同的發射條件下每一發彈的飛行軌跡與彈著點都不盡相同。

本文研究是以蒙地卡羅法將砲口的初速變化、砲口跳躍的角度產生符合隨機因素的量化值，加入起始條件中，建構成一隨機外彈道數學模型，以分析彈著精度散布與砲口影響參數，運用此模型模擬計算 M107 155 公厘榴彈砲的彈體飛行軌跡，並與其相關實測數據或射表進行驗證。

關鍵詞：六自由度模型、砲口初速、砲口跳躍、蒙地卡羅法。

王旭萍：修平科技大學機械工程系助理教授
楊伯華：修平科技大學機械工程系助理教授
洪浚瑋：修平科技大學精密機械與製造科技研究所研究生
投稿日期：99 年 11 月 29 日 接受刊登日期：100 年 6 月 8 日

Stochastic Exterior Ballistic Modeling of 6-DOF with Monte Carlo Solution

Shiu-Ping Wang, Pao-HwaYang, Chun-Wei Hung

Abstract

The six degrees of freedom (6-DOF) trajectory model was used to calculate the trajectory and altitude of the projectile. Under the same initial conditions, the solution of 6-DOF trajectory model is a unique solution. But from the really firing test, the projectile trajectory is hard to be same even though the firing conditions were kept. Muzzle velocity variance, muzzle jump, muzzle blast and aerodynamic jump are the random factors, which can affect the exterior ballistic of the projectile. Especially Muzzle velocity variance and muzzle jump are the main factors to cause the dispersion of the projectile.

A stochastic exterior ballistic model of Muzzle velocity variance and muzzle jump are constructed to analysis the dispersion of the projectile. Monte Carlo method was used to generate the random variance and quantize the direction of the muzzle jump. A sample of M107 155mm projectile trajectories was calculated by applying this model.

The computational result gives satisfactory agreement with experimental data.

Keywords: 6-DOF Modeling, Muzzle velocity, Muzzle jump, Monte Carlo.

Shiu-Ping Wang, Assistant Professor of Department of Mechanical Engineering, HUST.
Pao-Hwa Yang, Assistant Professor of Department of Mechanical Engineering, HUST.
Chun-Wei Hung, Graduate Student of the Department of Mechanical Engineering, HUST.
Received 29 November 2010; accepted 8 June 2011

壹、前言

近年來隨著計算機的計算速度大幅提昇，六自由度理論也隨之成為現今彈道研究一項不可或缺的基礎工具。用六自由度理論計算彈體飛行軌跡，輸入起始條件後，如砲口初始條件（初速、射角等），彈體飛行時依空氣動力特性，如阻力、翻轉力矩與旋轉摩擦力等，求取某一特定時距（time step）下之彈體速度與彈體質心位置變化，依此方式重覆計算直至彈體落地或上靶為止，運用此六自由度數學模型，計算在相同起始條件下之彈體飛行軌跡，其每一發彈的飛行軌跡與彈著點都是相同的。但實際上，在相同的射擊起始條件下，彈體在射擊過程中會受到砲口的初速變化、砲口跳躍、砲口的噴流及空氣動力改變等隨機因素影響，造成在相同的發射條件下每一發彈的飛行軌跡與彈著點都不盡相同。

本文研究的重點是如何將這些隨機因素加到六自由度數學模型中，建構成一隨機外彈道六自由度數學模型。而這些因素都是隨機的變量，於是利用蒙地卡羅法產生符合隨機變量的量化值，如砲口的初速變化、砲口跳躍的角度，加入數學模型中，模擬計算 M107 155 公厘榴砲彈的彈體飛行軌跡，並與其相關實測數據或射表進行驗證。

貳、文獻回顧

本研究範疇與開發之程式係屬於外彈道，研究探討具有一定初速之彈體，在空間運動中，不受任何機械力作用之彈體自由運動軌跡；彈體之自由飛行軌跡取決於彈體形狀於空氣中飛行時之空氣動力特性，目前常用的彈體形狀可分為旋轉穩定彈體與尾翼穩定彈體。旋轉穩定彈體係當彈體於砲管內向前飛行時，同時使彈體產生高速自旋運動，當彈體飛行於空氣中，作用其上之空氣動力將使彈體產生陀螺效應而使彈尖相對於彈體質心產生進動運動（precession）與章動運動（nutation），以保持彈尖向前而不翻滾；另一種尾翼穩定彈體係利用彈尾之尾翼設計，使尾翼彈體於飛行時，其空氣動力之壓心於彈體質心後方，以穩定彈尖向前而不翻滾。

尾翼穩定彈體，彈型以迫擊砲彈為主。尾翼穩定彈於空氣動力特性理論設計時，原則上以軸對稱或平面對稱為主要設計考量，然於實際生產製造，限於加工製造的工藝很難達到理論設計上的完全對稱，致使彈體飛行時所承受的空氣動力將隨實際彈體製造的不對稱性，而有所不同；不同的空氣動力作用將造成不同的彈體飛行姿態穩定與運動軌跡，1957 年 Charles H. Murphy 就對稱性彈體的俯仰（pitching）與偏擺（yawing）運動進行研究，並提出相關俯仰與偏擺力矩的預測

解算方法 [1]，1965 年 Anders S. Platou 探討彈體飛行時的馬格勒斯（Magnus）效應對俯仰與偏擺力矩的影響 [2]，1970 年 Gary T. Chapman and Donn B. Kirk 以實驗量測方式就彈體自由飛行數據進行分析研究，瞭解對稱性彈體的俯仰與偏擺運動間的耦合（couple）關係並提出俯仰力矩與偏擺力矩的實驗預測估算方法 [3]，1971年Charles H. Murphy 對輕微不稱性彈體之非線性運動進行研究 [4]，1972 年 G.W. Stone, E.L. Jr. Clark, 與 G.E. Burt 就非稱性彈體所產生之阻尼力矩(damping moment)效應進行研究 [5]，1973年 O. Walchner與 F.M. Sawyer研究細長型彈體的俯仰與偏擺運動，並推導其穩定特性 [6]，1980年 Charles H. Murphy 就對稱性彈體的動態不穩定運動特性進行研究 [7] 並於1988年將相關於此類對稱性彈體之空氣動力特性研究，不論是旋轉穩定彈體或尾翼穩定彈體，彙整於" Free Flight Motion of Symmetric Missiles”[8]；此後有關對稱性彈體之空氣動力特性研究，則多見於相關計算流力文章 [9~17]，1990 年 M. Nusca, S. Chakravarthy, 與U.Goldberg,以計算流力方法解析衝壓引擎彈底之流場結構以獲得其壓力分佈特性 [9]，1994 年 Walter Sturek 等人應用計算流力方法求取旋轉穩定彈與尾翼穩定彈之空氣動力特性 [10]，隨後 Paul Weinacht 與 Walter Sturek 亦以相同方法求取尾翼穩定彈旋轉時之空氣動力特性 [11], 2002 年 Mary Graham 等人以數值方法探討超音速側向噴流於尾翼穩定彈體之氣動力影響 [12]，2006年 Joseph, K., Costello, M. 與 Jubaraj, S.將計算流力計算之彈體氣動力直接與剛體動力（RBD, rigid body dynamic）方程式耦合，以求解即時性的彈體飛行軌跡與氣動力特性 [15]，2009 年Davis Bradford 等以嵌入遙測裝置與數位訊號處理器，量測側向噴流精準導引迫砲彈之飛行姿態數據與側噴時彈體之側向加速度等資料，以為側向噴流精準導引迫砲彈之氣動力特性、巡航、導引與飛控模式之研究討論 [17]。

彈體飛行軌跡數學模型的建立，其目的在於計算彈道飛行軌跡，而計算結果的準確性與實用性取決於彈體之空氣動力特性的完備與彈體飛行軌跡數學模型的解算方式；最早有關自由拋射物飛行軌跡計算理論的書籍是伽力略於西元1564-1642 年寫成，其後發展成外彈道學中的拋物線理論，適用於近射程、地球表面假設為平面、重力大小不變與不考慮空氣阻力影響之彈體飛行軌跡計算，至於不能忽視地表曲面及重力大小變化的遠程真空彈道，則發展成外彈道學中所謂的橢圓理論[18][19]。二十世紀中葉，隨著航

空工業與計算機的發展，彈體飛行軌跡的數學模型已直接與彈形之空氣動力特性構連在一起，1964 年 R.F. Lieske 與 R.L.McCoy 提出彈形剛體之飛行軌跡運動方程式 [20]，1966 年 R.F. Lieske 與 Mary L. Reiter 將彈體飛行時之定偏角（Yaw of repose）特性納入彈體飛行軌跡運動方程式中，以解決彈體飛行軌跡橫向飄移（draft）的問題 [21]；1970 年後，計算機的計算能量迅速的發展與計算機的體積大幅縮小，有關彈體飛行軌跡的計算已直接架構於六自由度（six-degree-of-freedom）運動方程式理論，除計算彈體飛行軌跡各點之座標值（射距、彈道高、彈道橫向飄移）外，亦可直接計算彈體飛行軌跡各點之彈丸飛行姿態（飛行攻角、偏角與側滑角），1986 年 G.C.Andrews, J.J. McPhee 與 G.W. Kraak 運用六自由度運動方程式進行彈體飛行穩定與彈著散佈精度研究 [22]；彈著散佈精度的預估研究為世界各國近二十年來的彈道研究重點，並將之歸屬於中間彈道學，換言之造成彈著散佈原因並非僅源於實際彈體製造的不對稱性致使彈體飛行時所承受的空氣動力變異，而產生彈體飛行軌跡與彈著不同；依前述的彈體飛行軌跡數學模型，若在相同的發射條件下是無法求得不同的彈著點，因而中間彈道學所研究的彈體出砲口後，在火藥氣體後放期其氣體與彈體之間作用關係與砲口跳躍等問題 [23]，如圖一、圖二所示，著實在研究提供彈體飛行軌跡數學模型不同的起始條件（initial condition），以模擬預估彈著散佈的問題。

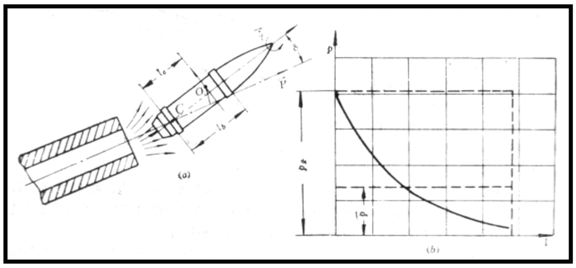

圖一、火藥氣體對彈體之後效期作用與壓力變化情形

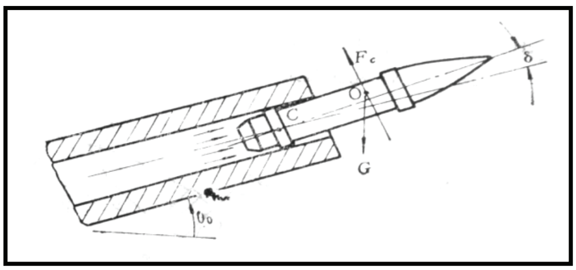

圖二、砲口跳耀對彈體之影響

叁、理論分析

一、彈道匹配與砲彈穩定飛行

火砲的任務在於提供砲彈穩定飛行與達到射程的初始條件；而彈道匹配則隨著火砲的戰術目的特性，於火砲、彈藥設計之初予以考量，以達戰術目的要求。砲彈穩定飛行是完成彈道匹配的基本考量；砲彈穩定飛行的方法區分為尾翼穩定（如迫擊砲彈、尾翼穩定脫殼穿甲彈 APFSDS、

高爆戰防彈 HEAT）與旋轉穩定（如高爆榴彈、穿甲彈 APDS）。若以碰炸式引信為彈頭終端引爆考量，則不論是尾翼穩定彈或旋轉穩定彈，其理想的彈道匹配如圖三所示，換言之彈體發射之初，其彈尖朝上，當彈體飛抵目標時則需彈尖朝下，並需滿足碰炸式引信之碰炸角度限制，以確保彈頭引爆，產生端引殺傷效應。

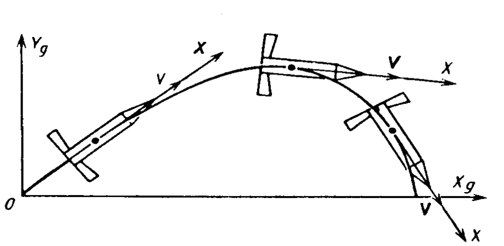

圖三、彈丸在彈道不同位置上之姿態

旋轉穩定彈係當彈體於砲管內向前飛行時，同時使彈體產生高速自旋運動，當彈體飛行於空氣中，作用其上之空氣動力將使彈體產生陀螺效應而使彈尖相對於彈體質心產生進動運動（precession）與章動運動（nutation），以保持彈尖向前而不翻滾。旋轉穩定彈的體形如圖四所示，飛行時其空氣動力之壓心（CP, Center of Pressure）於彈體質心（CG, Center of Gravity）前方。作用於壓心上的力對彈體質心產生一向彈尾翻轉的力矩，使彈尖向後翻滾，這種體形屬於靜態不穩定（static unstable）設計。尾翼穩定彈的體形如圖五所示，利用彈尾之尾翼設計，使彈體空氣動力壓心位於彈體質心後方，以使彈體於飛行時穩定彈尖向前而不翻滾；這種體形屬於靜態穩定（static stable）設計，彈體壓心與質心之間的距離稱為靜穩定儲量（stable margin），一般設計為全彈長度的 10% ~15%。以彈尖為原點，彈尖至壓心之間的距離為 L_p ，彈尖至質心之間的距離 L_g ，當

$L_g - L_p < 0$時，為靜態穩定

$L_g - L_p > 0$時，為靜態不穩定，需旋轉穩定

$L_g - L_p = 0$時，為中性穩定（neutral stable）

靜態不穩定的體形，需以彈體高速自旋運動以達彈體旋轉穩定，當彈體高速自旋時，將產生馬格勒斯效應（Magnus effect）與彈體橫向偏移（Drift）現象。

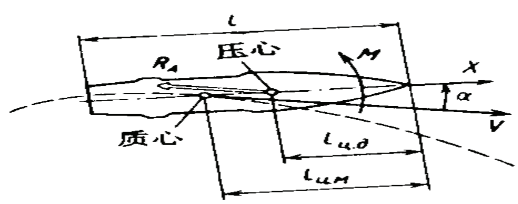

圖四、旋轉穩定彈之質心、壓心位置與氣動力矩作用

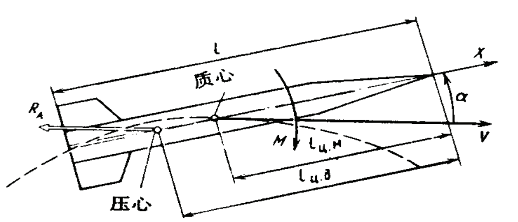

圖五、尾翼穩定彈之質心、壓心位置與氣動力矩作用

二、六自由度模式

六自由度程式基本上以輸入彈體物性、空氣動力係數，最後計算輸出彈體飛行軌跡特性資料。有關六自由度程式設計時所考慮的假設條件：

（1）彈體飛行時重心改變的飛行狀況

在計算彈體噴氣(Base Bload)或火箭的飛行軌跡時，其重心位置將為一時間函數，故軌跡計算時需考量該因素之影響。

（2）參考座標選取

為配合與地面量測數據比較，需將參考座標取決於地面座標系或地心座標。

（3）為解析彈體所受氣動力狀況，將參考座標取決於彈體座標系或彈體旋轉座標系。

（4）大氣中風速之影響。

（5）飛行環境資料

地球大氣密度、黏性、溫度、壓 力、音速等，係參考 Yang 及 ARDC 大氣模式計算法則做成高度函數以為計算。

（6）飛行體只受地球引力影響因飛行在地球表面之大氣層內飛行故月球及太陽系其他行星之影響省略不計

（7）彈體視為一剛體

依整個程式的設計目的而言，是為藉由一組運動方程式來瞭解整個飛行的運動狀況。而這組方程式須考量到飛行體在空中所受到的各種作用力，如：空氣動力、重力、推力、阻力與馬格勒斯力（Magnus force），然後依牛頓運動定律描繪出其作用合力與加速度之間的關係。彈體的整個運動狀態可分為移動運動與轉動運動，在移動運動裡依牛頓運動方程式可求得位置變化的情形，而在轉動運動裡則依尤拉方程式可求得其角度變化的情形。

牛頓方程式

$$\vec{F} = m\dot{\vec{v}} \tag{1}$$

在式中 $\vec{F}$ 和 $\dot{\vec{v}}$ 為對彈體重心的作用力總合和彈體之加速度，m 則為彈體質量。

尤拉方程式

$$\vec{M} = \frac{d}{dt}\vec{H} \tag{2}$$

式中 $\vec{M}$ 和 $\vec{H}$ 為對彈體重心作用於彈體上之力矩和彈體之角動量。

就整個運動而言，解出上述兩個方程式即可；但上述兩個方程式並無座標系統，所以我們必須加入座標以解析之。在座標選取上，一般皆以地面所能觀測為主，選取一地面參考座標。但實質上力和力矩係作用於彈體之上，故為解析上的方便，選取一彈體座標於彈體重心上，以求得力與力矩對彈體作用的情形。如此兩座標間

就存在著一座標相對運動的關係。假設此關係為彈體的轉動角速度，力和力矩係作用於彈體之上，故為解析上的方便，選取一彈體座標於彈體重心上以求得力與力矩對彈體作用的情形。如此，兩座標間就存在著一座標相對運動的關係。假設此關係為彈體的轉動角速度，其大小由彈體座標來表示為 $\vec{\omega}$ ，所以

$$\vec{F} = m\dot{\vec{v}} + m\vec{\omega}\times\vec{v} \qquad (3)$$

$$\vec{M} = \frac{d}{dt}\vec{H} + \vec{\omega}\times\vec{H} \qquad (4)$$

其中，$\vec{F}$ 為作用於彈體上之合力向量，m 為彈體質量，$\vec{\omega}$ 為彈體旋轉角速度，$\vec{V}$ 為彈體運動速度，$\dot{\vec{V}}$ 為彈體運動加速度，$\vec{M}$ 為作用於彈體之力矩向量，$\vec{H}$ 為彈體角動量。

方程式（3）與（4）只說明力矩在兩相對運動之角速度間座標的關係，並未真正的引入座標。接著將座標正式引入，選取一地面座標，沿射距方向為 X 軸，彈體飛行高度為 Y 軸，彈體偏移量為 Z 軸，因此可得 O-XYZ 地面座標；另於彈體上選取一彈體座標系統，以彈體之重心為原點，重心與彈尖之連線方向為 x 軸，垂直於 x 軸向上之方向為 y 軸，依左手定則決定軸之方向，因此可得 o-xyz 彈體座標系統；座標系統之建構如圖六所示。

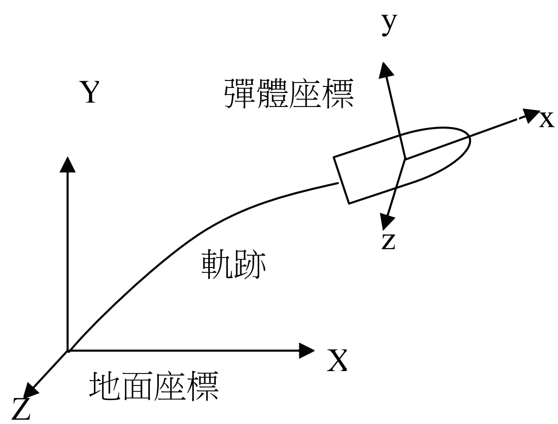

圖六、地面座標與彈體座標系統

將方程式（3）與（4）式中的各項向量以座標之分量表示，可得

$$\vec{F} = X\vec{i} + Y\vec{j} + Z\vec{k} \qquad (5)$$

X、Y、Z 為作用於彈體座標系 x、y、z 方向之總氣動力分量總和；

$$\vec{M} = L\vec{i} + M\vec{j} + N\vec{k} \qquad (6)$$

L、M、N 為作用於彈體座標系 x、y、z 方向之力矩分量；

$$\vec{V} = u\vec{i} + v\vec{j} + w\vec{k} \qquad (7)$$

u、v、k 為彈體座標系內彈體飛行速度在 x、y、z 軸上之分量；

$$\vec{\omega} = p\vec{i} + q\vec{j} + r\vec{k} \qquad (8)$$

p、q、r 為彈體座標系角速度在 x、y、z 上之分量；

$$\vec{H} = H_x\vec{i} + H_y\vec{j} + H_z\vec{k} \qquad (9)$$

H_x、H_y、H_z 為彈體座標系角動量在 x、y、z 上之分量；

將上述（1）（5）（7）代入（3）式可得

$$\begin{bmatrix} X \\ Y \\ Z \end{bmatrix} = m\begin{bmatrix} \dot{u} \\ \dot{v} \\ \dot{w} \end{bmatrix} + m\begin{bmatrix} 0 & -r & q \\ r & 0 & -p \\ -q & p & 0 \end{bmatrix}\begin{bmatrix} u \\ v \\ w \end{bmatrix} \qquad (10)$$

將重力考慮進來代入上式則變成

$$X - mg\sin\theta = m(\dot{u} + qw - rv) \qquad (11)$$

$$Y + mg\cos\theta\sin\phi = m(\dot{v} + ru - pw) \qquad (12)$$

$$Z + mg\cos\theta\cos\phi = m(\dot{w} + pv - qu) \qquad (13)$$

同理將式（6）、（8）、（9）代入式（4）式可得

$$\begin{bmatrix} L \\ M \\ N \end{bmatrix} = \begin{bmatrix} \dot{H}_x \\ \dot{H}_y \\ \dot{H}_z \end{bmatrix} + \begin{bmatrix} 0 & -r & q \\ r & 0 & -p \\ -q & p & 0 \end{bmatrix}\begin{bmatrix} H_x \\ H_y \\ H_z \end{bmatrix} \qquad (14)$$

又 H=Iw 所以

$$\begin{bmatrix} H_x \\ H_y \\ H_z \end{bmatrix} = \begin{bmatrix} I_{xx} & -I_{xy} & -I_{xz} \\ -I_{xy} & I_{yy} & -I_{yz} \\ -I_{xz} & -I_{yz} & I_{zz} \end{bmatrix}\begin{bmatrix} p \\ q \\ r \end{bmatrix} \qquad (15)$$

$$\begin{bmatrix} \dot{H}_x \\ \dot{H}_y \\ \dot{H}_z \end{bmatrix} = \begin{bmatrix} I_{xx} & -I_{xy} & -I_{xz} \\ -I_{xy} & I_{yy} & -I_{yz} \\ -I_{xz} & -I_{yz} & I_{zz} \end{bmatrix}\begin{bmatrix} \dot{p} \\ \dot{q} \\ \dot{r} \end{bmatrix}$$

$$+ \begin{bmatrix} \dot{I}_{xx} & -\dot{I}_{xy} & -\dot{I}_{xz} \\ -\dot{I}_{xy} & \dot{I}_{yy} & -\dot{I}_{yz} \\ -\dot{I}_{xz} & -\dot{I}_{yz} & \dot{I}_{zz} \end{bmatrix}\begin{bmatrix} p \\ q \\ r \end{bmatrix} \qquad (16)$$

因假設彈體為剛體（Rigid Body），故 $\dot{I} = 0$

$$\begin{bmatrix} \dot{H}_x \\ \dot{H}_y \\ \dot{H}_z \end{bmatrix} = \begin{bmatrix} I_{xx} & -I_{xy} & -I_{xz} \\ -I_{xy} & I_{yy} & -I_{yz} \\ -I_{xz} & -I_{yz} & I_{zz} \end{bmatrix}\begin{bmatrix} \dot{p} \\ \dot{q} \\ \dot{r} \end{bmatrix} \qquad (17)$$

將式（15）、（17）兩式代入式（14）式可得

$$\begin{bmatrix} L \\ M \\ N \end{bmatrix} = \begin{bmatrix} I_{xx} & -I_{xy} & -I_{xz} \\ -I_{xy} & I_{yy} & -I_{yz} \\ -I_{xz} & -I_{yz} & I_{zz} \end{bmatrix}\begin{bmatrix} \dot{p} \\ \dot{q} \\ \dot{r} \end{bmatrix}$$

$$+ \begin{bmatrix} 0 & -r & q \\ r & 0 & -p \\ -q & p & 0 \end{bmatrix}\begin{bmatrix} I_{xx} & -I_{xy} & -I_{xz} \\ -I_{xy} & I_{yy} & -I_{yz} \\ -I_{xz} & -I_{yz} & I_{zz} \end{bmatrix}\begin{bmatrix} p \\ q \\ r \end{bmatrix} \qquad (18)$$

因彈體軸對稱體，故 $I_{xy}=I_{yz}=I_{zx}=0$ 且 $I_{yy}=I_{zz}$ 將之代入上式可得

$$L = I_{xx}\dot{p} \qquad (19)$$

$$M = I_{yy}\dot{q} + (I_{xx} - I_{zz})rp \qquad (20)$$

$$N = I_{zz}\dot{r} + (I_{yy} - I_{xx})pq \qquad (21)$$

方程式（11）、（12）、（13）、（19）、（20）、（21）共計有六個方程式，這就是六自由度程式的統御方程式（Governing

Equation)。運用方程式求得彈體在彈體座標系內之線性加速度 $\dot{u}$ 、$\dot{v}$、 $\dot{w}$ 及角加速度 $\dot{p}$、$\dot{q}$、$\dot{r}$,再將所有之加速度積分,即可求得彈體在受力後所產生之線性速度與角速度,即 u、v、w 與 p、q、r。但此時所計算出來之速度與角速度乃是在機體座標下所獲得的結果,若直接積分則所獲得的位移與角位移亦即是對彈體座標而言。故須將上述計算的結果,再經過一座標轉換到地面座標系上,如此所獲得的結果也就可以與地面觀測的結果相互比較。

$$\dot{\phi} = p + q\sin\phi\tan\theta + r\cos\phi\tan\theta \qquad (22)$$

$$\dot{\theta} = q\cos\phi - r\sin\phi \qquad (23)$$

$$\dot{\psi} = (q\sin\phi + r\cos\phi)\sec\theta \qquad (24)$$

$$\begin{bmatrix} \dot{x}_E \\ \dot{y}_E \\ \dot{z}_E \end{bmatrix} = L_{VB} \begin{bmatrix} u \\ v \\ w \end{bmatrix} \qquad (25)$$

其中,$\dot{x}_E$,$\dot{y}_E$,$\dot{z}_E$ 為沿地面座標系三軸的速度分量;ϕ,θ,ψ 稱為尤拉角即地面座標系三軸與彈體座標系三軸之夾角;L_{VB} 為彈體座標系轉換到地面座標系之矩陣關係

$$L_{VB} = \begin{bmatrix} \cos\theta\cos\psi & \sin\phi\sin\theta\cos\psi - \cos\phi\sin\psi & \cos\phi\sin\theta\cos\psi + \sin\psi\sin\theta \\ \cos\theta\sin\psi & \sin\phi\sin\theta\sin\psi + \cos\phi\cos\psi & \cos\phi\sin\theta\sin\psi - \sin\phi\cos\psi \\ -\sin\theta & \sin\phi\cos\theta & \cos\phi\cos\theta \end{bmatrix} \qquad (26)$$

將方程式(11)、(12)、(13)、(19)、(20)、(21)計算後的結果輸入方程式(22)、(23)、(24)、(25),即可求得彈體在地面座標系裡之角加速度 $\dot{\phi}$ 、$\dot{\theta}$ 、$\dot{\psi}$ 與線性速度 $\dot{x}_E$ 、 $\dot{y}_E$ 、 $\dot{z}_E$,經積分後求得彈體在地面座標系內的線性位移 x_E 、 y_E 、 z_E 與角位移 ϕ 、 θ 、 ψ 。

三、蒙地卡羅法

蒙地卡羅法(Monte Carlo),是基於大數法則的實證方法,當實驗的次數越多,平均值也就會越趨近於理論值;也是一種數值方法,利用隨機亂數取樣來解決數學問題。所謂產生亂數,是從一開始給定的數集合中選出的數,稱為亂數,若數集合中的數被選中的機率相同,稱為均勻亂數。

砲彈在實際的射擊過程中,受到砲口初速變化、砲口跳躍、砲口的噴流及空氣動力改變等因素影響,導致每一發相同起始條件之彈體,其彈道軌跡與彈著點都不盡相同,上述這些砲口因素都是隨機的變量,因此本文使用蒙地卡羅法,產生符

合隨機因素之量化值。本研究做法為：在程式中利用符合隨機變量實際分布的隨機亂數產生器產生符合砲口初速變化與砲口跳躍角度之量化值，加入於每一發起始條件相同之彈體，並藉由六自由度數學模型模擬計算後，可得散佈的飛行軌跡與彈著點。

首先砲口跳躍角度方向有可能發生在砲口周圍 360 度，因此以彈體質心為基準可設想出一個三角圖錐，如圖七（a）與（b）所示，在理想的情況下不受砲口跳躍影響，彈體的發射點指向為 A 點位置，圖中假設彈體受到砲口跳躍影響，其發射點指向為 B 點位置，則要求得 B 點位置對初始速度影響，需將角錐分成兩個三角形(圖中平面 1 與平面 2)解析，δ為彈體跳躍角度大小、θ為彈體跳躍發生方向。

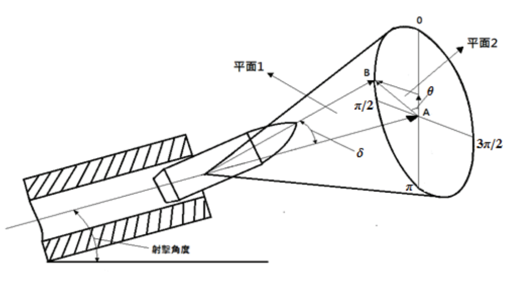

（a）

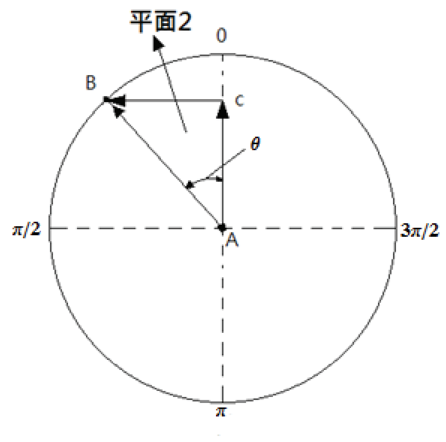

（b）

圖七、砲口跳躍角度示意圖

將兩個三角形作向量分解，如圖八所示，圖中 rnd(1)為初始速度變化，在本研究中採用值為正負 15 m/sec 為變化基準，rnd(2)為三角形(平面 1) δ角度以 0~10 度為變化基準，rnd(3)為三角形(平面 2) θ 角度以 0~360 度為變化基準。

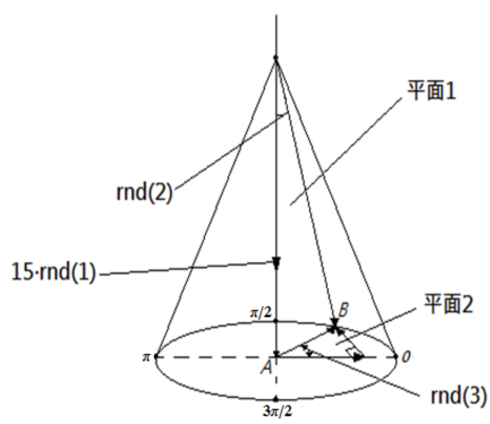

圖八、跳躍角度設想之角錐示意圖

兩個三角形間之關係，如圖九所示，圖中平面1與平面2分別為圖八角錐中與底面圓上之三角形，O為彈體的質心點、A為理想情況下之發射點、B為受到砲口跳躍影響之發射點。

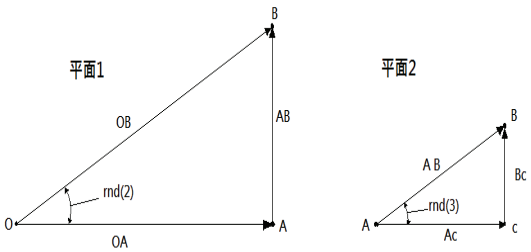

圖九、三角形間之關係示意圖

因此平面 1 之 OA、OB 及 AB 各段之向量可表示成

$$\left|\overrightarrow{OA}\right| = 15 \cdot rnd(1)$$

$$\left|\overrightarrow{OB}\right| = 15 \cdot rnd(1) \cdot cos[rnd(2)]$$

$$\left|\overrightarrow{AB}\right| = 15 \cdot rnd(1) \cdot sin[rnd(2)]$$

平面 2 之 AB 段向量與平面 1 之 AB 段相同，Ac 及 Bc 段之向量可表示成

$$\left|\overrightarrow{Ac}\right| = 15 \cdot rnd(1) \cdot sin[rnd(2)] \cdot sin[rnd(3)]$$

$$\left|\overrightarrow{Bc}\right| = 15 \cdot rnd(1) \cdot sin[rnd(2)] \cdot cos[rnd(3)]$$

接著經由各角度之向量轉換，可得到 B 點位置之 x、y、z 三個方向的速度方程式

$$V_x = 15 \cdot \mathrm{rnd}(1) \cdot \cos[\mathrm{rnd}(2)] \quad (27)$$

$$V_y = 15 \cdot \mathrm{rnd}(1) \cdot \sin[\mathrm{rnd}(2)] \cdot \sin[\mathrm{rnd}(3)] \quad (28)$$

$$V_z = 15 \cdot \mathrm{rnd}(1) \cdot \sin[\mathrm{rnd}(2)] \cdot \cos[\mathrm{rnd}(3)] \quad (29)$$

將這三個速度方程式寫成程式加入六自由度程式的起始條件中，藉此得到模擬砲口初始變化與砲口跳躍角度的隨機變量，使每一發起始條件相同之彈體，獲得不同飛行軌跡與彈著點。

四、程式流程

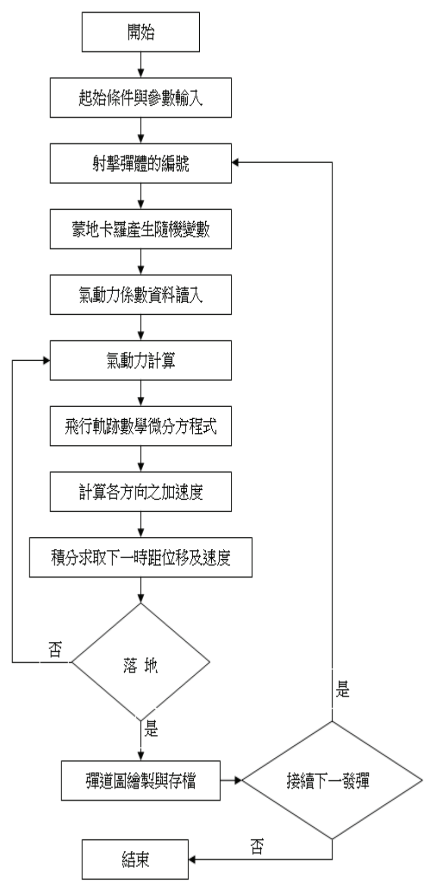

肆、結果與討論

本研究利用已收集之 155 mm M107 高爆榴彈，如圖十，之物性、幾何與發射條件及氣動力數據，進行六自由度旋轉穩定彈理論射表試算。

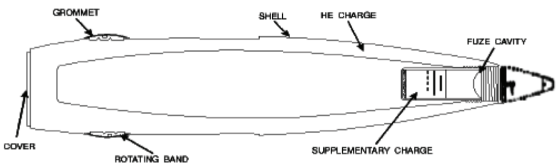

圖十、155mm M107高爆榴彈

每一發起始條件皆相同的彈體在六自由度數學模型模擬計算前已將隨機產生器產生之相關參數加入起始條件中，試算十發彈後，皆有不同的飛行軌跡與彈著點；圖十一為飛行距離對飛行時間關係；圖十二為飛行高度對飛行時間關係；圖十三為飛行高度對飛行距離關係；圖十四為偏移量對飛行距離關係；圖十五為彈著點散布圖；圖十六為飛行軌跡 3D 圖。表一為 M107 高爆榴彈物性；表二為依據計算結果編製之射表；表三為平均值與標準差，彈道諸元包括飛行時間（Flight Time）、射距（Range）與偏移量（Drift）。

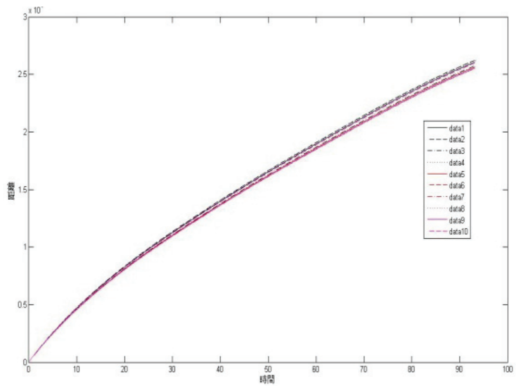

圖十一、飛行距離對飛行時間關係

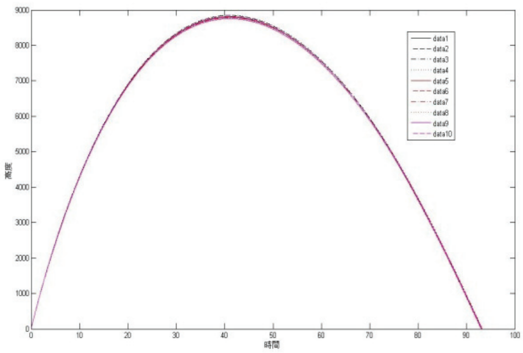

圖十二、飛行高度對飛行時間關係

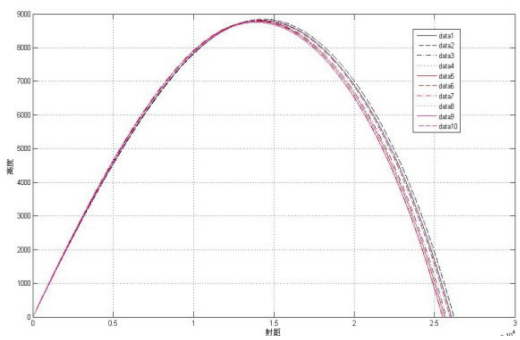

圖十三、飛行高度對飛行距離關係

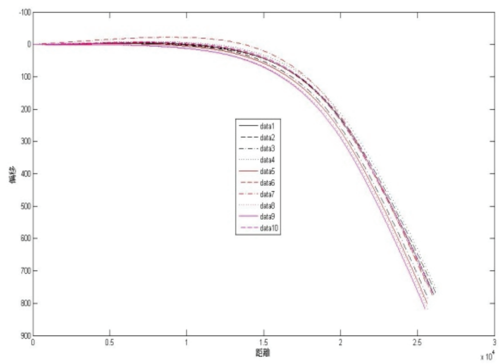

圖十四、偏移量對飛行距離關係

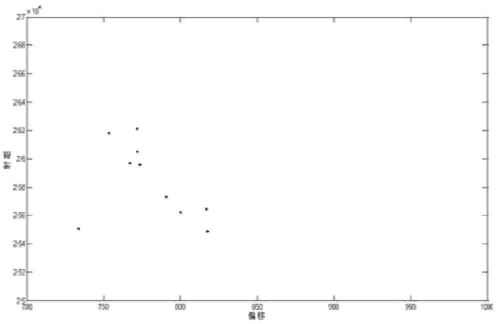

圖十五、彈著點散布圖

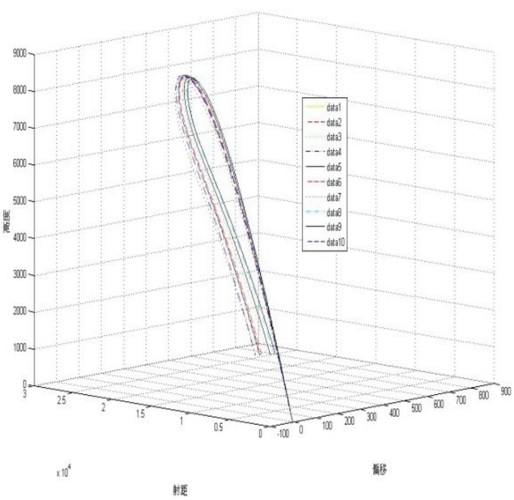

圖十六、飛行軌跡 3D 圖

表一、M107高爆榴彈物性

直徑(mm)	155
彈長(mm)	874.975
彈重(kg)	47.5
彈體重心(mm)	558
彈體 x 軸轉動慣量(kg-m^2)	0.1539
彈體 y,z 軸轉動慣量(kg-m^2)	2.2133

表二、計算結果編製之射表

編號	Flight Time (sec)	Range (m)	Drift (m)
1	93.09	26050.61	772.1
2	93.18	26212.92	771.84
3	93.14	25730.05	790.66
4	93.27	26183.28	753.65
5	93.18	25624.22	800.17
6	93.11	25958.05	773.53
7	93.19	25507.12	733.48
8	93.05	25645.85	817.01
9	93.01	25490.99	817.63
10	93.11	25969.92	766.95

表三、平均值與標準差

	Time	Range	Drift
平均值	93.133	25837.3	779.7
標準差	0.0717	257.094	25.51

伍、結論

在本文中藉由六自由度數學模型之建立並使用蒙地卡羅法來模擬砲口初速變化與砲口的跳躍等問題，已建構一可模擬六自由度彈道之計算程式，可用於彈道模擬器在輸入火砲發射條件後，計算對應之彈道諸元資料；本文中並以 M107 155 mm 火砲為例，計算其彈道軌跡與落點分布。

陸、參考文獻

[1] Charles H. Murphy, Jr.,"The Prediction of Nonlinear Pitching and Yawing Motion of Symmetric Missiles," Journal of the Aeronautical Science, Vol. 24, No. 7, pp.473-479, 1957.

[2] Anders S. Platou,"Magnus Characteristics of Finned and Nonfinned Projectiles, "AIAA Journal, Vol. 3, No. 1, pp.83-90,1965.

[3] Gary T. Chapman and Donn B. Kirk, "A Method for Extracting Aerodynamic Coefficients form Free-Flight Data, " AIAA Journal, Vol. 8, No. 4, pp.753-758, 1970.

[4] Charles H. Murphy, "Nonlinear Motion of a missile with Slight Configurational Asymmetries," Journal of Spacecraft and Rocket, Vol. 8, No. 3, pp.259-263, 1971.

[5] G.W. Stone, E.L. Jr. Clark, and G.E. Burt,"An Investigation of Nonsymmetric Aerodynamic Damping Moments," AIAA Paper 72-29, 1972.

[6] O. Walchner and F.M. Sawyer,"'In-Plane' and 'Out-of-Plane' Stability Derivatives of Slender Cones at Mach 14," Aerospace Research Laboratories, Wright-Patterson Air Force Base, Ohio, Report. ARL 73-0090, July 1973.

[7] Charles H. Murphy, "Symmetric Missile Dynamic Instabilities," Journal of Guidance and Control, Vol. 4, No.5, pp.464-471, 1980.

[8] Charles H. Murphy, "Free Flight Motion of Symmetric Missiles," June 20-24, 1988.

[9] Nusca, M.; Chakravarthy, S.; Goldberg, U. , "Computational Fluid Dynamics Capability for the Solid-Fuel Ramjet Projectile. " Journal of Propulsion and Power, Vol. 6, No.3, pp.256-262, 1990.

[10] Sturek, W.; Nietubicz, C.; Sahu, J.; Weinacht, P. ,"Applications of Computational Fluid Dynamics to the Aerodynamics of Army Projectiles." Journal of Spacecraft and Rockets, Vol. 31, No. 2, pp.186-199, 1994.

[11] Weinacht, P.; Sturek, W. ,

"Computation of the Roll Characteristics of a Finned Projectile. "Journal of Spacecraft and Rockets, Vol. 33, No. 6, pp.769-775, 1996.

[12] Graham, M.; Weinacht, P.; Bennett, J. , "Numerical Investigation of Supersonic Jet Interaction for Finned Bodies. " Journal of Spacecraft and Rockets , Vol. 39, No.3, pp.376-383, 2002.

[13] DeSpirito, J.; Heavey, K. , "CFD Computation of Magnus Moment and Roll-Damping Moment of a Spinning Projectile. ", AIAA Atmospheric Flight Mechanics Conference, AIAA-2004-4713, Providence, RI, 2004.

[14] Silton, S. , "Navier-Stokes Computations for a Spinning Projectile from Subsonic to Supersonic Speeds. " Journal of Spacecraft and Rockets, Vol. 42, No. 2, pp.223-231, 2005.

[15] Joseph, K., Costello, M. and Jubaraj, S. , " Generating an Aerodynamic Model for Projectile Flight Simulation using Unsteady Time Accurate Computational Fluid Dynamic Results. ", Army Research Laboratory, Aberdeen Proving Ground, USA, ARL-CR-577, 2006.

[16] Sahu, Jubaraj, " Time-Accurate Numerical Prediction of Free-Flight Aerodynamics of a Finned Projectile. " Journal of Spacecraft and Rockets , Vol. 45, No. 5, pp.946-954, 2008.

[17] Davis Bradford,Gregory Malejko, Rollie Dohrn,Scott Owens,Thomas Harkins and Gregory Bischer, " Addressing the Challenges of a Thruster-Based Precision Guided Mortar Munition With the Use of Embedded Telemetry Instrumentation. " ITEA Journal , Vol. 30, No. 1, pp.117-125, 2009.

[18] 浦發,芮筱亭,外彈道學,國防工業出版社,1989.

[19] 韓子鵬,薛曉中,張鶯,外彈道學,國防工業出版社,2000.

[20] R.F. Lieske and R.L.McCoy, "Equation of Motion of a Rigid Projectile," BRL Report No. 1244, 1964.

[21] R.F. Lieske and Mary L. R "Equation of Motion for a Modified Point Trajectory," BRL Report No. 1314, 1966.

[22] G.C.Andrews, J.J. McPhee and G.W. Kraak, "Simulating Projectile Motion to Evaluate Stability and Dispersion," Computers in Engineering, Vol. 2, PP319-326, 1988.

[23] 董量,王宗虎,馬素珍,彈箭飛行穩定性理論及其運用,兵器工業出版

社,1990

[24] 房玉軍、蔣建偉，子彈藥拋撒隨機外彈道模型及其蒙特卡洛解法，北京理工大學學報，2009。

Adaptive predictive PID controller based on Elman neural network with hierarchical BP algorithm

Chi-Huang Lu, Chi-Ming Lu, Yuan-Hai Charng

Abstract

This paper presents a predictive proportional-integral-derivative (PID) controller based on Elman neural network (ENN) for a class of nonlinear systems. The ENN with both online learning and well approximation capability is employed to estimate the nonlinear function of the controlled system. The weights of the ENN identifier are trained by the hierarchical backpropagation algorithm with the adaptive learning rate, the adaptive learning rate is suitable for the ENN identifier can be convergent. The predictive PID controller is derived via a predictive performance criterion and the adaptive optimal rate for guaranteeing the convergence of the proposed PID controller. The stability analysis of the closed-loop control system is presented by the discrete Lyapunov stability theorem. Numerical simulations reveal that the proposed control law gives satisfactory tracking and disturbance rejection performances.

Keywords: Elman neural network, hierarchical BP algorithm, model predictive control, PID controller.

Chi-Huang Lu, Associate Professor, Department of Electrical Engineering, HUST.
Chi-Ming Lu, Lecturer, Department of Electrical Engineering, HUST.
Yuan-Hai Charng, Lecturer, Department of Machine Engineering, HUST.
Received 3 April 2011; accepted 8 June 2011

基於 Elman 類神經網路與 Hierarchical 演繹法之適應預估 PID 控制器

呂奇璜、呂奇明、常元海

摘 要

本論文提出以 Elman 類神經網路（ENN）做為非線性系統之預估比例-微分-積分（PID）控制器。ENN 具備有及時學習與好的近似能力，是用來估測受控系統的非線性函數。ENN 辨識器係以 Hierarchical 演繹法與與適應學習率來學習 ENN 的權重值，適應學習率可確保 ENN 辨識器收斂。這預估 PID 控制器是藉由預估性能指標來推導，適應最佳率可確保所提 PID 控制器收斂；而閉迴路控制系統由離散 Lyapunov 穩定準則來進行穩定分析。數值模擬指出所提控制策略具備了滿意的設定點追蹤與擾動排除的性能。

關鍵詞：Elman 類神經網路、Hierarchical 演繹法、模型預估控制、PID 控制器。

呂奇璜：修平科技大學電機工程系副教授
呂奇明：修平科技大學電機工程系講師
常元海：修平科技大學機械工程系講師
投稿日期：100年4月3日 接受刊登日期：100年6月8日

1. Introduction

The Model predictive control (MPC) has been recognized as a powerful methodology for controlling of a wide class of nonlinear dynamic systems. Several theories and pragmatic design techniques have been proposed for a variety of physical systems and industry applications [1-4]. The MPC has also been recognized as a useful control means for nonlinear, time-delay and even multivariable systems. In the past decade, researchers have paid much effort in this quite challenging field of nonlinear model predictive control; some important theories and practices for nonlinear model predictive control have been documented in [5-9].

Since neural networks can approximate any nonlinear functions with arbitrary accuracy, they have been applied to develop adaptive control of nonlinear systems [10-13]. In particular, the recurrent neural network (RNN) is a dynamical mapping and demonstrates good control performance in the presence of unmodeled dynamics; each recurrent neuron has an internal feedback loop, and then captures the dynamic response of a system without external feedback through delays [14]. In the past decade, several researchers have extensively investigated RNN-based predictive control with its applications to nonlinear systems [15-17]. The most important characteristic of the recurrent neural networks is its connection to memorize feedback information of the history influence in the same neuron. In this paper, the adopted Elman neural network can be considered as a special type of RNN. The structure of ENN is more powerful than general self-recurrent neural networks to deal with nonlinear dynamic systems due to the cross-coupled interference and effect of each state can be approximated efficiently with the addition context layer [18,19].

Many industrial systems exhibit nonlinear behaviors, in that their mathematical relations between the controlled and manipulated variables depend heavily on the operating conditions. To control the nonlinear systems, most industrial controllers employ fixed-parameter PID controller. However, the control gains must be manually adjusted at different operation conditions in order to meet desired system performance; thus, the responses of nonlinear systems cannot be shaped into desirable performance using such controllers. Hence, the nonlinear systems reveal the need for adaptation of PID gains to achieve desired system response. As early as 1942, Ziegler and Nichols proposed the first PID tuning method [20]. Lee et al. presented the robust

PID controller design by fuzzy neural network [21]. Using a hybrid evolutionary-algebraic synthesis approach that combines linear matrix inequality (LMI) techniques based on K-S iteration with evolutionary search, a scheduled PID controller is designed by Kwiatkowski et al. [22]. Zheng et al. developed a self-tuning fuzzy PID controller for a switched reluctance motor direct drive volume control hydraulic press [23].

There are four objectives of this paper. The first is to propose the predictive PID controller based on ENN for a class of nonlinear systems. The PID gains of the proposed controller can be found using a scheme similar to a well-known MPC. The second is to solve the problem of the local minimum in the backpropagation (BP) algorithm and to improve the performance of the BP algorithm under the multilayer perceptron (MLP) structure of Elman neural network, one combine the hierarchical approach and the BP algorithm to implement the ENN identifier. The third is to guarantee the convergences of the ENN identifier and the predictive PID controller via the adaptive learning rate (ALR) and the adaptive optimal rate (AOR), respectively. The stability analysis of the closed-loop control system is studied by the discrete Lyapunov stability theorem. The fourth is to verify the feasibility and effectiveness of the predictive PID controller with its application to the nonlinear systems.

The rest of the paper is organized as follows. Section 2 describes how to construct the ENN identifier for a class of nonlinear discrete-time systems. Section 3 proposed that predictive PID control law is derived and the stability analysis is studied. Section 4 details the capabilities of the proposed controller utilizing computer simulations. Section 5 concludes this paper.

2. Elman neural network identifier

The section is devoted to developing the ENN identifier for a class of nonlinear systems. It is assumed that this nonlinear discrete-time system is generally described by the following nonlinear autoregressive moving averaging (NARMA) model

$$y(k) = f\big(u(k-1),\ \cdots,\ u(k-n_u),\ y(k-1),\ \cdots,\ y(k-n_y)\big) \tag{1}$$

where $u(\cdot): Z^+ \to \Re$ and $y(\cdot): Z^+ \to \Re$ are respectively the system input and output; $f(\cdot): \Re^{n_i} \to \Re$ denotes the nonlinear system function where $n_i = n_u + n_y$; $n_u \in Z^+$ and $n_y \in Z^+$ are the orders of the system input and the system output respectively.

The ENN architectures have been adopted to emulate the unknown nonlinear systems described in [19]. In the sequel, this output of the ENN to approximate the nonlinear system (1) is represented by $\hat{y}(k)$. Expressed mathematically

$$s_j(k) = \sigma\left(\sum_{i=1}^{n_i} w_{ij}^I x_i(k) + \sum_{j=1}^{n_j} s_j(k-1)\right) \tag{2}$$

$$\hat{y}(k) = \sum_{j=1}^{n_j} w_j^O s_j(k) \tag{3}$$

where $x_i(k)$ is the input variable of the input layer and the activation function is given by $\sigma(v) = 1/(1+e^{-v})$. w_{ij}^I and w_j^O are the weights for the ENN in the input layer, the hidden layer and the output layer, respectively.

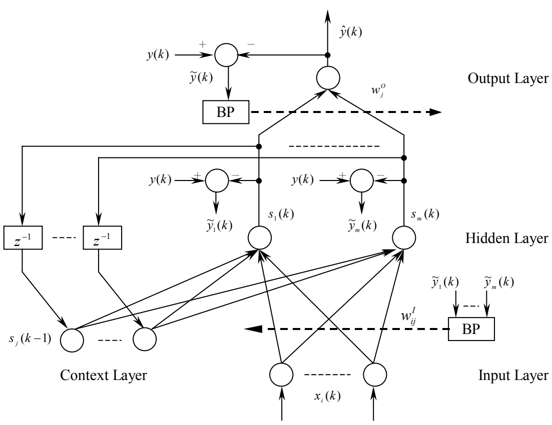

Figure 1. Structure of an ENN trained with the hierarchical BP algorithm.

2.1. Hierarchical BP algorithm

It is well known that the operation of the conventional BP algorithm will result in the occurrence of the local minimum that maybe leads to poor performance. Therefore, it is necessary to decrease the bad effects of the local minimum on the performance. The multilayer perceptron structure of Elman neural network, trained with the hierarchical BP algorithm is shown in Figure 1.When being trained with the proposed hierarchical BP algorithm, the entire MLP ENN is divided into two subnetworks and every single subnetwork is trained with an individual BP algorithm. Under this design, the ENN is determined by all BPs in the hierarchical BP algorithm, it can avoid the occurrence that the local minimum achieved by a single BP completely decides the ENN [24,25].

A weight updating rule for the ENN identifier using the hierarchical BP algorithm is adopted throughout the paper, and then the weights is recursively updated as

$$w_j^O(k) = w_j^O(k-1) + \Delta w_j^O = w_j^O(k-1) - \eta^o \frac{\partial \psi^o(k)}{\partial w_j^O}$$

$$= w_j^O(k-1) + \eta^o \widetilde{y}(k) s_j(k) \tag{4}$$

$$w_{ij}^I(k) = w_{ij}^I(k-1) + \Delta w_{ij}^I = w_{ij}^I(k-1) - \eta_j^I \frac{\partial \psi_j^I(k)}{\partial w_{ij}^I}$$

$$= w_{ij}^I(k-1) + \eta_j^I \widetilde{y}_j(k) x_i(k) \tag{5}$$

where η^o and η_j^I are the positive rates, and $\psi^o(k)$ and $\psi_j^I(k)$ of the performance criterions are defined by

$$\psi^o(k)=\left(y(k)-\hat{y}(k)\right)^2/2=\tilde{y}^2(k)/2 \tag{6}$$

$$\psi_j^I(k)=\left(y(k)-s_j(k)\right)^2/2=\tilde{y}_j^{\,2}(k)/2 \tag{7}$$

2.2. Adaptive learning rate

In general, if a small value is given for the learning rate, then the convergence of the neural network will be guaranteed, but the convergence rate may be rather slow. Conversely, if a large value for the learning rate is considered, then the neural network may become unstable. The following statement shows a guideline in selecting the learning rates properly, which leads to the ARLs of the Elman neural network.

Define a discrete Lyapunov function candidate as $\ell(k)=\tilde{y}^2(k)+\sum_{j=1}^{n_j}\tilde{y}_j^2(k)$. Then one obtains

$$\delta\ell(k)=\ell(k+1)-\ell(k)$$

$$=\tilde{y}(k)\left(2\tilde{y}(k)+\delta\tilde{y}(k)\right)+\sum_{j=1}^{n_j}\delta\tilde{y}_j(k)\left(2\tilde{y}_j(k)+\delta\tilde{y}_j(k)\right) \tag{8}$$

By the method in [17], $\delta\tilde{y}(k)$ and $\delta\tilde{y}_j(k)$ can be represented as

$$\delta\tilde{y}(k)=\frac{\partial\tilde{y}(k)}{\partial w_j^O}\Delta w_j^O=-\eta^o\tilde{y}(k)\left(\frac{\partial\tilde{y}(k)}{\partial w_j^O}\right)^2 \tag{9}$$

$$\delta\tilde{y}_j(k)=\frac{\partial\tilde{y}_j(k)}{\partial w_{ij}^I}\Delta w_{ij}^I=-\eta_j^I\tilde{y}_j(k)\left(\frac{\partial\tilde{y}_j(k)}{\partial w_j^O}\right)^2 \tag{10}$$

From (9) and (10), (8) can be expressed as

$$\delta\ell(k)=-\eta^o\tilde{y}^2(k)\left(\frac{\partial\tilde{y}(k)}{\partial w_j^O}\right)^2\left(2-\eta^o\left(\frac{\partial\tilde{y}(k)}{\partial w_j^O}\right)^2\right)$$

$$-\sum_{j=1}^{m}\eta_j^I\tilde{y}_j^2(k)\left(\frac{\partial\tilde{y}_j(k)}{\partial w_{ij}^I}\right)^2\left(2-\eta_j^I\left(\frac{\partial\tilde{y}_j(k)}{\partial w_{ij}^I}\right)^2\right) \tag{11}$$

To satisfy $\delta\ell(k)<0$, it is necessary to restrict to (11) which guarantees the convergence of the ENN with hierarchical BP algorithm. Before closing this section, one suggests that the ALRs be selected as following (12) and (13) in order to guarantee these selecting learning rates inside the stable region.

$$\eta^o=\frac{1}{\left(\frac{\partial\tilde{y}(k)}{\partial w_j^O}\right)^2}=\frac{1}{\sum_{j=1}^{n_j}s_j^2(k)} \tag{12}$$

$$\eta_j^I=\frac{1}{\left(\frac{\partial\tilde{y}_j(k)}{\partial w_{ij}^I}\right)^2}=\frac{1}{\sum_{i=1}^{n_i}x_i^2(k)}. \tag{13}$$

3. Predictive PID controller

In general, the PID controller in discrete form be represented by

$$u(k)=K_Pe(k)+K_I\sum_{\kappa=1}^{k}e(\kappa)+K_D\left(e(k)-e(k-1)\right) \tag{14}$$

where $e(k)=r(k)-y(k)$ and $r(k)$ is the input reference signal of the control system. The incremental PID controller can be given by

$$u(k) = u(k-1) + K_P\big(e(k) - e(k-1)\big) + K_I e(k) + K_D\big(e(k) - 2e(k-1) + e(k-2)\big). \quad (15)$$

The parameters K_P, K_I and K_D of PID controller is derived from the optimization of the predictive performance criterion based upon using the gradient descent method, that is

$$K_P(k) = K_P(k-1) + \Delta K_P = K_P(k-1) - \sum_{p=1}^{N_p} \lambda_p^P \frac{\partial J_P(k+p)}{\partial K_P} \quad (16)$$

$$K_I(k) = K_I(k-1) + \Delta K_I = K_I(k-1) - \sum_{p=1}^{N_p} \lambda_p^I \frac{\partial J_I(k+p)}{\partial K_I} \quad (17)$$

$$K_D(k) = K_D(k-1) + \Delta K_D = K_D(k-1) - \sum_{p=1}^{N_p} \lambda_p^D \frac{\partial J_D(k)}{\partial K_D} \quad (18)$$

where

$$J_P(k+p) = \frac{1}{2}\Big(\big(r(k+p) - \hat{y}(k+p)\big) - \big(r(k+p-1) - \hat{y}(k+p-1)\big)\Big)^2 = \frac{1}{2}\big(\hat{e}(k+p) - \hat{e}(k+p-1)\big) = \frac{1}{2}\hat{e}_P^2(k+p) \quad (19)$$

$$J_I(k+p) = \frac{1}{2}\hat{e}^2(k+p) = \frac{1}{2}\hat{e}_I^2(k+p) \quad (20)$$

$$J_D(k+p) = \frac{1}{2}\big(\hat{e}(k+p) - 2\hat{e}(k+p-1) + \hat{e}(k+p-2)\big)^2 = \frac{1}{2}\hat{e}_D^2(k). \quad (21)$$

N_p is the predictive output horizon and $\hat{y}(k+p)$ is the p-step-ahead prediction of $y(k)$. In order to reduce computational load of the predictive PID controller, let $u(k+N_p) = \cdots = u(k+2) = u(k+1) = u(k)$; then one has

$$\frac{\partial J_P(k+p)}{\partial K_P} = \frac{\partial J_P(k+p)}{\partial \hat{e}_P(k+p)} \frac{\partial \hat{e}_P(k+p)}{\partial \hat{y}(k+p)} \frac{\partial \hat{y}(k+p)}{\partial u(k)} \frac{\partial u(k)}{\partial K_P} = -\hat{e}_P(k+p)\left(\sum_{j=1}^{n_j} w_j^O s_j'(k+p) w_{1j}^I\right)\big(e(k) - e(k-1)\big) \quad (22)$$

$$\frac{\partial J_I(k+p)}{\partial K_I} = \frac{\partial J_I(k+p)}{\partial \hat{e}_I(k+p)} \frac{\partial \hat{e}_I(k+p)}{\partial \hat{y}(k+p)} \frac{\partial \hat{y}(k+p)}{\partial u(k)} \frac{\partial u(k)}{\partial K_I} = -\hat{e}_I(k+p)\left(\sum_{j=1}^{n_j} w_j^O s_j'(k+p) w_{1j}^I\right) e(k) \quad (23)$$

$$\frac{\partial J_D(k+p)}{\partial K_D} = \frac{\partial J_D(k+p)}{\partial \hat{e}_D(k+p)} \frac{\partial \hat{e}_D(k+p)}{\partial \hat{y}(k+p)} \frac{\partial \hat{y}(k+p)}{\partial u(k)} \frac{\partial u(k)}{\partial K_D} = -\hat{e}_D(k+p)\left(\sum_{j=1}^{n_j} w_j^O s_j'(k+p) w_{1j}^I\right)\big(e(k) - 2e(k-1) + e(k-2)\big) \quad (24)$$

where

$$s_j'(k+p) = \bar{\sigma}\left(\sum_{i=1}^{n_i} w_{i,j}^I x_i(k+p) + \sum_{j=1}^{n_j} s_j(k+p-1)\right),$$

$$\bar{\sigma}(v) = \frac{e^{-v}}{\left(1+e^{-v}\right)^2}. \quad (25)$$

3.1. Adaptive optimal rate

The following statement shows that the predictive PID controller is convergent via the adaptive optimal rate. Define a discrete Lyapunov function candidate as

$$\bar{\ell}(k) = \sum_{p=1}^{N_p} \big(\hat{e}_P^2(k+p) + \hat{e}_I^2(k+p) + \hat{e}_D^2(k+p)\big).$$

(26)

Then we have

$$\delta\bar{\ell}(k)=\bar{\ell}(k+1)-\bar{\ell}(k)$$

$$=\sum_{p=1}^{N_p}\delta\hat{e}_P(k+p)\big(2\hat{e}_P(k+p)+\delta\hat{e}_P(k+p)\big)$$

$$+\sum_{p=1}^{N_p}\delta\hat{e}_I(k+p)\big(2\hat{e}_I(k+p)+\delta\hat{e}_I(k+p)\big)$$

$$+\sum_{p=1}^{N_p}\delta\hat{e}_D(k+p)\big(2\hat{e}_D(k+p)+\delta\hat{e}_D(k+p)\big) \quad (27)$$

Since $\delta\hat{e}_P(k+p)$, $\delta\hat{e}_I(k+p)$ and $\delta\hat{e}_D(k+p)$ can be represented as

$$\delta\hat{e}_P(k+p)=\frac{\partial\hat{e}_P(k+p)}{\partial K_P}\Delta {K_P}^2$$

$$=-\lambda_p^P\hat{e}_P(k+p)\left(\frac{\partial\hat{e}_p(k+p)}{\partial K_P}\right) \quad (28)$$

$$\delta\hat{e}_I(k+p)=\frac{\partial\hat{e}_I(k+p)}{\partial K_I}\Delta K_I$$

$$=-\lambda_p^I\hat{e}_I(k+p)\left(\frac{\partial\hat{e}_I(k+p)}{\partial K_I}\right)^2 \quad (29)$$

$$\delta\hat{e}_D(k+p)=\frac{\partial\hat{e}_D(k+p)}{\partial K_D}\Delta K_D$$

$$=-\lambda_p^D\hat{e}_D(k+p)\left(\frac{\partial\hat{e}_D(k+p)}{\partial K_D}\right)^2. \quad (30)$$

From (28), (29) and (30), (27) can be expressed as

$$\delta\bar{\ell}(k)=-\sum_{p=1}^{N_p}\lambda_p^P\hat{e}_P^2(k+p)\left(\frac{\partial\hat{y}(k+p)}{\partial K_P}\right)^2\left(2-\lambda_p^P\left(\frac{\partial\hat{y}(k+p)}{\partial K_P}\right)^2\right)$$

$$-\sum_{p=1}^{N_p}\lambda_p^I\hat{e}_I^2(k+p)\left(\frac{\partial\hat{y}(k+p)}{\partial K_I}\right)^2\left(2-\lambda_p^I\left(\frac{\partial\hat{y}(k+p)}{\partial K_I}\right)^2\right)$$

$$-\sum_{p=1}^{N_p}\lambda_p^D\hat{e}_D^2(k+p)\left(\frac{\partial\hat{y}(k+p)}{\partial K_D}\right)^2\left(2-\lambda_p^D\left(\frac{\partial\hat{y}(k+p)}{\partial K_D}\right)^2\right)$$

(31)

To ensure a convergence of the predictive PID controller, the AOR can be set as (31), (32) and (33) so as to have $\delta\bar{\ell}(k)<0$; the AORs are given by

$$\lambda_p^P=\frac{1}{\left(\frac{\partial\hat{y}(k+p)}{\partial K_P}\right)^2}$$

$$=\frac{1}{\left(\left(\sum_{j=1}^{n_j}w_j^O s'_j(k+p)w_{1j}^I\right)\big(e(k)-e(k-1)\big)\right)^2} \quad (32)$$

$$\lambda_p^I=\frac{1}{\left(\frac{\partial\hat{y}(k+p)}{\partial K_I}\right)^2}$$

$$=\frac{1}{\left(\left(\sum_{j=1}^{n_j}w_j^O s'_j(k+p)w_{1j}^I\right)e(k)\right)^2} \quad (33)$$

$$\lambda_p^D=\frac{1}{\left(\frac{\partial\hat{y}(k+p)}{\partial K_D}\right)^2}$$

$$=\frac{1}{\left(\left(\sum_{j=1}^{n_j}w_j^O s'_j(k+p)w_{1j}^I\right)\big(e(k)-2e(k-1)+e(k-2)\big)\right)^2}$$

(34)

3.2. Stability analysis

The stability analysis of the

closed-loop control system is based upon the Lyapunov approach. Suppose the ENN identifier used for predictive PID controller design is stable. It is well known that the purpose of control is to force the output of the controlled system to track the desired trajectory of the system accurately. From this point view, one defines a discrete Lyapunov function as follows:

$$L(k)=\sum_{p=1}^{N_p}\boldsymbol{E}^T(k+p)\boldsymbol{E}(k+p)$$

$$+\sum_{p=1}^{N_p}\delta\boldsymbol{E}^T(k+p)\delta\boldsymbol{E}(k+p)\,. \qquad (35)$$

where

$$\boldsymbol{E}(k+p)=\left[\hat{e}_P(k+p),\ \hat{e}_I(k+p),\ \hat{e}_D(k+p)\right]^T$$

$$\delta\boldsymbol{E}(k+p)=\left[\delta\hat{e}_P(k+p),\ \delta\hat{e}_I(k+p),\ \delta\hat{e}_D(k+p)\right]^T$$

Then one has

$$\delta L(k)=\sum_{p=1}^{N_p}\delta\boldsymbol{E}^T(k+p)\left(2\boldsymbol{E}(k+p)+\delta\boldsymbol{E}(k+p)\right)$$

$$+\sum_{p=1}^{N_p}\delta\left(\delta\boldsymbol{E}^T(k+p)\right)\left(2\delta\boldsymbol{E}(k+p)+\delta\left(\delta\boldsymbol{E}(k+p)\right)\right)$$

$$=\delta\bar{\ell}(k)+\delta\breve{\ell}(k) \qquad (36)$$

where $\delta\bar{\ell}(k)$ is obtained from (31) and

$$\delta\breve{\ell}(k)=-\sum_{p=1}^{N_p}\lambda_p^P\delta\hat{e}_P^2(k+p)\left(\frac{\partial\hat{y}(k+p)}{\partial K_P}\right)^2\left(2-\lambda_p^P\left(\frac{\partial\hat{y}(k+p)}{\partial K_P}\right)^2\right)$$

$$-\sum_{p=1}^{N_p}\lambda_p^I\delta\hat{e}_I^2(k+p)\left(\frac{\partial\hat{y}(k+p)}{\partial K_I}\right)^2\left(2-\lambda_p^I\left(\frac{\partial\hat{y}(k+p)}{\partial K_I}\right)^2\right)$$

$$-\sum_{p=1}^{N_p}\lambda_p^D\delta\hat{e}_D^2(k+p)\left(\frac{\partial\hat{y}(k+p)}{\partial K_D}\right)^2\left(2-\lambda_p^D\left(\frac{\partial\hat{y}(k+p)}{\partial K_D}\right)^2\right)$$

(37)

From (32), (33) and (34).Then (37) becomes

$$\delta L(k)<-\sum_{p=1}^{N_p}\left(\hat{e}_P^2(k+p)+\hat{e}_I^2(k+p)+\hat{e}_D^2(k+p)\right)$$

$$-\sum_{p=1}^{N_p}\left(\delta\hat{e}_P^2(k+p)+\delta\hat{e}_I^2(k+p)+\delta\hat{e}_D^2(k+p)\right)$$

$$<-2\sum_{p=1}^{N_p}\left(\hat{e}_P^2(k+p)+\hat{e}_I^2(k+p)+\hat{e}_D^2(k+p)\right)$$

$$<-2\sum_{p=1}^{N_p}\boldsymbol{E}^T(k+p)\boldsymbol{E}(k+p)\,. \qquad (38)$$

Apparently the equilibrium point of the control system is $\left(\boldsymbol{E}(k+p),\ \delta\boldsymbol{E}(k+p)\right)=\left(\boldsymbol{0},\ \boldsymbol{0}\right)$; this implies that the output of the controlled system will accurately track the desired output and remain on the desired trajectories. Hence, the stability of the Elman-neural-network-based predictive PID control system is guaranteed.

4. Computer simulations

The examples of this section show the effectiveness of the predictive PID controller and the stability analysis of the control system. Simulations are performed on a personal computer using MATLAB program codes.

Example 1： Consider the control of a nonlinear dynamical system given by Sales and Billings [26]. The system model is described as follows:

$$y(k)=0.9722y(k-1)+0.3578u(k-1)-0.1295u(k-2)$$
$$-0.3103y(k-1)u(k-1)-0.04228y^2(k-2)$$
$$+0.1663y(k-2)u(k-2)-0.03259y^2(k-1)y(k-2)$$
$$-0.3513y^2(k-1)u(k-2)+0.3084y(k-1)y(k-2)u(k-2)$$
$$+0.1087y(k-2)u(k-1)u(k-2)+v(k)\,. \qquad (39)$$

The objective is to make the system output $y(k)$ tracks a reference input using the predictive PID controller, and the reference input $r(k)$ and the external disturbances $v(k)$ specified by

$$r(k)=\begin{cases}1, & 0<k\le 200\\ 0, & 200<k\le 400\end{cases}$$

$$v(k)=\begin{cases}0, & 0<k\le 100\\ 0.05, & 200<k\le 600\\ 0.2, & 600<k\le 800\end{cases}$$

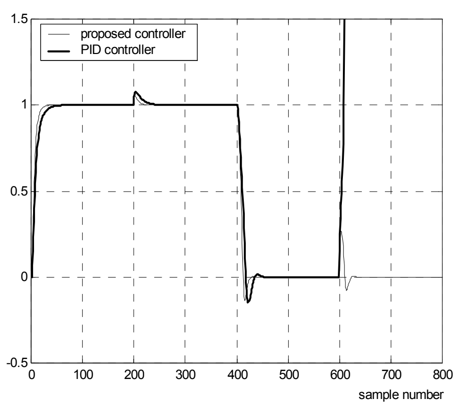

Figure 2 Output responses.

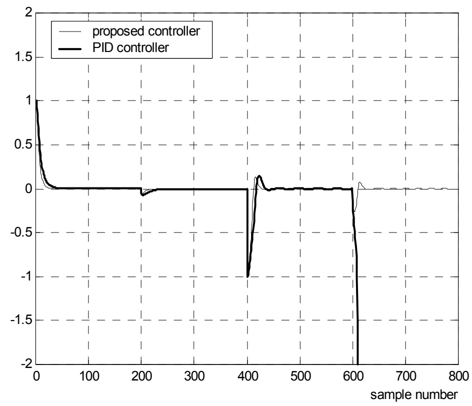

Figure 3. Control signals.

The prediction output horizon of the proposed controller is selected as $N_p=3$ and the hidden node of the ENN identifier is chosen as $n_j=3$. It is desirable to compare a proposed controller and a conventional velocity-type PID controller ($K_P=1.5$, $K_I=0.2$ and $K_D=0.01$).

Figures 2 and 3 show the output responses and the control signals of the proposed predictive PID controller and the conventional PID controller under setpoint changes and constant load disturbances, respectively. For the duration $200\le k<600$, the resultant maximum overshoots of the proposed controller and conventional PID controller were 11.3% and 13.9% , respectively. The results show that the proposed controller has good response in the disturbance $v(k)=0.2$ than the conventional PID controller.

In the presence of disturbance

$v(k) = 0.2$ for the duration $k \geq 600$, Figure 2 discloses that the conventional PID controller has an unstable tracking performance, which represents that conventional PID controller using the fixed parameters K_P, K_I and K_D is not capable of controlling nonlinear system under disturbance changes. As can be seen, the output performance of the proposed predictive PID controller is significantly better than this that can be obtained with the conventional PID controller.

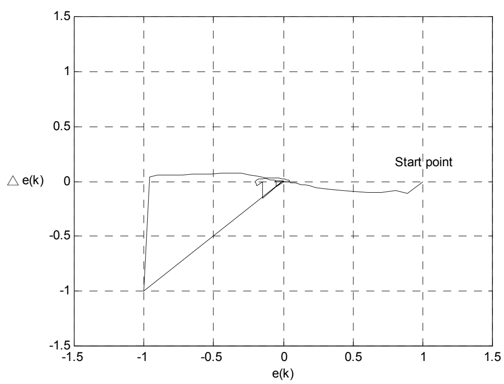

Figure 4. System response in the phase plane.

Figure 4 demonstrates the satisfactory phase plane, the system response indicates that the proposed predictive PID controller has zero steady-state tracking error and the resulting closed-loop system is stable.

Example 2: Consider the control of a discrete-time nonlinear dynamical system given by He and Jagannathan [27]. The system model is described as follows:

$$y(k) = \frac{5}{8}\left(\frac{y(k-1)}{1+y^2(k-1)}\right) + 0.3y(k-1) + u(k-1) + v(k)\ . \qquad (40)$$

The objective is to make the system output tracks a reference input using the proposed controller. The reference input and the disturbance specified by

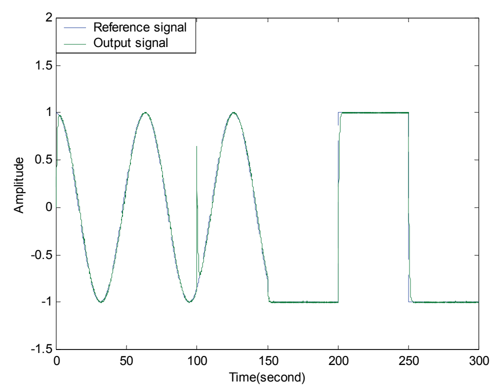

Figure 5. Output performance of the predictive PID controller.

$$r(k) = \begin{cases} \sin(\omega kT + \pi/2), \omega = 0.1, & 0 < k \leq 3000 \\ -1, & 3000 < k \leq 4000 \\ 1, & 4000 < k \leq 5000 \\ -1, & 5000 < k \leq 6000 \end{cases}$$

$$v(k) = \begin{cases} 0, & 0 < k \leq 2000 \\ 1.5, & 2000 < k \leq 6000. \end{cases}$$

where the sampling interval T is taken as 50 ms, and the white Gaussian noise with a standard deviation of 0.005 is added to the nonlinear system.

Figure 5 shows the reference signal and output response of the proposed controller under setpoint changes. The result indicates that the proposed control system has a good tracking performance. These results also reveal the usefulness of the predictive PID controller for this class of nonlinear systems.

5. Conclusions and Future Work

5.1. Conclusions

This paper has proposed a systematic design methodology to develop the predictive PID controller based on Elman neural networks for control of the nonlinear systems. The ENN identifier with the hierarchical BP algorithm has been used for the mathematical model of the nonlinear system and the proposed PID controller with the predictive performance criterion has been designed for control of the nonlinear systems. The stability analysis of the closed-loop control system is presented by the discrete Lyapunov stability theorem. The real-time control algorithm, including the adaptive learning rate and adaptive optimal rate for the ENN identifier and the predictive PID controller respectively, has been successfully applied to the illustrative nonlinear discrete-time systems.

5.2. Future work

This future work might be concerned with two directions. One is proposed controller for developing the nonlinear industrial systems. The other is to work toward the use of multi-input multi-output industrial systems to perform the tracking function the closed-loop systems so that the desired system specifications can be achieved.

References

[1] Clarke, D. W., & Mohtadi, C. (1989). Properties of generalized predictive control. Automatica, 25(6), 859-857.

[2] Camacho, E. F., & Bordons, C. (1999). Model Predictive Control. Springer-Verlag.

[3] Rawlings, J. B. (2000). Tutorial overview of model predictive control. IEEE Control Systems Magazine, 20(4), 38-52.

[4] Maciejowski, J. M. (2002). Predictive Control with Constraints. Prentice Hall.

[5] Allgöwer, F., & Zheng, A. (2000). Nonlinear Model Predictive Control. Birkhäuser Verlag.

[6] Kouvaritakis, B., & Cannon, M. (2001) Nonlinear Predictive Control – Theory and Practice. London: IEE.

[7] Huang, S., Tan, K. K., & Lee, T. H. (2002). Applied Predictive Control. Springer-Verlag.

[8] Granado, E., Colmenares, W.,

Bernussou, J., & García, G. (2003). Linear matrix inequality based model predictive controller. IEE Proc. Control Theory Appl, 150, 528-533..

[9] Lu, C. H., & Tsai, C. C. (2007). Generalized predictive control using recurrent fuzzy neural networks for industrial processes. Journal of Process Control, 17, 83-92.

[10] Narendra, K. S., & Parthasarathy, K. (1990). Identification and control of dynamical systems using neural networks. IEEE Transactions on Neural Networks, 1, 4-27.

[11] Adetona, O., Garcia, E., & Keel, L. H. (2000). A new method for the control of discrete nonlinear systems using neural networks. IEEE Transactions on Neural Networks, 11(1), 102-109.

[12] Ge, S. S., Zhang, J., & Lee, T. H. (2004). Adaptive neural network control for a class of MIMO nonlinear systems with disturbances in discrete-time. IEEE Transactions on Systems, Man, Cybernetics B, 34, 1630-1645.

[13] He, P., & Jagannathan, S. (2007). Reinforcement learning neural-network-based controller for nonlinear discrete-time systems with input constraints. IEEE Transactions on Systems, Man, Cybernetics B, 37(2), 425-436.

[14] Wai, R. J., & Lin F. J. (2001). Adaptive recurrent-neural-network control for linear induction motor. IEEE Transactions of Aerospace.

[15] Potocink, P., & Grabec, I. (2002). Nonlinear model predictive control of a cutting process. Neurocomputing, 43, 107-126.

[16] Yoo, S.J., Choi, Y. H., & Park, J. B. (2006). Generalized predictive control based on self-recurrent wavelet neural network for stable path tracking of mobile robots: adaptive learning rates approach. IEEE Transactions on Circuits and Systems I, 53(6), 1381-1394.

[17] Lu, C. H., & Tsai, C. C. (2008). Adaptive predictive control with recurrent neural network for industrial processes: an application to temperature control of a variable-frequency oil-cooling machine. IEEE Transactions on Industrial Electronics, 55(3), 1-10.

[18] Kremer, S. C. (1995). On the computational power of Elman-style recurrent networks. IEEE Transactions on Neural Networks, 6, 1000-1004.

[19] Lin, F. J., Hung, Y. C., & Chen, S. Y.

(2009). FPGA-based computed force control system using Elman neural network for linear ultrasonic motor. IEEE Transactions on Industrial Electronics, 56, 1238-1253.

[20] Ziegler, J. G., & Nichols, N. B. (1942). Optimum settings for automatic controller. Transactions on ASME, 62, 759-768.

[21] Lee, C. C., Lee, Y. H., & Teng, C. C. (2002). A novel robust PID controller design by fuzzy neural network. Asian Journal of Control, 4(4), 433-438.

[22] Kwiatkowski, A., Werner, H., Blath, J. P., Ali, A., & Schultalbers, M. (2009). Linear parameter varying PID controller design for charge control of a spark-ignited engine. Control Engineering Practice.

[23] Zheng, J. M., Zhao, S. D., & Wei, S.G. (2009). Application of self-tuning fuzzy PID controller for a SRM direct drive volume control hydraulic press 2009. Control Engineering Practice.

[24] Woo, T. K. Fast hierarchical least mean square algorithm. (2001). IEEE Signal Processing Letters, 8(11), 289-2914.

[25] Yang, S. S., Ho. C. L., & Lee, C. M. (2006). HBP: improvement in BP algorithm for an adaptive MLP decision feedback equalizer. IEEE Transactions on Circuits and Systems II. 53(3), 240-244.

[26] Sales, K. R., & Billings, S. A. (1999). Self-tuning control of nonlinear ARMAX model. International Journal of Control, 51, 753-769.

[27] He P. & Jagannathan S. (2007). Reinforcement learning neural-network-based controller for nonlinear discrete-time systems with input constraints. IEEE Transactions on Systems, Man, Cybernetics B. 37(2), 425-436, 2007.

壓克力磁力研磨加工特性之研究

蔡東憲、張浮明、江昇翰

摘 要

本文以切削加工後壓克力，利用磁場能量配合磨料進行研磨加工與去毛邊加工，並以不同主軸轉速、進給速率、磁力磨料尺寸、刀具與材料間隙等加工參數，研究加工前後壓克力表面透光性與表面粗糙度之特性，搭配不同材質磨料與工件配合磁場強度與轉速的相對關係，觀察磨料顆粒加工使用量的磁場變化和磨料移動關係，以獲得磨料加工製程效益與消耗程度，探討其磁場變化與磨料移動關係。本研究使用之磨料為可被磁鐵吸附的非導磁性 304 不鏽鋼，經設計不同狀態與條件之實驗過程，比較改善壓克力表面透光性與減少磨料損耗之要求，實驗結果顯示前者之重要性大於後者。以不同參數切削與研磨後，實驗顯示可獲得壓克力最佳表面粗糙度分別為 Ra 值 0.12 μm與 0.16 μm。

關鍵詞：綜合加工機、磁力研磨、壓克力、透光性。

蔡東憲：修平科技大學機械工程系副教授
張浮明：修平科技大學機械工程系副教授
江昇翰：修平科技大學精密機械與製造科技研究所研究生
投稿日期：100 年 5 月 19 日　接受刊登日期：100 年 7 月 1 日

The characteristics investigation of acrylic with magnetic abrasive finishing

Tung-Hsien Tsai, Fu-Ming Chang, Sheng-Han Chiang

Abstract

This article investigates on how to adopt magnetic field energy and abrasive to grinding and to burr an acrylic. Surface characteristics and roughness of acrylic material are investigated in different machining conditions such as spindle speed, feed rate, nano-magnetic abrasive size and the gap between tool and materials, respectively. The benefits of grinding process and consumption of abrasive are obtained by observing the relationship between the fluctuations of magnetic field with different abrasive amount and abrasive movement in various abrasives, magnetic intensity, and speeds. We use non-magnetic 304 stainless steel abrasive to reduce the abrasive wear through the design of different machining conditions and compare the improvement of the penetrability of the acrylic surface. The experiment results show that the maximum roughness was Ra $0.12\mu m$ and $0.16\mu m$ respectively for different machining and grinding parameters.

Keywords: Machine Center, Magnetic Abrasive Finishing, Acrylic、Transmittance.

Tung-Hsien Tsai, Associate Professor, Department of Mechanical Engineering, HUST.
Fu-Ming Chang, Associate Professor, Department of Mechanical Engineering, HUST.
Sheng-Han Chiang, Graduate Student, Graduate Institute of Precision Machinery and Manufacturing Technology, HUST.
Received 5 May 2011; accepted 1 July 2011

1. 前言

隨著人們生活形態改變,無論電子、光電、鏡頭、機械產品等加工成品，品質要求除具備充分的功能外，對於產品內、外觀的精度要求，使工件得到良好的表面等因素，日益殷切，因此常利用拋光等加工方式改善表面特性，而磁力研磨亦為近代發展不可缺的方法之一。磁力研磨因研磨機構設計、加工材料與磨料是否具有磁性之因素而有不同的研磨加工方式，基本上係利用磁場能量所形成之磁力線與具磁性磨料結合，將工件置於磁場中，與磨料形成具有撓性的磁性刷，進行研磨加工。視磨料的大小對於夾縫溝槽、管之內孔等不規則形狀，幾乎不受工件幾何外形影響，因加工應力小，表面不產生變質層，因此具有除去工件毛邊、拋光洗淨、不變形等優點，適合大量精密零件研磨,提高工件精度，較傳統研磨為優，使精密研磨的製程發展日益進步。

磁力研磨觀念最先由俄國學者提出[1]，發展至今已有許多效果，研究者與學者等更分別設計不同形式配合工件材料，分別利用磁場與振動再加鑽石磨料研磨工件，取不同影響加工表面參數，研究精密研磨得到鏡面加工表面，除磨料使用後容易處理並降低環境污染等優點，更可協助精密加工製程的改善與研究[2,3]。配合多種刀具應用CNC綜合加工機與複合式加工技術，工業界已開發成功使用，但配合銑床後直接研磨加工尚無運用，本研究將多種傳統磨床和非傳統研磨拋光技術，綜合設計使用在CNC銑床加工機上。Wang[4] 等以車床夾持管內孔旋轉,配合奈米電解腐蝕液，進行磁力研磨加工，研究經歷不同腐蝕時間之變化，達到表面拋光效果。Yan Wang[5]等以超音波配合磁力進行管內孔之研磨加工特性研究。林清田[6]等以釹鐵硼磁性圓柱刀具，吸附磨料與空心圓柱附凹槽溝刀具，研究不同形狀刀具且含拋光液研磨下，銑床加工鋁合金材料，尋找最佳參數。Jain [7]等研究工件間隙與研磨速度以改進研磨特性。曾柏昌[8]等使用真空燒結法製成研磨料，將磁性鐵與不帶磁性氧化鋁粉燒結成顆粒狀，粉末混和比例與黏著劑量和燒結溫度時間上變化，尋找最佳製程設計。El-Taweel[9]模式化分析6061鋁合金複合材料混合電化學旋轉磁力研磨特性之研究。Yamaguchi[10]等以陶瓷加鋁合金，進行內孔磁力研磨，研究加工特性。張浮明[11]等進行磁力研磨加工鋁合金6061-T6之特性研究，進行不同高度梯形狀之磁力與加工條件研磨拋光，以不同主軸轉數、進給速率、磁力磨料、刀具

與材料間隙、進給深度之因素為參數，比較加工前與加工後之表面粗糙度量測。使用反應曲面法（RSM）建立預測加工參數之數學模式與變異數分析，比較加工後之量測與預測結果，獲得各項加工參數的最佳化設定，可接近實驗值之95%的可信度。由實驗結果可知，各不同高度之表面粗糙度值皆有改善，其中以3mm之加工參數實際值最接近預測結果，其加工前Ra值為0.45 μm，磁力研磨拋光後可得到Ra值為0.09 μm。Yamaguchi[12]等使用被磁化之鋁合金配合陶磁材料之磨料，通過磁場與加工機構設計，研究不同參數進行孔內加工後，具有改善表面特性與增加材料移除的效果。

壓克力又稱為不碎玻璃，臺灣於1959年開始生產。壓克力(Acrylic)為一種樹脂透光度比玻璃為佳的高分子材料(甲基丙烯酸酯樹脂)。以塑膠製成壓克力玻璃具有高度透明度，耐候性強，常用在廣告招牌、照明器具及日常用品上，現代開發用於光電材料如手機、數位像機與3C產品等。惟材質硬脆，薄板型加工，尤不易達到良好的表面加工效果，若需要更精細的鏡面處理，只能以手工拋光費力耗時缺乏經濟效益。本研究即針對壓克力之特性，使用具磁場迴路吸附不鏽鋼材料之刀具，進行切削後磁力研磨，應用量測儀器探討其表面狀態，與磨料之損耗，比較不同加工參數之變化。

本文以壓克力為實驗材料，採用不同尺寸之磁粉，不同轉速、不同間隙與不同進給速率為實驗影響參數，研究表面粗糙度與磨料損耗率之探討。

2. 加工原理與磁力分佈

2.1 加工原理

使用永久磁鐵具磁力強度之磁極與端面設計吸附磨粒之刀具，吸附磨粒之刀具與工件表面，必須保持適當之加工間隙，形成含磁力之平面研磨加工，本設計磁極之刀具內為1000高斯之永久磁鐵，配合磁場強度吸附易磁化性質之奈米級磨料顆粒，使得具已磁化之磨粒，在磁場作用下沿磁力切線方向，構成一個封閉的磁場迴路與相互連結，形成具有可配合不同工件表面狀態研磨的撓性磁刷。磁力線產生的力量，使磨粒加壓至工件表面，以磁刷形式作為研磨的工具，當配合適當轉速時，磨粒尖端與工件表面形成相互運動之摩擦作用，工件在載物檯上之平面移動，進而達到研磨之拋光以及去毛邊等功能，磁場中磁力束刷，吸附磨料情況之示意圖與磁棒實際圖，如圖一與圖二所示。

2.2 磁力分佈

磁力研磨裝置設計必須考慮磁力線之分部，以正向力與磨擦係數之乘積為最大磨削力[13]，平面磁力研磨加工，當磨粒受磁場作用，具有磁位線之與磁力線之兩分力，其中磁力線為單位磁分子在磁場中受磁力運動之軌跡，為封閉曲線，由N極至S極，表示磁場的方向與大小，而本設計磁鐵內之磁力線為由S極往N極，磁鐵外由N極歸向S極，磁力線不相交且具互相排斥，線上任一點之切線方向，即為該點的磁場方向，磁力線愈密，磁場強度愈大，磁力線具有尋求最低磁阻的路徑。而視磁場強度相互吸附已磁化之磨粒與堆砌,達到一穩定重量。實驗數據顯式，磨粒吸附量，隨心軸轉速增加，因離心力增加，使得磨粒甩出而減少，因此當加工時心軸轉動超過1200 rpm時，才具有穩定之加工作用。本實驗採用磁場之磁力線由N極在下S極在上的永久磁鐵，刀具尺寸為16 mm圓棒，包覆1000高斯永久磁鐵，使得磁性磨料吸附在刀具棒頂端面同時加壓在工件表面，得以研磨加工表面之拋光，磨料相互吸引、堆疊等方式，形成撓性磁刷，利用磨粒在刀具與工件間隙之壓力進行加工。在研磨拋光過程當中，由於在加工區域內的磁場強度比加工區域外強，因此形成不均勻之集中磁場，加工區域外部的每一磁性磨粒，受到磁場的作用產生兩個分力法線方向(Fx)與切線方向(Fy)，兩者之合力(F)，其中Fx是在磁力線方向的分力，Fy是等磁位線方向的分力，其中法線方向垂直加壓磨粒於工件表面，使磁粒集中加工的方向與位置，如圖三所示。本實驗之磁性磨具設計，受磁場作用以切線方向之力達到磨擦加工作用，其合力F使磁性磨粒朝向加工區域集中，集中磁性磨粒在加工位置，並防止磁性磨粒，隨著因進給與轉速關係碰觸工件而殘留或飛散。磁力F之法線方向(Fx)與切線方向(Fy)其大小，受到磁場強度、磁極形狀、磁極尺寸影響極大。公式分別表示如下

$$Fx = \mu_0 V_0 X_m H (\partial H/ \partial x) \tag{1}$$

$$Fy = \mu_0 V_0 X_m H (\partial H/ \partial y) \tag{2}$$

其中μ_0為真空的導磁率，V_0為磁性磨粒之體積，X_m為磁性磨粒之磁化率，H為磁場強度,$(\partial H/ \partial x)$，$(\partial H/ \partial y)$分別表示在X、Y方向磁場強度的變化率。

磁性磨粒受到磁場的作用而吸附在刀具上，加工區域內，使得磁性磨粒之間，形成撓性排列之磁刷而產生壓力，作用於工件表面,此研磨壓力(Pz)為磨料對工件表面拋光的主要力量，其公式表示如下[14]

$$Pz = \left[\mu_0 H_0 \left(1 - \frac{1}{\mu_m}\right)\right] / 2 \quad (3)$$

其中μ_m為磁性磨粒子群的相對導磁率，H_0為真空之磁場強度。

3. 實驗規劃

3.1 機械設備

本加工實驗使用眾程科技之CNC綜合加工機EMV-600如圖四，其加工方式為開放式虎鉗夾持工件，虎鉗採用低膨脹係數及高硬度之防鏽鋼材料設計，切削液於磨削時噴向刀尖與虎鉗夾持工件區域，減低加工產生之熱應力，適用不同模具材料或表面切削加工，X-Y軸行程610 × 460 mm，Z軸行程480 mm，X-Y、U-V軸均採用AC伺服馬達驅動，本實驗採用Z軸為自動定位。機身的進給精度控制在0.001 mm之範圍內，主軸轉速Max. 15000 rpm，切削進給速度Max. 10000 mm/s，刀具直經Max. 65 mm，其加工條件，如表一所示。

3.2 磁力研磨

磁力研磨裝置設計必須考慮磁力線之分部，以正向力與磨擦係數之乘積為最大磨削力，本實驗研磨刀具磁力線之設計，以不銹鋼棒設計內含八個永久磁鐵串聯排列，磁通密度為1000高斯(Gauss)，N極朝下，S極朝上，建立磁場環繞並吸附含磁性的研磨料，其磨料吸附在磁棒N極形成磁力刷，使磨料包覆磁棒，磨料吸附於磁棒之磁場示意圖如圖二。研磨料規格尺寸，如圖五所示，吸附於磁棒上之磨料，為豪昱電子有限公司自行研發製造之磁性磨料，以三種不同規格尺寸 (a)氧化鐵奈米磨粒(125 μm)，(b)不鏽鋼奈米磨粒(200 μm)，(c) 200 μm不鏽鋼奈米磨粒加樹脂成分。本實驗以銑床主軸轉速、刀具與工件的間隙、刀具進給速率、刀具吸附磨粒、研磨時間等為加工參數。主軸轉速為800~1200 rpm範圍內做調整，刀具與工件間隙為固定0.5 mm作為基礎，刀具進給速率為200 mm/s。研磨時間600~1500秒做為調整觀察。磁性磨料在磁力研磨拋光中，所扮演的角色相當於加工機中之刀具，視為磁力研磨拋光極為重要的加工要素。磁性研磨材料必須具磁化性良好且易備被磁化性質，具有研磨能力的複合磨料，傳統使用的研磨材質，如氧化鋁、碳化矽、氮化硼、碳化硼與鑽石粉末等。由於奈米級磁性磨料，所需之製造設備昂貴，製造過程亦需要特殊的專業技術，導致目前國外進口磁性磨料價格居高不下。曾柏昌[8]等為探討燒結後磁性磨料之結合度的狀況，應用不銹鋼SUS304之表面粗糙度及材料移除率，採用真空燒結技術並配合田口實驗

法進行燒結實驗規劃，製造結合鐵與氧化鋁之磁性磨料，以獲得鐵粉粒度、氧化鋁粉粒度、成份比例、壓製成形壓力、黏結劑、燒結溫度、加熱時間等七個不同因子之最佳參數組合，並以SEM搭配EDS分析燒結後之磁性磨料。經過實際的拋光與實驗結果驗證，其研發的磁性磨料，已能將不銹鋼SUS304之表面拋光至鏡面程度（Ra 0.018 μm），足以媲美進口之磁性磨料，初步已展現出良好的研究成果。

本研究之主要目的，係利用三種不同規格奈米級之尺寸，進行加工，首先以125 μm之氧化鐵奈米磨粒，其次以200 μm之不鏽鋼奈米磨粒，再以200 μm不鏽鋼奈米磨粒加樹脂成分。進行研發304不鏽鋼，更優質、更耐磨且低成本的磁性磨料，及最佳配方參數之獲得。並將研發成功的磁性磨料廣泛的應用於內外徑、不規則平面、彎曲管與螺旋管等的內部等零件之研磨，期望將可為國內磁力研磨技術帶入另一個嶄新的境界。

3.3 實驗材料

壓克力之化學成分，如表二所示，其設計高度為平面凹槽為1 mm。使用磁棒進行磁力研磨不同平面600~1500秒進行實驗，壓克力材料實際加工平面如圖五。以壓克力為實驗材料，其化學成分，如表二所示，設計高度為凹槽狀 -1 mm深度之工件，使用磁棒進行磁力研磨以工件平面0 mm作為基準面加工平面與凹槽處，依照不同參數條件設定實驗，循溝槽邊環繞約單次加工60秒為研磨加工，如圖四。

研磨加工，以CNC綜合加工機之特性與作用為基準，分別研究表面粗糙度(Ra)與磨料損失率(MALR)等二項參數。首先使用MITUTOYO Surface Roughness Tester SJ-201儀器，磨削工件平面6 mm內每間隔2 mm之距離量測一次，取三次表面粗糙度之平均值為量測數據。量測磨粒的長、寬、高度與使用前之單位體積重量，比較加工前與加工後的體積損耗差異，為測定體積的重量損失消耗比。

4. 結果與討論

4.1 磨粒損失

本研究係延續磁力研磨加工鋁合金6061-T6之特性研究的後續實驗，以反應曲面法，決定品質因子之水準，經由品質設計程序、步驟、方法等，盡可能滿足產品的特性需求。結合數學和統計技巧的利用，對於影響製程不同的參數，對於問題的分析與建模，得到有意義的影響反應，進而求得最佳化的條件。獲得最佳二階模式預測磨料重量損耗率之模式，尋找磨粒最佳使用數量值，以實

現高品質低成本的研磨產品。從四個設計參數的調整變化得到使用磨粒數量，在主軸轉速1200 rpm、進給速率200 mm/s、刀具與工件間隙0.5 mm、研磨時間30分鐘參數為最高設定下，得到加工前磨粒20 g使用加工後損失剩餘10.1734 g，其獲得最佳加工性能。

若再調整提高加工參數，會發生磨粒飛散或甩出的情況，無法增加更高效益，由實驗得知，1000高斯之磁場強度，無法負荷主軸轉速超過1200 rpm以上，此時若以增加進給速率、降低間隙等，研磨時接觸工件與磁粒過度密集，會形成磁粒遲滯現象，影響磁場強度分布，隨著研磨時間的增加，效果不佳且會增高溫度，產生反效果，甚至在壓克力表面，有燒結碳化的情況，造成表面黑斑、刮痕等負面效果。

4.2 表面粗糙度

表面粗糙度是加工表面的狀況，目標值越小越佳，本研究係採用磁力研磨加工鋁合金6061-T6之特性研究的後續實驗，以反應曲面法，經由品質設計程序、步驟、方法等，決定品質因子之水準，結合數學和統計技巧的利用，對於影響製程不同的參數，盡可能滿足產品的特性需求，進行問題的分析與建模，得到有意義且得最佳化的條件，建立最佳二階模式預測表面粗糙度之模式，獲得最佳的表面粗糙度。

為提高加工效率與品質需求，使用四個實驗參數，調整得最佳參數值，於氧化鐵奈米磨粒125 μm尺寸，在主軸800 rpm、間隙0.5 mm、進給速率100 mm/s、加工時間20分鐘，得表面粗糙值最為平均效果良好，如表三所示。

當奈米磨粒尺寸為200 μm之不銹鋼材料時，在取主軸轉速1200 rpm、間隙0.5 mm、進給速率100 mm/s、加工時間20分鐘，以多點量測表面粗糙值經計算平均值，得到效果最為良好，如表四所示。綜合以上分析，得到最佳參數設計，磨粒尺寸大小的改善與不同主軸轉速，足以顯示具有提升加工品質的特性，效果顯著。對於200 μm不鏽鋼奈米磨粒加上樹脂成分，以相同主軸轉速加工後，量測表面粗糙度與觀察表面狀態，實驗結果發現，會增加表面透光性但表面粗糙度值變化不顯著。

5. 結論

本文使用CNC綜合加工機切削加工壓克力，係延續磁力研磨加工鋁合金6061-T6之特性研究之後續研究，鋁合金6061-T6，進行不同高度梯形狀之磁力研磨拋光，研究影響磁力研磨加工條件，以不同主軸轉數、進給速率、磁力磨料、刀具與材料間隙、進給深度之因素為參

數，比較加工前與加工後之表面粗糙度量測。使用反應曲面法（RSM）建立預測加工參數之數學模式與變異數分析，比較加工後之量測與預測結果，獲得各項加工參數的最佳化設定，可接近實驗值之95%的可信度。由實驗結果可知，在磨料顆粒0.08 mm、主軸轉速1000 rpm、間隙0.5 mm與進給速率100 mm/s，對磨料消耗的影響是最少的，磨料損耗率為0.0161 g。1~5 mm不同高度之表面粗糙度值皆有改善，皆從0.45 µm研磨過後改善至0.09 ~ 0.39 µm，其中以3 mm之加工參數磨料顆粒粗細0.08 mm、主軸轉速1000 rpm、間隙0.5 mm與進給速率100 mm/s，對表面粗糙度的改善影響最多，其Ra值最精細，實際值最接近預測結果，獲得加工性能表面粗糙度為Ra值 0.09 µm。

主軸轉速屆於800-1200 rpm之間，頻率為13-20 Hz間與夾持載台之自然頻率，皆屬低頻，因磁力研磨時磨料之運動，屬撓性行為，加工時配合工件曲面自動調整間隙，降低自然頻率之影響，進而不影響研磨精度。由以上實驗所獲得數據，觀察到在低轉速800 rpm以下表面粗糙度效果不佳，而高轉速1200 rpm以上磨料損失率因離心力飛甩出導致消耗磨料過多而無法得到好的粗糙度，而關於震動頻率由於本文所使用刀具吸附磨料顆粒，刀具本身沒有直接碰觸在這轉速範圍內工件，磨料更以吸附刀具端撓性運動，故頻率之影響於本文不列入考量。壓克力磁力研磨標準件規範目前沒有相關文獻於本文磨料類似規範，本文使用豪昱電子有限公司研發的奈米磨料，更加強實驗的可靠度，對於適當的主軸轉速、進給速率、磁力磨料、刀具與材料間隙、進給深度之因素的控制更有心得，提供未來業界使用印證考量之參考，可節省不必要的材料與時間的浪費。由於本文比較表面粗糙度與減少磨料損失率之研究，實驗結果表面粗糙度有改善降低但未達到工件透光性之要求，後續將竭盡所能加以改善，於本文暫無透光性量測數據，僅以觀察改善程度至透過壓克力可清晰或模糊看出工件下方之文字供參考。

本研究經由實驗及分析，獲得以下結論：(1)永久磁鐵刀具為平面設計，可增加磁場強度，形成類似多束刷式之研磨磁刷，增加磨粒對壓克力表面，有最佳的接觸面積與磨削力，提高研磨效率，改善表面粗糙度與降低磨粒損耗的成本。(2)實驗顯示，研磨前使用重量20 g的磨粒，磁場強度對磨料吸附率最佳，不會太多或太少，也就是不會不足或過量。實驗結果，取主軸轉速1200 rpm，進給速率200 mm/s，間隙0.5 mm，加工時間

20分鐘，為最佳的加工效率。(3)對表面粗糙度而言，於氧化鐵奈米磨粒125 μm尺寸，在主軸800 rpm、間隙0.5 mm、進給速率100 mm/s、加工時間20分鐘，得表面粗糙值0.12 μm，獲得最佳的表面粗糙度。對於尺寸200 μm不銹鋼奈米磨粒，在主軸轉速1200 rpm、間隙0.5 mm、進給速率100 mm/s、加工時間20分鐘，得表面粗糙值0.16 μm最為良好。對於200 μm不鏽鋼奈米磨粒加上樹脂成分，與未加樹脂成分，以相同條件加工後，觀察表面狀態與量測表面粗糙度，表面透光性增加，但表面粗糙度值變化不顯著。

誌　謝

本論文感謝豪昱電子有限公司，廖董事長提供實驗設備、磨粒材料與技術指導。

參考文獻

1. H-J. Ruben, in: A. NiKu-Lari, Advances in surface treatments, vol. 5, Pergamon Press, (1987) , pp. 239-256.
2. Dhirendra K. Singh1, V.K. Jain, V. Raghuram, Parametric study of magnetic abrasive finishing process. Journal of Materials Processing Technology, 149 (2004), pp 22–29.
3. T. Mori, K. Hirota, Y. Kawashima, Clarification of magnetic abrasive finishing mechanism. Journal of Materials Processing Technology, 143-144(2003), pp682-686.
4. A. C. Wang, S. J. Lee, Study the characteristics of magnetic finishing with gel abrasive. International Journal of Machine Tools and Manufacture, 49 (2009), pp1063-1069.
5. Yan Wang, Dejin Hu, Study on the inner surface finishing of tubing by magnetic abrasive finishing. International Journal of Machine Tools and Manufacture, 45 (2005), pp43-49.
6. 林清田，卓漢明，楊烈岱，曾柏昌，“AISI 304磁力研磨加工特性之研究”，磨粒加工學會年會暨加工技術研討會，(2009)。
7. V.K. Jain, P. Kumar, P.K. Behra, S.C. Jayswal, Effects of working gap and circumferential speed on the performance of magnetic abrasive finishing process, Wear 250 (2001), pp 384–390.
8. 曾柏昌，鄭振瑤，“鏡面拋光用磁性磨料製程研究”，磨粒加工學會年會暨加工技術研討會，(2009)。
9. T. A. El-Taweel, Modelling and analysis of hybrid electrochemical turning-magnetic abrasive finishing of 6061 Al/Al_2O_3 composite, The

International Journal of Advanced Manufacturing Technology, Volume 37(2008), pp705-714.
10. Hitomi Yamaguchi, Takeo Shinmura, Internal finishing process for alumina ceramic components by a magnetic field assisted finishing process, Precision Engineering 28 (2004), pp135–142.
11. 張浮明、蔡東憲、江昇翰，磁力研磨加工鋁合金6061-T6之特性研究，中國機械工程學會第二十七屆全國學術研討會論文集，DD07-006，台北市，(2010)。
12. 陳燕，巨東英，磁研磨裝置設計中的磁力線分析，Technology and Test, 2004,pp101-103.
13. H. Ysuwn, N.Ikawa, Y. Mori, K. Sugiyama, Numerically controlled elastic emission machining, Annals of the CIRP, vol.28 No.1, (1979), pp193-197.

附錄圖表

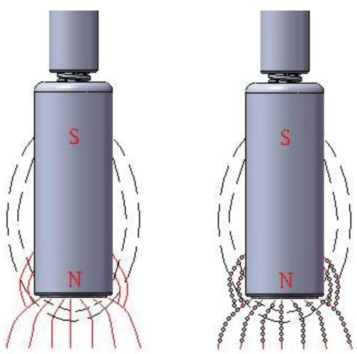

圖一、磁場中磁力束刷吸附磨料情況示意圖與磁棒實際圖

圖二、吸附於磁棒上之磨料圖

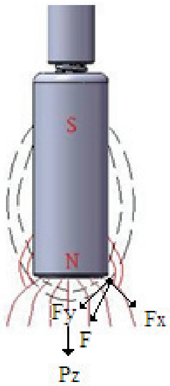

圖三、磁化線之分力分佈情形

圖四、CNC 銑床加工機(EMV-600)

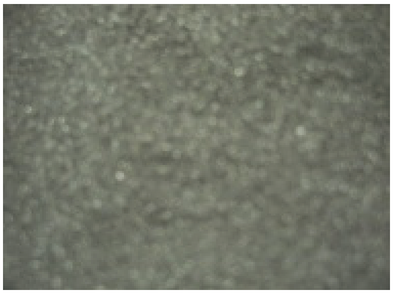
(a) 氧化鐵奈米磨粒(125μm),


(b) 不鏽鋼奈米磨粒(200μm),

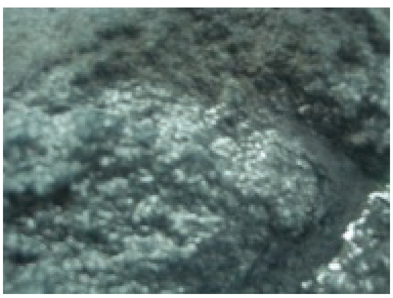
(c) 不鏽鋼奈米磨粒(200μm+樹脂)

圖五、吸附於磁棒上之磨料

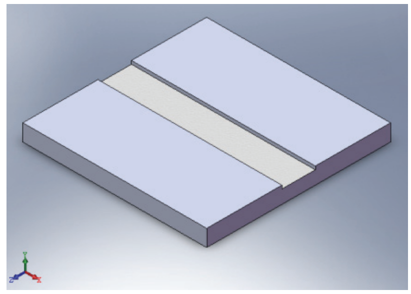
(a) 氧化鐵奈米磨粒(125μm)

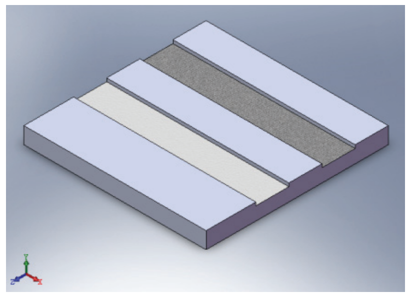
(b) 不鏽鋼奈米磨粒(200μm)

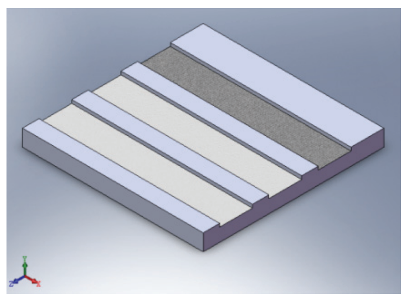
(c) 不鏽鋼奈米磨粒(200μm+樹脂)

圖六、工件加工示意圖

加工前:銑床加工銑削

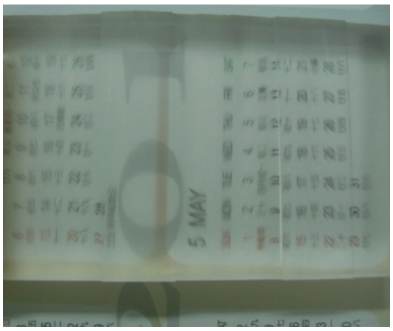

加工後:(a)氧化鐵奈米磨粒(125µm)

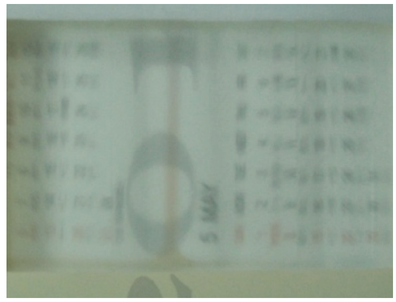

加工後: (b)不鏽鋼奈米磨粒(200µm)

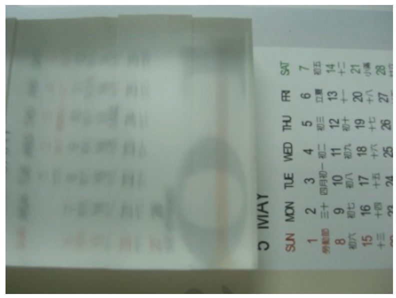

加工後: (c)不鏽鋼奈米磨粒(200µm+樹脂)

圖七、壓克力加工前與加工後比較圖

表一、加工條件與設備表

工作條件	單位	說明
磁力棒(刀具)		永久磁鐵
實驗材料		壓克力
工件尺寸	mm	120 x 120 x 10
氧化鐵奈米磨粒	µm	125µm磨料
不鏽鋼奈米磨粒	µm	200µm磨料
不鏽鋼奈米磨粒	µm	200µm磨料+樹脂
主軸轉速	rpm	800~1200
進給速率	mm/s	200
刀具與工件間隙	mm	0.5
研磨時間	sec	600~1500
切削液		樹脂

表二、壓克力工件化學成分表

過氧化二苯甲醯	甲基丙烯酸甲酯單體	壓克力
1	200	$(C_5O_2H_8)_n$

表三、氧化鐵奈米磨粒 125μm尺寸

工件號數	加 工 條 件		磁 力 研 磨			表面粗糙度 Ra(μm)		
	轉速 (rpm)	進給 (mm/s)	轉速(rpm)	進給(mm/s)	磨料			
初始條件	3000	200				0.95	0.90	0.89
1			800	800 (時間 10 分鐘)	125μm磨粒	0.55	0.52	0.47
2			800	100 (時間 5 分鐘)	125μm磨粒	0.19	0.13	0.12

表四、尺寸 200μm不銹鋼奈米磨粒

工件號數	加 工 條 件		磁 力 研 磨			表面粗糙度 Ra(μm)		
	轉速 (rpm)	進給 (mm/s)	轉速(rpm)	進給(mm/s)	磨料			
初始條件	3000	200				0.95	0.90	0.89
1			800	100	200μm磨粒	0.33	0.30	0.22
2			1200	100	200μm磨粒	0.26	0.17	0.16

表五、尺寸 200μm不銹鋼奈米磨粒加樹脂

工件號數	加 工 條 件		磁 力 研 磨			表面粗糙度 Ra(μm)		
	轉速 (rpm)	進給 (mm/s)	轉速(rpm)	進給(mm/s)	磨料含樹脂			
初始條件	3000	200				0.95	0.90	0.89
1			800	100	200μm磨粒	1.24	1.07	0.93
2			1200	100	200μm磨粒	1.11	1.21	1.98

修平科技大學《修平學報》徵稿要點

一、本刊為純學術性之刊物，專供本校同仁及校外人士發表研究成果及論著之用。

二、論述及研究報告文字（含圖表），以 20 頁為度，來稿須以 Word 格式排版，以電子郵件寄至圖書館校史組 (論文格式及版面規格，請至圖書館校史組網頁下載)。

三、無論中文或英文稿件皆須附上中英文題目、摘要，並註明作者姓名及系(所)職稱。他國文字稿件須附中文題目摘要，其字數以 500 字為度；並應列舉中、英文或他國文字之關鍵詞(keywords)。

四、文稿之審查依據「修平科技大學學報評審辦法」。

五、稿件格式按各專業學門標準格式或參考「修平學報論文格式」。

六、作者投稿後，若在作業程序中因故取消投稿者，則其後兩期不再接受其投稿。

七、所投稿件經編審委員審查同意刊登，稿件經刊印後，不得在他處刊印發表。如果已在其他刊物正式公開發表後，轉投本刊物，本委員會不負查核之責，相關著作權問題，由當事人自行負責。稿件若涉及一稿兩投或抄襲者，本學報得拒絕作者稿件五年。

八、經審查採用之文章，排版後送請作者校稿，作者僅能修正排版印刷之錯誤，且不得擅自於校稿過程中增減內容。

九、本刊每期以刊登二十篇論文為原則，經審查後決議可刊登者，如超過篇數，則按最後定稿時間先後排序，安排至下一期刊登。

十、本刊文之作者應對論文之內容及同意發表權之取得，負全部之責任。並請於投稿時即將「修平學報投稿授權聲明書」(附件)填妥後一併寄交。

十、本刊文之作者應對論文之內容及同意發表權之取得，負全部之責任。若著作人投稿於本刊經收錄後，同意授權本刊得再授權國家圖書館或其他資料庫業者，進行重製、透過網路提供服務、授權用戶下載、列印、瀏覽等行為。並請於接受刊登時即將「著作授權同意書」(附件)填妥後一併寄交。

十一、來稿經採用者，送當期學報光碟一份。

十二、本要點經學報編審委員會議通過，陳請校長核定後公布實施，修正時亦同。

修平科技大學學報評審辦法

第一條　來稿之評審係由學報編審委員會遴聘校外相關領域之專家學者擔任。

第二條　由執行編輯（校史組）收稿、登錄及分類後，交由學術副校長挑選二名校外專業人士或學者進行評審。

第三條　每篇稿件原則上由兩位評審，每位評審除於評審意見表上陳述意見外，並需對稿件作出下述三項之一建議：

一、接受刊登。
二、修正後再審。
三、不予刊登。

第四條　依據前述審查意見，處理方式如下表：

處理方式		第二位評審意見		
		接受刊登	修正後再審	不予刊登
第一位評審意見	接受刊登	刊登	寄回修改	＊第三位評審
	修正後再審	寄回修改	寄回修改	＊第三位評審
	不予刊登	＊第三位評審	＊第三位評審	退稿

＊1. 若第三位評審意見為「接受刊登」或「修正後再審」時，則請作者對不予接受之審查意見進行答覆外，將採兩正方評審意見予以刊登。

＊2. 若第三位評審意見為「不予刊登」時，將採兩負方評審意見予以退稿。

第五條　本刊將針對審查意見及結果函送投稿人，並說明處理方式。

第六條　評審作業相關人員，對評審委員身份應予以保密，以避免紛爭。

第七條　投稿人不得有打聽及干涉評審委員之言行。

第八條　本辦法經學報編審委員會議通過，陳請校長核定後公布實施，修正時亦同。

修　平　學　報

中華民國一〇〇年九月出版

發行人　鍾瑞國
出版者　修平科技大學圖書館校史組
地　址　41280 臺中市大里區工業路十一號
電　話　04-24961100
傳　真　04-24961187

編輯者　修平學報編審委員會
召 集 人—陳培中
編審委員—方世榮　江可達　林婉芳　張志凌
郭武彰　鄧作樑　盧志偉
（依姓氏筆劃排序）
執行編輯—郭武彰

印刷者　天空數位圖書有限公司
地　址　40255 台中市南區忠明南路 787 號 30 樓
電　話　04-22623893
傳　真　04-22623863

版權所有　請勿翻印

修平科技大學《修平學報》徵稿要點

一、本刊為純學術性之刊物，專供本校同仁及校外人士發表研究成果及論著之用。

二、論述及研究報告文字（含圖表），以 20 頁為度，來稿須以 Word 格式排版，以電子郵件寄至圖書館校史組 (論文格式及版面規格，請至圖書館校史組網頁下載)。

三、無論中文或英文稿件皆須附上中英文題目、摘要，並註明作者姓名及系(所)職稱。他國文字稿件須附中文題目摘要，其字數以 500 字為度；並應列舉中、英文或他國文字之關鍵詞(keywords)。

四、文稿之審查依據「修平科技大學學報評審辦法」。

五、稿件格式按各專業學門標準格式或參考「修平學報論文格式」。

六、作者投稿後，若在作業程序中因故取消投稿者，則其後兩期不再接受其投稿。

七、所投稿件經編審委員審查同意刊登，稿件經刊印後，不得在他處刊印發表。如果已在其他刊物正式公開發表後，轉投本刊物，本委員會不負查核之責，相關著作權問題，由當事人自行負責。稿件若涉及一稿兩投或抄襲者，本學報得拒絕作者稿件五年。

八、經審查採用之文章，排版後送請作者校稿，作者僅能修正排版印刷之錯誤，且不得擅自於校稿過程中增減內容。

九、本刊每期以刊登二十篇論文為原則，經審查後決議可刊登者，如超過篇數，則按最後定稿時間先後排序，安排至下一期刊登。

十、本刊文之作者應對論文之內容及同意發表權之取得，負全部之責任。並請於投稿時即將「修平學報投稿授權聲明書」(附件)填妥後一併寄交。

十、本刊文之作者應對論文之內容及同意發表權之取得，負全部之責任。若著作人投稿於本刊經收錄後，同意授權本刊得再授權國家圖書館或其他資料庫業者，進行重製、透過網路提供服務、授權用戶下載、列印、瀏覽等行為。並請於接受刊登時即將「著作授權同意書」(附件)填妥後一併寄交。

十一、來稿經採用者，送當期學報光碟一份。

十二、本要點經學報編審委員會議通過，陳請校長核定後公布實施，修正時亦同。

修平科技大學學報評審辦法

第一條　來稿之評審係由學報編審委員會遴聘校外相關領域之專家學者擔任。

第二條　由執行編輯（校史組）收稿、登錄及分類後，交由學術副校長挑選二名校外專業人士或學者進行評審。

第三條　每篇稿件原則上由兩位評審，每位評審除於評審意見表上陳述意見外，並需對稿件作出下述三項之一建議：

一、接受刊登。
二、修正後再審。
三、不予刊登。

第四條　依據前述審查意見，處理方式如下表：

<table>
<tr><td colspan="2" rowspan="2">處理方式</td><td colspan="3">第 二 位 評 審 意 見</td></tr>
<tr><td>接受刊登</td><td>修正後再審</td><td>不予刊登</td></tr>
<tr><td rowspan="3">第一位評審意見</td><td>接受刊登</td><td>刊登</td><td>寄回修改</td><td>＊第三位評審</td></tr>
<tr><td>修正後再審</td><td>寄回修改</td><td>寄回修改</td><td>＊第三位評審</td></tr>
<tr><td>不予刊登</td><td>＊第三位評審</td><td>＊第三位評審</td><td>退稿</td></tr>
</table>

＊1. 若第三位評審意見為「接受刊登」或「修正後再審」時，則請作者對不予接受之審查意見進行答覆外，將採兩正方評審意見予以刊登。

＊2. 若第三位評審意見為「不予刊登」時，將採兩負方評審意見予以退稿。

第五條　本刊將針對審查意見及結果函送投稿人，並說明處理方式。

第六條　評審作業相關人員，對評審委員身份應予以保密，以避免紛爭。

第七條　投稿人不得有打聽及干涉評審委員之言行。

第八條　本辦法經學報編審委員會議通過，陳請校長核定後公布實施，修正時亦同。

修　平　學　報

中華民國一〇〇年九月出版

發行人　鍾瑞國
出版者　修平科技大學圖書館校史組
地　址　41280 臺中市大里區工業路十一號
電　話　04-24961100
傳　真　04-24961187

編輯者　修平學報編審委員會
召 集 人—陳培中
編審委員—方世榮　江可達　林婉芳　張志淩
郭武彰　鄧作樑　盧志偉
（依姓氏筆劃排序）
執行編輯—郭武彰

印刷者　天空數位圖書有限公司
地　址　40255 台中市南區忠明南路 787 號 30 樓
電　話　04-22623893
傳　真　04-22623863

版權所有　請勿翻印

HSIUPING JOURNAL

VOL. 23
SEPTEMBER 2011

PUBLISHED BY
HSIUPING UNIVERSITY OF SCIENCE AND TECHNOLOGY
TAICHUNG, TAIWAN, R. O. C.

ISSN 1817-2954